

14P

FINAL TECHNICAL REPORT ON

A PRELIMINARY DESIGN OF A DRAG-FREE SATELLITE  
AND ITS APPLICATION TO GEODESY

Principal Investigators

Professor Benjamin O. Lange  
Dr. Daniel B. DeBra  
Stanford University

Professor William M. Kaula  
University of California  
at Los Angeles

(NASA-CR-125606) A PRELIMINARY DESIGN OF A  
DRAG-FREE SATELLITE AND ITS APPLICATION TO  
GEODESY Final Technical Report B.O.  
Lange, et al (Stanford Univ.) May 1969  
191 D

N72-18869

Unclas

17339

FACI

(NASA CR OR TMX OR AD NUMBER)

CSCL 22B G3/31

(CATEGORY)

Submitted to the National Aeronautics and Space Administration  
Electronics Research Center, Cambridge, Massachusetts

by the

Department of Aeronautics  
and Astronautics  
Stanford University

Institute of Geophysics  
and Planetary Physics  
University of California  
at Los Angeles

NAS-12-695

MAY 1969



STANFORD UNIVERSITY

CENTER FOR SYSTEMS RESEARCH

**Final Technical Report on  
A Preliminary Design of a Drag-Free Satellite  
and its Application to Geodesy**

**Principal Investigators**

**Professor Benjamin O. Lange**

**Dr. Daniel B. DeBra**  
**Stanford University**

**Professor William M. Kaula**  
**University of California at**  
**Los Angeles**

*Geodesy and its application to geodesy*

## TABLE OF CONTENTS

<u>Chapter</u>	<u>Page</u>
FOREWORD . . . . .	1
FOREWORD REFERENCES . . . . .	2
I. <u>TIDAL FRICTION WITH LATITUDE-DEPENDENT AMPLITUDE AND PHASE</u> <u>ANGLE</u> . . . . .	3
A. INTRODUCTION . . . . .	4
B. DEVELOPMENT OF DISTURBING FUNCTION . . . . .	5
C. EFFECTS ON LUNAR ORBIT EVOLUTION . . . . .	12
D. EFFECTS ON CLOSE SATELLITE ORBITS . . . . .	17
CHAPTER I: REFERENCES . . . . .	23
II. <u>ORBIT ANALYSIS</u> . . . . .	28
A. THE SELECTION OF ORBITS FOR THE DETERMINATION OF THE TESSERAL HARMONIC TERMS OF THE GRAVITATION POTENTIAL . .	28
1. Analysis of Medium and Long-Period Perturbations . .	28
2. The Selection of Resonant Orbits . . . . .	36
3. Computation of the Amplitude of $M_{lmpq}$ . . . . .	37
4. Additional Advantage of the Drag-Free Satellite for Orbits of Small Major Axes . . . . .	46
CHAPTER II: REFERENCES . . . . .	49
III. <u>SATELLITE DESIGN</u> . . . . .	50
A. MAGNETIC ATTITUDE CONTROL OF A SPINNING DRAG-FREE GEODESY SATELLITE . . . . .	51
1. The Attitude Dynamics of Rigid Spinning Spacecraft .	52
2. Disturbance Torques . . . . .	57
3. State Estimation by Filtering Horizon Sensor Data . .	62
4. Magnetic Attitude Control of the Symmetric Spinning Vehicle . . . . .	72
B. TRANSLATIONAL CONTROL MECHANIZATION FOR SPINNING SATELLITE	91
1. The Trapping Phenomenon . . . . .	93
2. Control Mechanizations Investigated . . . . .	97
3. State Estimation Techniques . . . . .	98

## TABLE OF CONTENTS (Cont)

<u>Chapter</u>	<u>Page</u>
III. (Cont)	
4. Conclusions . . . . .	106
C. INTERACTION BETWEEN TRANSLATIONAL CONTROL AND GRAVITY STABILIZED ATTITUDE MOTION . . . . .	107
1. Nonlinear Equations of Motion . . . . .	107
2. Measured Quantities, Control Forces, and Torques . .	112
3. Equilibrium Orientations and Positions . . . . .	114
4. Stability . . . . .	115
CHAPTER III: REFERENCES . . . . .	121
<u>APPENDIX A</u> . . . . .	123
<u>APPENDIX B</u> . . . . .	134
<u>APPENDIX C</u> . . . . .	163
<u>APPENDIX D: DOCUMENTATION OF DRAG-FREE SATELLITE FUEL COMPUTATION PROGRAM</u> . . . . .	172

## FOREWORD

Stanford University and the University of California at Los Angeles record in this Final Report, the results of a nine-months study on the application of a Drag-Free Satellite to geodesy. The work was performed under NASA Grant NAS-12-695 which was awarded in response to our proposal [Refs. 1 and 2] "To Prepare a Preliminary Design of a Drag-Free Satellite and Study Its Application To Geodesy," and the Addendum dated January, 1968. The work reported is principally in two areas: the first is the feasibility of making geophysical measurements which are not possible with conventional satellites, and the second area, preliminary design work on attitude and translation-control systems for spinning vehicle and possible coupling of attitude and translation control for gravity stabilized vehicles.

A Drag-Free Satellite control reference is an unsupported proof mass shielded from all external surface forces by the satellite. Since only gravitational forces act on the proof mass, it follows a purely gravitational orbit. A control system in a satellite senses the relative position of the satellite with respect to the proof mass and actuates reaction jets forcing the satellite to follow the proof mass. The satellite therefore also follows a purely gravitational orbit [Refs. 3 and 4]. This concept has been developed to a high degree at Stanford under NASA Grant NsG 582 and was independently proposed at UCLA for aeronomy studies in 1962 [Ref. 5]. There are two principal advantages of a Drag-Free Satellite for geodesy. First, the satellite cancels surface forces which might mask the small variations in the gravitational field; hence, it protects the long period perturbations due to weak effects from distortion and allows them to become large enough to be measured. Secondly, the perigee of the satellite can be made lower without introducing additional disturbances to the satellite ephemeris. It is possible, therefore, to enhance the effect of higher gravitational harmonics.

Two types of geodesy information have been considered in detail. The first is an improved analytical model of the effect of tidal forces on the earth. Latitude and longitude dependence of the elastic deformation and energy dissipation have been included. From this mathematical model, it is hoped to determine accurately, the tidal interaction of the earth, moon, and sun. Some fixed tesseral harmonics of the earth's gravitational field have been measured by conventional satellites. A large number of tesseral harmonics (72 pairs) were selected as being uncertain and of interest. Through careful analysis, four orbits have been selected in which a Drag-Free Satellite can identify 69 of these 72 pairs of tesseral harmonics. The necessary theory for this evaluation has been reviewed and the analysis leading to the selections of these four orbits is presented in detail.

In the design of the Drag-Free Satellite, there are two different types of performances that concern the designer. The control system which thrusts the satellite so that it follows the proof mass must be efficient in the utilization of propellant. Low propellant expenditure and tight control are the most important measures of control performance.

A very different type of performance is discussed in evaluating how closely one achieves a purely gravitational orbit. The proof mass may be perturbed by a sensor, gradients in local magnetic field, mass attraction from the satellite, and many other phenomena. Mass attraction of the satellite on the proof mass is the largest of these very small forces which prevent the orbit from being purely gravitational. When the average value of these disturbances are along-track, they produce significant perturbations. To reduce this effect by several orders of magnitude, the satellite may be spun. Therefore, a thorough preliminary design study was made on a spinning vehicle, attitude and translation control system for a drag-free operation to establish the feasibility of achieving this significant improvement of performance in case it is needed. The importance of adding a Drag-Free Satellite control system to an existing satellite was also recognized and hence, feasibility studies were performed to insure that special coupling effects would not degrade the translation control system performance. These are presented herewith in detail.

#### REFERENCES

1. "Proposal To Prepare A Preliminary Design of a Drag-Free Satellite And Study Its Application To Geodesy," Stanford University, submitted to NASA, Nov 1967.
2. Addendum to the above, Jan 1968.
3. "Proposal to Develop and Operate a Sustaining Earth Satellite in Two Orbital Flights," submitted to NASA by Stanford University, Feb. 1966.
4. Lange, Benjamin O., "The Control and Use of Drag-Free Satellites," Ph.D Dissertation, Stanford University, Department of Electrical Engineering, Aeronautics and Astronautics SUDAER Rept. No. 194, June 1964.
5. "Proposal for Phase I Studies of the Sustaining Orbiting Geophysical Observatory," vol. 1, Scientific/Technical, prepared by the University of California at Los Angeles, Institute of Geophysical and Planetary Physics Space Center for NASA, Dec 1962.

## 1.

### TIDAL FRICTION WITH LATITUDE-DEPENDENT AMPLITUDE AND PHASE ANGLE

Tidal disturbing functions were developed in which the amplitude factor  $k$  and lag angle  $\epsilon$  are expressed as sums of zonal spherical harmonics.

In regard to the current evolution of the moon's orbit, the existence of a second degree harmonic in the lag angle could make a significant contribution to energy transfer to the moon; it is unlikely, however, that it has an important effect on the overall time-scale of the orbit evolution.

If the moon formed in an equatorial orbit about the earth, tidal friction could do nothing to incline the orbit. Once the orbit was inclined, tidal friction could increase the inclination further if there was a commensurability between the earth's rotation and the moon's revolution.

Latitudinal variations in tidal properties would have appreciable effects on close satellite orbits. An appreciable second degree harmonic in the phase lag is needed, however, to reconcile the available data with the rate of the earth's rotational deceleration. Further progress requires satellites free from surface force effects.

## A. INTRODUCTION

As has been established by various studies in recent years, integration of the moon's orbit back in time under the influence of tidal friction with the dissipation factor  $1/Q$  inferred from observations of lunar & solar motion bring the moon close to the earth only  $1.0$  to  $2.0 \times 10^9$  years ago (Gerstenkorn, 1955; MacDonald, 1964; Goldreich, 1966). Furthermore, at the closest point the moon's orbit has an appreciable inclination with respect to the earth's equator, which would rule out a fission origin. Goldreich (1966) and Munk (1968) suggested, however, that an asymmetric tidal response of the earth may have had a significant effect on the orbital evolution of the moon.

Additional data which have recently been developed use the effects of tidal potentials on artificial satellite orbits. Kozai (1968) analyzed perturbations of the inclination of three satellites of  $33^\circ$  to  $50^\circ$  inclination. He obtained Love numbers  $k_2$  varying from  $0.23$  to  $0.33$  with uncertainties less than  $\pm .03$ , and phase lags from  $0^\circ$  to  $9^\circ$  with uncertainties of  $\pm 5$  to  $7^\circ$ . Newton (1968) analyzed perturbations of the node and inclination of four polar satellites. He obtained Love numbers  $k_2$  varying from  $0.28$  to  $0.44$  with uncertainties less than  $\pm .03$ , and phase lags from  $0.7^\circ$  to  $2.5^\circ$ , with uncertainties less than  $\pm 0.8^\circ$ . Newton emphasized that there appeared to be significant rate-dependence of both amplitude and phase angle. However, we still might hope to explain some of the differences among artificial satellite analyses, as well as the discrepancies from the  $2^\circ$  -  $2.5^\circ$



lags inferred from the deceleration of the earth's rotation by an asymmetric tidal response: i.e., one which is a function of location within the earth.

## B. DEVELOPMENT OF DISTURBING FUNCTION

Let the disturbing function of the sun or moon be represented in terms of the Kepler elements of the disturbing body and the spherical coordinates of the point of calculation of the potential (Kaula, 1964):

$$U = \sum_{l,m,p,q} B_{lm}^* C_{lmpq}^* r^l P_{lm}(\sin\varphi) \cdot \begin{cases} \cos \\ \sin \end{cases}_{l-m \text{ even/odd}}^{l-m} \{v_{lmpq}^* - m(\lambda + \theta)\}, \quad (1)$$

where  $r$ ,  $\varphi$ ,  $\lambda$  are radius, latitude, and longitude respectively;  $\theta$  is the Greenwich sidereal time;  $P_{lm}(\sin\varphi)$  is the Legendre Associated function; and

$$B_{lm}^* = Gm^* \frac{(l-m)!}{(l+m)!} (2 - \delta_{0m}) \quad (2)$$

$$C_{lmpq}^* = \frac{1}{a^{*l+1}} F_{lmp}(l^*) G_{lpq}(e^*) \quad (3)$$

$$v_{lmpq}^* = (l-2p)\omega^* + (l-2p+q)M^* + m\Omega^* \quad (4)$$

where  $G$  is the gravitational constant;  $m^*$ ,  $a^*$ ,  $e^*$ ,  $l^*$ ,  $M^*$ ,  $\omega^*$ ,  $\Omega^*$  are the mass and Kepler elements of the disturbing body; and  $F_{\ell mp}(l^*)$  and  $G_{\ell pq}(e^*)$  are polynomials as derived by Kaula (1966).

Now, regardless of the nature of the tidal response of the earth -- oceanic, bodily, or otherwise -- so long as there is no significant non-linearity (i.e., tidal terms interacting with themselves or other terms), then the tidal potential at the earth's surface  $r = R$  can be written as:

$$\begin{aligned}
 T(R, \varphi, \lambda) = & \sum_{\ell mpq} k_{\ell}(\varphi, \lambda) R^{\ell} B_{\ell m}^* C_{\ell mpq}^* \\
 & \cdot P_{\ell m}(\sin \varphi) \begin{cases} \cos & \ell-m \text{ even} \\ \sin & \ell-m \text{ odd} \end{cases} \\
 & \cdot \left\{ v_{\ell mpq}^* - \epsilon_{\ell mpq}(\varphi, \lambda) - m(\lambda + \theta) \right\} \quad (5)
 \end{aligned}$$

We should expect the Love number  $k_{\ell}(\varphi, \lambda)$  and phase lag  $\epsilon_{\ell mpq}(\varphi, \lambda)$  to be rather smoothly varying functions of position, and hence representable by spherical harmonics; this would certainly be true of that portion of their effect which would affect satellite orbits. The full development of Eq. (5) would involve products of tesseral harmonics, and hence would be most conveniently done in complex representation, along the lines of Kaula (1967). But a fairly elementary consideration shows that any longitude-dependent part of the product  $k_{\ell} \epsilon_{\ell mpq}$  will have its effect on any orbit "averaged out" by the earth's rotation.

Hence for the purpose of orbital analysis let us assume  $k_\ell$  and  $\epsilon_{\ell mpq}$  to be functions of latitude only, which allows us to retain a real representation:

$$k_\ell = \sum_h \kappa_{\ell h} P_{ho}(\sin\varphi) \quad (6)$$

and

$$\epsilon_{\ell mpq} = \sum_n \epsilon_n(\ell mpq) P_{no}(\sin\varphi) \quad (7)$$

In derivations where the frequency dependence of  $\epsilon_n$  is not being emphasized, we shall drop the argument  $(\ell mpq)$ .

If it is assumed that all the  $\epsilon_n$  are small enough that  $\sin(\epsilon_{\ell mpq}) = \epsilon$ ,  $\cos(\epsilon_{\ell mpq}) = 1$ , then the tidal potential at the surface can be written:

$$\begin{aligned} T(R) = & \sum_{\ell mpqh n} K_{\ell mpq} \kappa_{\ell h} P_{ho}(\sin\varphi) P_{\ell m}(\sin\varphi) \\ & \cdot \left[ \begin{matrix} \cos \\ \sin \end{matrix} \right]_{\ell-m \text{ odd}}^{\ell-m \text{ even}} \left\{ v_{\ell mpq} - m(\lambda+\theta) \right\} \\ & + \epsilon_n P_{no}(\sin\varphi) \left\{ \begin{matrix} \sin \\ -\cos \end{matrix} \right\}_{\ell-m \text{ odd}}^{\ell-m \text{ even}} \left\{ v_{\ell mpq} - m(\lambda+\theta) \right\} \end{aligned} \quad (8)$$

where

$$K_{\ell mpq} = R^{\ell} B_{\ell m}^* C_{\ell mpq} \quad (9)$$

The product  $P_{\ell m}(\sin\varphi) P_{j0}(\sin\varphi)$  can be converted to a sum:

$$P_{\ell m} P_{j0} = \sum_{k=m}^{\ell+j} Q_{\ell j km} P_{km} \quad (10)$$

Values of  $Q_{\ell j km}$  are given in Table 1. Applying Eq. (10) to all products in Eq. (8) allows us to write the tidal potential  $T(r)$  at any radius  $r > R$  as:

$$\begin{aligned} T(r) = & \sum_{\ell mpq h n k s} K_{\ell mpq} \kappa_{\ell h} Q_{\ell h km} \\ & \cdot \left[ \left( \frac{R}{r} \right)^{k+1} P_{km} \begin{Bmatrix} \cos \\ \sin \end{Bmatrix}_{\ell-m}^{\ell-m \text{ even}} \left\{ v_{2mpq}^* - m(\lambda+\theta) \right\} \right. \\ & \left. + \epsilon_n Q_{kns m} \left( \frac{R}{r} \right)^{s+1} P_{sm} \begin{Bmatrix} \sin \\ -\cos \end{Bmatrix}_{\ell-m}^{\ell-m \text{ even}} \left\{ v_{2mpq}^* - m(\lambda+\theta) \right\} \right] \quad (11) \end{aligned}$$

Using the usual conversion from spherical coordinates to Kepler elements of the perturbed satellite orbit (Kaula, 1966, p. 37),

$$\begin{aligned} & \left( \frac{R}{r} \right)^{\ell+1} P_{\ell m}(\sin\varphi) \begin{Bmatrix} \cos \\ \sin \end{Bmatrix}_{m\lambda} \\ & = \left( \frac{R}{a} \right)^{\ell+1} \sum_{jg} F_{\ell mj}(I) G_{\ell jg}(e) \begin{Bmatrix} \cos & \sin \\ \sin & -\cos \end{Bmatrix}_{\text{even } (\ell-m) \text{ odd}} \\ & \cdot \left\{ v_{\ell mpq} - m\theta \right\} \quad (12) \end{aligned}$$

we get

$$\begin{aligned}
T = & \sum_{\ell m p q h n k s j g} K_{\ell m p q} u_{\ell h} Q_{\ell h k m} \\
& \cdot \left[ \left( \frac{R}{a} \right)^{k+1} F_{k m j}(l) G_{k j g}(e) \begin{cases} \cos & (k-l) \text{ even} \\ (-1)^m \sin & (k-l) \text{ odd} \end{cases} \right. \\
& \cdot \{v_{k m j g} - v_{\ell m p q}^*\} + \epsilon_n Q_{k n s m} \left( \frac{R}{a} \right)^{s+1} F_{s m j}(l) \\
& \cdot G_{s j g}(e) \begin{cases} -\sin & (s-l) \text{ even} \\ (-1)^m \cos & (s-l) \text{ odd} \end{cases} \left. \{v_{s m j g} - v_{\ell m p q}^*\} \right] \quad (13)
\end{aligned}$$

To simplify, let us substitute  $(k_\ell \epsilon)_h$  for  $u_{\ell h} \sum_n \epsilon_n Q_{k n s m}$ :  
then we can write

$$\begin{aligned}
T = & \sum_{\ell m p q h k j g} K_{\ell m p q} \left( \frac{R}{a} \right)^{k+1} F_{k m j}(l) G_{k j g}(e) Q_{\ell h k m} \\
& \cdot \left[ u_{\ell h} \begin{cases} \cos & (k-l) \text{ even} \\ (-1)^m \sin & (k-l) \text{ odd} \end{cases} + (k_\ell \epsilon)_h \begin{cases} -\sin & (k-l) \text{ even} \\ (-1)^m \cos & (k-l) \text{ odd} \end{cases} \right] \\
& \cdot \{v_{k m j g} - v_{\ell m p q}^*\} \quad (14)
\end{aligned}$$

For analysis of the moon's orbital evolution, we require  
(1) zero rate:

$$\dot{v}_{k m j g} - \dot{v}_{\ell m p q}^* = 0, \quad (15)$$

or, from Eq. (4),

$$j = \frac{1}{2}(k-l) + p \quad (16)$$

$$g = q; \quad (17)$$

and (2) small "damping" factor  $(a^{*l+1} a^{k+1})^{-1}$ , or

$$lk = 20, 22, 24, 33, \text{ or } 42 \quad (18)$$

The combination 31 for  $lk$  is excluded because a first degree harmonic would represent a shift of the origin, the earth's center of mass. For lunar orbit evolution then let us write

$$T = T_0 + T_2 + T_4$$

where

$$\left. \begin{aligned} T_0 &= \sum_{qh} K_{201q} \left(\frac{R}{a}\right) F_{000} G_{00q} Q_{2h00} \psi_{201hq} \\ T_2 &= \sum_{qhmp} K_{2mpq} \left(\frac{R}{a}\right)^3 F_{2mp} G_{2pq} Q_{2h2m} \psi_{22mphq} \\ T_4 &= \sum_{\ell=2}^4 \sum_{qhmp} K_{\ell mpq} \left(\frac{R}{a}\right)^{7-\ell} F_{(6-\ell)mj} G_{2jq} \\ &\quad \cdot Q_{(6-\ell)h\ell m} \psi_{(6-\ell)\ell mphq} \end{aligned} \right\} \quad (19)$$

in which

$$\psi_{\ell k m p h q} = \left( \kappa_{\ell h} \cos - (k_{\ell} \epsilon)_h \sin \right) \left( v_{k m j q} - v_{\ell m p q}^* \right)$$

and  $j$  is related to  $k$ ,  $\ell$ , and  $p$  by Eq. (16).

For analysis of tidal perturbations of artificial satellites, we require (1) no short period terms, or

$$g = 2j - k \quad (20)$$

and (2) small "damping" factor  $(a^* \ell + 1)^{-1}$ , or

$$\ell = 2 \quad (21)$$

Eq. (14) thus becomes

$$\begin{aligned} T = & \sum_{m p q h k j} K_{2 m p q} \left( \frac{R}{a} \right)^{k+1} F_{k m j} G_{k j (2j-k)} Q_{2 h k m} \\ & \cdot \left[ \kappa_{2 h} \left\{ \begin{matrix} \cos & k \text{ even} \\ (-1)^m \sin & k \text{ odd} \end{matrix} \right\} + (k_{\ell} \epsilon)_h \left\{ \begin{matrix} -\sin & k \text{ even} \\ (-1)^m \cos & k \text{ odd} \end{matrix} \right\} \right] \\ & \cdot \left[ v_{k m j (2j-k)} - v_{2 m p q}^* \right] \quad (22) \end{aligned}$$

Values of the amplitude factors  $K_{\ell m p q}$  and associated rates  $v_{\ell m p q}^*$  are given in Table I-1.

### C. EFFECTS ON LUNAR ORBIT EVOLUTION

Of the terms in Eq. (19), those with  $\ell_{mpq} = 2010$  are meaningless because  $\dot{v}_{0000}$  is zero. The lowest value of  $h$  which gives a non-zero  $Q_{2h00}$  is 2. From Table I-2,  $K_{2011}$  is appreciably larger than  $K_{201-1}$ .  $G_{001}$  is the coefficient of  $\cos M$  in the expansion of  $a/r$ , or  $e$ . Writing out the parts of  $K_{2011}$  and evaluating  $Q_{2200}$  from Table I we get

$$T_0 = \frac{Gm^*}{Ra^*} \left[ \frac{3}{4} \sin^2 i^* - \frac{1}{2} \right] \left[ \frac{3}{2} e^* + \frac{27}{16} e^{*3} + \dots \right] \\ \cdot \left( \frac{R}{a^*} \right)^3 \left( \frac{R}{a} \right) e \frac{1}{5} (\kappa_{22} \cos - \kappa_{20} \epsilon_2 \sin) (M - M^*) \quad (23)$$

From the Lagrangian planetary equations-of-motion, we get (dropping asterisks after differentiating  $T_0$ ):

$$\dot{a}_0 = \frac{2}{na} \frac{\partial T_0}{\partial M} \\ = - \frac{Gm^*}{na^2} \frac{2e(R/a)^4}{5R} \left[ \frac{3}{4} \sin^2 i - \frac{1}{2} \right] \left[ \frac{3}{2} e + \frac{27}{16} e^3 + \dots \right] (\kappa_2 \epsilon_2) \\ \approx \frac{3Gm^* e^2 (R/a)^4}{10na^2 R} \kappa_{20} \epsilon_2 \quad (24)$$

and



$$\dot{e}_0 = \frac{1-e^2}{na^3} \frac{\partial T_0}{\partial M}$$

$$= - \frac{Gm^*}{na^3} \frac{(1-e^2)}{5R} \left(\frac{R}{a}\right)^4 \left[ \frac{3}{4} \sin^2 i - \frac{1}{2} \right] \left[ \frac{3}{2}e + \frac{27}{16}e^3 + \dots \right]$$

$$\cdot (k_2 e_2)$$

$$\approx \frac{3Gm^*e}{20na^3R} \left(\frac{R}{a}\right)^4 \kappa_{20} e_2 \quad (25)$$

These terms express the effect of the interaction of the eccentricity of the moon's orbit with a variation of the tidal dissipation in the earth which is symmetric about the equator. Since the earth's rotation is not involved, there is no angular momentum transfer: only energy transfer. Eq. (24) states that if dissipation is concentrated near the poles in the earth, the moon will move away faster; while if it is concentrated near the equator it will move away more slowly. Eq. (25) is merely consistent with conservation of angular momentum, or  $a^{\frac{1}{2}}(1-e^2)^{\frac{1}{2}}$ .

Putting in numbers, we have for the present lunar orbit, from Eq. (24), in planetary units

$$\dot{a}_0 = 1.08 \times 10^{-13} \kappa_{20} e_2 (2011) \quad (26)$$

From Eq. (41) of Kaula (1964),

$$\dot{a}_2 \approx \frac{3Gm^*}{na^2R} \left(\frac{R}{a}\right)^6 \kappa_{20} \epsilon_0(2200)$$

$$= 0.97 \times 10^{-13} \kappa_{20} \epsilon_0(2200) \quad (27)$$

The frequency (in an earth reference frame) for  $\ell_{mpq} = 2200$  is about 55 times that for  $\ell_{mpq} = 2011$ . Hence, since a significant part of the tidal dissipation is in the oceans, probably

$$\epsilon_0(2011) \ll \epsilon_0(2200) \quad (28)$$

Furthermore, we would expect  $\epsilon_0 + \epsilon_2 P_2$  to be greater than zero everywhere, so probably

$$-\epsilon_0(2011) < \epsilon_2(2011) < 2\epsilon_0(2011) \quad (29)$$

Thus it seems unlikely that the effect on the lunar orbit evolution of non-uniformity of dissipation can explain the discrepancy between the lag angle inferred from lunar & solar motions (most recently by Curott, 1966) and that from artificial satellite orbits by Newton (1968). Since  $\dot{h}_y/\dot{h}$  is positive, for non-uniform dissipation to explain some of the discrepancy its contribution to  $\dot{h}_y$  should be negative and hence  $\dot{a}_0$  should be positive, corresponding to a predominance around the poles (see Kaula, 1968, p. 197).

The most significant result of Goldreich (1966) was that if dissipation has been uniform over the earth's surface, the inclination to the equator could never have been less than  $10^\circ$

within 10 earth radii. Goldreich suggested that strong local dissipation in a few places in the earth's oceans or crust may lead to unanticipated deviations from his results. No matter how "local" was this dissipation, and no matter how close the moon, the main effect on the orbit must be expressible in spherical harmonics -- just as is the case for satellite orbit perturbations by gravity anomalies fixed in the earth. A faster rate of rotation such as prevailed early in the earth's history would make this all the more true.

For the inclination to be changed by the disturbing function of Eq. (19), the combination  $F_{\ell mp} F_{kmj} [(k-2j) \cot i - m \csc i]$  must be non-zero (see, e.g., Kaula, 1966, p. 40). For  $i = 0$ , this never occurs:  $F_{\ell mp} F_{kmj}$  contains a non-zero factor only for  $m = k-2j$ . If  $m \neq k-2j$ ,  $F_{\ell mp} F_{kmj}$  is at least order  $i^2$ . All of which goes to say that purely latitudinal variations in tidal properties can do nothing to wrench the moon out of an equatorial orbit. What is necessary is an interaction such that

$$[(k-2j) - (\ell-2p)] (\dot{\omega} + \dot{M}) + (s-m) (\dot{\Omega} - \dot{\theta}) \approx 0 \quad (30)$$

with  $s \neq m$ : i.e., a resonance. To maintain such a resonance long enough to have significant effect,  $\dot{n}/\ddot{\theta}$  must have about equaled  $n/\dot{\theta}$ , where  $n$  is the mean motion, related to  $\mu = G(M+m^*)$  by Kepler's third law,

$$n = \mu^{\frac{1}{2}} a^{-3/2} \quad (31)$$

From conservation of angular momentum (Eq. (59), Kaula, 1964):

$$C\ddot{\theta} = \frac{1}{3}m^* \mu^{2/3} n^{-4/3} \dot{n} \quad (32)$$

where  $C$  is the earth's moment of inertia, or

$$\begin{aligned} \dot{n}/\ddot{\theta} &= 3Cm^{*-1} \mu^{-2/3} n^{4/3} \\ &= 3Cm^{*-1} a^{-2} \\ &\approx 81/a^2 \end{aligned} \quad (33)$$

for  $a$  in earth radii. Integrating the moon back close to the earth gives a rotation period of about five hours (Fig. 9, Goldreich, 1966), or 0.28 for  $\dot{\theta}$  in the "planetary" units of radians/807 sec. Setting  $n$  as equal to  $0.28 \times 81/a^2$  and equating it to  $n$  by Kepler's law (Eq. (31)), we get an absurdly large semi-major axis  $a$ . Hence it seems unlikely that any longitudinal variation in tidal properties ever had a significant effect on the lunar orbit. This holds true even for nonlinearities in the tides, since in Eq. (30) the tidal harmonic  $k$ s now has a completely independent specification from  $\ell$ m.

The next, more desperate, possibility is that an irregularity in tidal properties would affect  $\dot{n}$  so much in a direction counter to the central tidal term as to hold the moon at a resonance point where its inclination could be changed. A situation might have existed which is mathematically similar

to that of Mimas and Tethys, with a tidal bulge taking the place of the inner satellite Mimas. However, the treatment of Allan (1968) indicates that the inclinations must have been non-zero before these satellites became coupled, and that the subsequent increase in the inclinations depends on a factor of order  $I^2$ .

We thus seem to be forced back to the conclusion that at least part of the moon was captured. The interesting question then is how small a portion of the moon needs to be captured, taking into account that resonance with longitudinal variations in tidal properties may help to further feed the inclination. Since the mixed capture-fission hypothesis would involve several more ramifications than either theory alone (see the discussion & conclusions of Goldreich, 1966), it seems appropriate to defer further consideration thereof to another paper.

In regard to the time-scale problem of the lunar orbit evolution, the conclusion of Eqs. (26) - (27) that latitudinal variation in tidal lag can account for only a minor part of the current evolution indicates that it was of even less significance in the past, and hence a less important effect than changes in the extent of shallow seas, as suggested by the most recent paleontological work (Panella et al., 1968).

#### D. EFFECTS ON CLOSE SATELLITE ORBITS

We wish to examine the behavior of artificial satellites of small  $a/R$  under the influence of the disturbing function

given by Eq. (22) with a view to explaining results already obtained and suggesting specification of future orbits to determine tidal properties of the earth.

In his analysis, Kozai (1968) determined  $k$  and  $\epsilon$  from the perturbation of the inclination  $\Delta i$  of argument  $\Omega$ . Hence he used only the term  $mpqhkj = 110021$  of Eq. (22), or

$$T_2 = K_{2100} \left( \frac{R}{a} \right)^3 \left[ -\frac{3}{2} \sin i \cos i \right] (1-e^2)^{-3/2} \cdot \kappa_{20} (\cos -\epsilon_0 \sin) (\Omega - \Omega^*) \quad (34)$$

Newton (1968) determined  $k$  and  $\epsilon$  from the perturbations of inclination  $\Delta i$  and node  $\Delta \Omega$  with arguments containing  $\Omega$  and  $2\Omega$ . He obtained the lunar and solar-orbit dependent factors by numerical integration, which would be equivalent to using all 6 terms  $m = 1, 2$  and  $p = 0, 1, 2$ , with  $qhkj = 0021$  in Eq. (22):

$$T_2 = \sum_{mp} K_{2mp0} \left( \frac{R}{a} \right)^3 F_{2m1}(i) (1-e^2)^{-3/2} \cdot \kappa_{20} (\cos -\epsilon_0 \sin) m(\Omega - \Omega^*) \quad (35)$$

Since the perigee argument  $\omega$  is absent from the disturbing functions (34) and (35), odd zonal variations  $h = 1, 3, 5 \dots$  in  $k_2$  and  $\epsilon$  could not have given rise to perturbations of the same period as equations (34) and (35); only even variations  $h = 2, 4 \dots$ . Hence in the expressions for perturbation of

$\Delta l$  (dependent on  $\partial R/2\Omega$ ) containing the Love number  $k$  we can make the substitution

$$\left(\frac{R}{a}\right)^3 F_{2m1} G_{210} \left\{ \begin{matrix} k_l \\ k_l \epsilon \end{matrix} \right\} = \sum_{k,h} \left(\frac{R}{a}\right)^{k+1} F_{kmk/2} G_{k(k/2)0} \cdot Q_{2hkm} \left\{ \begin{matrix} k_{2h} \\ (k_a \epsilon)_h \end{matrix} \right\}, \quad (36)$$

$m = 1, 2; \quad h, k \text{ even}$

and in the expressions for the perturbation  $\Delta\Omega$  (dependent on  $\partial R/\partial l$ ), the substitution

$$\left(\frac{R}{a}\right)^3 \frac{\partial F_{2m1}}{\partial l} G_{210} \left\{ \begin{matrix} k_\Omega \\ k_\Omega \epsilon \end{matrix} \right\} = \sum_{k,h} \left(\frac{R}{a}\right)^{k+1} \frac{\partial F_{kmk/2}}{\partial l} G_{k(k/2)0} \cdot Q_{2hkm} \left\{ \begin{matrix} k_\Omega \\ (k_a \epsilon)_h \end{matrix} \right\} \quad (37)$$

$m = 1, 2; \quad h, k \text{ even}$

Let us define

$$J_{hm} = \sum_k \left(\frac{R}{a}\right)^{k+1} F_{kmk/2} G_{k(k/2)0} Q_{2hkm} \quad (38)$$

and

$$J'_{hm} = \partial J_{hm} / \partial l \quad (39)$$

Then (36) and (37) become

$$J_{0m} \left\{ \begin{matrix} k_1 \\ k_1 \epsilon \end{matrix} \right\} = \sum_h J_{hm} \left\{ \begin{matrix} x_{2h} \\ (k_2 \epsilon)_h \end{matrix} \right\} \quad (40)$$

$$J'_{0m} \left\{ \begin{matrix} k_\Omega \\ k_\Omega \epsilon \end{matrix} \right\} = \sum_h J'_{hm} \left\{ \begin{matrix} x_{2h} \\ (k_2 \epsilon)_h \end{matrix} \right\} \quad (41)$$

Kozai (1968) used satellites of essentially two specifications:  $a/R = 1.30$ ,  $i = 33^\circ$ ,  $e = 0.16$ ; and  $a/r = 1.22 \pm .04$ ,  $i = 48.6^\circ \pm 1.5^\circ$ ,  $e = .01$ . Newton (1968) used satellites of one specification  $a/R = 1.157 \pm .016$ ,  $i = 90.2^\circ \pm 0.3^\circ$ ,  $e < .008$ . Values of  $J_{hm}$  corresponding to the  $m$  values of terms used in these analyses are given in Table I-3.

In Table I-4 are summarized the results obtained by Kozai and Newton. Newton's values for  $k$  and  $k\delta$  are based mainly on solar perturbations and are combinations of values ranging from 0.31 to 0.38 which are weighted inversely proportionate to their radiation pressure perturbations. In combining Kozai's values for his  $47.2^\circ$  and  $50.1^\circ$  inclination satellites we have utilized a similar weighting:  $1/.21$  for the  $47.2^\circ$  (ECHO 1 ROCKET CASE) and  $1/.07$  for the  $50.1^\circ$  (ANNA 1B). In defining the lag angle we have accepted the Darwinian assumption, used by Newton, that it is proportionate to frequency: i.e.,  $\epsilon = \delta$  for  $m = 1$  and  $\epsilon = 2\delta$  for  $m = 2$ .

We also have included in Table IV the lag inferred from the earth's deceleration, using the rate derived by Curott (1966). It appears in the column  $k_1\delta$ , since it depends on  $\lambda R/\lambda M$  and the  $\ell_{mpq} = 2200$  term is dominant (Kaula, 1968, pp. 198-203).



Applying Eqs. (40) - (41) to the close satellite data in Table IV we get as observation equations:

$$\begin{Bmatrix} -.310, & -.086, & +.042 \\ -.429, & -.204, & +.126 \\ .986, & .155, & -.304 \\ .986, & -.008, & -.026 \end{Bmatrix} \begin{Bmatrix} \kappa_{20}, (\kappa_2 \delta)_0 \\ \kappa_{22}, (\kappa_2 \delta)_2 \\ \kappa_{24}, (\kappa_2 \delta)_4 \end{Bmatrix} = \begin{Bmatrix} -.0967, & .0000 \\ -.1072, & -.0149 \\ +.337, & .0053 \\ +.346, & .0073 \end{Bmatrix} \quad (42)$$

Which yield

$$k_2 = .372 - .240 P_{20} - .013 P_{40} \quad (43)$$

$$(k\delta)_2 = .006 - .093 P_{20} - .079 P_{40} \quad (44)$$

The large  $\kappa_{22}$  of  $-.240$  makes significant terms  $\kappa_{2h} e_n$ , when both  $h$  and  $n$  are non-zero, appearing in Eq. (13). If we let

$$\sum_{l,n} Q_{lnko} \kappa_{2l} \delta_{2n} = (k\delta)_{2k} \quad (45)$$

we get

$$\delta_2 = .003 - .028 P_{20} - .263 P_{40}, \quad (46)$$

which is even more implausible.

An alternative procedure would be to use Newton's data alone for  $\kappa_{20}$  and  $\kappa_{22}$ , and then use Newton's data with the moon for  $(k\delta)_{20}$ ,  $(k\delta)_{22}$ ,  $(k\delta)_{24}$ . We get

$$k_2 = .351 - .055 P_{20} \quad (47)$$

$$(k\delta)_2 = .0072 - .0121 P_{20} - .0004 P_{40} \quad (48)$$

and

$$\delta_2 = .0195 - .0331 P_{20} - .0028 P_{40} \quad (49)$$

Eq. (47) is much more reasonable than Eq. (43), and Eq. (49) is somewhat more reasonable than Eq. (46). Physical necessity requires only that  $\delta_{20}$  is positive; the existence of ocean tides makes it possible that one of the zonal coefficients can be larger than  $\delta_{20}$ . Eq. (49) says that beyond the latitude where  $P_{20}$  is  $.0195/.0331$ ,  $58^\circ$ , phase leads should predominate over phase lags in the tide meter readings. A statistical analysis would be worthwhile. A major effect by ocean tides would invalidate the Darwinian assumption and make it impossible to extrapolate any inferences to rates other than semi-diurnal & diurnal, such as the monthly rate which Eq. (26) suggests might be important in lunar orbit evolution.

With the data on hand we get only a tentative indication of significant latitudinal variation in the earth's tidal properties. But it is certainly a good enough indication to warrant further effort in two directions: (1) the placing in

orbit of artificial satellites which are instrumented to compensate for any surface forces, in order to determine long-periodic (fortnightly or more) variations in the orbit; and (2) the transformation of tidal models of the earth to a form compatible with the potential of Eq. (13) or (14).

#### ACKNOWLEDGEMENTS

This work has been supported by NASA contracts NGR 05-007-138 and NAS 12-695.

#### REFERENCES

- Allan, R.R. 1968, Royal Aircraft Est. Tech. Rep. 68169.
- Curott, D.R. 1966, Astron J. 71, 264.
- Gerstenkorn, H. 1955, Z. Astrophys. 26, 245.
- Goldreich, P. 1966, Revs. Geophys. 4, 411.
- Kaula, W.M. 1964, Revs. Geophys. 2, 661.
- Kaula, W.M. 1966, Theory of Satellite Geodesy (Blaisdell, Waltham, Mass.).
- Kaula, W.M. 1967, Revs. Geophys. 5, 83.
- Kaula, W.M. 1968, An Introduction to Planetary Physics: the Terrestrial Planets (Wiley, New York).
- Kozai, Y. 1968, Bull. Geod. 89, 355.
- MacDonald, G.J.F. 1964, Revs. Geophys. 2, 467.
- Munk, W.H. 1968, Quart. J. Roy. Astron. Soc. 9, 352.
- Newton, R.R. 1968, Geophys. J. Roy. Astron. Soc. 14, 505.
- Panella, G., C. MacClintock, & M.N. Thompson 1968, Science 162, 792.

TABLE 1-1. FACTORS FOR PRODUCT TO SUM CONVERSION  
OF LEGENDRE ASSOCIATED POLYNOMIALS\*

$$P_{lm} P_{no} = \sum_k Q_{lnkm} P_{km}$$

$l$	$m$	$n$	$Q_{ln0m}$	$Q_{ln1m}$	$Q_{ln2m}$	$Q_{ln3m}$	$Q_{ln4m}$	$Q_{ln5m}$	$Q_{ln6m}$
2	0	0			1				
2	0	1		2/5		3/5			
2	0	2	1/5		2/7		18/35		
2	0	3		9/35		4/15		10/21	
2	0	4			2/7		20/77		5/11
2	1	0			1				
2	1	1		3/5		2/5			
2	1	2			10/21		9/35		
2	1	3		-9/35		1/15		4/21	
2	1	4			-4/21		3/77		5/33
2	2	0			1				
2	2	1				1/5			
2	2	2			-2/7		3/35		
2	2	3				-2/15		1/21	
2	2	4			1/21		-6/77		1/33
3	0	0				1			
3	0	1			3/7		4/7		
3	0	2		9/35		4/15		10/21	
3	0	3	1/7		4/21		18/77		100/231
3	1	0				1			
3	1	1			4/7		3/7		
3	1	2		18/35		1/5		2/7	
3	1	3			2/21		9/77		50/231

\*Neumann or Ferrers type:

$$P_{lm}(\cos\theta) = \sin^m\theta \sum_t \frac{(-1)^t (2l-2t)!}{2^l t!(l-t)!(l-m-2t)!} \cos^{l-m-2t}\theta$$

TABLE 1-2. AMPLITUDE FACTORS OF TIDAL TERMS

"Planetary" units: length  $6.37 \times 10^8$  cm, mass  $5.97 \times 10^{27}$  g,  
time 806.8 sec.

$l$	$m$	$p$	$q$	MOON $K_{lmpq}$	SUN $K_{lmpq}$
2	0	0	-1	$.632 \cdot 10^{-10}$	$.929 \cdot 10^{-11}$
			0	$-.229 \cdot 10^{-8}$	$-.111 \cdot 10^{-8}$
			1	$-.440 \cdot 10^{-9}$	$-.651 \cdot 10^{-10}$
		1	-1	$-.122 \cdot 10^{-8}$	$-.180 \cdot 10^{-9}$
		1	1	$-.123 \cdot 10^{-8}$	$-.180 \cdot 10^{-9}$
		2	-1	$-.440 \cdot 10^{-9}$	$-.651 \cdot 10^{-10}$
			0	$-.229 \cdot 10^{-8}$	$-.111 \cdot 10^{-8}$
			1	$.632 \cdot 10^{-10}$	$.929 \cdot 10^{-11}$
2	1	0	-1	$-.122 \cdot 10^{-8}$	$-.180 \cdot 10^{-9}$
			0	$.441 \cdot 10^{-7}$	$.213 \cdot 10^{-7}$
			1	$.852 \cdot 10^{-8}$	$.125 \cdot 10^{-8}$
		1	-1	$-.350 \cdot 10^{-8}$	$-.515 \cdot 10^{-9}$
			0	$-.427 \cdot 10^{-7}$	$-.204 \cdot 10^{-7}$
			1	$-.350 \cdot 10^{-9}$	$-.515 \cdot 10^{-9}$
		2	-1	$-.365 \cdot 10^{-9}$	$-.540 \cdot 10^{-10}$
			0	$-.189 \cdot 10^{-8}$	$-.921 \cdot 10^{-9}$
			1	$.525 \cdot 10^{-10}$	$.774 \cdot 10^{-11}$
2	2	0	-1	$-.584 \cdot 10^{-8}$	$-.859 \cdot 10^{-9}$
			0	$.212 \cdot 10^{-6}$	$.103 \cdot 10^{-6}$
			1	$.409 \cdot 10^{-7}$	$.606 \cdot 10^{-8}$
		1	-1	$.153 \cdot 10^{-8}$	$.223 \cdot 10^{-9}$
			0	$.186 \cdot 10^{-7}$	$.888 \cdot 10^{-8}$
			1	$.153 \cdot 10^{-8}$	$.223 \cdot 10^{-9}$
		2	-1	$.634 \cdot 10^{-10}$	$.112 \cdot 10^{-10}$
			0	$.393 \cdot 10^{-9}$	$.190 \cdot 10^{-11}$
			1	$-.109 \cdot 10^{-10}$	$-.160 \cdot 10^{-11}$

TABLE 1-3. INFLUENCE COEFFICIENTS OF TIDAL PARAMETERS ON SATELLITE ORBITS

a	e	i	m	$J_{0m}$	$J'_{0m}$	$J_{2m}$	$J'_{2m}$	$J_{4m}$	$J'_{4m}$
1.30	.16	33°	1	-.310	-.276	-.086	-.284	.042	.303
1.20	.01	49°	1	-.429	.121	-.204	-.278	.126	-.123
1.16	.00	90°	{1	.000	.986	.000	-.008	.000	-.026
			2	.986	.000	.155	.000	-.304	.000
60.27	.055	23.5°	2	$1.04 \times 10^{-6}$	---	$-.30 \times 10^{-6}$	---	$.05 \times 10^6$	---

TABLE 1-4. SUMMARY OF ORBIT ANALYSES FOR TIDAL PARAMETERS

a	e	i	$k_1$	$k_1^\delta$	$k_\Omega$	$k_\Omega^\delta$
1.30	.16	33°	.312	.0000	--	--
1.20	.01	49°	.250	.0348	--	--
1.16	.00	90°	.342	.0054	.351	.0074
60.27	.055	23.5°	--	.0107	--	--

## II. ORBIT ANALYSIS

### A. THE SELECTION OF ORBITS FOR THE DETERMINATION OF THE TESSERAL HARMONIC TERMS OF THE GRAVITATIONAL POTENTIAL

When candidate orbits are selected for geodesy satellites, it is necessary to consider all possible ways in which measurable information can be obtained from such orbits. Existing satellites, of course, yield useful geodetic information. Drag-free orbits are therefore essential only in determining otherwise unknown and unobtainable data. Geodesy information obtainable from existing satellites is being considered, with results reported in Refs. 2-1 to 2-4. From these reports, it appears that the tesseral harmonic coefficients of degree 7-15 and order 3-10 are the 72 pairs of coefficients which are least well known and probably of most current interest. Figure 2-1, taken from Ref. 2-4, indicates one group's opinion of the status of the tesseral harmonics.

Improved values of the coefficients of order 11-16 have been measured by tracking the perturbations of existing satellites although the effect of atmospheric forces may cast some doubt on the validity of the data.

Previous studies have discussed (and we have verified) the optimum orbits for measuring the unknown tesseral coefficients [Refs. 2-7, 2-8]. But it is of more practical importance to know the minimum number of drag-free orbits required to adequately determine all of these coefficients.

In this Chapter, we review the pertinent perturbation theory and show how a drag-free orbit increases measurability by protecting long-period perturbations from distortions and allowing operation at lower perigee altitude. We conclude that 69 of the 72 pairs of coefficients of interest can be determined by Drag-Free Satellites in only four carefully selected orbits which are specified and discussed.

#### 1. Analysis of Medium and Long-Period Perturbations.

Medium-period perturbations will be defined as those with periods which are fractions of a day. Long-period perturbations are those with periods of several days. Perturbation analysis is begun by considering the gravitational potential expressed in the form



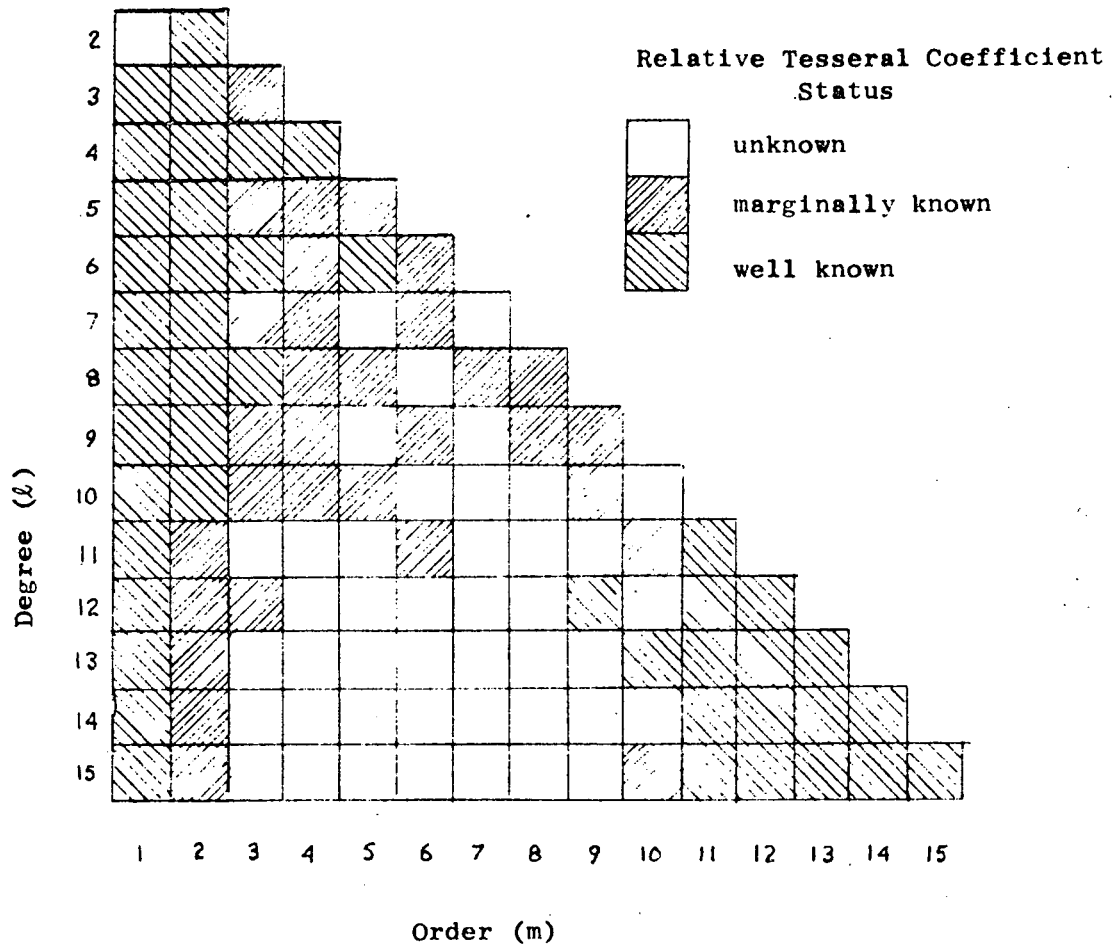


FIG. 2-1. STATUS OF KNOWLEDGE OF TESSERAL COEFFICIENTS  
ACCORDING TO REFERENCE 2-4.

$$V = \frac{u}{r} + \sum_{\ell=2}^{\infty} \sum_{m=0}^{\ell} \sum_{p=0}^{\ell} \sum_{q=-\infty}^{\infty} R_{\ell mpq} \quad (2.1)$$

in which

$$R_{\ell mpq} = \frac{u}{a} \left( \frac{a_E}{a} \right)^{\ell} J_{\ell m} F_{\ell mp}(i) G_{\ell pq}(e) \begin{cases} \cos \\ \sin \end{cases} \begin{matrix} (\ell-m)\text{even} \\ (\ell-m)\text{odd} \end{matrix} \psi_{\ell mpq} \quad (2.2)$$

and

$$\psi_{\ell mpq} = [(\ell - 2p)\omega + (\ell - 2p + q)M + m(\Omega - \theta_E - \lambda_{\ell m})]. \quad (2.3)$$

The quantities  $a$ ,  $e$ ,  $i$ ,  $\Omega$ ,  $\omega$ , and  $M$  are the standard orbital elements, and  $u$  is the earth mass times the universal gravitation constant.

$J_{\ell m}$  and  $\lambda_{\ell m}$  are the amplitude and phase angle associated with the tesseral coefficients of degree  $\ell$  and order  $m$ . The angle  $\theta_E$  is the hour angle of Greenwich and  $a_E$  is the earth's equatorial radius. The function  $F_{\ell mp}(i)$ , known as the inclination function, results from the potential being rotated into the orbit plane. It is given by Kaula [Ref. 2-5]

$$F_{\ell mp}(i) = \sum_t \frac{(2\ell - 2t)!}{t! (\ell - t)! (\ell - m - 2t)! 2^{2(\ell - t)}} \sin^{\ell - m - 2t} i \quad (2.4)$$

$$\times \sum_{s=0}^m \binom{m}{s} \cos^s i \sum_c \binom{\ell - m - 2t + s}{c} \binom{m - s}{p - t - c} (-1)^{c - k}$$

where  $k$  is the integer part of  $(\ell - m)/2$ ,  $t$  is summed from 0 to the lesser of  $p$  or  $k$ , and  $c$  is summed over all values for which the binomial coefficients are non-zero. The eccentricity function  $G_{\ell pq}(e)$  comes from converting orbit radius and true anomaly into  $a$ ,  $e$ , and  $M$ . For  $(\ell - 2p + q) = 0$ , it is given by

$$G_{\ell pq}(e) = \frac{1}{(1 - e^2)^{\ell - \frac{1}{2}}} \sum_{d=0}^{p' - 1} \binom{\ell - 1}{2d + \ell - 2p'} \binom{2d + \ell - 2p'}{d} \left( \frac{e}{2} \right)^{2d + \ell - 2p'} \quad (2.5)$$

where  $p' = p$  for  $p < \ell/2$

$= (\ell - p)$  for  $p > \ell/2$ .

For  $(\ell - 2p + q) \neq 0$ ,  $G_{\ell pq}(e)$  is given by

$$G_{\ell pq}(e) = (-1)^{|q|} (1 + \beta^2)^\ell \beta^{|q|} \sum_{k=0}^{\infty} P_{\ell pqk} Q_{\ell pqk} \beta^{2k} \quad (2.6)$$

where

$$\beta = \frac{e}{(1 + \sqrt{1 - e^2})},$$

$$P_{\ell pqk} = \sum_{r=0}^h \binom{2(p' - \ell)}{h - r} \frac{(-1)^r}{r!} \left( \frac{(\ell - 2p' + q')e}{2\beta} \right)^r,$$

$$\begin{aligned} h &= k + q', \quad q' > 0 \\ &= k, \quad q' \leq 0; \end{aligned}$$

and

$$Q_{\ell pqk} = \sum_{r=0}^h \binom{-2p'}{h - r} \frac{1}{r!} \left( \frac{(\ell - 2p' + q')e}{2\beta} \right)^r,$$

$$h = \begin{cases} k, & q' > 0 \\ k - q', & q' \leq 0. \end{cases}$$

Here,

$$p' = p, \quad q' = q \quad \text{for } p \leq \ell/2,$$

$$p' = \ell - p, \quad q' = -q \quad \text{for } p > \ell/2.$$

The instantaneous time rate of change of the orbital elements due to any one term in the gravitational potential is found from the Lagrange planetary equations

$$\begin{aligned} \dot{a} &= \frac{2}{an} \frac{\partial R}{\partial M} \\ \dot{e} &= \frac{\sqrt{1 - e^2}}{na^2 e} \left( \sqrt{1 - e^2} \frac{\partial R}{\partial M} - \frac{\partial R}{\partial \omega} \right) \\ \dot{\omega} &= - \frac{\cos i}{na^2 \sqrt{1 - e^2} \sin i} \frac{\partial R}{\partial i} + \frac{\sqrt{1 - e^2}}{na^2 e} \frac{\partial R}{\partial e}, \end{aligned} \quad (2.7)$$

$$\dot{i} = \frac{1}{na^2 \sqrt{1-e^2} \sin i} \left( \cos i \frac{\partial R}{\partial \omega} - \frac{\partial R}{\partial \Omega} \right) \quad (2.7)$$

Cont.

$$\dot{\Omega} = \frac{1}{na^2 \sqrt{1-e^2} \sin i} \frac{\partial R}{\partial i}$$

$$\dot{M} = n - \frac{1-e^2}{na^2 e} \frac{\partial R}{\partial e} - \frac{2}{na} \frac{\partial R}{\partial a},$$

where  $R = R_{\ell mpq}$  given in Eq. 2.2 and  $n$  is the mean orbital rate. Approximate solutions to these equations are found by treating the  $\psi_{\ell mpq}$  as linear functions of time [Ref. 2-5].

The medium-period perturbations of the in-track position of the satellite can be found for any given  $J_{\ell m}$  and  $\lambda_{\ell m}$  from the closed-form approximate solutions of Eq. 2.7 for the expression  $(\Delta\omega + \Delta M + \Delta\Omega \cos i)$ . These perturbations, which fluctuate with a frequency of  $m$  times per day, are obtained by choosing particular combinations of the indices  $p$  and  $q$  such that  $(\ell - 2p + q) = 0$ , i.e., the effect of the rapidly changing mean anomaly  $M$  is missing from the angle  $\psi_{\ell mpq}$ . For this case, the amplitude of the in-track angular displacement,  $(\Delta\omega + \Delta M + \Delta\Omega \cos i)$  is

$$\begin{aligned} (\Delta\omega + \Delta M + \Delta\Omega \cos i)_{\max} &= \\ &= \left| \frac{\mu a_E^{\ell} J_{\ell m}}{na^{\ell+3} [(\ell-2p)\dot{\omega} + m(\dot{\Omega} - \dot{\theta}_E)]} \left[ \left\{ \frac{\sqrt{1-e^2} - (1-e^2)}{e} \right\} F \frac{dG}{de} + 2(\ell+1)FG \right] \right| \end{aligned} \quad (2.8)$$

where the indices have been dropped from  $F_{\ell mp}$  and  $G_{\ell pq}$ . The rates  $\dot{\omega}$  and  $\dot{\Omega}$  are found by the usual first-order approximations

$$\dot{\omega} = - \frac{3n J_{20} a_E^2}{4(1-e^2)^2 a^2} [1 - 5 \cos^2 i],$$

and

$$\dot{\Omega} = - \frac{3n J_{20} a_E^2}{2(1-e^2)^2 a^2} \cos i.$$

Equation 2.8 is valid for any orbit, so this perturbation represents a quantity which, if measurable, can be used to determine the coefficients  $J_{\ell m}$  and  $\lambda_{\ell m}$ . Additional perturbations to the cross-track and radial positions of an orbiting satellite also give a measure of the coefficients' magnitude, although the latter two are not as large as the in-track perturbation. In general, the medium-period fluctuations of the orbital elements are not large, and it is necessary to examine the long-period or resonant perturbations in order to obtain the desired coefficients more accurately.

The closed-form linear solutions to the Lagrange planetary equations all have the rate term

$$\dot{\psi}_{\ell mpq} = (\ell - 2p)\dot{\omega} + (\ell - 2p + q)\dot{M} + m(\dot{\Omega} - \dot{\theta}_E)$$

in the denominator. For instance,

$$\Delta a = \frac{2\mu a_E^\ell}{na^{\ell+2} \dot{\psi}_{\ell mpq}} FG(\ell - 2p + q) \begin{cases} \cos & (\ell - m) \text{ even} \\ \sin & (\ell - m) \text{ odd} \end{cases} \dot{\psi}_{\ell mpq}$$

These solutions are valid except when this rate term is very small. If  $\dot{\psi}_{\ell mpq}$  is small, the sine and cosine terms in the planetary equations change very slowly, allowing large amplitude buildup. Then, the assumption of small perturbations leading to the closed-form solution is not valid. The condition  $\dot{\psi}_{\ell mpq} \cong 0$  occurs when  $(\ell - 2p + q)\dot{M} \cong m\dot{\theta}_E$  because  $\dot{\omega}$  is small compared with  $\dot{M}$ , and  $\dot{\Omega}$  is small compared with  $\dot{\theta}_E$ . This is, of course, the condition of resonance for which the orbital frequency is an integer multiple of the earth's rate.

No general closed-form solution of the planetary equations, valid for the resonant case, is known at this time. Vagners [Ref. 2-6] obtained a solution for orbits of small eccentricity and  $(\ell - 2p + q) = 1$  by combining the von Zeipel method with perturbation techniques of Hamiltonian mechanics. There are special cases where a pendulum solution for the osculating value of the nodal longitude of the mean satellite is quite accurate [Ref. 2-7]. In general, however, the exact solution

to the perturbations of the elements, due to those tesseral harmonic terms which are in resonance with the orbit, can be found only by numerical integration of Eqs. 2.7. The solutions depend on initial conditions and the degree of commensurability that the orbit has with the resonant condition.

Consider the case where the number of revolutions per day equals the order  $m$ , that is,  $(\ell - 2p + q) = 1$ . For this

$$\begin{aligned}\dot{\psi}_{\ell m_1}(q) &= (1 - q)\dot{\omega} + \dot{M} + m_1(\dot{\Omega} - \dot{\theta}_E) \\ &= C_1 - q\dot{\omega}\end{aligned}\tag{2.9}$$

where  $C_1$  is a constant dependent upon the mean elements of the particular orbit. Thus, for a given resonant orbit, there is a large set of beat frequencies  $\dot{\psi}_{\ell m}(q)$  corresponding to each  $q$  (assuming the inclination is not too close to the critical inclination. For the case of  $(\ell - 2p + q) = 2$

$$\begin{aligned}\dot{\psi}_{\ell m_2}(q) &= (2 - q)\dot{\omega} + 2\dot{M} + m_2(\dot{\Omega} - \dot{\theta}_E) \\ &= C_2 - q\dot{\omega} = 2C_1 - q\dot{\omega}\end{aligned}$$

Hence, another large set of beat frequencies exists and, in fact, many other sets exist for  $C_1 \neq 0$  or some multiple of  $\dot{\omega}$ . Because of this spectrum of beat frequencies, it is theoretically possible to detect the effect of many tesseral harmonic coefficients from a given resonant orbit.

The physical reason for the existence of the multiple beat frequency phenomenon is due to the combination of two effects. Orbital eccentricity causes a satellite to be more strongly attracted by the bulges due to tesseral coefficients at one part of the orbit (near perigee) than the other. In addition, the argument of perigee has the rate  $\dot{\omega}$  which slowly moves the point of strongest attraction around the orbit. The tesseral harmonics have both zonal ( $\ell$ , latitude) and sectoral ( $m$ , longitude) dependence. The earth's rotation makes a family of the tesseral harmonics (common  $m$ ) resonate with the orbit.

The members of this family each have a different latitude dependence, however, and so the point of maximum attraction dwells for different durations and with different frequency near each. Thus, the long-period perturbations associated with a slightly-off resonant condition does not exactly coincide with the repeatability of the node passing through a wave length of the sectoral dependence; rather, the long-period effects are different, in general, for each latitude dependence. These effects show up in expanded powers of  $e$  and multiples of  $\omega$ .

The rates  $\dot{\Omega}$ ,  $\dot{M}$ , and  $\dot{\omega}$  are not usually constant in the resonant situation, so, following Ref. 2-7, consider the acceleration of the elements. If the elements are designated  $x_i$  where  $i = 1, \dots, 6$ , then

$$\begin{aligned} \frac{d^2 x_i}{dt^2} &= \sum_{j=1}^6 \frac{\partial \dot{x}_i}{\partial x_j} \frac{dx_j}{dt} + \frac{\partial \dot{x}_i}{\partial t} \\ &= \frac{\partial \dot{x}_i}{\partial \psi} \dot{\psi} + \sum_{x_j=a, e, i} \frac{\partial \dot{x}_i}{\partial x_j} \dot{x}_j \end{aligned}$$

All quantities but  $\ddot{M}$  are of order  $J_{\ell m}$ . For acceleration of mean anomaly,

$$\begin{aligned} \ddot{M}_{\ell mpq} &= -\frac{3}{2} \frac{n}{a} \dot{a}_{\ell mpq} + O(J_{\ell m} \cdot \dot{\psi}_{\ell mpq}) + O(J_{\ell m}^2) \\ &\approx -\frac{3}{2} \frac{n}{a} \left( \frac{2}{na} \frac{\partial R}{\partial M} \right) \\ &= -\frac{3\mu}{a^3} \left( \frac{a_E}{a} \right)^\ell (\ell-2p+q) F_{\ell mp}(i) G_{\ell pq}(e) J_{\ell m} \begin{cases} -\sin & (\ell-m) \text{ even} \\ \cos & (\ell-m) \text{ odd} \end{cases} \psi_{\ell mpq} \end{aligned} \quad (2.10)$$

Although Eq. 2.10 is an approximation, it can be used to determine the relative magnitudes of the perturbations to the in-track position of a satellite in a near-resonant orbit. Two remarks can be made about this equation:

- (1) Because  $\ddot{M}_{\ell mpq} \sim (a_E/a)^\ell$ , the effects of higher degree terms are attenuated.

2.  $G_{\ell pq}(e)$  is proportional to  $e^{|q|}$ . Thus, higher values of  $|q|$  tend to decrease  $M_{\ell mpq}$ . This is especially true for small eccentricity. The highest possible eccentricity is therefore desirable.

For a resonant orbit, the number of pairs  $(J_{\ell m}, \lambda_{\ell m})$  of unknowns which can be determined is equal to the number of distinct beat frequencies which can be measured from the in-track perturbation. This is true, provided that the satellite remains in the orbit for at least one-half the period of the smallest required beat frequency. Thus, it is important that the orbit be "tuned" closely enough to exact commensurability so that the resonant effect is a large one, and yet preferably not so close that one beat period is too long to observe in the satellite lifetime.

To determine which resonant orbits should be used to obtain particular  $(J_{\ell m}, \lambda_{\ell m})$ , the magnitude of  $\ddot{M}_{\ell mpq}$  is computed (using hypothetical values for  $J_{\ell m}$ ) and examined for measurability. The eccentricity is assigned a value which seems very comfortable for a Drag-Free Satellite and the dependence upon inclination is investigated by letting inclination range from  $0^\circ$  to  $90^\circ$ .

## 2. The Selection of Resonant Orbits

The above analysis suggests that the following procedures should be used in selecting resonant orbits for determination of poorly known tesseral harmonic coefficients.

- (a) Determine which tesseral harmonic terms can be adequately measured by observing the medium-period perturbations of existing satellites.
- (b) For important terms not obtainable from existing satellites, investigate the possibility of determination from satellites placed in resonant orbits. The order ( $m$ ) of the terms determines the semi-major axis of the orbit required. The inclination of the orbit should be chosen so the resulting accelerations in mean anomaly ( $\ddot{M}$ ) for each term of order  $m$  is large enough to produce a detectable effect. The total effect can be determined by computing  $\ddot{M}$  vs  $i$  for the various combinations of  $(\ell, m, p, q)$  of interest. For example, suppose it is determined from a series of  $\ddot{M}$  vs  $i$  plots that an inclination exists such that in-track perturbations are measurable for  $q$  in the range  $-3$  to  $+3$ . Then seven pairs  $(J_{\ell m}, \lambda_{\ell m})$  can be determined from this orbit. If



there are ten pairs of coefficients required with this particular order  $m$ , then at least two orbits will be required for this particular semi-major axis.

- (c) This procedure can be repeated for each  $m$  in the range of orders of the  $(J_{\ell m, \lambda_{\ell m}})$  terms sought. If a range of acceptable inclinations exists for any two adjacent values of  $m$ , then satellites can be put into both these orbits, using the same booster, without a plane-change maneuver.
- (d) If a desired pair of coefficients  $(J_{\ell m, \lambda_{\ell m}})$  can be only marginally determined from a particular resonant orbit, a comparison must be made of the relative merits of establishing that orbit or trying to determine the coefficients from the medium-period perturbations on another orbit.

As indicated before, coefficients of degree 7-15 and order 3-10 are of primary interest. It is feasible to determine all these coefficients from four satellites which have orbital frequencies of 3, 4, 5, and 7 times per day.

### 3. Computation of The Amplitude of $\ddot{M}_{\ell mpq}$

$|\ddot{M}|_{\max}$  vs  $i$  computations have been made for different coefficients in both Refs. 2-7 and 2-9. In these studies, however, the value of  $q$  was limited to 0 and  $\pm 1$ . Here, because we are looking for a measure of the perturbations due to many beat frequencies, these computations need to be expanded.

The hypothetical value of  $J_{\ell m}$  used in the computation of the amplitude of  $\ddot{M}_{\ell mpq}$  is

$$J_{\ell m} = \left[ \frac{(\ell - m)! (4\ell + 2)}{(\ell + m)!} \right]^{1/2} \bar{J}_{\ell m} \quad (2.11)$$

where  $\bar{J}_{\ell m}$  is the normalized coefficient. Kaula [Ref. 2-5] gives the approximation

$$\bar{J}_{\ell m} = \frac{\sqrt{2} \times 10^{-5}}{\ell^2} \quad (2.12)$$

and Allan [Ref. 2-9] uses

$$\bar{J}_{\ell m} = \left[ \frac{12.2 \times 10^{-10}}{(2\ell + 1)^2 (2\ell + 3)} (0.93)^{2\ell+3} \right]^{1/2}$$

which are nearly equivalent. Although published estimates of actual  $(J_{\ell m}, \lambda_{\ell m})$  through (15, 15) exist, these only tend to confuse this analysis, so Eq. 2.12 is used instead.

To determine coefficients of degree 7-15 from a single orbit, at least nine beat frequencies must be detectable. To get an idea of how the perturbation is attenuated by increasing  $|q|$ , a series of computer runs of  $|\ddot{M}|$  vs  $i$  was made for  $m = 7$ ,  $\ell$  ranging from 7 through 15, and  $q$  ranging from -4 to +6. The altitude of perigee was chosen as 450 km which is easily within the capability of a long-life Drag-Free Satellite. The semi-major axis was established as that required for a satellite to orbit the earth seven times per day. The output of these runs consists of a series of plots of  $|\ddot{M}|$  (denoted by  $|MDDOT|$ ) vs  $i$  and is found in Appendix A. Here, the index  $s$  is the number of orbits per day. The quantity  $(\ell - 2p + q)$  in Eq. 2.10 is replaced by  $(m/s)$ .

Referring to Appendix A, it is seen that, in general, the magnitude of  $|\ddot{M}|$  does indeed decrease with increased  $\ell$  and  $|q|$ . It was desired to determine how large the in-track resonant orbit perturbations are due to the relevant coefficients of order  $m = s$ . It also was necessary to determine if measurable perturbations exist corresponding to each beat frequency. Consequently, the index  $q = 0$  was assigned to the  $(\ell, p) = (15, 7)$  combination and other  $q$ 's were assigned to other combinations of lower degree  $\ell$ .

Another series of computations of  $|\ddot{M}|$  was made for resonant orbits with  $s = m$  ranging from 3-6 and 8-12 with altitude of perigee at 450 km. The combinations of  $(\ell, p, q)$  investigated in particular were (15, 7, 0), (14, 7, 1), (13, 7, 2), (12, 5, -1), (11, 4, -2), (10, 6, 3), (9, 6, 4), (8, 2, -3), and (7, 1, -4) although some other combinations were included. The plots from these runs are presented in Appendix B.

By examining the plots of Appendices A and B, it can be seen that the general level of  $|\ddot{M}|$  over the range of inclinations increases with

increasing order  $m$ . This is primarily due to the decrease in semi-major axis as  $m$  is increased with perigee altitude held constant. It can also be seen that there are several places where  $|\ddot{M}|$  sharply decreases and then increases as inclination is changed. These places correspond to points where the inclination function  $F(i)$  changes signs. Such crossover inclinations should be avoided. If one removes from consideration, the near neighborhood of critical inclination, those inclinations corresponding to crossover points, and those with  $\ddot{M}$  less than what can be regarded as a minimum detectable level, then what remains are those ranges of  $i$  constituting possible inclinations for a geodesy satellite.

If the minimum beat period is 60 days, an acceleration with maximum value of  $10^{-5}$  deg/day<sup>2</sup> will result roughly in an intrack perturbation of amplitude between 100 and 1,000 meters. Thus, one can consider an  $|\ddot{M}|$  of  $10^{-5}$  deg/day<sup>2</sup> or larger as constituting a substantially measurable effect,  $|\ddot{M}|$  between  $10^{-6}$  and  $10^{-5}$  deg/day<sup>2</sup> as being marginally detectable, and  $|\ddot{M}|$  less than  $10^{-6}$  deg/day<sup>2</sup> as being undetectable. Applying this criterion to the data of Appendix B, one can see that the  $J_{15,3}$ ,  $J_{14,3}$ ,  $J_{13,3}$ ,  $J_{7,3}$ , and  $J_{15,4}$  terms for the combinations of  $(p,q)$  chosen are only marginally detectable. (In fact, the general magnitude of the acceleration of  $J_{15,3}$  is so small that unless close tuning can be achieved, it can be as accurately predicted from medium period effects on low satellites.) The rest of the coefficient combinations tend to have large ranges of quite detectable accelerations.

As an example of the mean anomaly accelerations  $|\ddot{M}|$ , for the distinct combinations of  $(\ell, m, p, q)$  investigated, Table 2-1 was prepared for various values of  $m$ . Two values of inclination are shown for the orbits with  $s = 3-6$ . For the inclinations shown, only  $J_{15,3}$  is not detectable,  $J_{14,3}$ ,  $J_{13,3}$ ,  $J_{12,3}$ ,  $J_{7,3}$ ,  $J_{15,4}$ ,  $J_{7,4}$ , and  $J_{7,6}$  are marginally detectable, and the rest are easily detectable by the criterion given above. This is dependent, of course, upon the particular combinations of  $(p,q)$  chosen.

Consider now the possibility of determining coefficients from orbits where  $m = 2s$ ,  $3s$ , and  $4s$ , i.e., conditions of greater than one-day

TABLE 2-1

MAXIMUM ACCELERATION OF MEAN ANOMALY,  $|\ddot{a}| \times 10^5$  DEG/DAY<sup>2</sup>,  
FOR GIVEN INCLINATION AND INDICES L, M, P, Q WITH S = M

L P Q	m = 3 i = 36°	m = 3 i = 58°	m = 4 i = 34°	m = 4 i = 50°	m = 5 i = 38°	m = 5 i = 52°	m = 6 i = 46°
15 7 0	.05	.03	.33	.13	2.00	1.22	2.00
14 7 1	.16	.20	1.27	1.44	3.46	2.71	15.05
13 7 2	.49	.40	2.60	1.93	9.66	10.00	10.99
12 5 -1	.50	.55	3.93	3.10	12.59	9.47	27.62
11 4 -2	1.26	.58	2.52	2.60	11.82	10.46	21.91
10 6 3	5.03	3.72	10.57	8.71	17.71	27.64	32.61
9 6 4	2.61	1.30	2.34	9.12	2.82	12.20	4.68
8 2 -3	1.90	1.28	4.89		7.51	4.56	3.44
7 1 -4	.38	.31	.23	.67	1.11	.58	.18
L P Q	m = 6 i = 50°	m = 7 i = 50°	m = 8 i = 50°	m = 9 i = 44°	m = 10 i = 44°	m = 11 i = 44°	m = 12 i = 44°
15 7 0	4.60	10.17	38.14	60.30	138.22	169.28	(*63.25)
14 7 1	14.80	25.74	14.78	117.56	119.90	84.71	(*103.87)
13 7 2	6.21	30.12	78.08	59.23	35.10	14.66	(*59.94)
12 5 -1	18.54	45.67	12.16	156.46	148.00	85.22	(* 7.73)
11 4 -2	12.34	34.24	9.40	87.95	66.31	24.86	* for
10 6 3	4.17	35.38	19.54	2.39	(*12.92)		L, P, Q =
9 6 4	7.59	3.54	1.08	(*3.16)	* for		15 6 -2
8 2 -3	8.43	14.74	23.18	* for	L, P, Q =		14 6 -1
7 1 -4	.60	1.89		L, P, Q =	10 3 -3		13 6 0
				9 2 -4			12 6 1

commensurability. Since

$$|\ddot{M}_{\ell mpq}| = -\frac{3\mu}{a^3} \left(\frac{a_E}{a}\right)^\ell \left(\frac{m}{s}\right) F_{\ell mp}^{(i)} G_{\ell pq}^{(e)} J_{\ell m},$$

then for fixed  $(\ell, m, p)$ , the attenuation of  $|\ddot{M}|$  for the higher orbit will be

$$\frac{|\ddot{M}_2|}{|\ddot{M}_1|} = \left(\frac{a_1}{a_2}\right)^{\ell+3} \left(\frac{s_1}{s_2}\right) \left(\frac{G_2(e)}{G_1(e)}\right). \quad (2.13)$$

Here, the indices 1 and 2 represent those quantities corresponding to the lower and higher orbit respectively. The value of  $q_2$  corresponding to  $G_2(e)$  is equal to  $(q_1 + S_1/S_2)$  where  $q_1$  corresponds to  $(\ell + 2p + q_1) = m/s_1$ . Tables 2-2, 2-3, and 2-4 show ratios of  $|\ddot{M}_2|/|\ddot{M}_1|$  for  $m = 6, 9$ , and  $12$  in the  $s = 3$  orbit,  $m = 8$  and  $12$  in the  $s = 4$  orbit, and  $m = 10$  in the  $s = 5$  orbit. Table 2-5 shows the resulting values of  $|\ddot{M}|$  for inclinations of  $58^\circ$  for  $s = 3$ ,  $50^\circ$  for  $s = 4$ , and  $52^\circ$  for  $s = 5$  orbits. It can be seen that except for  $J_{15,6}$ , all overtone coefficients are at least marginally detectable in the  $s = 3$  orbit. For  $s = 4$ , only the  $J_{12,8}$  term is marginally detectable with the rest being quite detectable by the above criteria. For  $s = 5$ , all  $m = 10$  terms are quite detectable. It must be remarked that no special effort was made to maximize the effect of the overtone terms in selecting the inclinations used for Table 2-5. With further effort, there can undoubtedly be improvement. The point is that a great deal of information can be obtained from the  $s = 3, 4$ , and  $5$  resonant orbits in addition to what is obtainable from the fundamental beat frequencies. In fact, all but three of the 72 pairs of the desired coefficients can be found from those orbits. It also must be emphasized that the choice of cutoff points between what are referred to as undetectable, marginal, and quite detectable perturbations is strongly dependent upon uncertainties due to tracking and perturbing surface forces on the satellite. For a Drag-Free Satellite, the effect of surface forces can be attenuated to the point where tracking uncertainty is the major limiting factor.

M	L	P	Q1	Q2	G(0.4663) S = 6	G(0.6638) S = 3	(A1/A2)**(L+3)	MDD(2)/MDD(1)
6	15	7	0	1	0.4114724E 03	0.2499720E 05	0.2441413E-03	0.2966346E-01
	14	7	1	2	0.3729592E 03	0.2262122E 05	0.3875503E-03	0.4701244E-01
	13	7	2	3	0.2213335E 03	0.1375805E 05	0.6151977E-03	0.7648110E-01
	12	5	-1	0	0.1053418E 03	0.2233471E 04	0.9765655E-03	0.4141054E-01
	11	4	-2	-1	0.3465096E 02	0.1057808E 04	0.1550201E-02	0.9464753E-01
	10	6	3	4	0.2576006E 02	0.1068145E 04	0.2460790E-02	0.2040740E 00
	9	2	-4	-3	0.4931422E 00	0.2611052E 02	0.3906257E-02	0.4136510E 00
	8	2	-3	-2	0.1044890E 01	0.3098537E 02	0.6200798E-02	0.3677590E 00
	7	5	4	5	0.8508028E 00	0.2067940E 02	0.9843152E-02	0.4784902E 00

M	L	P	Q1	Q2	G(0.3006) S = 9	G(0.6638) S = 3	(A1/A2)**(L+3)	MDD(2)/MDD(1)
9	15	7	0	2	0.2832899E 02	0.4409143E 05	0.1881684E-05	0.8785989E-02
	14	7	1	3	0.2230350E 02	0.3333880E 05	0.3914060E-05	0.1755195E-01
	13	7	2	4	0.1137298E 02	0.1746933E 05	0.8141570E-05	0.3751728E-01
	12	5	-1	1	0.8413002E 01	0.4075726E 04	0.1693514E-04	0.2461297E-01
	11	4	-2	0	0.2447608E 01	0.8923994E 03	0.3522651E-04	0.3853081E-01
	10	3	-3	-1	0.3647965E 00	0.2542462E 03	0.7327407E-04	0.1532059E 00
	9	2	-4	-2	0.2329785E-01	0.2936353E 02	0.1524162E-03	0.5762946E 00

M	L	P	Q1	Q2	G(0.1527) S = 12	G(0.6638) S = 3	(A1/A2)**(L+3)	MDD(2)/MDD(1)
12	15	6	-2	1	0.6898279E 00	0.2064687E 05	0.5960498E-07	0.7136013E-02
	14	6	-1	2	0.1621167E 01	0.2398181E 05	0.1501952E-06	0.8887306E-02
	13	6	0	3	0.2472869E 01	0.1951319E 05	0.3784681E-06	0.1194583E-01
	12	6	1	4	0.1649502E 01	0.1111163E 05	0.9536789E-06	0.2569726E-01

TABLE 2-2. ATTENUATION OF THE m = 6, 9, and 12 COEFFICIENT ACCELERATIONS IN THE s = 3 ORBIT.

M	L	P	Q1	Q2	G(0.3534) S = 8	G(0.5927) S = 4	(A1/A2)**(L+3)	MDD(2)/MDD(1)
8	15	7	0	1	0.6600482E 02	0.6106805E 04	0.2441406E-03	0.4517607E-01
	14	7	1	2	0.5381236E 02	0.5122363E 04	0.3875492E-03	0.7378107E-01
	13	7	2	3	0.2880846E 02	0.2902432E 04	0.6151958E-03	0.1239611E 00
	12	5	-1	0	0.1829340E 02	0.7023538E 03	0.9765627E-03	0.7498795E-01
	11	4	-2	-1	0.5565388E 01	0.3113899E 03	0.1550197E-02	0.1734706E 00
	10	6	3	4	0.3766256E 01	0.2406877E 03	0.2460784E-02	0.3145193E 00
	9	2	-4	-3	0.6278861E-01	0.6857068E 01	0.3906250E-02	0.8531936E 00
	8	2	-3	-2	0.1925093E 00	0.9928094E 01	0.6200783E-02	0.6395738E 00

M	L	P	Q1	Q2	G(0.1527) S = 12	G(0.5927) S = 4	(A1/A2)**(L+3)	MDD(2)/MDD(1)
12	15	6	-2	0	0.6898279E 00	0.2572443E 04	0.1881679E-05	0.2105095E-01
	14	6	-1	1	0.1621167E 01	0.3467806E 04	0.3914051E-05	0.2511740E-01
	13	6	0	2	0.2472869E 01	0.3156320E 04	0.8141554E-05	0.3117514E-01
	12	6	1	3	0.1649502E 01	0.1962298E 04	0.1693511E-04	0.6043959E-01

TABLE 2-3. ATTENUATION OF THE  $m = 8$  and 12 COEFFICIENT ACCELERATIONS IN THE  $s = 4$  ORBIT.

M	L	P	Q1	Q2	G(0.2497) S = 10	G(0.5273) S = 5	(A1/A2)**(L+3)	MDD(2)/MDD(1)
10	15	7	0	1	0.1273480E 02	0.1790253E 04	0.2441386E-03	0.6864178E-01
	14	7	1	2	0.9779472E 01	0.1398694E 04	0.3875459E-03	0.1108562E 00
	13	7	2	3	0.4696593E 01	0.7420310E 03	0.6151912E-03	0.1943923E 00
	12	5	-1	0	0.4110580E 01	0.2584683E 03	0.9765557E-03	0.1228092E 00
	11	4	-2	-1	0.1120265E 01	0.1085586E 03	0.1550186E-02	0.3004398E 00
	10	3	-3	-2	0.1505170E 00	0.2334720E 02	0.2460769E-02	0.7633958E 00

TABLE 2-4. ATTENUATION OF THE  $m = 10$  COEFFICIENT ACCELERATIONS IN THE  $s = 5$  ORBIT.



TABLE 2-5.

COMPARISON OF MAXIMUM ACCELERATIONS OF THE MEAN ANOMALY,  
 $|M| \times 10^5 \text{ DEG/DAY}^2$ , DUE TO HIGHER OVERTONE TERMS

( $s = m$ ), FOR  $s = 3, 4$ , and  $5 \text{ REVS/DAY}$ .

$s=3$			$s=4$			$s=5$		
$m=3$			$m=4$			$m=5$		
$i=58^\circ$			$i=50^\circ$			$i=52^\circ$		
$Q2=Q1+1$			$Q2=Q1+1$			$Q2=Q1+1$		
$m=9$			$m=12$			$m=10$		
$Q2=Q1+2$			$Q2=Q1+2$			$Q2=Q1+1$		
L	P	Q1	L	P	Q1	L	P	Q1
15	7	0	15	7	0	15	7	0
		.03			.13			1.22
14	7	1	15	6	-2	14	7	1
		.20			-			2.71
13	7	2	14	7	1	13	7	2
		.40			1.44			10.00
12	5	-1	14	6	-1	12	5	-1
		.55			-			9.47
11	4	-2	13	7	2	11	4	-2
		.58			1.93			10.46
10	6	3	13	6	0	10	6	3
		3.72			-			27.64
10	3	-3	12	5	-1	10	3	-3
		-			3.10			16.39
9	2	-4	12	6	1	9	2	-4
		.07			-			1.60
8	2	-3	11	4	-2	8	2	-3
		1.28			2.60			4.56
7	5	4	10	6	3	7	5	4
		8.06			8.71			5.16
			9	2	-4			
					.20			
			8	2	-3			
					3.94			
			7	5	4			
					6.79			
					-			

#### 4. Additional Advantage of the Drag-Free Satellite for Orbits of Small Major Axes.

To determine the coefficients of the harmonic expansion of the earth's gravitational potential from satellite perturbations, it is important that these perturbations not be obscured by other forces such as those due to radiation pressure and atmospheric pressure. Because these forces are always present to some degree, their effective removal by use of a Drag-Free Geodetic Satellite will always produce more confidence in the validity of the tracking data. The situation in which greatest improvement would be obtained is with orbits of low perigee altitude.

In the literature [Refs. 2-1 through 2-4], it is reported that there are a number of resonant satellites in the range  $s = 11-15$  and that the coefficients with these orders can be reasonably well determined. If one considers a circular orbit with a frequency of 14 rev/day, because of the  $e^{|q|}$  factor in the  $G(e)$  function, only the beat frequency corresponding to  $q = 0$  is detectable. One cannot assume that for  $\ell > 14$ , the tesseral coefficients are so small that their effect is negligible if Eq. 2.11 and 2.12 are valid. In other words, for a circular orbit, the  $J_{15,14}$ ,  $J_{17,14}$ , and  $J_{19,14}$  coefficients will all significantly affect the  $q = 0$  perturbation. Thus, one must make the orbit as eccentric as possible to obtain these coefficients by increasing the number of detectable beat frequencies. A Drag-Free Satellite can contribute significantly here by allowing the low perigee altitudes necessary for increasing eccentricity to an acceptable value.

To illustrate the effect of an increase in eccentricity, Table 2-6 was prepared showing the change in the magnitude of the  $G_{\ell mp q}(e)$  function for the  $s = 14$  orbit. The values of degree  $\ell$  ranged from 14-20 and  $q$  from -3 to +3 which would produce 7 beat frequencies. The eccentricities used correspond to perigee altitudes of 350, 500, 650, and 800 km. Appendix C contains the  $|\ddot{M}|$  vs  $i$  plots corresponding to this range of indices for an altitude of 350 km. To determine the  $|\ddot{M}|$  for any other perigee altitude, multiply  $|\ddot{M}|_{350}$  by  $G(e)/G(0.0748)$ . For example, when  $i = 50$ , the following results are obtained in a

M	L	P	Q1	Q2	G(0.4663) S = 6	G(0.6638) S = 3	(A1/A2)**(L+3)	MDD(2)/MDD(1)
6	15	7	0	1	0.4114724E 03	0.2499720E 05	0.2441413E-03	0.2966346E-01
	14	7	1	2	0.3729592E 03	0.2262122E 05	0.3875503E-03	0.4701244E-01
	13	7	2	3	0.2213335E 03	0.1375805E 05	0.6151977E-03	0.7648110E-01
	12	5	-1	0	0.1053418E 03	0.2233471E 04	0.9765655E-03	0.4141054E-01
	11	4	-2	-1	0.3465096E 02	0.1057808E 04	0.1550201E-02	0.9464753E-01
	10	6	3	4	0.2576006E 02	0.1068145E 04	0.2460790E-02	0.2040740E 00
	9	2	-4	-3	0.4931422E 00	0.2611052E 02	0.3906257E-02	0.4136510E 00
	8	2	-3	-2	0.1044890E 01	0.3098537E 02	0.6200798E-02	0.3677590E 00
	7	5	4	5	0.8508028E 00	0.2067940E 02	0.9843152E-02	0.4784902E 00

M	L	P	Q1	Q2	G(0.30061) S = 9	G(0.6638) S = 3	(A1/A2)**(L+3)	MDD(2)/MDD(1)
3	15	7	0	2	0.2832899E 02	0.4409143E 05	0.1881684E-05	0.8785989E-02
	14	7	1	3	0.2230350E 02	0.3333880E 05	0.3914060E-05	0.1755195E-01
	13	7	2	4	0.1137298E 02	0.1746933E 05	0.8141570E-05	0.3751728E-01
	12	5	-1	1	0.8413002E 01	0.4075726E 04	0.1693514E-04	0.2461297E-01
	11	4	-2	0	0.2447608E 01	0.8923994E 03	0.3522651E-04	0.3853081E-01
	10	3	-3	-1	0.3647965E 00	0.2542462E 03	0.7327407E-04	0.1532059E 00
	9	2	-4	-2	0.2329785E-01	0.2936353E 02	0.1524162E-03	0.5762946E 00

M	L	P	Q1	Q2	G(0.1527) S = 12	G(0.6638) S = 3	(A1/A2)**(L+3)	MDD(2)/MDD(1)
12	15	6	-2	1	0.6898279E 00	0.2064687E 05	0.5960498E-07	0.7136013E-02
	14	6	-1	2	0.1621167E 01	0.2398181E 05	0.1501952E-06	0.8887306E-02
	13	6	0	3	0.2472869E 01	0.1951319E 05	0.3784681E-06	0.1194583E-01
	12	6	1	4	0.1649502E 01	0.1111163E 05	0.9536789E-06	0.2569726E-01

TABLE 2-6. COMPILATION OF THE G(e) FUNCTION FOR THE s = 14 ORBIT CORRESPONDING TO PERIGEE ALTITUDES OF 350, 500, 650, and 800 km.

comparison of the 350 and 800 km perigee altitude cases.

<p style="text-align: center;"><u>TABLE 2-6</u> COMPARISON OF MEAN ANOMALY ACCELERATIONS FOR FOR PERIGEES OF 350 and 800 KM</p>				
$\ell$	p	q	deg/day <sup>2</sup>	
			$ \ddot{M}_{350}  \times 10^5$	$ \ddot{M}_{800}  \times 10^5$
14	5	-3	2.752	0.013
15	6	-2	32.754	0.850
16	9	3	1.240	0.006
17	9	2	24.748	0.622
18	8	-1	196.01	26.38
19	9	0	332.51	209.20
20	10	1	171.72	21.82

It is evident that the eccentricity effect is significant for  $|q| > 2$ . The perturbations due to coefficients of degree  $\ell > 15$  seem to be substantial.

## CHAPTER II: REFERENCES

- 2-1. Wagner, C.A., "A Survey of Existing Satellites in Resonant Orbits for Geodetic Purposes," NASA-GSFC-X-643-68-256, Greenbelt, Md., Jul, 1968.
- 2-2. Wagner, C.A., "Resonant Perturbations of Earth Satellites in Two Day Commensurable Orbits," NASA-GSFC-X-643-68-373, Greenbelt, Md., Sept., 1968.
- 2-3. Douglas, B.C., and Wagner, C.A., "A Perturbation Analysis of Existing Resonant Satellites," NASA-GSFC-X-643-68-338, Greenbelt, Md., Aug., 1968.
- 2-4. Strange, W.E., Calabria, F.M., Rainey, H.T., and Gunshal, L.P. "Requirements for Resonant Satellites," AAS National Specialist Symposium on Orbital Resonance, Jan 1968.
- 2-5. Kaula, W.M., Theory of Satellite Geodesy, Blaisdell Publishing Company, Waltham, Mass., 1966.
- 2-6. Vagners, J., "Some Resonant and Nonresonant Perturbations of Earth and Lunar Orbiters," SUDAAR No. 317, Dept. of Aeronautics and Astronautics, Stanford University, Stanford, Calif., Aug 1967.
- 2-7. Douglas, B.C., Palmiter, M.T., and Gedeon, G.S., "Resonant Satellite Geodesy Study," TRW Report No. 09128.6001-R000, TRW Systems Group, Redondo Beach, Calif., 1968.
- 2-8. Winn, C.B., and Garvey, D.C., "Theoretical Investigation of a Maneuverable Geodetic Satellite," Paper No. 69-1, Dept. of Mechanical Engineering, Colorado State University, Fort Collins, Colo., Sept 1968.
- 2-9. Allan, R.R., "Resonance Effects Due to the Longitude Dependence of the Gravitational Field of a Rotating Primary," Planet. Space Sci., vol 15, 1966.

### III. SATELLITE DESIGN

Since 1963, Stanford University has been developing drag-free technology for application to several possible missions (e.g., an aeronomy mission, and an unsupported gyroscope mission). Throughout this work, we have become convinced that it is possible to build the basic mechanism (proof mass, pickoff, processing electronics, and thrusting system) with standard state-of-the-art flight hardware and techniques. The interface of the drag-free device with the rest of the satellite can be simple or complicated depending on the requirements for the other aspects of the mission (other experiments, physical configuration constraints, kind of telemetry desired from the drag-free mechanism, etc.). Reference 3-1, for example, proposes a very simple complete Drag-Free Satellite for use in a low altitude aeronomy mission.

The discussion in this part of the report has therefore been limited to the feasibility of applying the drag-free principle to geodesy missions. In particular, it is concerned with any special requirements arising through application to geodesy.

The drag-free device very effectively cancels the disturbing accelerations due to surface forces such as atmospheric drag and solar radiation pressure. The largest remaining non-geodetic disturbing acceleration is that due to the mass attraction of the satellite itself on the proof mass. This acceleration can be as low as  $10^{-11}$  g or as high as perhaps  $10^{-8}$  g depending on the care with which one manages the mass distribution within the satellite (particularly the masses within say, 10 cm of the proof mass).

The principal component of this mass attraction is due to the fact that the satellite mass center does not necessarily coincide with a point of zero mass attraction. Since the proof mass is nominally at the satellite mass center and the points of zero mass attraction are fixed points in the satellite, spinning the satellite about an axis normal to the orbit plane will tend to average the orbit plane components of this force. This will reduce the intrack disturbing acceleration by about 2 orders of magnitude below that attainable without spin.

Sections A and B which follow, present solutions to problems which arise for a spinning Drag-Free Geodetic Satellite. First, active attitude control to maintain the spin axis normal to the orbit plane; then, phenomena in the translational control uniquely associated with spin and the system mechanization are discussed.

It is not necessary, of course, that a Drag-Free Geodesy Satellite be spin stabilized. Quite useful geodetic information could be obtained with a gravity stabilized Drag-Free Satellite, such as GEOS-C with a modular, add-on drag-free package. With such a satellite, there is the question of whether or not the translational control system could couple into attitude motion (through misalignment errors in the pickoff and thrusters) in such a way as to cause attitude instability. This topic is discussed in the final section of this Chapter.

#### A. MAGNETIC ATTITUDE CONTROL OF A SPINNING DRAG-FREE GEODESY SATELLITE

As discussed in Chapters I and II, in-track perturbation of a Drag-Free Satellite is the effect which contains the most significant geodetic information. It is desirable to minimize as much as possible, the effect of all other in-track disturbances from these measurements. This can be done most easily with a spinning Drag-Free Satellite with spin axis normal to the orbit plane. The spinning motion allows very effective averaging in the orbit plane of the major components of mass attraction of the satellite mass on the proof mass.

Because many disturbance torques are present which can drive the spin axis from the orbit plane normal and change the satellite's spin speed, an attitude control system must be provided to correct for these. An excellent method of providing this attitude control for the orbits of interest is to make use of the earth's magnetic field. By creating a magnetic dipole moment in the satellite, a torque is produced on the satellite as this moment tries to align with the earth's magnetic field. By controlling the direction of the dipole moment, one has the ability to control both the pointing direction and spin speed of the satellite.

The basic idea of magnetic attitude control is not new and has been studied extensively and used in several satellite systems. In the following sections, a new method of three-axis magnetic attitude control

is developed which can rely on a single magnetic coil. First, the linearized equations of attitude motion are developed and the effect of a nutation damper is added. Then, a brief review of disturbance torques acting on the satellite is presented. Following this is a discussion of the use of a state estimator driven by horizon sensors to determine the attitude errors. With this information, the magnetic attitude control system is developed for a satellite with mass symmetry about the spin axis. This system has three modes so that both pointing control and spin control can be achieved. A procedure for determining control gains which will provide an average optimum performance is presented. Stability is demonstrated by using Lyapunov and averaging techniques. Then, a brief summary is made of the analog and digital simulations of this attitude control system.

## 1. The Attitude Dynamics of Rigid Spinning Spacecraft

In this part, equations representing the dynamics of the spinning spacecraft with respect to relevant coordinate systems are developed as a means of notation and coordinate system definition.

### a. Spacecraft Kinetics.

If it is assumed that the control axes (the axes about which control torques can be applied) are the principal inertia axes for the spacecraft mass center, then the kinetic equations describing the vehicle's attitude motion are the well-known Euler equations

$$\begin{aligned}\dot{\omega}_x &= \frac{1}{I_{xx}} [T_y + (I_{yy} - I_{zz}) \omega_y \omega_z] \\ \dot{\omega}_y &= \frac{1}{I_{yy}} [T_x + (I_{zz} - I_{xx}) \omega_x \omega_z] \\ \dot{\omega}_z &= \frac{1}{I_{zz}} [T_z + (I_{xx} - I_{yy}) \omega_x \omega_y] .\end{aligned}\tag{3.1}$$

Here,  $(I_{xx}, I_{yy}, I_{zz})$  are the principal moments of inertia. The vector  $\bar{\omega}^{B-I}$  is the instantaneous angular velocity of the body with respect to an inertial reference frame. The quantities  $(\omega_x, \omega_y, \omega_z)$  are the measure numbers in the body-fixed frame aligned with the principal



axes. The quantities  $(T_x, T_y, T_z)$  are the measure numbers in the same body-fixed frame of the external torques acting on the satellite.

#### b. Coordinate Systems and Spacecraft Kinematics.

The coordinate systems of interest are shown in Figs. 3-1 to 3-3. The primary inertial reference frame is defined by the  $\hat{x}_I$  axis pointing to the Vernal equinox, the  $\hat{z}_I$  axis pointing along the earth's spin axis, and  $\hat{y}_I$  completing the right-hand orthogonal set.

Figure 3-2 shows the "local" reference frame with  $\hat{x}_L$  along the direction of the vector  $\bar{R}$  from the geocenter to the satellite. The axis  $\hat{z}_L$  is normal to the orbit plane and along the orbit's angular momentum vector, and  $\hat{y}_L$  completes the right-hand orthogonal set. The angles  $i, \Omega, g,$  and  $f$  have the usual definitions of inclination, right ascension of ascending node, argument of perigee, and true anomaly. The local frame will be used as the reference set (R) later, in the study of controlling alignment of the spin axis with the normal to the orbit plane.

#### c. Linearized Equations of Motion

When it is desired to keep the spin axis aligned normal to the orbit plane, the natural axes about which to apply control torques are the local axes (L) of Figure 3-2. These correspond to the reference axes (R) of Figure 3-1. However, the closest possible positions of the principal axes of the satellites are the intermediate axes labeled (P) in Figure 3-1. These axes correspond to the orientation of the body-fixed axes at the time when the angle  $\psi$  equals zero.

Assume that the angles  $\phi$  and  $\theta$  (corresponding to yaw and roll angles about  $\hat{x}_R$  and  $\hat{y}_P$  respectively in Fig. 3-1) are small enough so that the approximations

$$\sin \phi \cong \phi ,$$

$$\sin \theta \cong \theta ,$$

$$\cos \phi \cong \cos \theta \cong 1 ,$$

can be made.

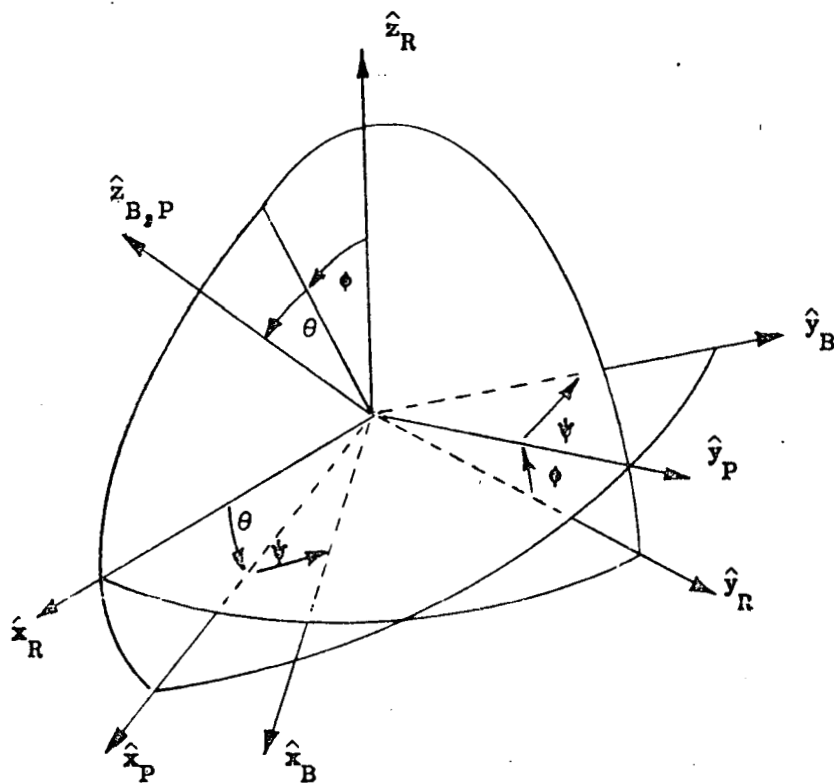


FIG. 3-1. NONCLASSICAL EULER ANGLE TRANSFORMATION FROM A REFERENCE FRAME (R) TO A BODY-FIXED FRAME (B) BY SUCCESSIVE ROTATIONS ABOUT THE  $x$ ,  $y$ , and  $z$  AXES THROUGH ANGLES  $\phi$ ,  $\theta$ , and  $\psi$ .

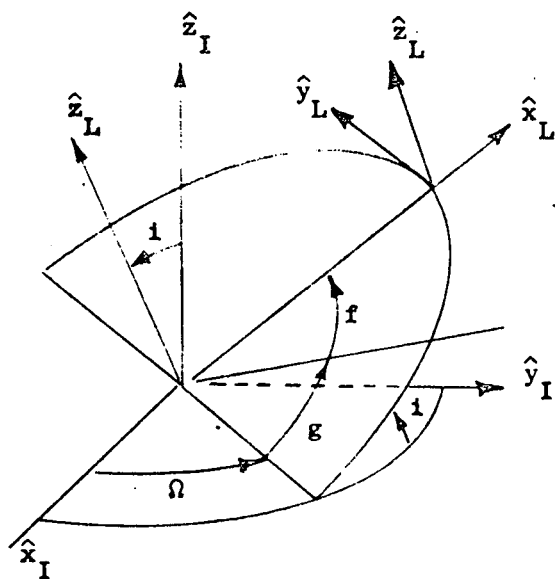


FIG. 3-2. ORIENTATION OF THE LOCAL (L) REFERENCE FRAME

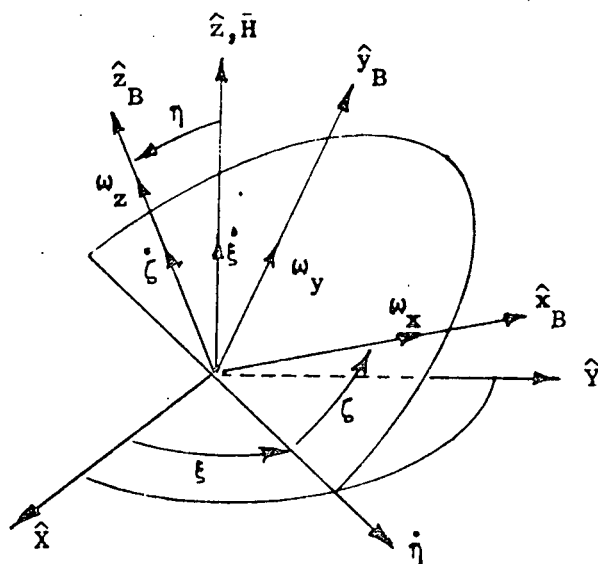


FIG. 3-3. GEOMETRY OF THE ANGLES AND ANGULAR RATES OF THE WOBBLE PROCESS.

Assume also that  $\omega_z = \dot{\psi} = \text{constant} \gg \dot{g} + \dot{f}$ . Then, for a satellite with mass symmetry about the spin axis (i.e.,  $I_{xx} = I_{yy}$ ), Eq. 3.1 can be written in the constant matrix form

$$\begin{bmatrix} \dot{\alpha}_x \\ \dot{\alpha}_y \\ \dot{\phi} \\ \dot{\theta} \end{bmatrix} = \begin{bmatrix} 0 & -D & 0 & 0 \\ D & 0 & 0 & 0 \\ 1 & 0 & 0 & n \\ 0 & 1 & -n & 0 \end{bmatrix} \begin{bmatrix} \alpha_x \\ \alpha_y \\ \phi \\ \theta \end{bmatrix} + \begin{bmatrix} 1 & 0 \\ 0 & 1 \\ 0 & 0 \\ 0 & 0 \end{bmatrix} \begin{bmatrix} T_{x_L} \\ T_{y_L} \end{bmatrix}. \quad (3.2)$$

In this equation,  $\alpha_x$  and  $\alpha_y$  are the  $\hat{x}_P$  and  $\hat{y}_P$  measure numbers of the angular velocity of the body with respect to the inertial frame, and  $T_{x_L}$  and  $T_{y_L}$  are the  $\hat{x}_L$  and  $\hat{y}_L$  of the torques applied to the body (normalized by  $I_{xx}$ ).  $D$  is the ratio of the moments of inertia times the spin rate,

$$D \triangleq I_{zz} \omega_z / I_{xx}.$$

The constant  $n$  corresponding to mean orbital rate, has also been substituted for  $\dot{g} + \dot{f}$ , which is time varying for an elliptic orbit.

#### d. Addition of a Wobble Damper.

Figure 3-3 depicts the geometry of the angles and angular rates of the wobble process. The body axes  $\hat{x}_B, \hat{y}_B, \hat{z}_B$  are rotated from an inertially fixed set  $\hat{X}, \hat{Y}, \hat{Z}$  through the classical Euler angles  $\xi, \eta$ , and  $\zeta$ . The  $\hat{Z}$  axis is aligned with the total angular momentum vector  $\vec{H}$ . The rates  $\dot{\xi}$  and  $\dot{\eta}$  are the inertial precession and nutation. The nutation angle  $\eta$  is described by

$$\cos \eta = I_{zz} \omega_z / H. \quad (3.3)$$

The term "wobble damping" is defined as the driving of  $\eta$  to zero. If the nutation angle  $\eta$  is small, and  $\omega_z$  is held approximately constant, then the so-called "energy sink approximation" technique yields the relationship  $\dot{\eta} = -d\eta$  where  $d$  is the time-constant of

the wobble damping process.

After a bit of algebra, it can be shown that the effect of the damper is the addition of two diagonal terms in the  $4 \times 4$  system matrix of Eq. 3.2. Equation 3.2 thus becomes,

$$\begin{bmatrix} \dot{\alpha}_x \\ \dot{\alpha}_y \\ \dot{\phi} \\ \dot{\theta} \end{bmatrix} = \begin{bmatrix} -d & -D & 0 & 0 \\ D & -d & 0 & 0 \\ 1 & 0 & 0 & n \\ 0 & 1 & -n & 0 \end{bmatrix} \begin{bmatrix} \alpha_x \\ \alpha_y \\ \phi \\ \theta \end{bmatrix} + \begin{bmatrix} 1 & 0 \\ 0 & 1 \\ 0 & 0 \\ 0 & 0 \end{bmatrix} \begin{bmatrix} T_{xL} \\ T_{yL} \end{bmatrix} \quad (3.4)$$

Equation 3.4 will be used throughout (this) section, A, to determine the desired control system for a spinning symmetric geodesy satellite. The exact equations of a mechanical wobble damper are generally more complex than has been assumed by the energy-sink procedure used here and require evaluation of a higher-order system [Refs. 3-2, 3-3, and 3-4]. However, most references on the subject indicate that the energy-sink approximation gives results reasonably close to actual behavior, so the method will be retained rather than increasing the order of the system equations which would be necessary for a closer investigation of the effect of a particular type of damper.

## 2. Disturbance Torques

Disturbance torques acting on the satellite can be broken into three categories. Two, referred to as "inertially-fixed" and "body-fixed" torques, are those which tend to move the spin axis from the reference and are about the vehicle's lateral axes. The third type of torque is about the spin axis and tends to change the rate of spin speed.

Short discussions of the following important inertially-fixed torques will be presented here

- a. atmospheric
- b. radiation pressure
- c. misalignment of translation control jets
- d. magnetic effects
- e. reference-frame kinematics.

Full developments can be found in the indicated references.

a. Atmospheric torques

Consider the atmospheric torque acting on a cylindrical satellite with uniform wall material. If  $\delta z$  is the distance from the mass center along the axis of symmetry to the geometric center, then, from the analysis of Ref. 3-5, it can be shown that the inertially fixed torque magnitude acting on the satellite is

$$T_{\text{aero}} = (T_{\text{end}} + P_{\text{cyl}})\delta z \quad (3.5)$$

where, for diffuse reflection

$$\begin{aligned} P_{\text{cyl}} &= 2\ell r \rho V_i^2 \sin \eta_L [\sin \eta_L + \pi/6 (V_r/V_i)] \\ T_{\text{end}} &= \pi r^2 \rho V_i^2 \sin \eta_i \cos \eta_i \end{aligned}$$

and

- $\ell \triangleq$  cylinder length
- $r \triangleq$  cylinder radius
- $\rho \triangleq$  atmospheric density
- $V_i \triangleq$  relative speed of incoming molecules
- $V_r \triangleq$  relative speed of outgoing molecules
- $\eta_i \triangleq$  angle between incoming velocity and the wall surface.

The ratio  $V_r/V_i \cong \sqrt{1 - \alpha}$ , where  $\alpha$  is the accommodation coefficient for the particular surface. References 3-5 and 3-6 present accommodation coefficients ranging from 0.3 to 0.95 depending on the wall material and gaseous medium involved. The relative velocity  $\bar{V}_i$  is found by

$$\bar{V}_i = -\bar{V} + K\bar{\omega}_e \times \bar{R} \quad (3.6)$$

where  $\bar{V}$  = inertial velocity of the spacecraft

$\bar{\omega}_e$  = earth spin velocity

$\bar{R}$  = radius vector from the geocenter

$K$  = wind constant.

The angular velocity of the upper atmosphere has been determined by examining changes in inclinations of various satellites by King-Hele [Ref. 3-7]. He found  $K = 1.46$  for nine satellites at heights of 200 to 300 km. The atmospheric model used here is developed in Refs. 3-8 and 3-9.

b. Radiation pressure torques.

Direct solar radiation pressure in the vicinity of the earth is

$$Ra_1 \cong 4.66 \times 10^{-5} \text{ dyne/cm}^2. \quad (3.7)$$

Earth emitted radiation pressure is

$$Ra_3 \cong 7.53 \times 10^{-6} \text{ dyne/cm}^2. \quad (3.8)$$

By numerical integration of the solar energy reflected from the earth to a satellite, the following empirical relationships have been found for the pressure due to this reflected energy.

$$Ra_3 \cong 1.80 \times 10^{-5} \exp(-3 \times 10^{-4} h) \cos \beta \text{ dyne/cm}^2, \quad (3.9a)$$

in which  $h$  is the satellite altitude in km, and  $\beta$  the angle between the earth-satellite radius vector and the earth-sun line.  $Ra_3$  is assumed zero for  $\beta > \pi/2$ . The reflected radiation vector is at an angle of  $(\beta + \nu)$  rad from the earth-sun line, where

$$\nu \cong f_1 (\beta/f_1)^{2.4} \text{ rad} \quad (3.9b)$$

and

$$f_1 \cong 4.89 - h(5.82 \times 10^{-4}) \text{ rad}. \quad (3.9c)$$

According to Evans [Ref. 3-10], the pressure and shear stress components due to a radiation source vector  $\bar{Ra}$  striking a wall at an angle  $\zeta$  range from

$$p = (Ra) \sin \zeta (\sin \zeta + 2/3 \rho) \quad (3.10)$$

$$\tau = (Ra) \sin \zeta \cos \zeta$$

for diffuse reflection to

$$p = (Ra)(1 + \rho) \sin^2 \zeta \quad (3.11)$$

$$\tau = (Ra)(1 - \rho) \sin \zeta \cos \zeta$$

for spectral reflection. Here,  $\rho$  is the surface reflectivity. Because the radiation pressures can be formulated as vectors, the radiation disturbance torque evaluation is done in exactly the same fashion as for aerodynamic torques.

c. Torques due to translational control thrusters.

There are two apparent ways in which translation control jets could cause disturbance torques to the satellite attitude. If the line of action of a translational control thruster does not pass through the satellite center of mass, the system will produce torques which could affect both the pointing accuracy and the spin speed. In addition, a leak in a pneumatic system either at a joint or in a valve could also produce torques.

d. Magnetic torques.

Magnetic disturbance torques are primarily caused by current loops in the spacecraft and materials subject to permanent or induced magnetism. The instantaneous torque is the vector cross product of the spacecraft's effective dipole moment  $\bar{M}_s$  and the magnetic induction of the local field  $\bar{B}$  or

$$\bar{T}_m = \bar{M}_s \times \bar{B} \quad (3.12)$$

Here,  $\bar{M}_s$  is considered to include all but the dipole generated by the control coils. For a spinning satellite, the inertially fixed torque will equal the product of the dipole component along the spin axis and the lateral component of the magnetic field.



Because the satellite spins with respect to the magnetic field vector, torques due to the induced currents (eddy currents) and the irreversible magnetism of permeable materials (hysteresis effects) must also be considered. Smith [Ref. 3-11] has developed a theoretical expression for determining the eddy current torques in rotating shells which is used in this analysis.

The magnetic field assumed for the analysis of these disturbance torques is modeled in Ref. 3-12. Coefficients used in this analytical model are presented in Ref. 3-13.

e. Reference frame kinematics.

For a satellite in an earth orbit with inclination  $i$ , the instantaneous orbit precession rate is, to first order,

$$\dot{\Omega} = -\frac{3\mu J_2 R_e^2 \cos i \sin^2 \sigma}{HR^3} \quad (3.13)$$

Here,  $\mu$  is the universal gravitation constant times the earth mass,  $\sigma$ , is the sum of the orbit's argument of perigee and the true anomaly,  $H$  is the orbit's angular momentum with respect to the earth, and  $J_2$  is the first harmonic term in the expansion of the earth's potential. If the spin axis of the satellite is to be maintained normal to the orbit plane, a torque, "kinematic disturbance torque," must be exerted on the satellite to precess the spin axis as the orbit normal precesses. A simple consideration of required rate of change of satellite angular momentum yields the torque expression

$$\bar{T}_K = \dot{\Omega} \sin i I_{zz} \omega_z \hat{y}_K, \quad (3.14)$$

where  $\hat{y}_K$  is a unit vector along the line of nodes.

f. Total torques

To determine the total disturbance torque acting on any particular cylindrical spinning satellite, a digital computer program was written to evaluate these five torques. This program computes the

torques as a function of the parameters which change with orbital position of the satellite in its nominal orientation. Examples of inertially fixed yaw and roll torques were computed using this program and are presented as functions of orbital position in Figs. 3-4 and 3-5. For these examples, the orbit is inclined at  $45^\circ$  and the orbital frequency is 15 times/day. Perigee occurs at 300 km over the equator which is positioned in the center of the atmospheric bulge. The dimensions and other parameters used for the cylindrical spacecraft of this example are

length  $\ell$  = 0.5 m,  
radius  $r$  = 0.5 m and 0.75 m (two cases),  
skin thickness = 0.1 cm of aluminum,  
spin speed = 1 rad/sec,  
accommodation coefficients = 0.64 and 0.84 (two cases),  
decimeter flux index = 300 and 100 (two cases),  
reflectivity = 0.0 and 1.0 (two cases),  
spin axis dipole =  $0.6 \text{ amp m}^2$ ,  
c.m. offset from c.p. = 0.5 cm,  
jet misalignment moment arm = -0.5 cm.

Such plots are useful for illustrating the relative magnitudes and characteristics of the various disturbance torques.

### 3. State Estimation by Filtering Horizon Sensor Data

By proper placement of a pair of infrared horizon sensors (bolometers), it is possible to measure directly the roll error,  $\theta$ . Because of the structure of the satellite's state equations, the system is "observable." That is, a filter can be constructed which will produce estimates of the other state variables from the roll error measurements. To account for driving noise (disturbance torques) and measurement noise, an optimum steady-state (Kalman) filter is developed which gives "best" estimates of these states. This system is developed as follows.

#### a. Horizon-sensor determination of roll angle, spin speed, and orbital rate.

Roll-error measurement can be provided using the output of

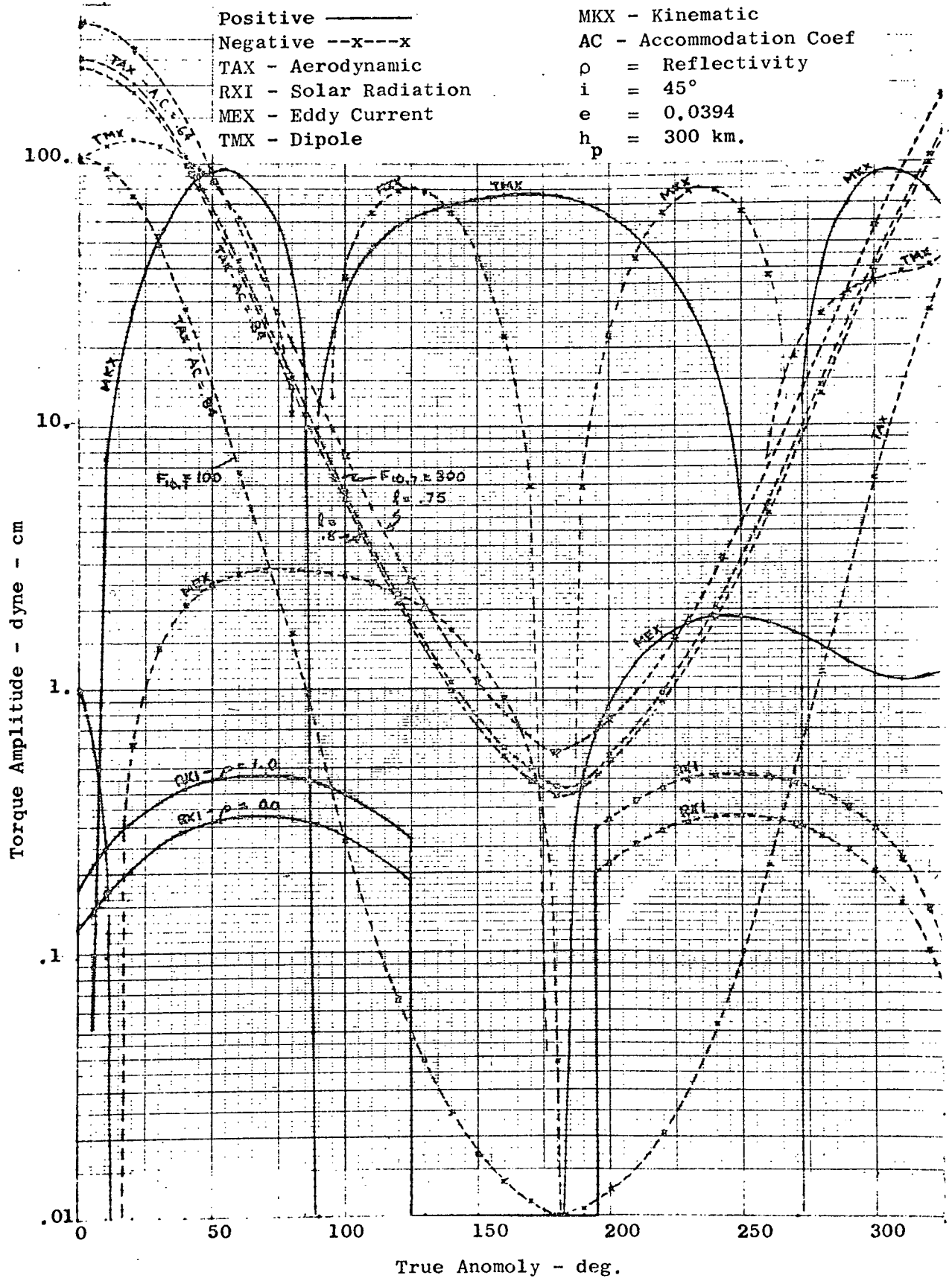


FIG. 3-4. TYPICAL YAW TORQUE COMPONENTS

TAY - Aerodynamic	RY1 - Direct Solar Radiation
RY2 - Earth Radiation	RY3 - Reflected Radiation
MEY - Eddy Current	i = 45°
MKY - Kinematic	e = 0.0394
TMY - Dipole	h <sub>p</sub> = 300 km

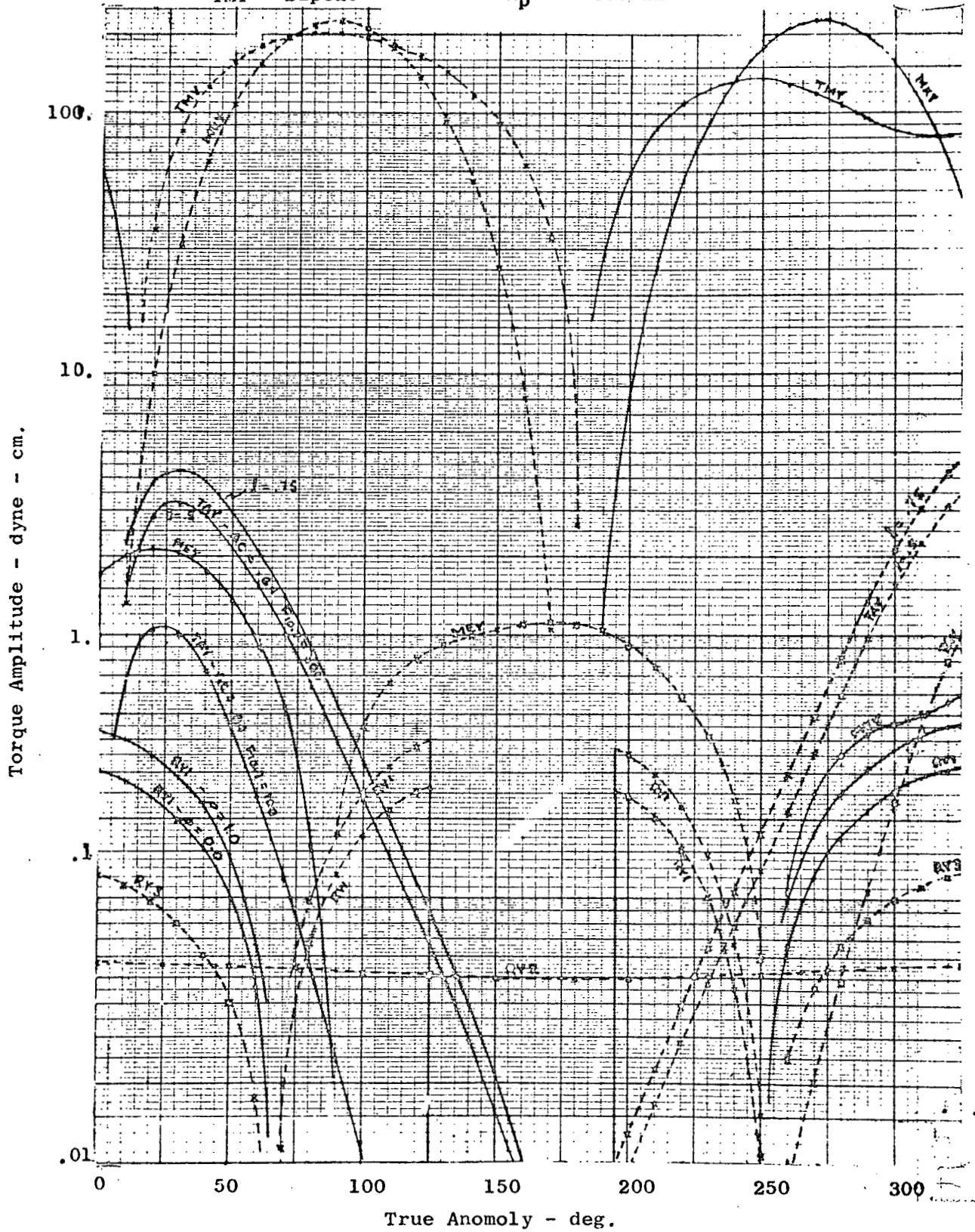


FIG. 3-5. TYPICAL ROLL TORQUE COMPONENTS

two infrared bolometers arranged with their optical axes in a "Vee" configuration as shown in Fig. 3-6. The optical axes lie in a plane containing the vehicle spin axis. As the satellite spins, the optical axes sweep out two conical surfaces in space. The sensors produce signals related to the change in received radiant energy as optical axes sweep from cold outer space through the warmer infrared earth, and back to space again after each spin revolution.

The intersection of these sensor paths with the earth and the corresponding sensor output is shown in Fig. 3-7. When the spin axis is normal to the earth-satellite radius vector, the sensor pulse outputs will have the same width and occur at the same time for an ideal spherical earth. If a roll error exists, the relationship among pulses will be as shown. Errors in yaw cannot be instantaneously detected. However, since the satellite spin axis is approximately fixed in inertial space, a pointing error in yaw at any particular instant will become an error in roll  $90^\circ$  later in the orbit due to the rotation of the local reference frame.

The geometry of the horizon sensor scheme is depicted in Fig. 3-8 where

$\theta$  = roll error

$\delta$  = half-vee angle

$\alpha$  =  $90^\circ - \delta$

$\beta$  =  $\sin^{-1} (Re/R)$

$t_1$  = time between horizon pulses for right sensor

$\dot{\psi}$  = local spin rate  $\cong \omega_z - \dot{f} - \dot{g}$

$\gamma$  =  $\dot{\psi} t_1 / 2$

The earth sweep time for the right sensor,  $t_1$ , can be written

$$t_1 = \frac{2}{\dot{\psi}} \cos^{-1} \frac{\cos \beta + \sin \theta \sin \delta}{\cos \theta \cos \delta} \quad (3.15)$$

Equation 3.15 was used to compute the output characteristics

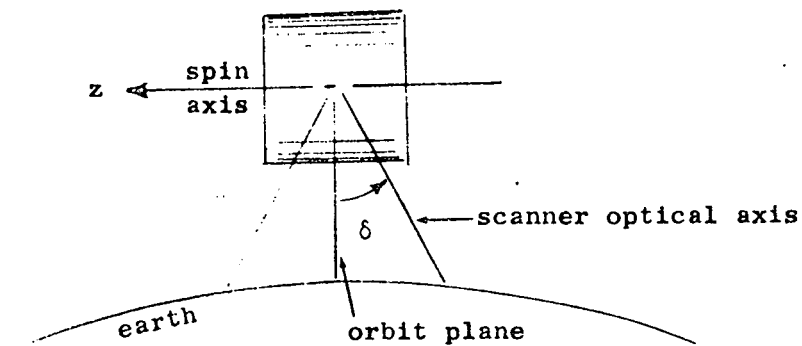


FIG. 3-6. HORIZON SENSOR "VEE" CONFIGURATION

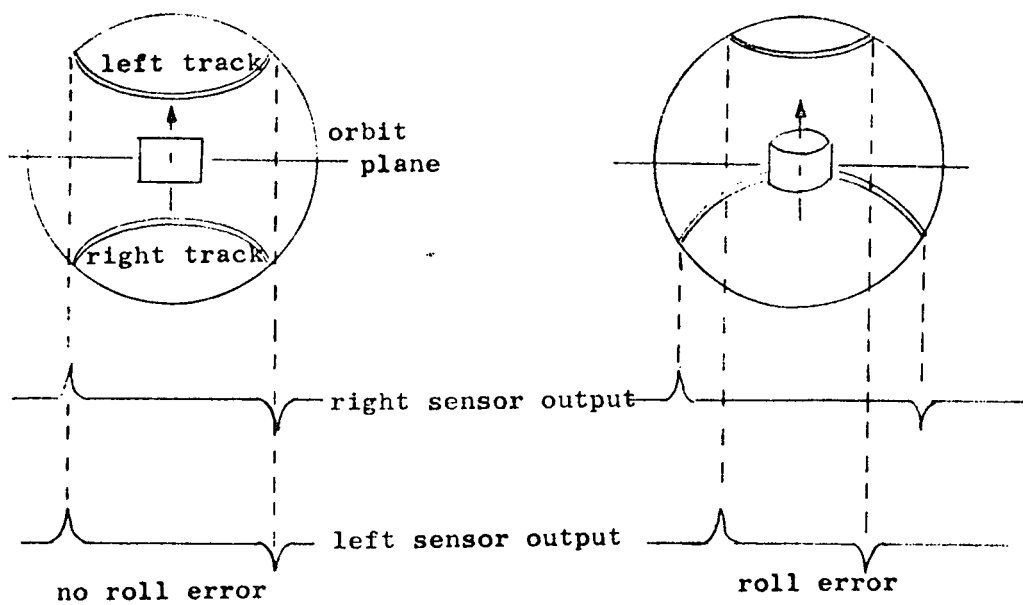


FIG. 3-7. HORIZON SENSOR OUTPUT WITH AND WITHOUT ROLL ERRORS.

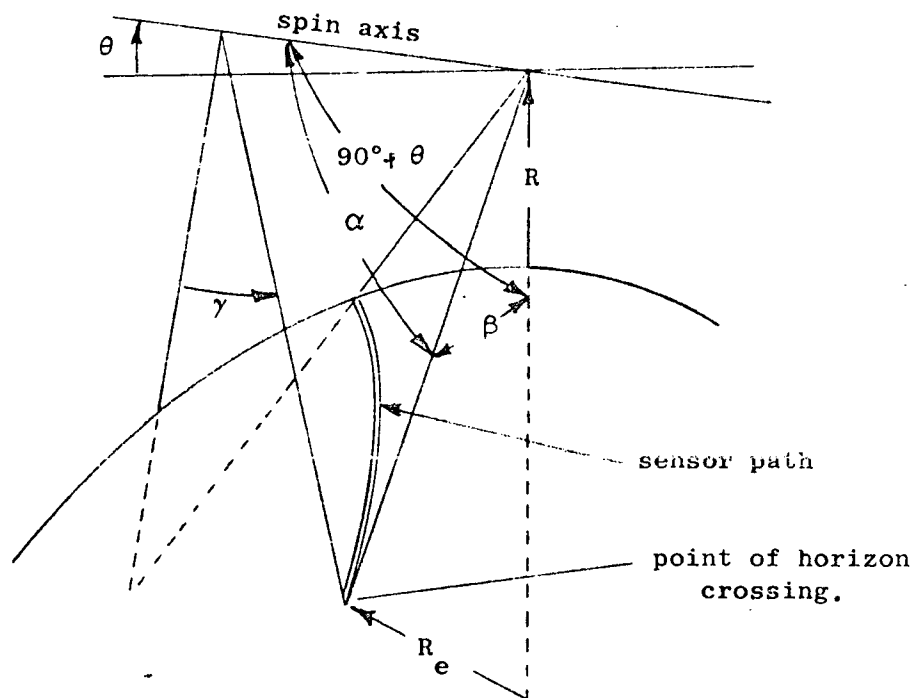


FIG. 3-8. GEOMETRY OF THE HORIZON SENSOR SCHEME.

of sensors with half-vee angles of  $3^\circ$ ,  $6^\circ$ , and  $9^\circ$  for an elliptic orbit having 3 revs/day. Define  $\Delta t$  and  $T_{avg}$  as

$$\Delta t \triangleq \frac{t_2 - t_1}{2}$$

where  $t_2$  is the time between horizon pulses for the left sensor, and  $T_{avg} \triangleq (t_2 + t_1)/2$ . Then Fig. 3-9 shows roll-angle error as a function of  $\Delta t$  for a  $9^\circ$  half-vee angle for various values of satellite radius. The roll error is found by multiplying  $\Delta t$  by a gain (slope of curves such as those in Fig. 3-9) which is radius dependent. This gain, as a function of  $T_{avg}$ , is shown in Fig. 3-10 for the three sensor angles investigated here. The quantity  $T_{avg}$  average remains fairly constant at a given altitude for small values of roll error. As can be seen from Eq. 3.15, the sensors will produce a larger error signal with a larger half-vee angle. However, a trade-off must be made because larger sensor angles will cause the sensor to miss the earth for high altitudes of highly eccentric orbits.

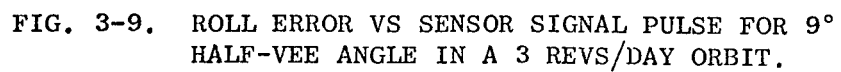
Because the horizon sensors produce a pulse train, with  $T_{avg}$  a function of satellite altitude, this output can also be used to give a direct measurement of the vehicle's spin speed and the current orbital rate,  $\dot{f} + \dot{g}$ , of the vehicle.

#### b. Kalman filter for state estimation.

The linearized state equations of the symmetric spinning satellite was summarized in matrix form in Eq. 3.4. This equation, as it stands, is observable from a measurement of the roll error  $\theta$ . That is, with a signal proportional to the roll error  $\theta$ , a state observer can be constructed to estimate values of the yaw error  $\phi$  and the two inertial rates  $\alpha_x$  and  $\alpha_y$ .

It would be nice if the disturbance torques could also be treated as states and estimated as part of the observer's function. However, a constant torque about the x-axis (yaw axis) (e.g., aerodynamic torque) is not observable from roll error measurements of a symmetric vehicle. Therefore, for the time being, it will be assumed that the disturbance torques can be treated as white driving noise. If it is





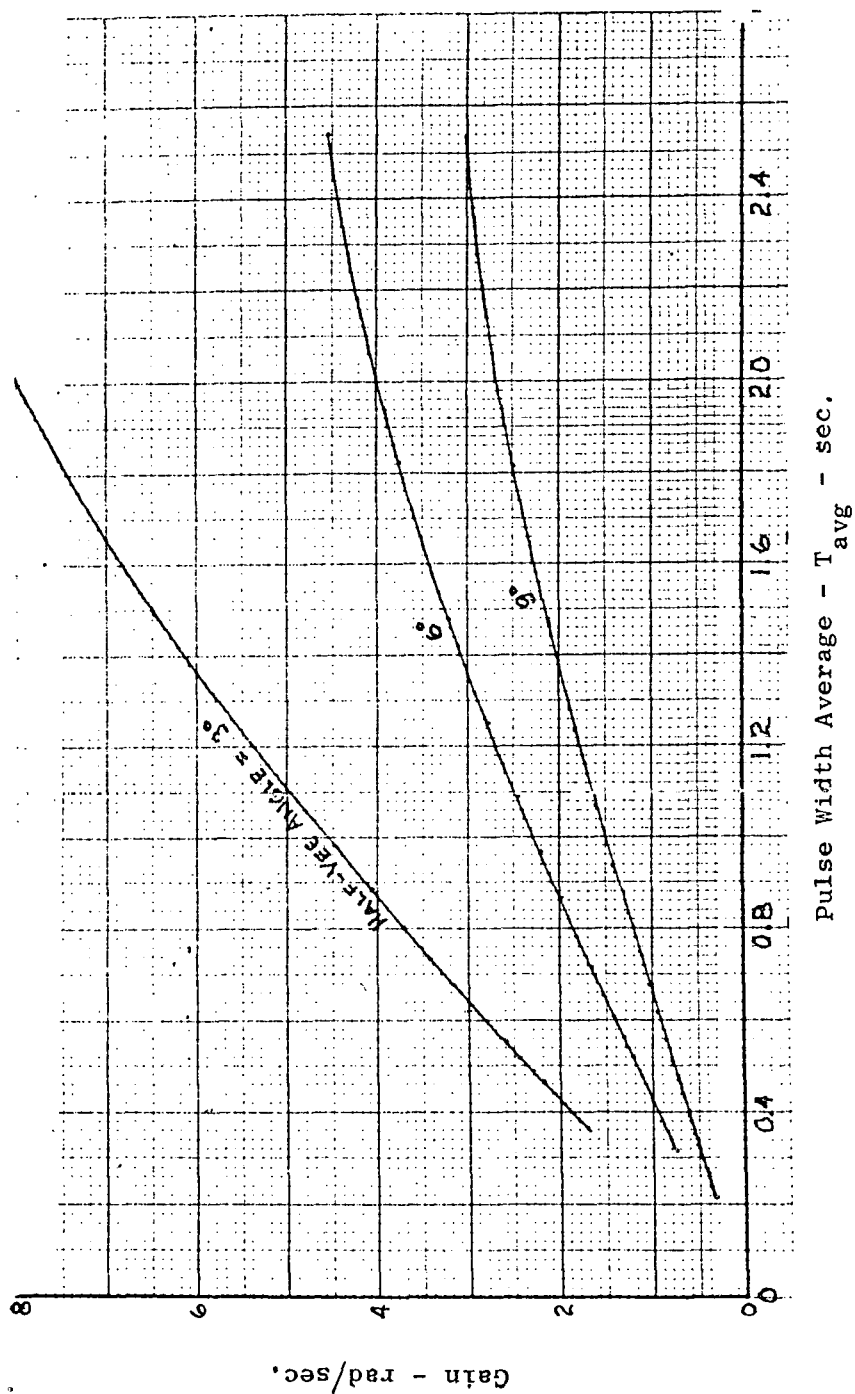


FIG. 3-10. ERROR GAIN VS PULSE WIDTH FOR DIFFERENT HALF-VEE ANGLES IN A 3 REVS/DAY ORBIT.

assumed that the driving noise and measurement noise are stationary, white, uncorrelated processes, a Kalman filter [Ref. 3-14] can be mechanized to determine the linear least squares estimates of  $\alpha_x$ ,  $\alpha_y$ , and  $\phi$ .

The state and observation equations are expressed in general form as

$$\begin{aligned} \dot{x} &= Fx + Gu + Lv \\ y &= Hx + w \end{aligned} \quad (3.16)$$

where  $u$  is the normalized control input, and  $v$  and  $w$  are white noise with covariances

$$\begin{aligned} E\{v(t)v^T(\tau)\} &= Q\delta(t - \tau) \\ E\{w(t)w^T(\tau)\} &= R\delta(t - \tau) \end{aligned}$$

and

$$E\{w(t)v^T(\tau)\} = E\{v(t)x^T(0)\} = E\{w(t)x^T(0)\} = 0.$$

$Q$  is a positive semi-definite diagonal matrix and  $R$  is a scalar constant. The  $(4 \times 1)$  matrix  $x(0)$  is the value of the state vector  $x$  at time zero. The estimator equations are then

$$\dot{\hat{x}} = F\hat{x} + G\hat{u} + \Sigma H^T R^{-1} (y - H\hat{x}), \quad (3.17)$$

where  $\Sigma$  is the covariance of the error  $(x - \hat{x})$  which is determined by finding the steady state solution to the Riccati equation

$$\dot{\Sigma} = F\Sigma + \Sigma F^T + LQL^T - \Sigma H^T R^{-1} H\Sigma. \quad (3.18)$$

It can be seen by dividing Eq. 3.18 by  $R$  that the steady-state solution of  $\Sigma$  depends solely on the matrix  $Q/R$ . Thus, for

$LQL^T$  of the form

$$\frac{Q}{R} = \begin{bmatrix} q & 0 & 0 & 0 \\ 0 & q & 0 & 0 \\ 0 & 0 & 0 & 0 \\ 0 & 0 & 0 & 0 \end{bmatrix},$$

the amount of work required to solve Eq. 3.18 is greatly simplified.

Equation 3.18 was solved by numerical integration for a wide range of the parameter  $q$  and the results are shown in Fig. 11. In this plot,  $[K_1, K_2, K_3, K_4] = [\Sigma H^T R^{-1}]^T$ , the gain matrix of the filter. For driving noise with variance  $v = 10^{-4} \text{ sec}^{-2}$  and measurement error  $\omega = 10^{-3}$  radians,  $q$  would be 0.01. The solutions of Fig. 3-11 are for parameter values of  $D = 1.5 \text{ sec}^{-1}$  mean orbital rate and  $n = 1.09 \times 10^{-3} \text{ sec}^{-1}$ , corresponding to the 15 rev/day. Changing  $n$  to  $2.18 \times 10^{-4} \text{ sec}^{-1}$  for 3 rev/day, changed the steady-state gains by less than 2%. Thus, there seems to be no need to use time-varying gains computed by continuous integration of the Riccati equations to account for the change in the orbital rate due to the elliptic orbit.

Since the input to the Kalman estimator is not continuous in nature but comes as a sampled signal, the familiar Shannon sampling theorem requires that this signal have a sample rate which is at least twice as fast as the variation in the state which one is trying to produce. The rate terms  $\alpha_x$  and  $\alpha_y$  oscillate with a frequency  $D$ , therefore it is necessary to sample at least  $2I_{zz}/I_{xx}$  times per satellite revolution. Thus, the horizon sensor heads must either be spun at least  $2I_{zz}/I_{xx}$  times faster than the satellite spin rate or more than  $2I_{zz}/I_{xx}$  sensor pairs must be used on the satellite.

#### 4. Magnetic Attitude Control of the Symmetric Spinning Vehicle.

Given the ability to determine the three unknown states of the vehicle attitude, one can proceed to develop a control system making use of these states. Then, once a control law has been formulated, the implementation of the required control torques must be considered. The control problem studied here is that of a regulator. It is desired to keep the spin axis as close as possible to the orbit plane normal and maintain the spin speed of the satellite within some acceptable bounds.

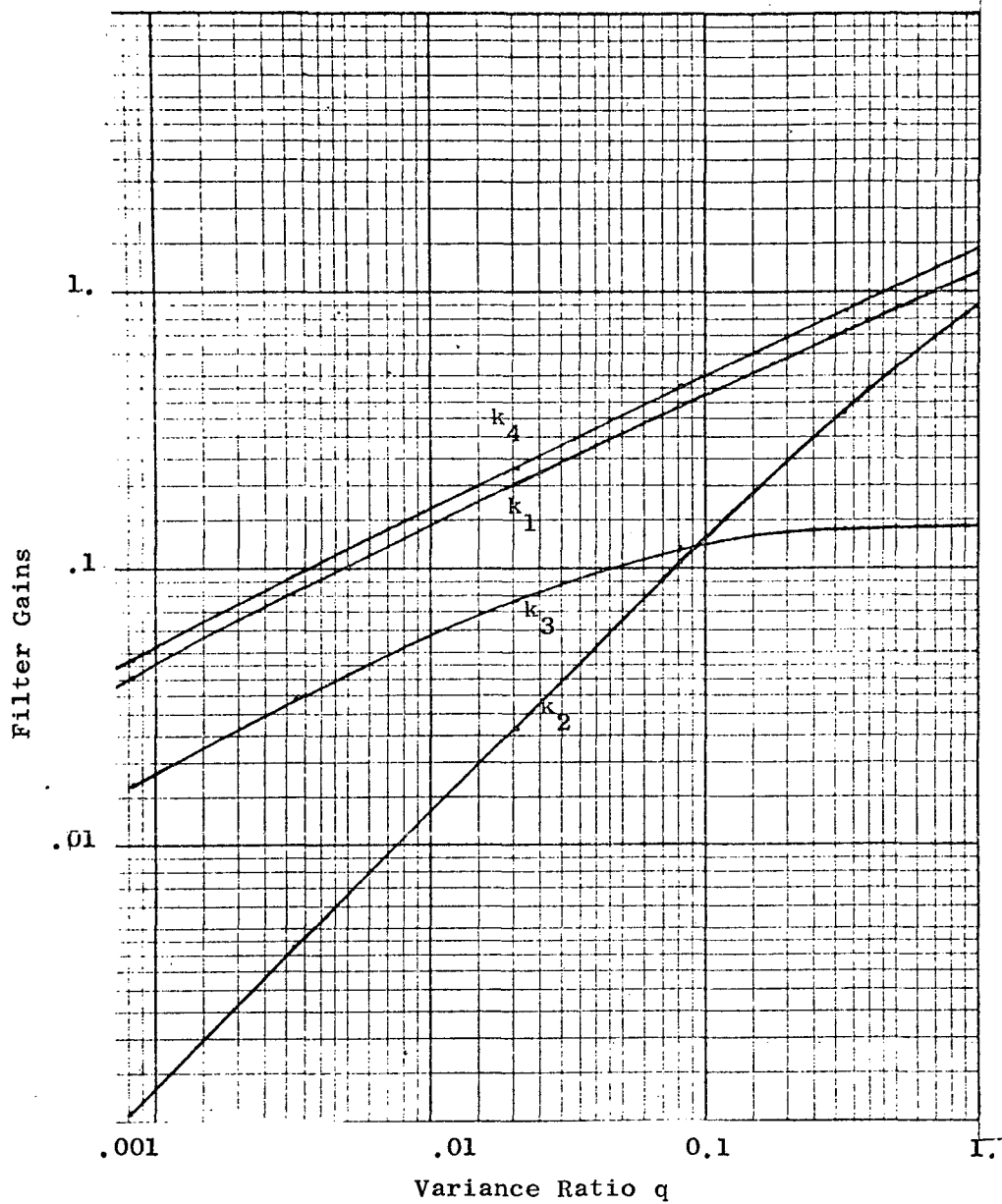


FIG. 3-11. KALMAN FILTER GAINS VS NOISE VARIANCE RATIO FOR SPINNING SATELLITE.

In this part, a new method of magnetically controlling the attitude of a spinning spacecraft is developed. It will be shown that this magnetic attitude control system is simple and requires very little power requirements for geodesy satellites in orbits between 15° and 75° inclinations. This system, possibly supplemented with a passive nutation damper, thus becomes a strong candidate in any geodesy mission for which active attitude control is required.

a. Magnetic implementation of the control law.

The desired control torque will usually consist of components about the roll and yaw axes to correct wobble motion and pointing error and a component about the spin axis to correct spin speed error. To implement a torque magnetically, one makes use of the relationship

$$\bar{T} = \bar{m} \times \bar{B} \quad (3.19)$$

where  $\bar{m}$  is the magnetic dipole created by producing electromagnets or passing current through coils fixed to the satellite. The vector  $\bar{B}$  is the local value of the earth's magnetic field and  $\bar{T}$  is the resultant torque.

Because  $\bar{B}$  has an arbitrary direction (see Fig. 3-12), it is not always possible to solve Eq. 3.19 for  $\bar{m}$  to produce a desired  $\bar{T}$ . Thus, it is assumed that the spin component of desired torque is ignored except in cases where the spin speed has deviated so far from the nominal value that corrective action must be taken.

For maximum efficiency, it is necessary to create a magnetic dipole in the spacecraft normal to the earth's magnetic field at any given instant. Thus,

$$\bar{m} \cdot \bar{B} = 0 \quad (3.20)$$

By solving Eqs. 3.19 and 3.20 with the assumption that the component of  $\bar{T}$  along the spin axis is zero, one obtains

$$\begin{aligned} m_z &= (T_{yD} B_x - T_{xD} B_y) / |\bar{B}|^2 \\ m_x &= (m_z B_x - T_{yD}) / B_z \\ m_y &= (m_z B_y + T_{xD}) / B_z \end{aligned} \quad (3.21)$$

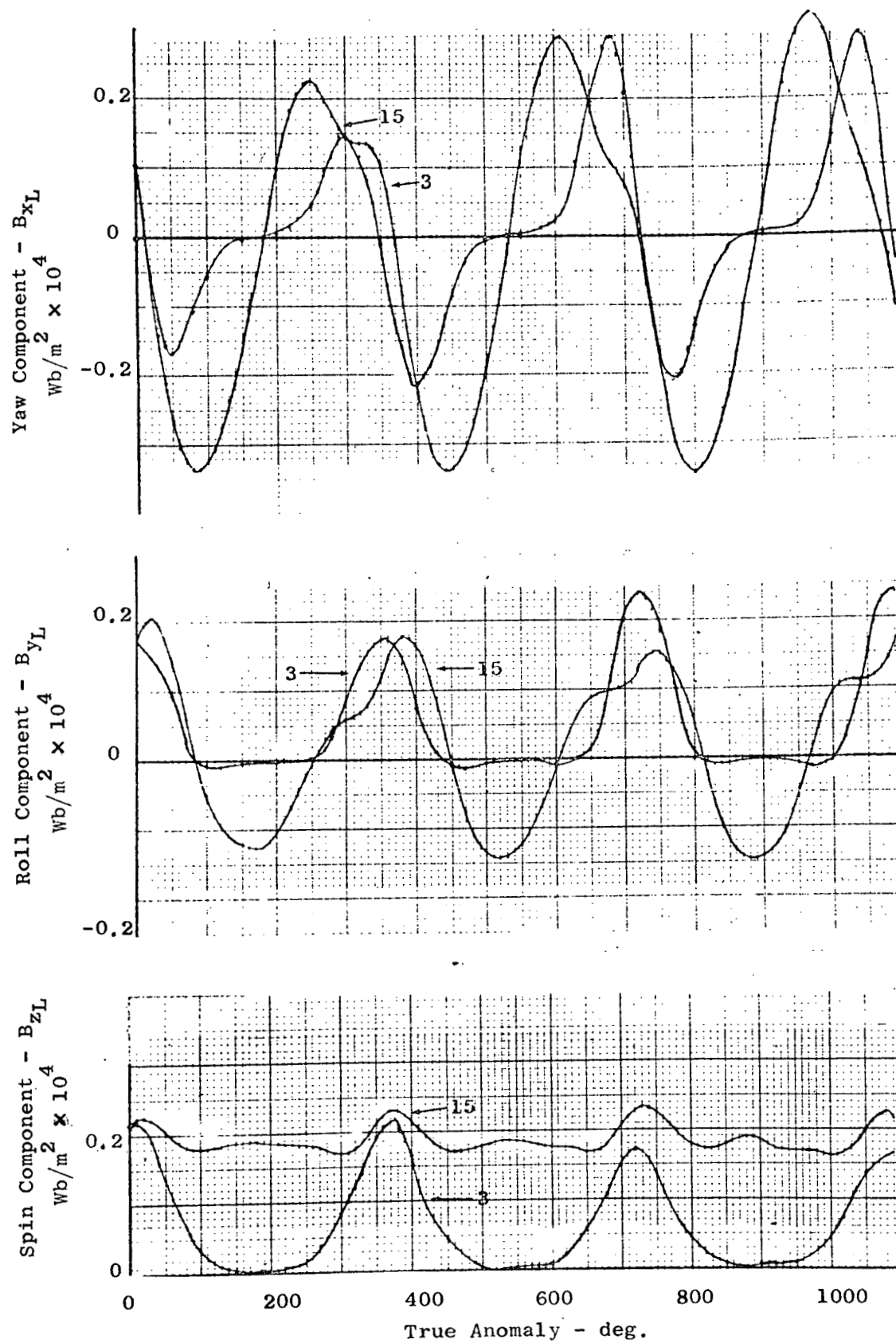


FIG. 3-12. EARTH'S MAGNETIC FIELD COMPONENT VARIATION FOR 3 REVS/DAY AND 15 REVS/DAY ORBITS INCLINED AT  $45^\circ$ .

where  $T_{yD}$  and  $T_{xD}$  are the desired control torques and the subscripts x, y, z on all quantities denote measure numbers in the local (L) reference frame. Equations 3.20 is basic to magnetic attitude control and have been used in modified form in several mechanizations since appearing in Ref. 3-15.

To mechanize a control system along the lines of Eq. 3.21 requires the measurement of three components of the magnetic field. It also requires seven multiplications and two divisions. Although this is complex in itself, the worst problem arises from the requirements for division by  $B_z$  and  $|\bar{B}|^2$ . For a highly elliptic orbit (see Fig. 3-12),  $B_z$  alone varies over two orders of magnitude in size.

One method of control mechanization which greatly simplifies Eq. 3.21 is to set  $m_z = 0$  and assume an average value of the spin component of magnetic field  $B_z$ . Then, for  $K = 1/B_{z \text{ average}}$ ,

$$\begin{aligned} m_x &= -KT_{yD} \\ m_y &= KT_{xD} \end{aligned} \quad (3.22)$$

The resulting actual torque acting on the vehicle will then be

$$\begin{aligned} T_x &= (KB_z)T_{xD} \\ T_y &= (KB_z)T_{yD} \\ T_z &= -K(B_y T_{yD} + B_x T_{xD}) \end{aligned} \quad (3.23)$$

The spin torque  $T_z$  should average to nearly zero over several orbits under such a scheme.

Pointing control can also be achieved with the z-coil alone. If one assumes that the magnetic field  $\bar{B}$  is normal to the required torque  $\bar{T}_D$ , then

$$\bar{m} = K_1 (\bar{B} \times \bar{T}_D)$$

where  $K_1$  is some appropriate gain. Thus

$$m_z = K_1 (B_x T_{yD} - B_y T_{xD})$$

Spin-coil control has the disadvantage that the resulting pointing control torque is not usually in the exact direction of the desired torque but has the advantage of creating no undesired spin torques.



b. Spin control

If the spin speed deviates from the nominal value, this can be detected by variations in the periodic signal coming from the horizon sensors. The desired control torque to correct such a deviation  $\Delta\omega_z$  would be

$$T_{z_D} = -K_z \Delta\omega_z$$

or

(3.24)

$$T_{z_D} = -K_z \operatorname{sgn}(\Delta\omega_z)$$

when  $|\Delta\omega_z|$  exceeds some deadband value. There are two ways in which this spin control can be implemented.

The first implementation of spin control follows from Eqs. 3.23. From these it is seen that a spin torque will exist because of the presence of pointing control. Thus, one might incorporate logic into the control system such that pointing control is only actuated when the resulting spin torque is in the desired direction.

The second possible scheme is to apply current to the x and y coils in such a way that the resulting magnetic moment is normal to the component of the magnetic field in the X-Y plane. Thus

$$m_x = K_z B_y \operatorname{sgn}(\Delta\omega_z)$$

(3.25)

$$m_y = -K_z B_x \operatorname{sgn}(\Delta\omega_z)$$

c. Complete control logic

The preceding two sections (a & b), can be combined to yield a control system which provides both pointing control and spin-speed control. Two constants  $C_1$  and  $C_2$  are defined which represent boundaries of the deadbands associated with the spin speed. Let  $C_1$  be the value such that when  $|\Delta\omega_z| > C_1$ , one should provide some sort of spin control. Let  $C_2$  be the value for which, when  $|\Delta\omega_z| > C_2$ , it is mandatory that spin control action be taken. Then suitable logic governing the currents

put into three orthogonal coils would be

for:  $-C_1 \leq \Delta\omega_z \leq C_1$  (Mode 1)

$$m_x = -K T_{y_D}$$

$$m_y = K T_{x_D} \quad (3.26)$$

$$m_z = 0 ;$$

for:  $C_1 < \Delta\omega_z \leq C_2$  (Mode 2)

if  $\text{sgn} [-K(B_y T_{y_D} + B_x T_{x_D})] = \text{sgn}(-\Delta\omega_z)$ , use Mode 1;

if  $\text{sgn} [-K(B_y T_{y_D} + B_x T_{x_D})] = -\text{sgn}(-\Delta\omega_z)$

(3.27)

$$m_x = 0$$

$$m_y = 0$$

$$m_z = K_1 (B_x T_{y_D} - B_y T_{x_D}) ;$$

for:  $C_2 \leq |\Delta\omega_z|$  (Mode 3)

$$m_x = K_z B_y \text{sgn}(\Delta\omega_z)$$

$$m_y = -K_z B_x \text{sgn}(\Delta\omega_z)$$

(3.28)

$$m_z = K_1 (B_x T_{y_D} - B_y T_{x_D}) .$$

If the gains are set properly and care is exercised in design and construction of the vehicle, Mode 3 will not be required during normal operation. However, it should be provided for use during initial spin-up or for the case where spin speed changes but no pointing error accumulates.

This control mechanization requires the presence of three orthogonal coils about the three orthogonal control axes. The z-coil (spin coil) could be provided with a ferromagnetic core so that weight and power requirements would be lowered.

The control system must also have the ability to measure the magnetic-field components,  $B_x$  and  $B_y$  when in Modes 2 and 3. This is done with a two-axes fluxgate magnetometer [Ref. 3-16], a device with reasonable linearity. The magnetometer's sensitive axes must be mounted such that no interference is created from the magnetic field produced by the control coil. For the case where the magnetic components  $m_x$  and  $m_y$  are both being generated, this interference can best be prevented by a time-sharing procedure. Here, the coil currents are cut off momentarily once each cycle of spacecraft spin. At this time the magnetic-field measurements could be sampled and held during the controlled portion of the cycle.

d. Skewed-coil magnetic control.

It is possible to simplify to a great extent, the mechanization of the control system suggested in the previous section. This can be done by replacing the three coils by a single coil skewed at  $45^\circ$  to the spin axis as shown in Fig. 3-13. A further simplification is to use only one magnetometer with its sensitive axis along the node of the skewed coil and the x-y plane as indicated. Such a magnetometer would not require time-shared measurements. For such a system, if the current in the coil is constant, an average magnetic dipole moment is generated along the spin axis. If a constant current has its direction switched every  $180^\circ$ , the average magnetic moment is in the x-y plane pointing in the direction  $90^\circ$  from the switch points. Thus, one has the ability to generate all three components of the desired magnetic dipole  $\bar{m}$  averaged over a spin cycle of the satellite. A disadvantage to such a system is that it can only generate the average required magnetic components in the x and y directions over one cycle. Thus, it does not have the ability to generate control forces which fluctuate faster than spin rate such as wobble damping terms. Therefore, the skewed-coil must be supplemented with a nutation damper. At any rate, the

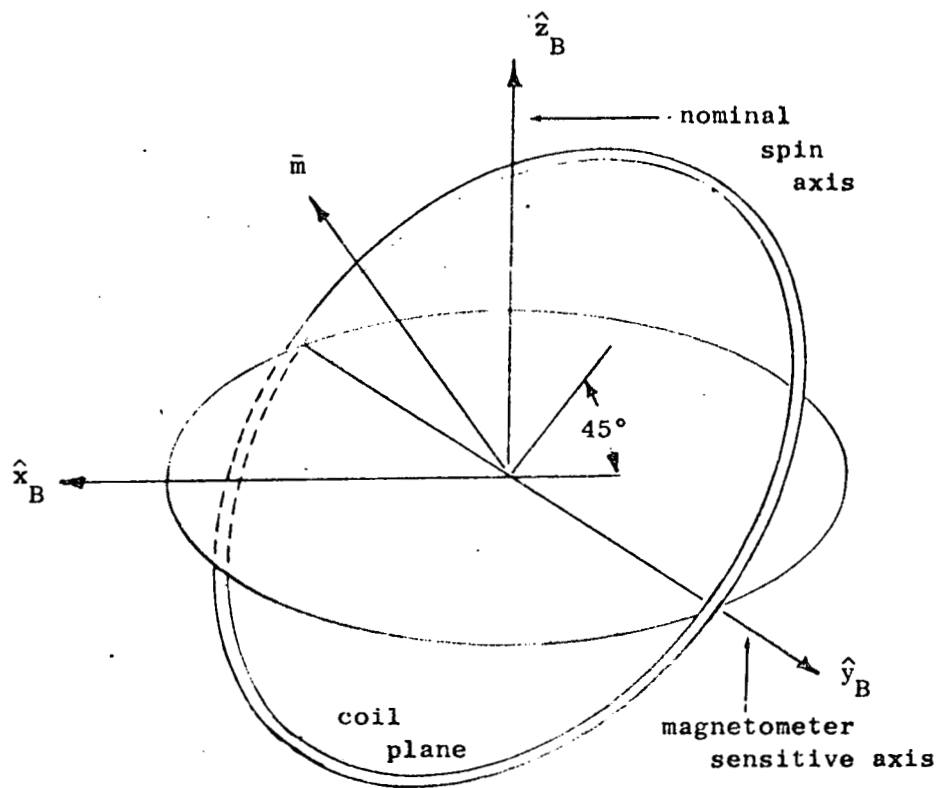


FIG. 3-13. GEOMETRY OF SKEWED COIL IN SPINNING SPACE-CRAFT. MAGNETOMETER SENSITIVE AXIS LIES IN PLANE OF COIL.

packaging advantages of a system with a single coil and magnetometer seem to make the skewed coil mechanization worthy of consideration.

e. Minimum power optimal pointing control.

The normal mode of operation of the magnetic control system will be Mode 1. It is necessary to specify what the desired control torque components  $T_{x_D}$  and  $T_{y_D}$  are for this mode and what appropriate gains should be. A reasonable criteria for selecting the control torques to be applied is to choose  $T_{x_D}$  and  $T_{y_D}$  which yields the response desired and minimizes the power used to achieve this. The expressions for the idealized pointing control torques will now be presented below.

Power consumption is proportional to current squared and the magnetic moment of a coil equals the product of the current, the coil area, and the number of turns of the coil. Thus, for a single coil one should try to minimize the control current squared. For two orthogonal coils, minimum power is obtained by minimizing the sum of the squares of the coil currents. Thus, the optimization problem considered is that of minimizing the performance index  $J$  subject to the system differential equations 3.4, where

$$J = \int_{-\infty}^{t_f} (q_1 \alpha_x^2 + q_1 \alpha_y^2 + q_2 \theta^2 + q_2 \phi^2 + T_{D_x}^2 + T_{D_y}^2) dt .$$

For a fourth-order system whose equations of motion have complex symmetry, the solution of this problem is well known (e.g., Ref. 3-17) and yields an optimal control of the form

$$\begin{aligned} T_{D_x} &= -K_v \phi - K_{p1} \phi - K_{p2} \theta \\ T_{D_y} &= -K_v \theta + K_{p2} \phi - K_{p1} \theta , \end{aligned} \tag{3.29}$$

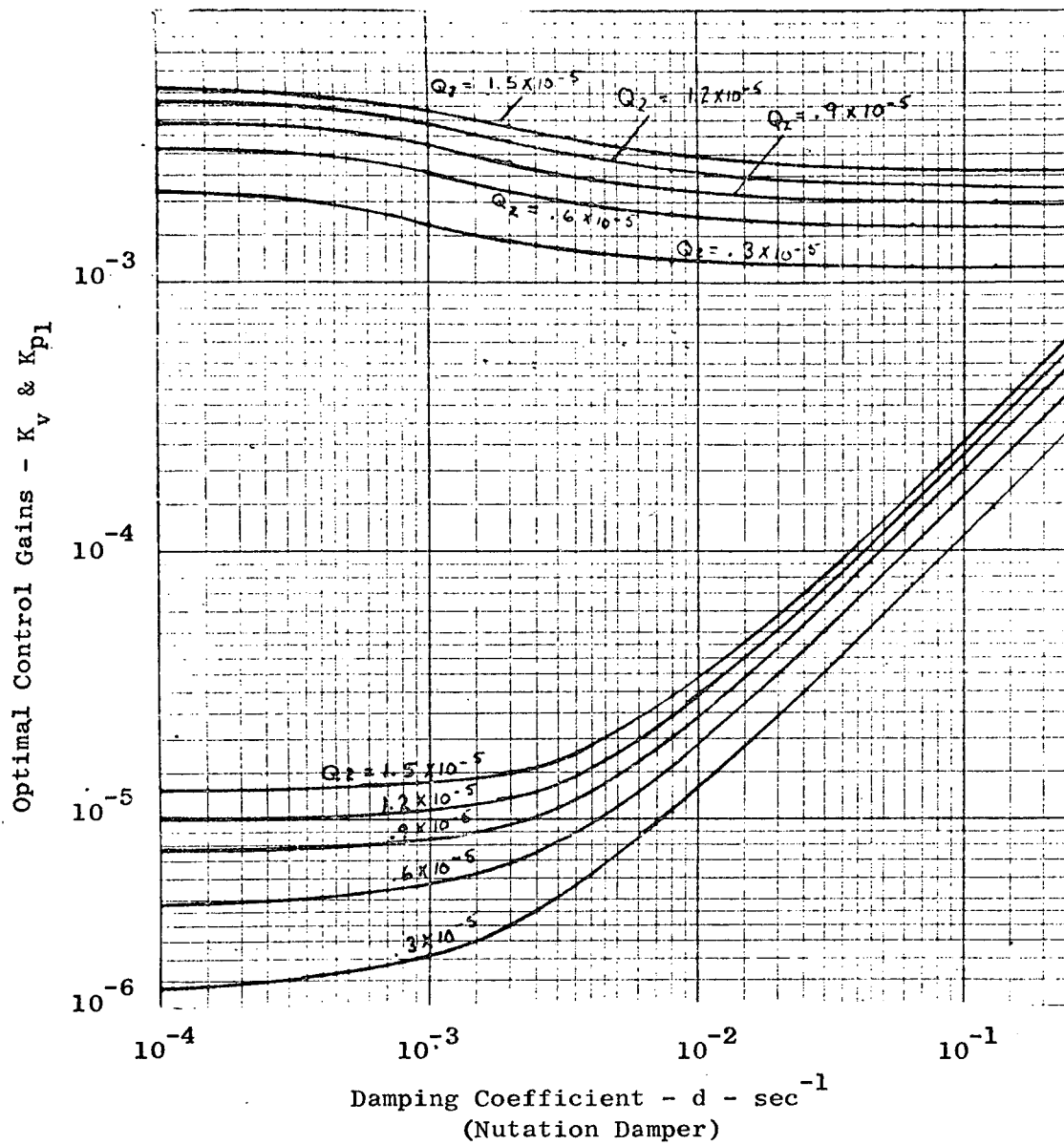
where the three coefficients of Eq. 3.29 are solutions to the equations

$$\begin{aligned}
 & 2(K_{p1})^3 + (D^2 + 2Dn + n^2 + d^2 + q_1)(K_{p1})^2 + 2(Dnq_1 - q_2)K_{p1} \\
 & - (d^2q_2 + d^2n^2q_1 + q_1q_2) = 0 \\
 & K_v = -d + \sqrt{d^2 + 2K_{p1} + q_1} \\
 & K_{p2} = dn + \sqrt{(dn)^2 + q_2 - (K_{p1})^2 - 2DnK_{p1}}.
 \end{aligned} \tag{3.30}$$

The solutions to Eq. 3.30 for  $D = 1.5$  rad/sec,  $n = 1.09 \times 10^{-3}$  rad/sec,  $q_1 = 0$ , with  $q_2$  treated as a parameter are shown in Fig. 3-14. The nutation damping coefficient,  $d$ , is varied from  $10^{-4}$  to  $10^{-1}$ . Changing the mean orbital rate,  $n$ , to  $2.18 \times 10^{-4}$ , corresponding to a 3 revs/day orbit had no markable change on the solutions. The choice of actual gains to be used for power minimization depends upon the coefficient of the nutation damper used and the response desired which is determined by choice of the parameter  $q_2$ .

#### f. Stability considerations

In the previous section, gains from minimum power control were determined with the assumption that the resulting idealized torque would always be mechanized exactly. However, using the simplified control mechanization specified in Eqs. 3.26, 3.27, and 3.28, one would only be able to actuate the coils to produce control torques which would be optimum in some average time sense. For instance, if Eq. 3.26 is being used and the gain  $K$  is chosen as the average value of  $1/B_z$ , then the actual control torque produced varies considerably from the "optimum." It is known from optimal theory that the optimal gains, when mechanized exactly, will result in a stable system. But when the actually mechanized control torques are time varying, depending upon the time history of  $B_z$ , the question of stability remains open. The subsequent discussion is intended to be a summary of the stability investigation. A more detailed development may be found in Ref. 3-19.



	$q_2$	$1.5 \times 10^{-5}$	$1.2 \times 10^{-5}$	$9 \times 10^{-5}$	$0.6 \times 10^{-5}$	$0.3 \times 10^{-5}$
Position Control Gain $K_{p2}$ :	$K_{p2}$	$3.8 \times 10^{-3}$	$3.5 \times 10^{-3}$	$3.0 \times 10^{-3}$	$2.4 \times 10^{-3}$	$1.7 \times 10^{-3}$

FIG. 3-14. OPTIMUM CONTROL GAINS FOR POWER MINIMIZATION AS A FUNCTION OF DAMPING. THE PARAMETER  $q_2$  IS CHOSEN FOR RESPONSE CONSIDERATIONS.

Consider the case of the skewed-coil controller. Let the damping terms of Eq. 3.29 be lumped in with the nutation damper so that the desired magnetic torques are

$$\begin{aligned} T_{D_x} &= -K_{p1} \phi - K_{p2} \theta \\ T_{D_y} &= K_{p2} \phi - K_{p1} \theta \end{aligned} \quad (3.31)$$

From Eqs. 3.23 and 3.26, the actual position control gains are

$$\begin{aligned} T_x &= -K(K_{p1} \phi + K_{p2} \theta) B_z(t) \\ &= -K_1(t)(K_{p1} \phi + K_{p2} \theta); \end{aligned} \quad (3.32a)$$

$$\begin{aligned} T_y &= -K(-K_{p2} \phi + K_{p1} \theta) B_z(t) \\ &= -K_1(t)(-K_{p2} \phi + K_{p1} \theta); \end{aligned} \quad (3.32b)$$

where  $K_1(t) = KB_z(t)$ . Substituting Eqs. 32 into Eq. 4 yields

$$\begin{bmatrix} \dot{\alpha}_x \\ \dot{\alpha}_y \\ \dot{\phi} \\ \dot{\theta} \end{bmatrix} = \begin{bmatrix} -d & -D & -K_1(t)K_{p1} & -K_1(t)K_{p2} \\ D & -d & K_1(t)K_{p2} & -K_1(t)K_{p1} \\ 1 & 0 & 0 & n \\ 0 & 1 & -n & 0 \end{bmatrix} \begin{bmatrix} \alpha_x \\ \alpha_y \\ \phi \\ \theta \end{bmatrix} \quad (3.33)$$

One must determine what range of  $K_1(t)$  can be allowed and yet be assured that Eq. 3.33 remains stable.

Referring to Fig. 3-14, it is seen that  $K_{p2} \gg K_{p1}$ , so replace  $K_1(t)K_{p2}$  by  $K$  and  $K_1(t)K_{p1}$  by zero in Eq. 3.33. Then, one can proceed to determine what value of the constant gain  $K$  would cause the resulting system to be unstable.

For the values of  $d$  and  $n$ , typical of the satellite considered here, application of Routh's criteria produces the approximate condition



$$Dd > K_1(t) . \quad (3.34)$$

Equation 3.34 gives an approximation to the upper limit on  $K_1(t)$ . As a more rigorous approach, a Lyapunov function has been constructed which demonstrates asymptotic stability for  $K_1(t)$  less than an upper limit agreeing very well with Eq. 3.34. The system is stable for  $K_1(t) < 5.398$ , for example, using the Lyapunov approach with parametric values,

$$\begin{aligned} D &= 1.5 \\ d &= 1.26 \times 10^{-2} \\ n &= 1.09 \times 10^{-3} \\ K_{p1} &= 2.85 \times 10^{-5} \\ K_{p2} &= 3.5 \times 10^{-3} . \end{aligned}$$

Again, the time variation of orbital rate has only a slight effect on the results.

A method of determining the limits on the allowable position gain has now been established. Suppose one sets the gains of the control system so the system is optimal for the average magnetic field. Then the previous technique determines whether or not stability is maintained over the entire range of magnetic field variations for that particular orbit. The average magnetic field for an orbit can be found from plots such as Fig. 3-15 taken from Ref. 3-18 by using the semi-major axis as the average radius.

One must also investigate the stability of Mode 2 control, i.e., the situation when only the spin component of the magnetic moment is used for pointing control. Consider again the case where the magnetic control is for position control only. By requiring that the average magnitudes of  $\alpha_x$ ,  $\alpha_y$ ,  $\theta$ , and  $\phi$  be always decreasing, one can obtain the condition

$$d > \frac{K_1(B_x^2 + B_y^2)}{2D} \quad (3.35)$$

and  $K_{p1} = 0$  for all  $(B_x^2 + B_y^2)$  of the orbit. The spin magnetic moment during Mode 2 and 3 control should then be

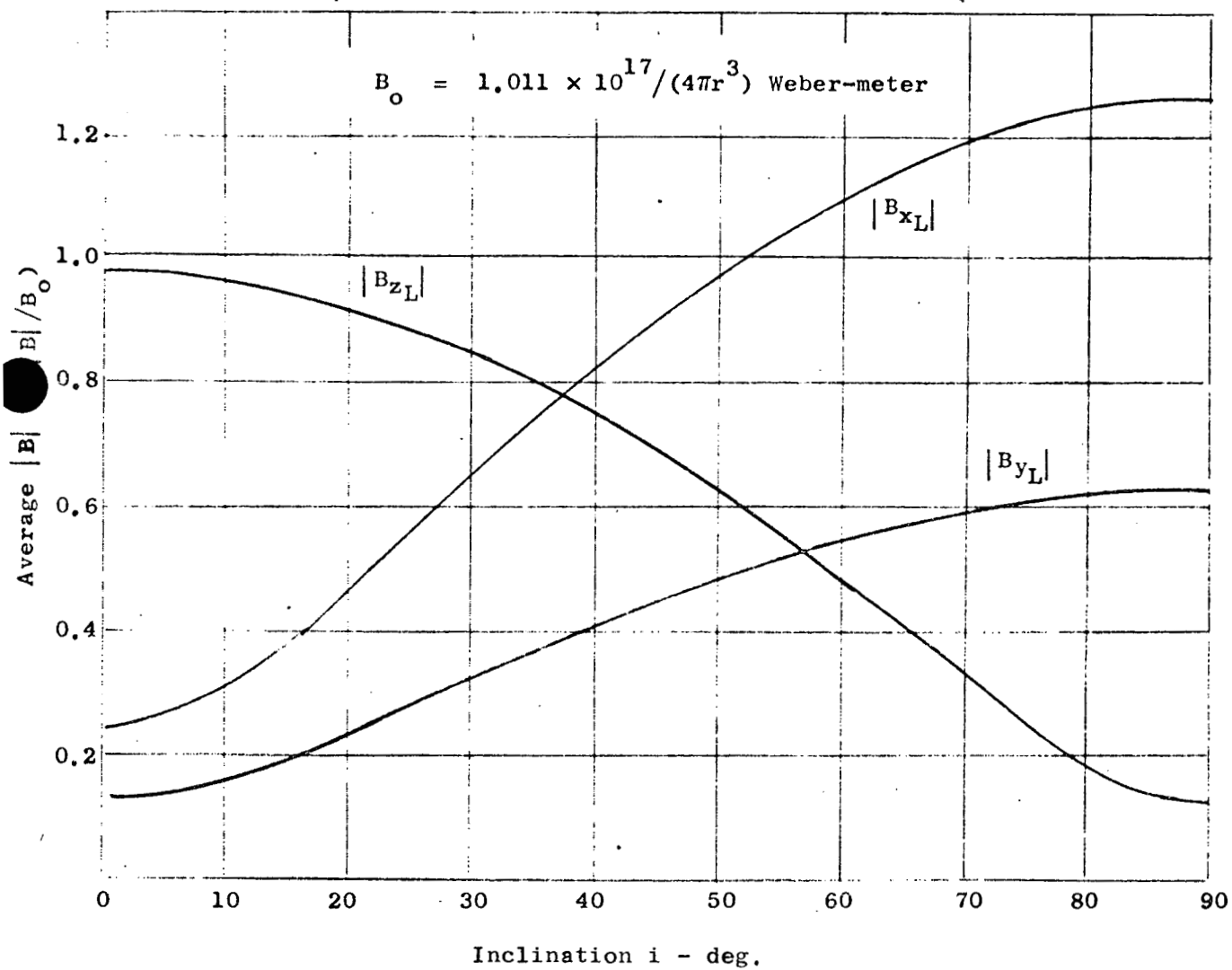


FIG. 3-15. MAGNETIC FIELD AVERAGES FOR CIRCULAR ORBITS.

$$m_z = K_1 K_{p2} [\phi B_x + \theta B_y] \quad (3.36)$$

where  $K_1$  is chosen so that Eq. 3.35 is satisfied.

g. Simulation results.

Throughout this study, analog and digital simulations of the system have been made to verify the analytical results. A brief summary of some of the findings of these simulations will be mentioned here.

In deciding to use a state estimator as part of the control system, it was necessary to compare the system response with that which would occur when no estimator was used. Without an estimator the magnetic position control could be

$$\begin{aligned} T_{D_x} &= -K_p \theta \\ T_{D_y} &= 0 \end{aligned} \quad (3.37)$$

where  $\theta$  is the roll error signal coming directly from the horizon sensors. This control would, of course, be supplemented with a nutation damper.

Assuming, the exact control torque is applied as specified by the control laws 3.37 and 3.31, the response times were compared for driving the states to zero from a variety of initial conditions. For the cases considered, the system with the estimator was found to be all the way from equally-as-fast to twenty-times-as-fast as the system with no estimator.

This speed of response has two advantages. Because disturbance torques are going to move the satellite spin axis away from normal to the orbit plane, fast response means that the average deviation is less. Also, because the control torque depends upon the magnetic field available (which fluctuates considerably in elliptic orbits), it is desirable to apply control when the magnetic field strength is sufficiently high. However, without an estimator,

the detectable error (roll component) might only be present when the magnetic field strength is low. Thus, without an estimator (which serves as a memory of the error), it could take much longer to drive the system to the null position.

Analysis and simulation showed no advantage of the estimator for offsetting a steady state yaw disturbance torque. But since actual disturbances (see Figs. 3-4 and 3-5) are fluctuating, the advantage is realized. The steady state error due to a constant yaw torque is approximately  $\phi \cong T_x / (Dn)$  where  $T_x$  is the normalized yaw torque.

Other points studied by analog simulation were the effect of putting a sampled signal into the estimator and using the constant parameter  $n$  in the estimator equations rather than a time-variable  $\dot{f} + \dot{q}$ . Comparing a sampled input signal with the continuous estimate of the roll error  $\hat{\theta}$  causes no problem if damping is done solely by nutation damper. But such a mechanization causes the estimates of the rate terms  $\hat{\alpha}_x$  and  $\hat{\alpha}_y$  to have a phase lag behind the actual rates. The lag angle depends upon the speed of sampling. Figures 3-16a, b, show the response of the rates  $\alpha_x$  and  $\hat{\alpha}_x$  when sampling rate is four times per second. It can be seen that damping is poor and finally nonexistent when  $\hat{\alpha}_x$  goes to zero. This problem can be rectified either by sampling  $\hat{\theta}$  before comparing with the input  $\theta$  or by putting a lead angle in the rate damping control signal. If  $\hat{\alpha}_x$  and  $\hat{\alpha}_y$  lag  $\alpha_x$  and  $\alpha_y$  by an angle  $\Delta$ , then the damping control should be

$$\begin{aligned} T_{D_x} &= -K_v (\cos \Delta \hat{\alpha}_x - \sin \Delta \hat{\alpha}_y) \\ T_{D_y} &= -K_v (\sin \Delta \hat{\alpha}_x + \cos \Delta \hat{\alpha}_y) . \end{aligned} \tag{3.38}$$

Figures 3-16c, d show  $\alpha_x$  and  $\hat{\alpha}_x$  using Eq. 3.38 with  $\Delta = 60^\circ$ .

An uneven response was the effect of using a constant  $n$  in the estimator instead of a variable  $\dot{f} + \dot{g}$  (which is available from the horizon sensors) to account for orbital rate. The trajectories followed by the satellite spin axis were highly dependent upon initial conditions in such cases and often resulted in limit cycles about some point near the origin. No evidence of (instability) was seen from this

4 samples/rev with no lead on damping  $\alpha_x$  and  $\hat{\alpha}_x$  -

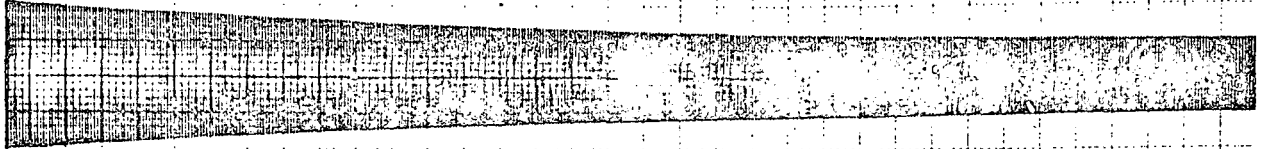


FIG. 3-16a. ACTUAL RATE  $\alpha_x$  - NO LEAD IN CONTROL.  
RATE ONLY PARTIALLY DAMPENS.

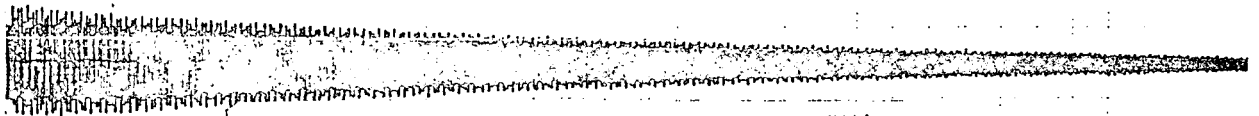


FIG. 3-16b. ESTIMATED RATE  $\alpha_x$  - NO LEAD

FIG. 3-16a and b: SAMPLING EFFECT ON ACTIVE RATE  
DAMPING. SAMPLE RATE: 4 TIMES/  
ROTATION.

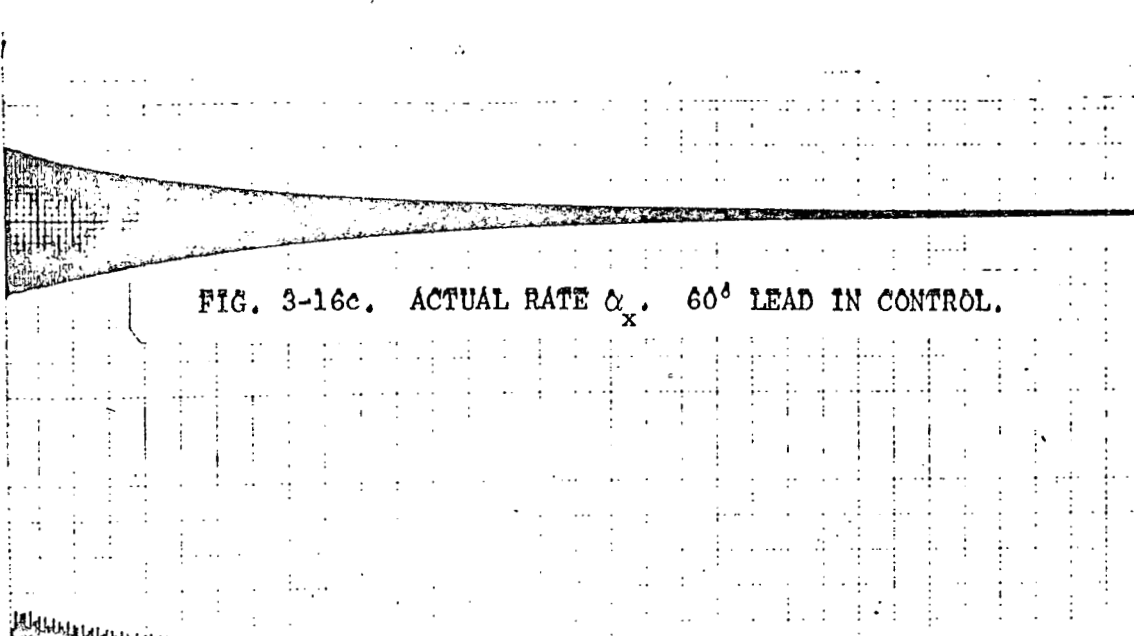


FIG. 3-16c. ACTUAL RATE  $\alpha_x$ .  $60^\circ$  LEAD IN CONTROL.

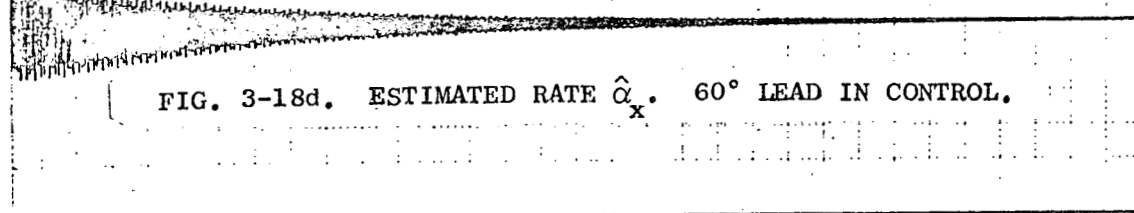


FIG. 3-18d. ESTIMATED RATE  $\hat{\alpha}_x$ .  $60^\circ$  LEAD IN CONTROL.

FIG. 3-16c and d: SAMPLING EFFECT ON ACTIVE RATE  
DAMPING. SAMPLE RATE: 4 TIMES/  
ROTATION.

condition, however.

A final point which required investigation was the performance of the system during Mode 3 spin control. It can be shown that to keep the pointing error as small as possible due to the spin control torque, this torque should be applied over a  $180^\circ$  segment of the orbit. For greatest efficiency, this segment should be centered about the perigee point. To check the spin correction performance of this control and also observe the effect on the pointing error, several digital runs were made with the actual magnetic field and realistic disturbance torques included.

Figure 3.17 is an example of the response of spin speed, roll, and yaw errors during Mode 3 control of a 15 revs/day orbit. For this example, the magnetic moment components are

$$m_x = -10^5 B_y \operatorname{sgn}(\Delta\omega_z)$$

$$m_y = 10^5 B_x \operatorname{sgn}(\Delta\omega_z)$$

$$m_z = 3.5 \times 10^6 (\phi B_x + \theta B_y)$$

measured in Amp - m<sup>2</sup>. The magnetic field components are in Webers/m<sup>2</sup>. The parameters  $d$  and  $D$  were  $0.0126 \text{ sec}^{-1}$  and  $1.5 \text{ sec}^{-1}$ . These runs were based on boundary constants between Modes 1, 2, and 3 of  $C_1 = 0.01 \text{ rad/sec}$  and  $C_2 = 0.02 \text{ rad/sec}$  with nominal spin speed of one rad/sec.

#### B. TRANSLATIONAL CONTROL MECHANIZATION FOR SPINNING SATELLITE

The function of the translational control system is to keep the satellite centered about the proof mass in the presence of disturbing forces. This is accomplished by actuation of gas jets based on an error signal derived from the position of the proof mass with respect to a null point fixed in the satellite. As previously pointed out, spinning the satellite attenuates the problem of placing this null point where there is zero mass attraction of the satellite on the proof

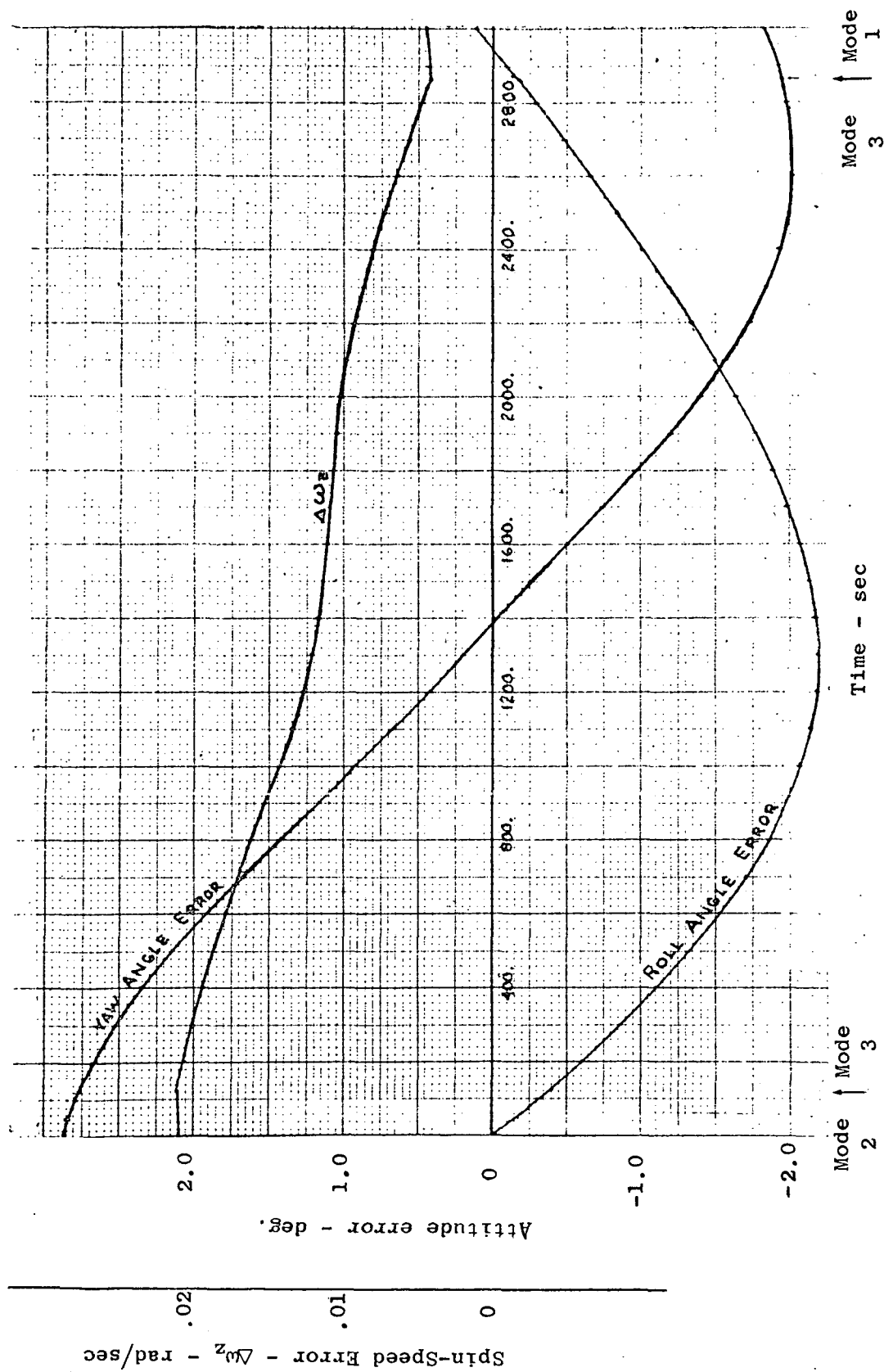


FIG. 3-17. TYPICAL RESPONSE OF SPIN SPEED, ROLL, AND YAW ERRORS DURING MODE 3 CONTROL.



mass. Hence, spinning makes possible improved performance; however, it modifies the mechanization of the translational control. Assuming a linear controller, Lange [Ref. 3-20] showed that a simple correction term can be added to the controller for a non-spinning vehicle to stabilize a spinning vehicle. A practical mechanization of this has been simulated on analog and digital computers and built in our laboratory simulator. Under controlled conditions, this mechanization works very well; however, stringent requirements on the electronic tolerances and the mass-center/null point alignment are necessary to prevent a certain phenomenon which we call "trapping". Accordingly, control mechanizations have been investigated which will alleviate the trapping problem in the simplest way possible.

#### The Trapping Phenomenon

The existing control mechanization for the two-degree-of-freedom laboratory simulator consists of pulse-width pulse-frequency modulators with deadbands and lead compensation in each axis and the  $\vec{\omega} \times \vec{p}$  cross-coupling terms. The deadbands along each body-fixed axis create a square deadspace in a plane. In Fig. 3-18 below, lines of control

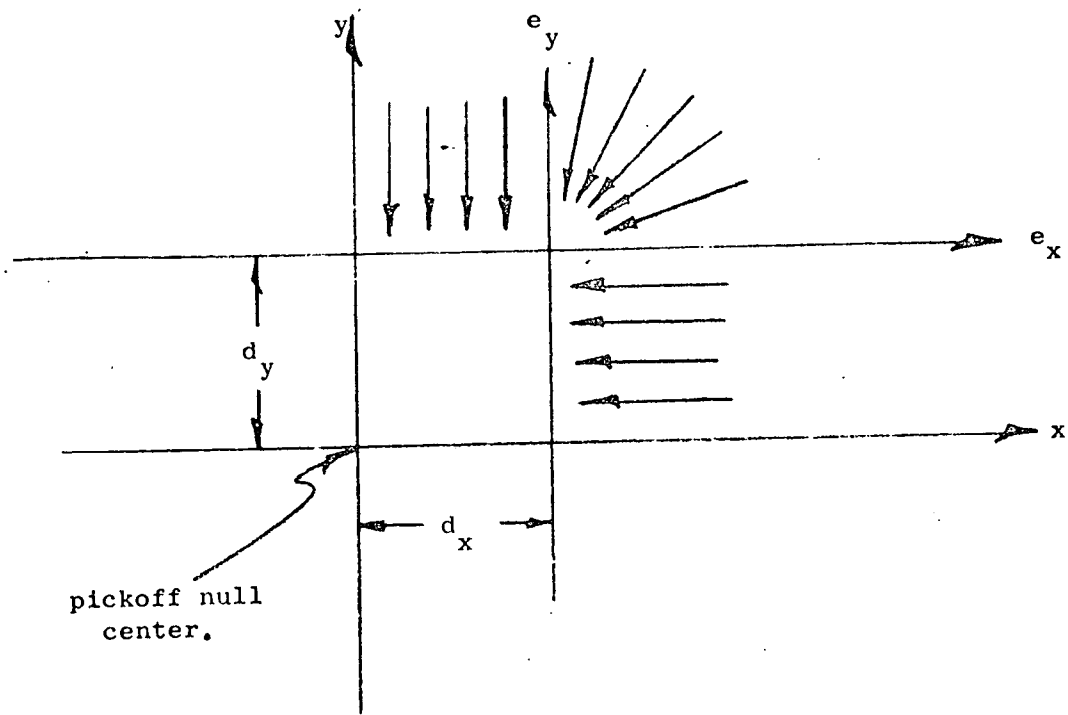


FIG. 3-18. PLANAR DEADSPACE

direction are sketched in the first quadrant around the deadspace. Note that in the vicinity of the deadspace corner, the force is in the wrong direction except on the  $45^\circ$  line (it should point towards the origin). This fact, coupled with small errors in deadspace squareness, cross-coupling terms, or mass-center alignment gives rise to control-force directions sufficiently erroneous to cause the proof mass to become trapped near a deadspace corner. Because the satellite is spinning, the mass center (origin in Fig. 3-18) is describing circles in inertial space. This state is stable and the control force continues with just the right direction and magnitude to balance the centrifugal force of the mass center's circular motion, thus wasting propellant.

The point where the center of the proof mass becomes trapped is readily calculated by assuming the control force is linear after crossing the deadspace threshold. The control law given by Lange [Ref. 3-20] is modified by the square deadspace yielding an expression for the control error signal valid in the shaded region of Fig. 3-18 as follows:

$$e_x = x + \gamma(\dot{x} - \omega y) - d_x \quad (3.39)$$

$$e_y = y + \gamma(\dot{y} + \omega x) - d_y \quad (3.40)$$

where

$$\begin{aligned} \gamma &\triangleq \text{rate gain/position gain} \\ \omega &\triangleq \text{vehicle spin rate} \\ (d_x, d_y) &\triangleq \text{deadband parameters} \end{aligned}$$

The approach taken is to assume the vehicle is in the trapped state (observed experimentally on the laboratory simulator and duplicated on the analog computer) and to look for points which will maintain it. The observed limit cycle consisted of constant values of  $e_x$ ,  $e_y$ ,  $\dot{x}$ , and  $\dot{y}$  with  $\ddot{x} = \ddot{y} = 0$ . Constant  $\dot{x}$  and  $\dot{y}$  imply the center of mass is traversing circles in inertial space if it lies anywhere other than at those values of  $x$  and  $y$ . Maintaining this state requires control action in the direction and magnitude to provide the centrifugal

acceleration of this circular motion.

Assuming the center of mass (c.m.) is located at  $(x_e, y_e)$ , we are looking for a point  $(x, y)$  where

$$1) \frac{e_y}{e_x} = \frac{y - y_e}{x - x_e} \quad (\text{direction requirement})$$

$$2) K_p \sqrt{e_x^2 + e_y^2} = \sqrt{(x - x_e)^2 + (y - y_e)^2} \cdot \omega_a^2 \cdot m_v \quad (\text{magnitude requirement})$$

$K_p$  = control force gain,

$\omega_a$  = actual vehicle rotation rate,

$m_v$  = vehicle mass.

The direction requirement, coupled with equations 3.39 and 3.40 with  $\dot{x} = \dot{y} = 0$ , yield a circular locus of points with center at

$$e_x = e_{xc} = \frac{d_y - \gamma \omega d_x - (\gamma^2 \omega^2 + 1)y_e}{2\omega\gamma} \quad (3.41)$$

$$e_y = e_{yc} = -\frac{d_x + \gamma \omega d_y - (\gamma^2 \omega^2 + 1)x_e}{2\omega\gamma} \quad (3.42)$$

$$\text{and radius} = \sqrt{e_{xc}^2 + e_{yc}^2} \quad (3.43)$$

Similar expressions can be derived for the other three possible quadrants.

Trapping will be maintained at some point on the circle if there is a portion of the circle in the assumed quadrant ( $e_x > 0, e_y > 0$ ), since values of  $K_p$  are typically large enough to satisfy the magnitude requirement. A portion of the circular locus appears in the assumed quadrant when

$$e_{xc} > 0$$

or

$$d_y - \gamma \omega d_x - (\gamma^2 \omega^2 + 1)y_e > 0 \quad (3.44)$$

In the laboratory simulator,  $\gamma \omega = 1$  and with  $x_e = y_e = 0$  and  $d_x = d_y$  (square deadspace) there is no solution. However,  $d_y > d_x$  or  $y_e < 0, x_e = 0$  yield solutions.

The influence of the term  $\gamma\omega$  is interesting:

$\gamma\omega < 1$ : there always exists a trapping solution in some quadrant even with a square deadspace and no center of mass error.

$\gamma\omega > 1$ : the requirement for perfect squareness diminishes. However, the affect of c.m. error is amplified by the factor  $(\gamma^2\omega^2 + 1)/2\gamma\omega$ .

It is also interesting to calculate the c.m. displacement ( $y_e$ ) at which the trapping locus just appears: assume a square deadspace, i.e.,

$$d_x = d_y = d$$

then the locus just appears when

$$d - \gamma\omega d - (\gamma^2\omega^2 + 1)y_e = 0$$

or

(3.45)

$$\frac{y_e}{d} = \frac{1 - \gamma\omega}{\gamma^2\omega^2 + 1}$$

Differentiating this expression with respect to  $\gamma\omega$  and setting equal to zero yields a maximum permissible excursion ( $y_e^*$ ) with a perfect square deadspace

$$\frac{y_e^*}{d} = 0.206$$

for

$$\gamma\omega = 2.4$$

With a circular deadspace, the solution is no longer quadrant dependent, and the locus of possible solutions is again a circle

$$\begin{aligned} \text{center: } x_c &= -\left(\frac{\gamma^2\omega^2 + 1}{2\omega\gamma}\right)y_e \\ y_c &= \left(\frac{\gamma^2\omega^2 + 1}{2\omega\gamma}\right)x_e \end{aligned} \quad (3.46)$$

$$\text{radius: } r = \sqrt{x_c^2 + y_c^2}$$

The requirement for trapping is that the above circle diameter exceed the deadspace radius. Hence, the ratio of allowable center of mass excursion ( $r_{cm}$ ) to deadspace radius  $r_{db}$  is given as

$$\frac{r_{cm}}{r_{db}} = \frac{\omega \gamma}{\omega^2 \gamma^2 + 1} \quad (3.47)$$

Again, the maximum permissible center of mass excursion ( $\Gamma_{cm}^*$ ) is readily calculated

$$\frac{\Gamma_{cm}^*}{r_{db}} = \frac{1}{2}$$

at

(3.48)

$$\gamma \omega = 1$$

Analysis of an octagonal deadspace follows along similar lines as the round and square deadspaces and yields

$$\frac{d_{cm}^*}{d} = 0.45$$

at

(3.49)

$$\gamma \omega = 2$$

## 2. Control Mechanizations Investigated

Basic ideas considered for the elimination or attenuation of the trapping phenomena have centered around modification of the deadspace shape and introduction of state estimation techniques. Desirable properties of estimators include

- (a) noise attenuation,
- (b) ability to estimate c.m. position ( $x_e$ ,  $y_e$ ) and control to it, rather than sensor null.
- (c) high bandwidth enabling simpler modulators.

Susceptibility to trapping is affected by (1) center of mass displacement from the sensor null point ( $x_e$  and  $y_e$ ), and (2) errors in

mechanization of the control law. Results of analysis of the first category (carried out in Section 1 above) are given in Table 3-1. The maximum values of the allowable excursion are tabulated along with the value of  $\gamma\omega$  which produces the maximum. Trapping, however, is not the only consideration in selecting the best value of  $\gamma\omega$  for a control system design. The value of  $\gamma$  (rate gain/position gain) must be compatible with good control system performance in the presence of large disturbing forces and large initial conditions. The angular spin rate ( $\omega$ ) is influenced by attitude control and mass-attraction averaging considerations. These factors may dictate choice of a  $\gamma\omega$  value allowing less c.m. excursion than that tabulated.

Mechanization errors arising from component tolerances and amplifier biases typically cause control signals to be off about 10% of full scale or about 20% of the deadband. This translates roughly one to one into an equivalent c.m. excursion, hence, a system could be on the verge of trapping from mechanization errors alone if a square deadspace was used.

Table 3-1 also indicates relative complexities of the systems without compensation or estimator. The primary factor making systems ① and ④ simple compared to other schemes is the square deadspace. Overall system complexity is a strong function of the estimator configuration which will be discussed next.

### 3. State Estimation Techniques.

If a dynamical system is thought to obey the set of system equations

$$\dot{\mathbf{x}} = \mathbf{F}\mathbf{x} + \mathbf{G}\mathbf{u}$$

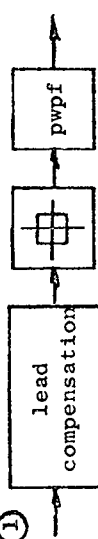
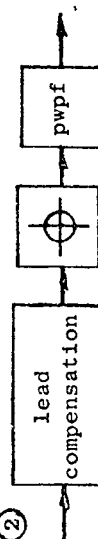
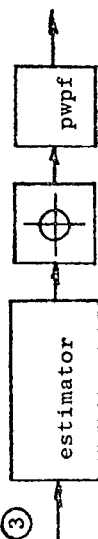
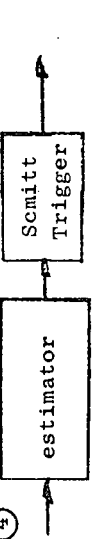
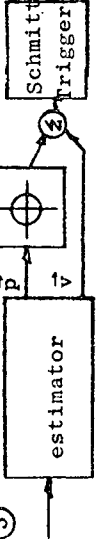
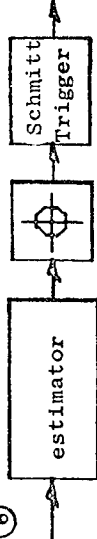
where

$\mathbf{x} \triangleq$  state vector,

$\left. \begin{matrix} \mathbf{F} \\ \mathbf{G} \end{matrix} \right\} \triangleq$  constant matrices,

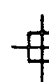
$\mathbf{u} \triangleq$  known control vector,

TABLE 3-1. SUMMARY OF MECHANIZATIONS INVESTIGATED

DESCRIPTION	TRAPPING SUSCEPTIBILITY		COMPLEXITY (ignoring lead compensation or estimator)	REMARKS
	allowable c.m. excursion at optimum $\gamma\omega$ (deadband units)	optimum $\gamma\omega$		
① 	0.2	2	simpler	former laboratory simulator mechanization.
② 	0.5	1	most complex	being built on laboratory simulator.
③ 	0.5	1	most complex	
④ 	0.2	2	simplest	rotating equivalent of derived rate modulator when 2-state estimator used.
⑤ 	0.5	1	less complex	
⑥ 	0.45	2	less complex	

DEFINITIONS:

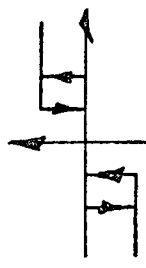
p-w p-f  $\Delta$  pulse-width pulse-frequency modulator


  $\Delta$  square deadspace

  $\Delta$  circular deadspace

$\vec{p}$   $\Delta$  position of mass center with respect to proof mass

$\dot{\vec{v}}$   $\Delta$  time rate of change of  $\vec{p}$  in an inertial frame.

 Schmitt Trigger  $\Delta$

  $\Delta$  octagonal deadspace  
 $\gamma\omega \Delta \left( \frac{\text{rate gain}}{\text{position gain}} \right)$  (angular rotation rate)

an "estimator" or "observer" for this system is

$$\dot{\hat{x}} = F\hat{x} + Gu + K(y - H\hat{x}) \quad (3.50)$$

where

- $\hat{x} \triangleq$  estimated state vector
- $K \triangleq$  constant estimator gain matrix
- $y \triangleq$  measurement vector
- $H \triangleq$  constant matrix.

When the measurement vector is also a state, the estimated state vector need not include these states and Eq. 3.50 is somewhat modified. This is sometimes referred to as a "reduced state observer" or "minimal-order observer". Recent references covering the theory of these state estimation techniques are Ref. 3-21 and 3-22.

The normalized translational equations of planar motion of a rotating body in body coordinates may be written

$$\begin{bmatrix} \dot{x} \\ \dot{y} \\ \dot{v}_x \\ \dot{v}_y \end{bmatrix} = \begin{bmatrix} 0 & 0 & 1 & 0 \\ 0 & 0 & 0 & 1 \\ \omega^2 & 0 & 0 & +2\omega \\ 0 & \omega^2 & -2\omega & 0 \end{bmatrix} \begin{bmatrix} x \\ y \\ v_x \\ v_y \end{bmatrix} + \begin{bmatrix} 0 & 0 \\ 0 & 0 \\ 1 & 0 \\ 0 & 1 \end{bmatrix} \begin{bmatrix} f_x^c \\ f_y^c \end{bmatrix} + \begin{bmatrix} 0 \\ 0 \\ f_x^d - \omega^2 x_e \\ f_y^d - \omega^2 y_e \end{bmatrix} \quad (3.51)$$

where

- $x, y \triangleq$  position of mass center with respect to inertial space,
- $v_x, v_y \triangleq$  time rate of change of position,
- $f_x^c, f_y^c \triangleq$  control accelerations,
- $\omega \triangleq$  spin rate,
- $f_x^d, f_y^d \triangleq$  disturbance accelerations,
- $x_e, y_e \triangleq$  center of mass displacement.



If we assume

(a) disturbances and c.m. displacement negligible ( $f_x^d - \omega^2 x_e = 0$ , etc.)

(b)  $x, y$  are measured directly,

then, one of the most simple examples of an estimator is example (b) in Table 3-2.

$$\begin{bmatrix} \dot{\hat{x}} \\ \dot{\hat{y}} \\ \dot{\hat{v}}_x \\ \dot{\hat{v}}_y \end{bmatrix} = \begin{bmatrix} 0 & 0 & 1 & 0 \\ 0 & 0 & 0 & 1 \\ \omega^2 & 0 & 0 & 2\omega \\ 0 & \omega^2 & -2\omega & 0 \end{bmatrix} \begin{bmatrix} \hat{x} \\ \hat{y} \\ \hat{v}_x \\ \hat{v}_y \end{bmatrix} + \begin{bmatrix} 0 \\ 0 \\ f_x^c \\ f_y^c \end{bmatrix} + \begin{bmatrix} K_{11} & K_{12} \\ K_{21} & K_{22} \\ K_{31} & K_{32} \\ K_{41} & K_{42} \end{bmatrix} \begin{bmatrix} x - \hat{x} \\ y - \hat{y} \end{bmatrix}. \quad (3.52)$$

If  $f^d$  and c.m. displacement are not negligible, errors will be present in the estimate of the states ( $\hat{x}$  and  $\hat{v}$ ). If these errors are not acceptable or if we desire knowledge of the unknown quantities, then the state vector is augmented with these errors as constants to be estimated. The estimator equations then become (example (e) in Table 3-2)

$$\begin{bmatrix} \dot{\hat{x}} \\ \dot{\hat{y}} \\ \dot{\hat{v}}_x \\ \dot{\hat{v}}_y \\ \dot{\hat{x}}_e \\ \dot{\hat{y}}_e \end{bmatrix} = \begin{bmatrix} 0 & 0 & 1 & 0 & 0 & 0 \\ 0 & 0 & 0 & 1 & 0 & 0 \\ \omega^2 & 0 & 0 & 2\omega & -\omega^2 & 0 \\ 0 & \omega^2 & -2\omega & 0 & 0 & -\omega^2 \\ 0 & 0 & 0 & 0 & 0 & 0 \\ 0 & 0 & 0 & 0 & 0 & 0 \end{bmatrix} \begin{bmatrix} \hat{x} \\ \hat{y} \\ \hat{v}_x \\ \hat{v}_y \\ \hat{x}_e \\ \hat{y}_e \end{bmatrix} + \begin{bmatrix} 0 \\ 0 \\ f_x^c \\ f_y^c \\ 0 \\ 0 \end{bmatrix} + \begin{bmatrix} K \\ K \\ K \\ K \\ 0 \\ 0 \end{bmatrix} \begin{bmatrix} x - \hat{x} \\ y - \hat{y} \\ x - \hat{x} \\ y - \hat{y} \end{bmatrix}. \quad (3.53)$$

A reduced state estimator with a revised state formulation can also be mechanized for this system. If we define

TABLE 3-2.  
COMPENSATION/ESTIMATOR SUMMARY

Description	Noise Rejection	Electronic Tolerance Requirements	C.M. Tolerance Requirements	Number of Operational Amplifier
(a) lead compensa- tion	bad	best	see Table 3-1	2
(b) 4-state (x, v) estimator	best	good	see Table 3-1	6
(c) 2-state (v) estimator (reduced state)	good	bad	see Table 1	4
(d) 4-state (v, c.m.) estimator (reduced state)	good	bad	best	8
(e) 6-state (x, v, c.m.) estimator	best	good	best	8

$$\left. \begin{aligned} v_x &\triangleq \dot{x} - \omega y \\ v_y &\triangleq \dot{y} + \omega x \end{aligned} \right\} \text{inertial velocity in body coordinates,}$$

then the equations of motion are

$$\begin{bmatrix} \dot{x} \\ \dot{y} \\ \dot{v}_x \\ \dot{v}_y \end{bmatrix} = \begin{bmatrix} 0 & \omega & 1 & 0 \\ -\omega & 0 & 0 & 1 \\ 0 & 0 & 0 & \omega \\ 0 & 0 & -\omega & 0 \end{bmatrix} \begin{bmatrix} x \\ y \\ v_x \\ v_y \end{bmatrix} + \begin{bmatrix} 0 & 0 \\ 0 & 0 \\ 1 & 0 \\ 0 & 1 \end{bmatrix} \begin{bmatrix} f_x \\ f_y \end{bmatrix} \quad (3.54)$$

The system matrix of Eq. 3.54 is partitioned as shown in line with the states being directly observed. This defines the following submatrices:

$$\begin{aligned} F_{11} &\triangleq \begin{bmatrix} 0 & \omega \\ -\omega & 0 \end{bmatrix} \\ F_{12} &\triangleq \begin{bmatrix} 1 & 0 \\ 0 & 1 \end{bmatrix} \\ F_{22} &\triangleq \begin{bmatrix} 0 & \omega \\ -\omega & 0 \end{bmatrix} \\ G_2 &\triangleq \begin{bmatrix} 1 & 0 \\ 0 & 1 \end{bmatrix} \end{aligned} \quad L \triangleq \begin{bmatrix} K_{11} & K_{12} \\ K_{21} & K_{22} \end{bmatrix} \quad \begin{array}{l} \text{estimator gain} \\ \text{matrix} \end{array}$$

and the reduced state estimator in block diagram form coupled with a simple pulse modulator is as shown in Fig. 3-19.

This estimator/modulator configuration is the rotating vehicle equivalent of the derived rate controller in common use today [Ref. 3-23].

Other estimator forms considered include variations of the state definitions as well as the number of states being estimated. In addition,

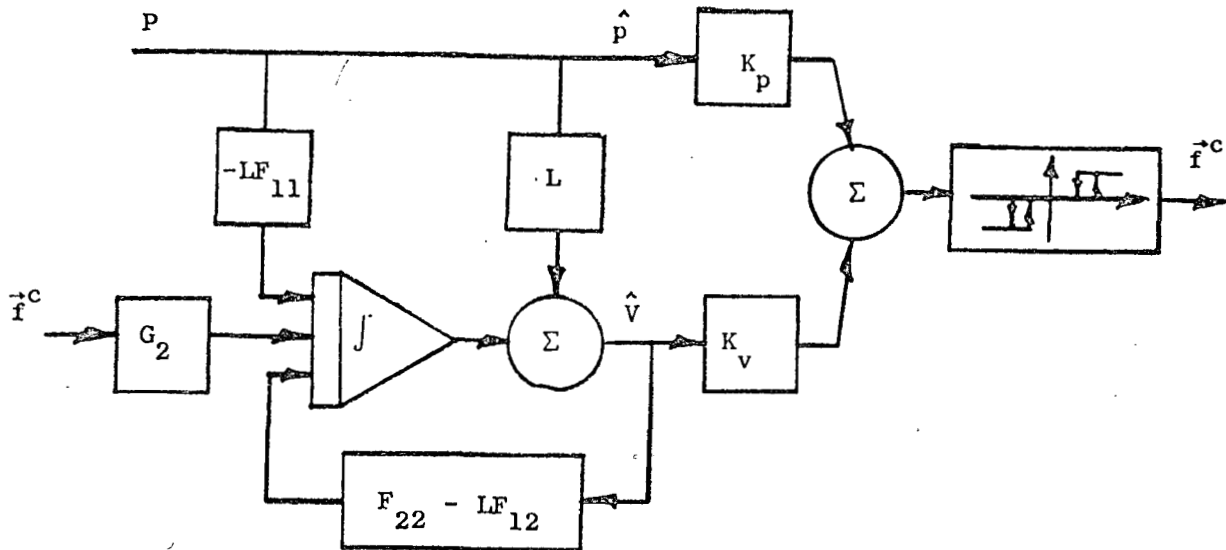


FIG. 3-19. ROTATING VEHICLE DERIVED RATE CONTROLLER

various mechanizations are possible for a given estimator form. For example, the subtraction of  $(x - \hat{x})$  and  $(y - \hat{y})$  in full state estimators (e.g. Eqs., 3.53 and 3.54) can be performed in a separate amplifier or in each integrator of the system. A vector block diagram illustrating this mechanization difference is given in Fig. 3-20, a and b.

Results of the analysis of the different forms and mechanizations can be summarized as follows:

- (1) State redefinition so that the error signal is a state:
  - (a) reduces errors due to component tolerance
  - (b) reduces number of amplifiers required;
- (2) Mechanizing extra amplifiers for computing the difference between measured quantities and estimated quantities in full state estimators substantially reduces errors due to component tolerances;
- (3) Reduced state estimators are inherently sensitive to component tolerances because the step suggested in (2) above is not possible.

Table 3-2 summarizes some of the characteristics of various estimator forms and lead compensation. All the estimator forms share a common characteristic response to a control pulse. The control signal is

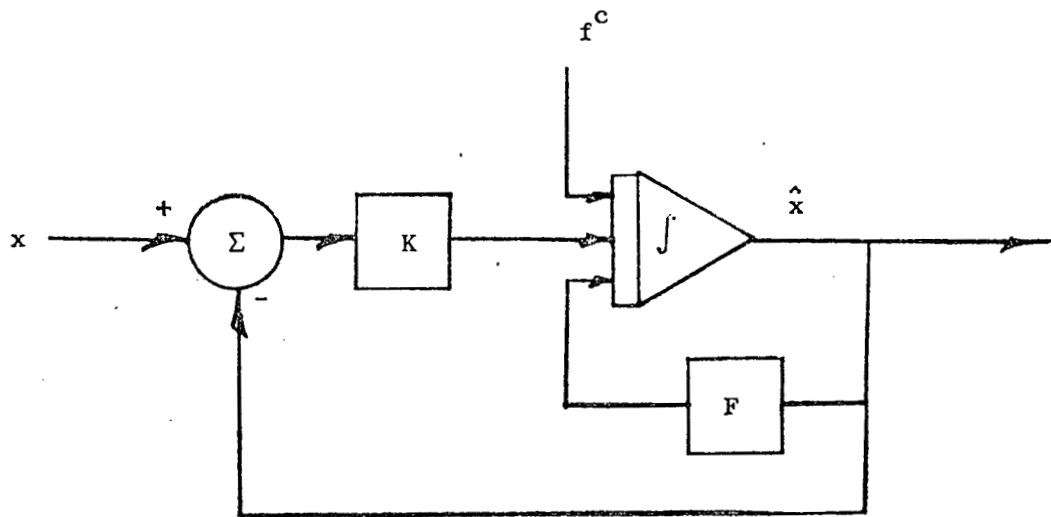


FIG. 3-20a: ESTIMATOR WITH SUMMATION AMPLIFIER

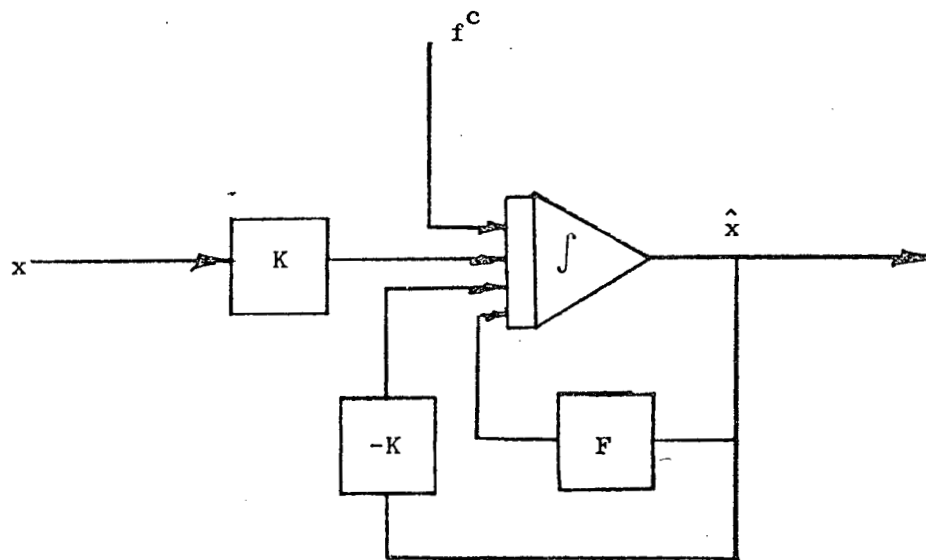


FIG. 3-20b: ESTIMATOR WITHOUT SUMMATION AMPLIFIER

fed into a velocity state integrator essentially duplicating the response of the actual dynamical system. Thus, one could say the bandwidth of the response to a control pulse is infinite. This is fundamentally different from lead compensation which relies on sensing a change in velocity from observed position data. This high bandwidth to control pulses allows use of simpler modulators with estimators.

#### 4. Conclusions

Utilization of a square deadspace appears marginal even with perfect c.m. location, eliminating schemes with square deadspace (1) and (4) in Table 3-1.

Two desirable characteristics of the estimators are (1) noise rejection, and (2) ability to estimate c.m. location and control to it, rather than to sensor null, thus relaxing the requirement of physical control of the c.m. location.

If an estimator is required, systems utilizing the high bandwidth to simplify the modulator appear to be the logical choice (schemes (5) and (6) over (3) in Table 3-1). Although lead compensation may be adequate from a noise and c.m. standpoint, its selection over a simple estimator form (such as (b) or (c) in Table 3-2) is not immediate. The additional complexity in the modulator required when using lead compensation is balanced by the additional complexity of the estimator. This choice essentially reduces to pulse-width pulse-frequency or "rotating derived rate". Unlike  $1/s^2$  plants, where the derived rate is clearly the simpler controller, the rotating plant requires additional complexity in the estimator making the choice an even one.

Mechanization of a system with circular deadbands, lead compensation, and a p-w p-f modulator (scheme (2) in Table 3-1) on our laboratory simulator is nearing completion. This should allow verification of our analog and digital simulations of the system. In addition, a six-state estimator (Form (e) in Table 3-2) is being built for substitution in place of the lead compensation (thus producing scheme (3) in Table 3-1). This will provide laboratory verification of the estimator concept.

### C. INTERACTION BETWEEN TRANSLATIONAL CONTROL AND GRAVITY STABILIZED ATTITUDE MOTION

This section gives attention to the analysis of a phenomenon which can occur with a drag-free gravity-stabilized vehicle. This situation could arise, for example, if the currently planned GEOS-C geodesy satellite was to be made drag-free by the addition of an "add-on drag-free device". The phenomenon is the possibility of attitude instability as a result of coupling (or interaction) between the translational control system and the gravity stabilized attitude motion.

If the pickoff null and satellite mass center are not coincident, the pickoff interprets attitude motion of the satellite about the mass center as a change in the position of the proof mass, and the control actuators are commanded accordingly to null out this position change. If the actuators can exert a moment about the satellite mass center, then there is the possibility that attitude motion itself can generate attitude torques in such a way that the system is unstable.

#### 1. Nonlinear Equations of Motion.

Consider a rigid, gravity-stabilized Drag-Free Satellite to which there is applied a collection of translational control forces,  $\Sigma \bar{F}_j$ , where the subscript  $j$  denotes the  $j^{\text{th}}$  control actuator. If  $\bar{R}_{c-pm}$  denotes the position vector of the satellite composite mass center (c) with respect to the proof mass (pm) [Fig. 3-21], we can then write

$$\frac{d^2}{dt^2} \bar{R}_{c-pm} = \frac{1}{m_t} \left[ \bar{F}_G + \Sigma \bar{F}_j \right] - \frac{1}{m_{pm}} \bar{F}^{pm}_G + \frac{1}{m_t} \bar{F}_D . \quad (3.55)$$

In Eq. 3.55,  $\bar{F}_G$  and  $\bar{F}^{pm}_G$ , denote respectively, the gravitational forces acting on the satellite body and on the proof mass.  $\bar{F}_D$  is the collection of external disturbance forces on the satellite, and  $m_t$  and  $m_{pm}$  denote respectively the masses of the satellite and proof mass.

For the relative acceleration between the satellite's mass center, c, and the proof mass, pm, due to the gravitational forces, one has

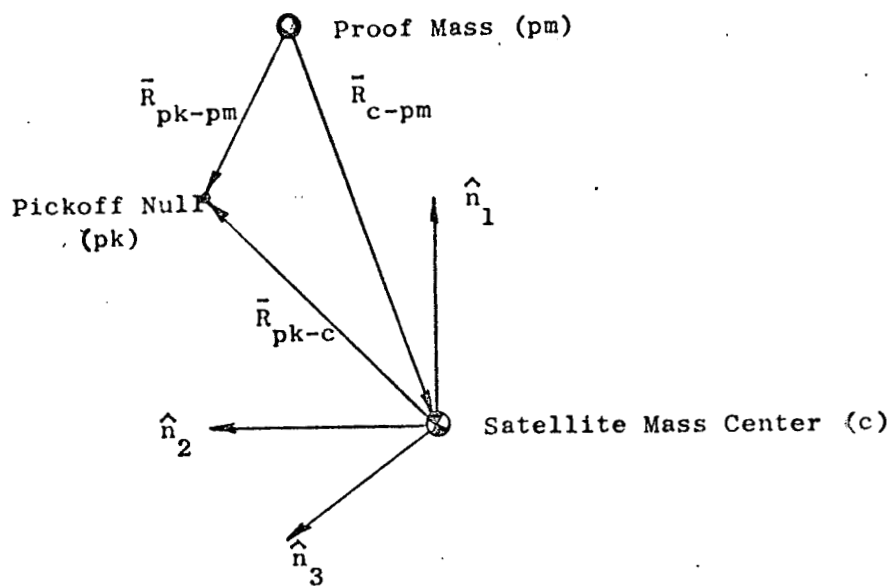


FIG. 3-21: GEOMETRY OF THE PICKOFF NULL, SATELLITE MASS CENTER, AND PROOF MASS.



$$\begin{aligned}
\frac{\bar{F}_G}{m_t} - \frac{\bar{F}_G^{pm}}{m_{pm}} &= -\frac{Gm_\oplus}{R_c^3} \bar{R}_c + \frac{Gm_\oplus}{R_{pm}^3} \bar{R}_{pm} \\
&= \omega_o^2 \bar{R}_{pm} \left[ \frac{R_c^3}{R_{pm}^3} - 1 \right] - \omega_o^2 \bar{R}_{c-pm}
\end{aligned}$$

where  $m_\oplus$  denotes the mass of the earth, and  $\omega_o$  is the (constant) orbital angular velocity of  $c$  about the earth.

$$\frac{\bar{F}_G}{m_t} - \frac{\bar{F}_G^{pm}}{m_{pm}} \approx -\omega_o^2 \bar{R}_{c-pm} \cdot \left[ \hat{1} - 3 \frac{\hat{R}_{pm} \hat{R}_{pm}}{R_{pm}^2} \right] \quad (3.56)$$

where  $\hat{1}$  denotes the unit diadic and  $\hat{R}_{pm}$  is the unit vector in the direction of  $\bar{R}_{pm}$  ( $\hat{R}_{pm} \triangleq \bar{R}_{pm}/R_{pm}$ ).

To write the scalar equations of motion of the Satellite, let  $\{\hat{\theta}\} = (\hat{\theta}_1, \hat{\theta}_2, \hat{\theta}_3)$  be a set of reference orthogonal unit vectors centered at [Fig. 3-22];  $\hat{\theta}_1$  is the unit vector in the direction from the earth's mass center to  $c$ ,  $\hat{\theta}_3$  is the unit vector in the direction of the orbital angular velocity  $\bar{\omega}_o$ , and  $\hat{\theta}_2$  is such that  $\hat{\theta}_2 = \hat{\theta}_3 \times \hat{\theta}_1$ .  $\{\hat{\theta}\}$  is rotating in space with angular velocity  $\bar{\omega}_o = \omega_o \hat{\theta}_3$ . Let  $\{\hat{N}\} = (\hat{n}_1, \hat{n}_2, \hat{n}_3)$  be a set of orthogonal unit vectors centered at  $c$  and fixed in the satellite. The orientation of  $\{\hat{N}\}$  is such that it is coincident, at any instant of time, with the principal inertia axes of the satellite.

Any orientation of the satellite with respect to the reference frame  $\{\hat{\theta}\}$  is obtained by aligning  $\{\hat{N}\}$  with  $\{\hat{\theta}\}$  and then performing three successive right-hand Euler rotations as shown in Fig. 3-22:  $\hat{\theta}_1$  about the axis aligned with  $\hat{n}_1$ ,  $\hat{\theta}_2$  about the new direction of the axis aligned with  $\hat{n}_2$ , and  $\theta_3$  about the final direction of the axis aligned with  $\hat{n}_3$ . This set of rotations produces the so-called nonclassical Euler angles.

The relation between the unit vectors  $\hat{\theta}_i$  and  $\hat{n}_i$  ( $i = 1, 2, 3$ ) can be immediately obtained as

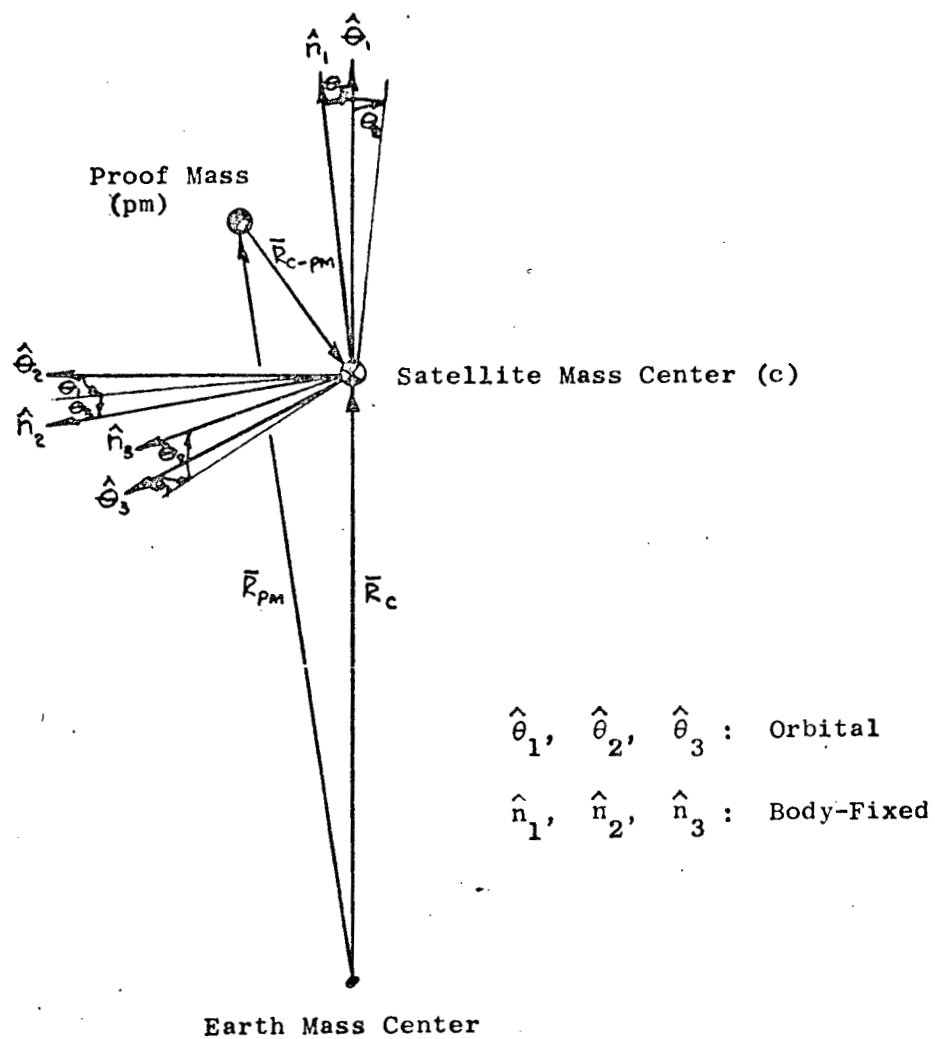


FIG. 3-22: GEOMETRY OF THE ORBITAL AND BODY-FIXED REFERENCE FRAMES.

$$\begin{bmatrix} \hat{\theta}_1 \\ \hat{\theta}_2 \\ \hat{\theta}_3 \end{bmatrix} = \begin{bmatrix} \cos\theta_2 \cos\theta_3 & -\cos\theta_2 \sin\theta_3 & \sin\theta_2 \\ \cos\theta_1 \sin\theta_3 + \sin\theta_1 \sin\theta_2 \cos\theta_3 & \cos\theta_1 \cos\theta_3 - \sin\theta_1 \sin\theta_2 \sin\theta_3 & -\sin\theta_1 \cos\theta_2 \\ \sin\theta_1 \sin\theta_3 - \cos\theta_1 \sin\theta_2 \cos\theta_3 & \sin\theta_1 \cos\theta_3 + \cos\theta_1 \sin\theta_2 \sin\theta_3 & \cos\theta_1 \cos\theta_2 \end{bmatrix} \times \\
\times \begin{bmatrix} \hat{n}_1 \\ \hat{n}_2 \\ \hat{n}_3 \end{bmatrix} \triangleq c \begin{bmatrix} \hat{n}_1 \\ \hat{n}_2 \\ \hat{n}_3 \end{bmatrix} \quad (3.57)$$

By noticing that

$$\left. \begin{aligned} \bar{R}_{c-pm} &\triangleq x\hat{\theta}_1 + y\hat{\theta}_2 + z\hat{\theta}_3 \\ \bar{F}_j &\triangleq f_{j1}\hat{n}_1 + f_{j2}\hat{n}_2 + f_{j3}\hat{n}_3 \end{aligned} \right\} \quad (3.58)$$

and by expressing the left hand side of Eq. 3.54 in the coordinate system  $\{\hat{\theta}\}$ , the three following scalar equations describing the translation motion of  $c$  with respect to proof mass in the absence of external disturbances,  $\bar{F}_D$ , are obtained

$$\begin{aligned} m_t [\ddot{X} - 2\omega_o \dot{Y} - 3\omega_o^2 X] &= \sum [f_{j1} \cos\theta_3 - f_{j2} \sin\theta_3] \cos\theta_2 + f_{j3} \sin\theta_2 \\ m_t [\ddot{Y} + 2\omega_o \dot{X}] &= \sum [f_{j1} (\sin\theta_3 \cos\theta_2 + \cos\theta_3 \sin\theta_2 \sin\theta_1) + f_{j2} (\sin\theta_3 \sin\theta_2 \sin\theta_1 - \cos\theta_3 \cos\theta_1) \\ &\quad - f_{j3} \cos\theta_2 \sin\theta_1] \\ m_t [\ddot{Z} + \omega_o^2 Z] &= \sum [f_{j1} (\sin\theta_3 \sin\theta_1 - \cos\theta_3 \sin\theta_2 \cos\theta_1) + f_{j2} (\sin\theta_3 \sin\theta_2 \cos\theta_1 + \cos\theta_3 \sin\theta_1) \\ &\quad + f_{j3} \cos\theta_2 \cos\theta_1] . \end{aligned} \quad (3.59)$$

If  $\bar{r}_j (= r_{j1}\hat{n}_1 + r_{j2}\hat{n}_2 + r_{j3}\hat{n}_3)$  denotes the vector from the  $j^{\text{th}}$  translational control actuator to  $c$ , the moment  $\bar{T}_j$  about  $c$ , due to  $\bar{F}_j$ , is then

$$\bar{T}_j = \bar{r}_j \times \bar{F}_j = (r_{j2}^F r_{j3}^F - r_{j3}^F r_{j2}^F) \hat{n}_1 + (r_{j3}^F r_{j1}^F - r_{j1}^F r_{j3}^F) \hat{n}_2 + (r_{j1}^F r_{j2}^F - r_{j2}^F r_{j1}^F) \hat{n}_3$$

$$\Delta \equiv T_{j1} \hat{n}_1 + T_{j2} \hat{n}_2 + T_{j3} \hat{n}_3 \quad (3.60)$$

If  $I_1$ ,  $I_2$ , and  $I_3$  are the three principal moments of inertia of the satellite (excluding the proof mass, which never touches the satellite), application of the angular momentum principle gives the three following equations, describing the rotational motion of the vehicle about c

$$\begin{aligned} I_1 \dot{\omega}_1 + [(I_3 - I_2) \omega_3 + h] \omega_2 &= 3\omega_o^2 (I_2 - I_3) \sin\theta_2 \cos\theta_2 \sin\theta_3 + \sum T_{j1} \\ I_2 \dot{\omega}_2 + [(I_1 - I_3) \omega_3 - h] \omega_1 &= 3\omega_o^2 (I_1 - I_3) \sin\theta_2 \cos\theta_2 \cos\theta_3 + \sum T_{j2} \\ I_3 \dot{\omega}_3 + (I_2 - I_1) \omega_1 \omega_2 &= 3\omega_o^2 (I_1 - I_2) \cos^2\theta_2 \sin\theta_3 \cos\theta_3 + \sum T_{j3} \end{aligned} \quad (3.61)$$

In Eq. 3.61,  $\omega_1$ ,  $\omega_2$ , and  $\omega_3$  are the three measure numbers of the components of the angular velocity of the satellite (with respect to inertial space), expressed in  $\{\hat{N}\}$ , and  $\bar{h}$  is the constant angular momentum (with respect to the satellite body) of a yaw coupling rotor connected to the satellite in such a way that  $\bar{h} = h\hat{n}_3$ .

The expressions for  $\omega_i$  in terms of the attitude angles  $\theta_i$  ( $i = 1, 2, 3$ ) are

$$\begin{aligned} \omega_1 &= (\dot{\theta}_2 + \omega_o \sin\theta_1) \sin\theta_3 + (\dot{\theta}_1 \cos\theta_2 - \omega_o \cos\theta_1 \sin\theta_2) \cos\theta_3 \\ \omega_2 &= (\dot{\theta}_2 + \omega_o \sin\theta_1) \cos\theta_3 - (\dot{\theta}_1 \cos\theta_2 - \omega_o \cos\theta_1 \sin\theta_2) \sin\theta_3 \\ \omega_3 &= \dot{\theta}_3 + \dot{\theta}_1 \sin\theta_2 + \omega_o \cos\theta_1 \cos\theta_2 \end{aligned} \quad (3.62)$$

## 2. Measured Quantities, Control Forces, and Torques.

The quantities sensed by the proof mass position sensors are the three measure numbers of the components of the vector from the "pickoff null" (pk) to the proof mass (pm). Let  $g_1$ ,  $g_2$ , and  $g_3$  denote the three measured quantities (i.e.,  $\bar{r}_{pk-pm} = g_1 \hat{n}_1 + g_2 \hat{n}_2 + g_3 \hat{n}_3$ ) and

$\epsilon_1$ ,  $\epsilon_2$ , and  $\epsilon_3$  the three measure numbers of the components of  $\bar{R}_{pk-c}$  expressed in  $\{\hat{N}\}$ . Then

$$\bar{R}_{pk-pm} = \bar{R}_{pk-c} + \bar{R}_{c-pm}$$

and it follows that

$$\begin{bmatrix} g_1 \\ g_2 \\ g_3 \end{bmatrix} = \begin{bmatrix} \epsilon_1 \\ \epsilon_2 \\ \epsilon_3 \end{bmatrix} + C^T \begin{bmatrix} X \\ Y \\ Z \end{bmatrix} \quad (3.63)$$

where the superscript  $T$  denotes matrix transposition. The quantities  $\epsilon_1$ ,  $\epsilon_2$ , and  $\epsilon_3$  can be thought of as bias in the pickoff signal due to non-coincidence of the pickoff null and the vehicle mass center.

The three measure numbers  $f_{ji}$  ( $i = 1, 2, 3$ ) of the control force applied to the satellite by the  $j$ th control actuator are assumed, for purposes here, to be linear functions of the sensed quantities and their rates.

$$\Sigma f_{ji} = -(k_p g_i + k_v \dot{g}_i) \quad (3.64)$$

where  $k_p$  and  $k_v$  are "position" and "rate" gain constants respectively.

For the measure numbers of the control torque,  $\Sigma T_j$ , a linear relationship is assumed of the form

$$\begin{bmatrix} \Sigma T_{j1} \\ \Sigma T_{j2} \\ \Sigma T_{j3} \end{bmatrix} = L \begin{bmatrix} \Sigma f_{j1} \\ \Sigma f_{j2} \\ \Sigma f_{j3} \end{bmatrix} \quad (3.65)$$

where  $L$  is a constant  $3 \times 3$  matrix of effective force moment arms about the satellite mass center,  $c$ , and is generally non-zero due to errors in alignment and physical constraints on placement of actuators.

### 3. Equilibrium Orientations and Positions

To determine equilibrium solutions of Eq. 3.59 and 3.61, assume

$$\begin{aligned}
 \theta_i &= \text{constant} \triangleq \theta_{ie} \quad (i = 1, 2, 3) \\
 X &= \text{constant} \triangleq X_e \\
 Y &= \text{constant} \triangleq Y_e \\
 Z &= \text{constant} \triangleq Z_e
 \end{aligned}
 \tag{3.66}$$

By substituting Eq. 3.66 into Eq. 3.59 and 3.61, and by assuming that all quantities in Eq. 3.66 are "small" (so that products of small quantities in Eq. 3.59 and Eq. 3.61 may be dropped), yields the equilibrium solution

$$\begin{aligned}
 \theta_{1e} &= \theta_{2e} = \theta_{3e} = 0 \\
 X_e &= -\epsilon_1 \\
 Y_e &= -\epsilon_2 \\
 Z_e &= -\epsilon_3
 \end{aligned}
 \tag{3.67}$$

Also assumed in this solution is that  $|k_p| \gg 3\omega_o^2 m_t$ , (i.e., the translational control natural frequency is very much higher than orbital frequency) a condition actually satisfied in practice.

Equations 3.67 simply state that in equilibrium, without external disturbing forces, the proof mass is coincident with the pickoff null and the body principal axes are aligned with the orbital reference frame.

#### 4. Stability

To a first approximation, the measured quantities  $g_i$  ( $i = 1, 2, 3$ ) can be expressed, from Eq. 3.63, as

$$\begin{bmatrix} g_1 \\ g_2 \\ g_3 \end{bmatrix} \approx \begin{bmatrix} X_s \\ Y_s \\ Z_s \end{bmatrix} + \begin{bmatrix} 0 & \epsilon_3 & -\epsilon_2 \\ -\epsilon_3 & 0 & \epsilon_1 \\ \epsilon_2 & -\epsilon_1 & 0 \end{bmatrix} \begin{bmatrix} \theta_{1s} \\ \theta_{2s} \\ \theta_{3s} \end{bmatrix} \quad (3.68)$$

where the subscript  $s$  denotes a perturbation from the equilibrium solution.

Assuming that there are two translational control actuators for each axis of the satellite, mounted in opposition to each other, the matrix  $L$  can be written as

$$L = \begin{bmatrix} 0 & -l_3 & l_2 \\ l_3 & 0 & -l_1 \\ -l_2 & l_1 & 0 \end{bmatrix} \quad (3.69)$$

Linearizing Eqs. 3.59 and 3.61 about the equilibrium solution given in Eq. 3.67, and writing the result in the Laplace transform domain (leaving out initial conditions) after taking into consideration that  $|k_p| \gg 3\omega_o^2 m_t$ , the following equations of motion are obtained

3

$$\begin{bmatrix}
 I_1 s^2 + (I_3 - I_2) \omega_o^2 + h \omega_o + (k_p + sk_v)(l_2 \epsilon_2 + l_3 \epsilon_3) & [(I_3 - I_1 - I_2) \omega_o^2 + h \omega_o] s + -(k_p + sk_v) l_3 \epsilon_1 \\
 [(I_1 + I_2 - I_3) \omega_o - h] \omega_o s + - (k_p + sk_v) l_1 \epsilon_2 & I_2 s^2 - [4(I_1 - I_3) \omega_o - h] \omega_o + -(k_p + sk_v) l_3 \epsilon_2 \\
 -(k_p + sk_v) l_1 \epsilon_3 & -(k_p + sk_v) l_2 \epsilon_3 \\
 & I_3 s^2 + 3 \omega_o^2 (I_2 - I_1) + (k_p + sk_v)(l_1 \epsilon_1 + l_2 \epsilon_2)
 \end{bmatrix}
 \begin{bmatrix}
 \theta_{1s} \\
 \theta_{2s} \\
 \theta_{3s}
 \end{bmatrix}
 +
 \begin{bmatrix}
 0 \\
 0 \\
 0
 \end{bmatrix}
 =
 \begin{bmatrix}
 0 \\
 0 \\
 0
 \end{bmatrix}
 \quad (3.71)$$

and

$$\begin{bmatrix}
 m_t s^2 + sk_v + k_p & -2 \omega_o m_s & 0 \\
 2 \omega_o m_s & m_t s^2 + sk_v + k_p & 0 \\
 0 & 0 & m_t s^2 + sk_v + k_p
 \end{bmatrix}
 \begin{bmatrix}
 X_s \\
 Y_s \\
 Z_s
 \end{bmatrix}
 =
 -(k_p + sk_v)
 \begin{bmatrix}
 0 & \epsilon_3 & -\epsilon_2 \\
 -\epsilon_3 & 0 & \epsilon_1 \\
 \epsilon_2 & -\epsilon_1 & 0
 \end{bmatrix}
 \begin{bmatrix}
 \theta_{1s} \\
 \theta_{2s} \\
 \theta_{3s}
 \end{bmatrix}
 \quad (3.72)$$



Equations 3.71 and 3.72 represent the full six-degree-of-freedom system for small motion about the equilibrium solutions given in Eqs. 3.67. It is obvious from the equations that the parameters  $\epsilon_1, \epsilon_2, \epsilon_3$  (pickoff null offsets from the satellite mass center) and  $\ell_1, \ell_2, \ell_3$  (effective moment arms of the control actuators about the satellite mass center) cause coupling between the equations of translation and attitude. The stability of these equations as a function of these parameters is the primary interest here.

To simplify the analysis initially, assume that  $\epsilon_3$  and  $\ell_3$  are zero and investigate stability of the motion in the plane of the orbit. The equations for this may be written

$$\begin{aligned} & \left[ I_3 s^2 + 2\xi_G \omega_G I_3 s + 3\omega_o^2 (I_2 - I_1) + (k_p + sk_v)(\ell_1 \epsilon_1 + \ell_2 \epsilon_2) \right] \theta_{3s} + \\ & + (k_p + sk_v) (\ell_1 Y_s - \ell_2 X_s) = 0 ; \end{aligned} \quad (3.73)$$

$$\begin{aligned} & (m_t s^2 + sk_v + k_p) X_s - (2\omega_o m_t s) Y_s - \left[ \epsilon_2 (k_p + sk_v) \right] \theta_{3s} = 0; \\ & (m_t s^2 + sk_v + k_p) Y_s + (2\omega_o m_t s) X_s + \left[ \epsilon_1 (k_p + sk_v) \right] \theta_{3s} = 0. \end{aligned}$$

The characteristic equation of this set of equations can be approximated very closely by the equation

$$1 + \frac{K(p + k)p \left[ p(p^2 + \frac{r^2}{k}p + r^2) - G(\frac{r^2}{k}p + r^2) \right]}{\left( p^2 + \frac{r^2}{k}p + r^2 \right)^2 (p^2 + 2\xi_G p + 1)} = 0 \quad (3.74)$$

where  $K \triangleq \frac{k_v(\ell_1 \epsilon_1 + \ell_2 \epsilon_2)}{I_3 \omega_G}$

$$\omega_G \triangleq \omega_o \left[ \frac{3(I_2 - I_1)}{I_3} \right]^{1/2}$$

$$r \triangleq \frac{\sqrt{k_p/m_t}}{\omega_G}$$

$$k \triangleq \frac{k_p}{k_v \omega_G}$$

$$p \triangleq \omega_G s$$

$$G \triangleq 2 \frac{\omega_0}{\omega_G} \frac{(\ell_1 \epsilon_2 - \ell_2 \epsilon_1)}{(\ell_1 \epsilon_1 + \ell_2 \epsilon_2)}$$

The parameter  $\xi_\theta$  has been included in Eqs. 3.73 and 3.74 to account for some rate-dependent damping of the gravity stabilized attitude librations. This damping was not included explicitly in the original equations because the form in which it enters the equations is so dependent on mechanization.

Viewing the characteristic Eq. 3.14 as a function of two parameters,  $K$ , and  $G$ , it is possible to sketch the loci of the roots as a function of  $K$  while holding  $G$  constant. There are, of course, six poles for the loci, four corresponding to the  $X$  and  $Y$  translational mode with normalized undamped natural frequency of  $r = \sqrt{k_p/m_t}/\omega_G$ , and two corresponding to the gravity stabilized pitch attitude with normalized natural frequency of 1. There are five zeros for the loci, one on the negative real axis at  $-k$ , two very near the translational mode roots (the exact location depends on  $G$ ), and two very near the origin on the real axis.

Fig. 3-23 is a plot of the roots of the system calculated directly from Eqs. 3.73 (not the approximate characteristic equation, Eq. 3.74) for the parameter values indicated in the figure. Since realistic values of the frequency ratio  $r$  are around 100, it is necessary to show the loci with two different scalings, a macro-view to illustrate the behavior of the roots of the translational mode and a micro-view to observe the behavior of the gravity stabilized roots very near the origin. For the case illustrated ( $G > 0$ ) it is seen that the loci cross the real axis relatively quickly for values of  $K > 0$ , but that for  $K < 0$ , the system is stable until relatively large negative values of  $K$  are reached. A similar loci plot for  $G < 0$  would show that the zero on the real axis near  $+2$  moves to the left-half plane and the loci again cross the imaginary axis for relatively small values of  $K$ , this time for  $K < 0$ .

To obtain an analytical relationship among the four parameters  $\epsilon_1$ ,  $\epsilon_2$ ,  $\ell_1$ , and  $\ell_2$  and system stability, the Routhian array may be constructed from the approximate characteristic equation, Eq. 3.74, and conditions for imaginary axis crossover deduced from this. This yields the stability criterion,

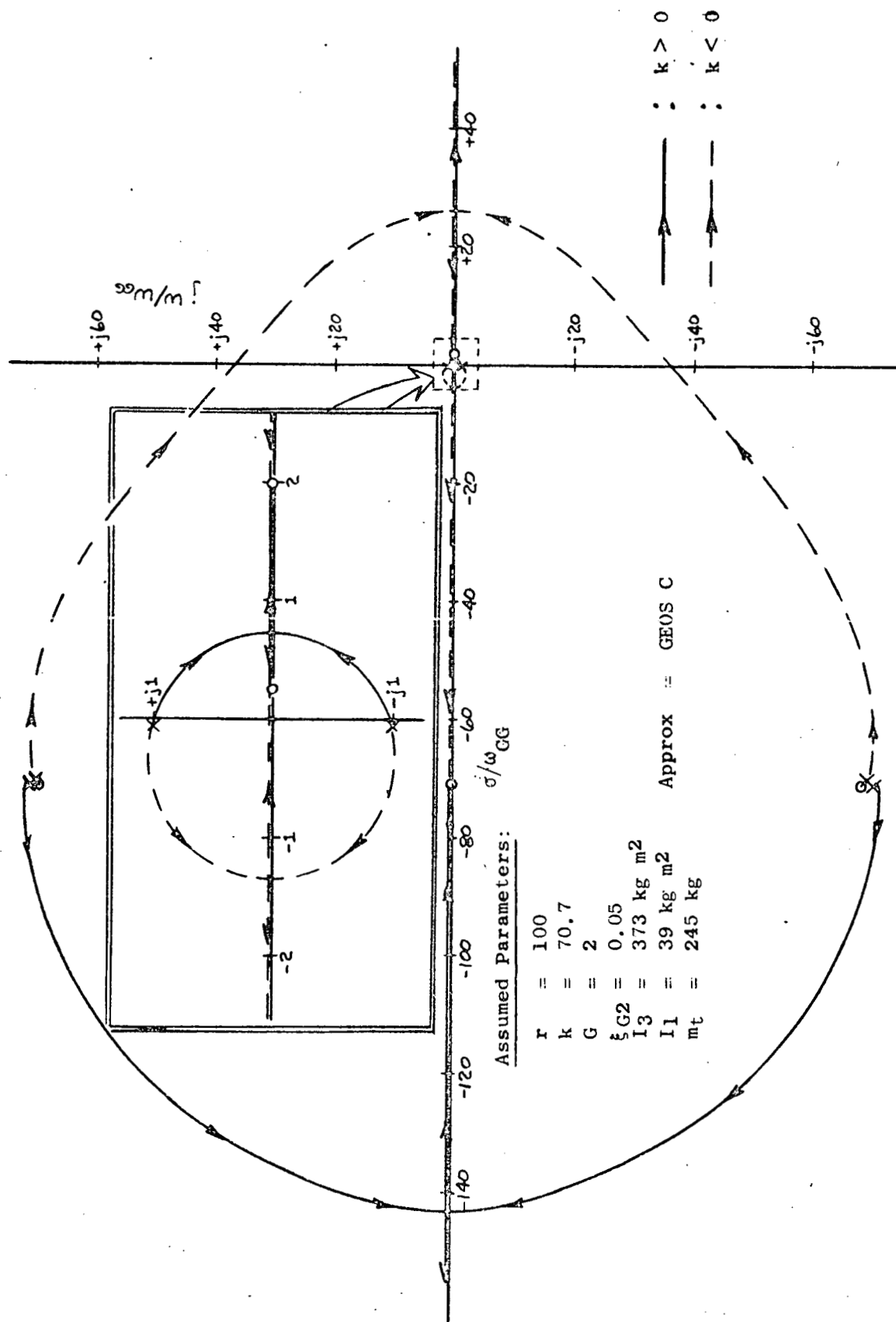


FIG. 3-23. ROOT LOCI AS A FUNCTION OF  $k$  FOR TRANSLATIONAL AND ATTITUDE MOTION IN THE PLANE OF THE ORBIT ( $G$  held constant).

$$(\ell_1 \epsilon_2 - \ell_2 \epsilon_1) < \frac{\xi_G \sqrt{3I_3(I_2 - I_1)}}{m_t} \quad (3.75)$$

for

$$\left| \sqrt{\frac{I_3}{3(I_2 - I_1)}} \frac{(\ell_1 \epsilon_2 - \ell_2 \epsilon_1)}{(\ell_1 \epsilon_1 + \ell_2 \epsilon_2)} \right| \ll k .$$

This relationship governs the imaginary axis crossover for the loci originating at the gravity stabilized poles and is the primary constraint on specification of the allowable values of pickoff null offset ( $\epsilon_1$  and  $\epsilon_2$ ) and control actuator moment arms ( $\ell_1$  and  $\ell_2$ ). From Eq. 3.75 using approximate GEOS-C parameters

$$(\ell_1 \epsilon_2 - \ell_2 \epsilon_1) < 0.125$$

( $\ell_1, \ell_2, \epsilon_1, \epsilon_2$  in meters) for stability. This agrees very well with values obtained from the calculations of the roots of Eq. 3.73 used in plotting the loci of Fig. 3-23.

Even though one must be careful not to violate Eq. 3.75 in the vehicle design, this requirement does not seem to be a difficult design constraint. For example, with  $\epsilon_1 = \pm 1$  cm, and  $\epsilon_2 = \pm 1$  cm, we can safely have  $\ell_1$  and  $\ell_2 = \pm 1$  meter for  $\xi_G = 0.05$ .

The question of stability in roll-yaw and the effect of non-zero  $\epsilon_3$  and  $\ell_3$  has yet to be fully investigated, but considerations as above are expected to yield similar results: tolerances on pickoff null to mass center and control actuator moment arm specifications which are quite comfortable from the design point-of-view.

### CHAPTER III: REFERENCES

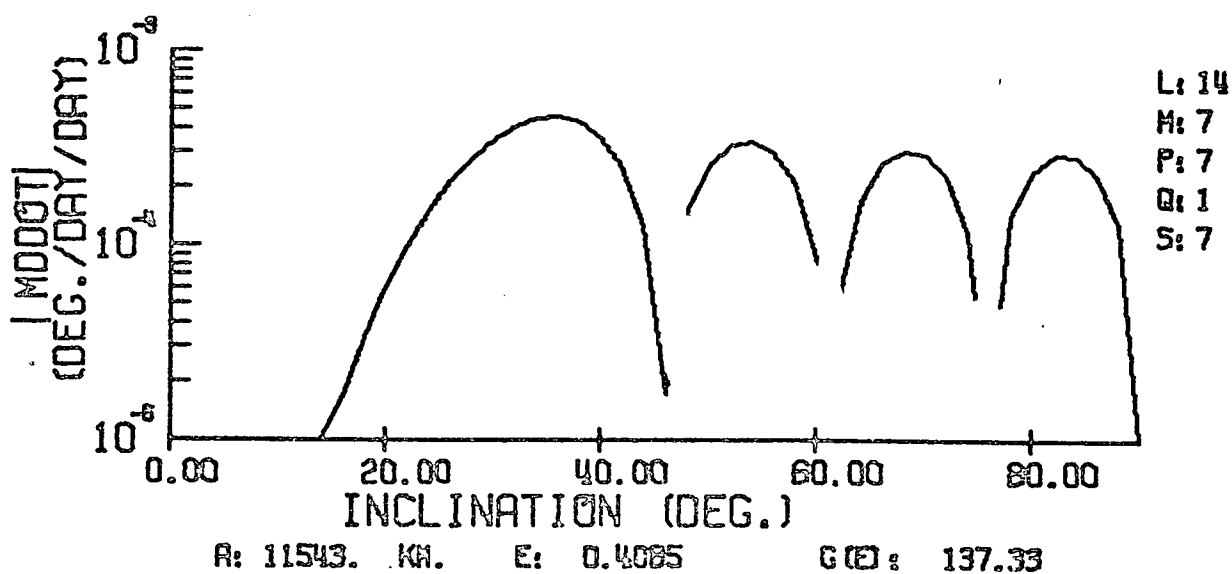
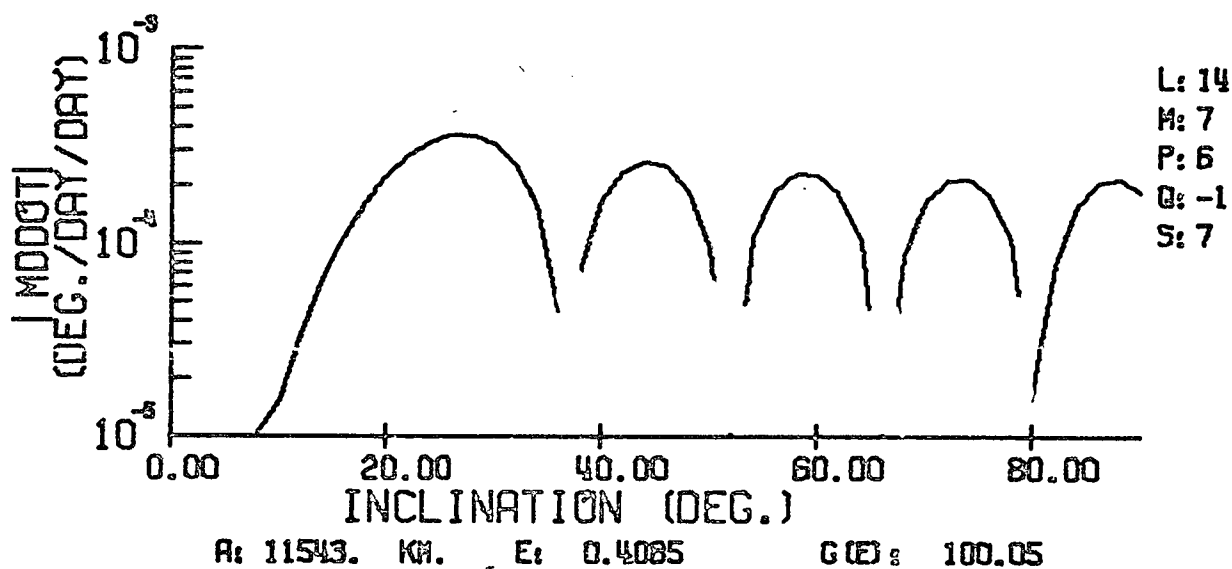
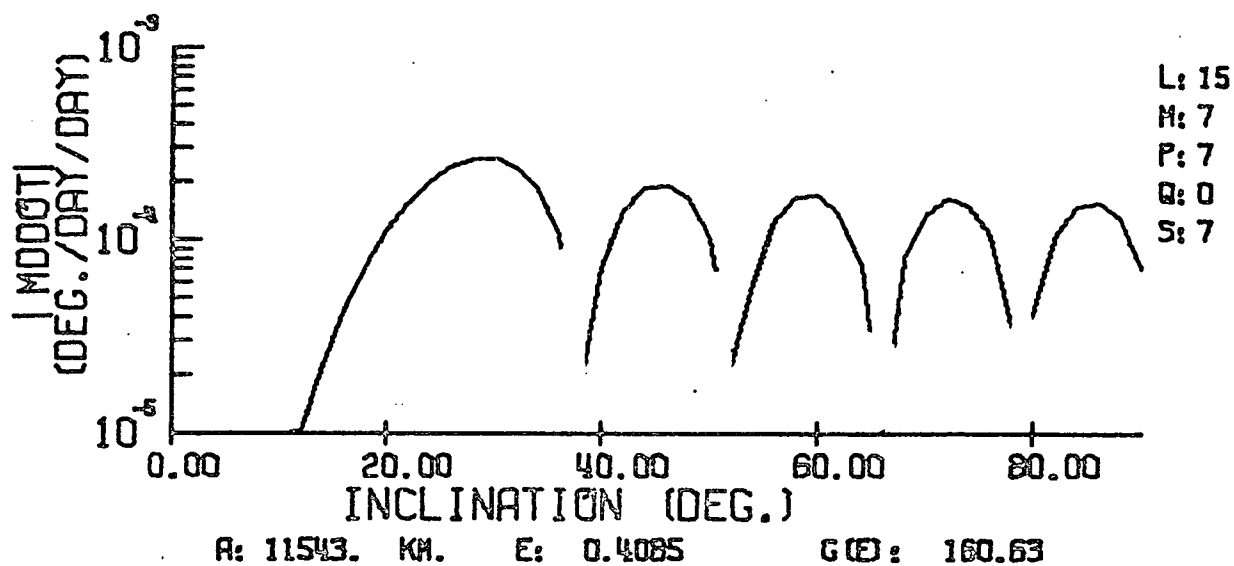
- 3-1. "Proposal To Develop and Operate a Sustaining Earth Satellite in Two Orbital Flights," submitted to NASA by Stanford University, February 1966 (with addendum dated Sept. 1966).
- 3-2. Yu, E.Y., "Spin Decay, Spin Precession Damping and Spin Axis Drift of the Telstar Satellite," The Bell System Technical Journal, vol. XLII, no. 5, Sept. 1963.
- 3-3. Bhuta, P.G., and Koval, E.R., "A Viscous Ring Damper for a Freely Precessing Satellite," Int. J Mech Sci., vol. 8, 1966.
- 3-4. Spencer, T.M., "Cantilevered-mass Nutation Damper for a Dual-Spin Spacecraft," Proc. of the Symposium on Attitude Stabilization and Control of Dual-Spin Spacecraft, Aerospace Report No. TR-0158(3307-01)-16, Aerospace Corp., El Segundo, Calif., Nov. 1967.
- 3-5. Schamberg, R., "A New Analytical Representation of Surface Interaction for Hyperthermal Free Molecule Flow with Application to Neutral-Particle Drag Estimates of Satellites," RM-2313, The Rand Corporation, Santa Monica, Calif., 1959.
- 3-6. Moe, K., "Recent Experimental Evidence Bearing on Satellite Drag Coefficients," AIAA J., vol 6, no. 7, July 1968.
- 3-7. King-Hele, D.G., "The Rotational Speed of the Upper Atmosphere Determined from Changes in Satellite Orbits," Space Research V, (King-Hele, D.G., Muller, P., and Righini, G., editors), North Holland Publishing Co., Amsterdam, 1965.
- 3-8. Jacchia, L.G., "Static Diffusion Models of the Upper Atmosphere with Empirical Temperature Profiles," Smithsonian Contributions to Astrophysics, vol. 8, no. 9, Smithsonian Institution Astrophysical Observatory, Washington, D.C., 1965.
- 3-9. Keating, G.M., and Prior, E.J., "Latitude and Seasonal Variations in Atmospheric Densities Obtained during Low Solar Activity by Means of the Inflatable Air Density Satellite," Space Research VII, vol. 2, (Smith-Rose, R.L., and King, J.W., editors), North Holland Publishing Co., Amsterdam, 1967.
- 3-10. Evans, W.J., "Aerodynamic and Radiation Disturbance Torques on Satellites Having Complex Geometry," Torques and Attitude Sensing in Earth Satellites, (S.F. Singer, editor), Academic Press, New York, 1964.
- 3-11. Smith, G.L., "A Theoretical Study of the Torques Induced by a Magnetic Field on Rotating Cylinders and Spinning Thin-Wall Cones, Cone Frustums, and General Body of Revolution," NASA TR-129, Washington, D.C., 1962.

### CHAPTER III REFERENCES (Cont)

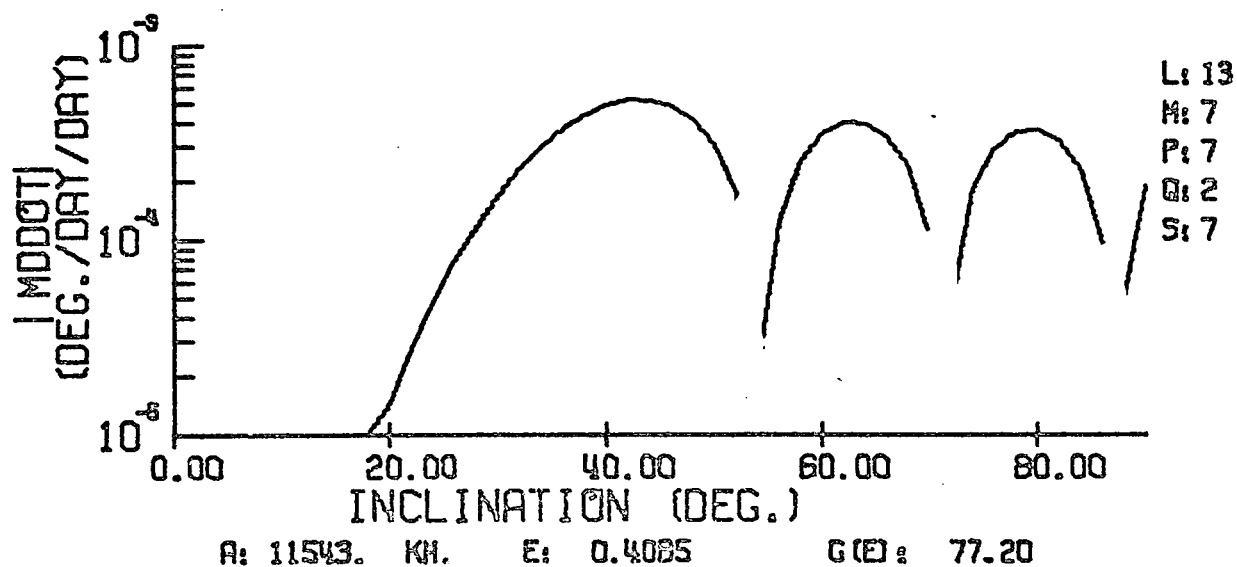
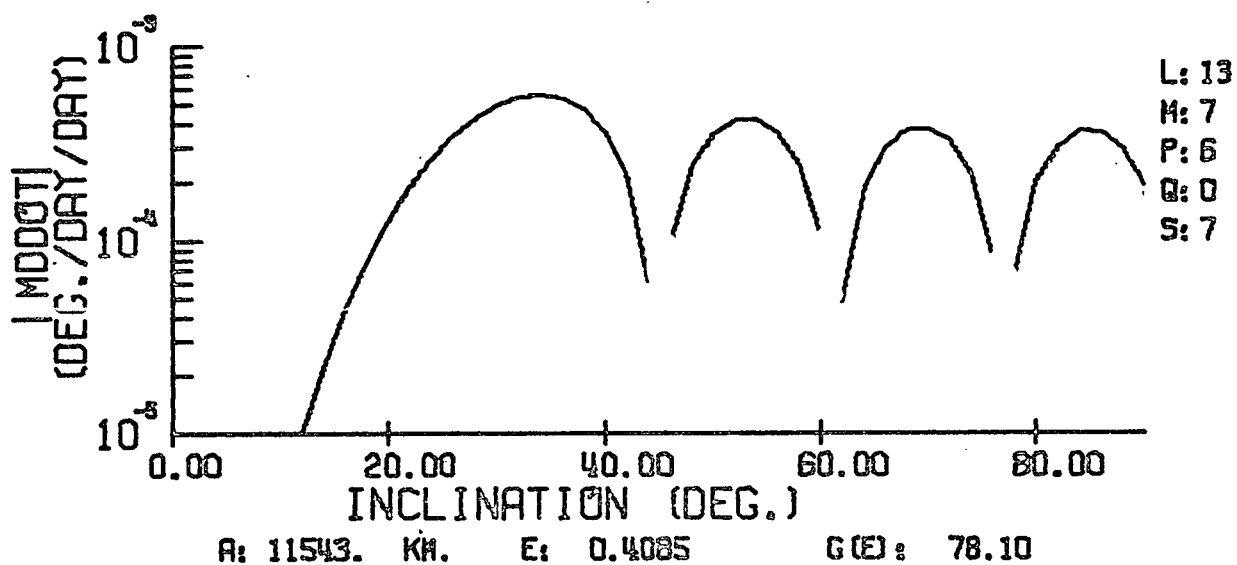
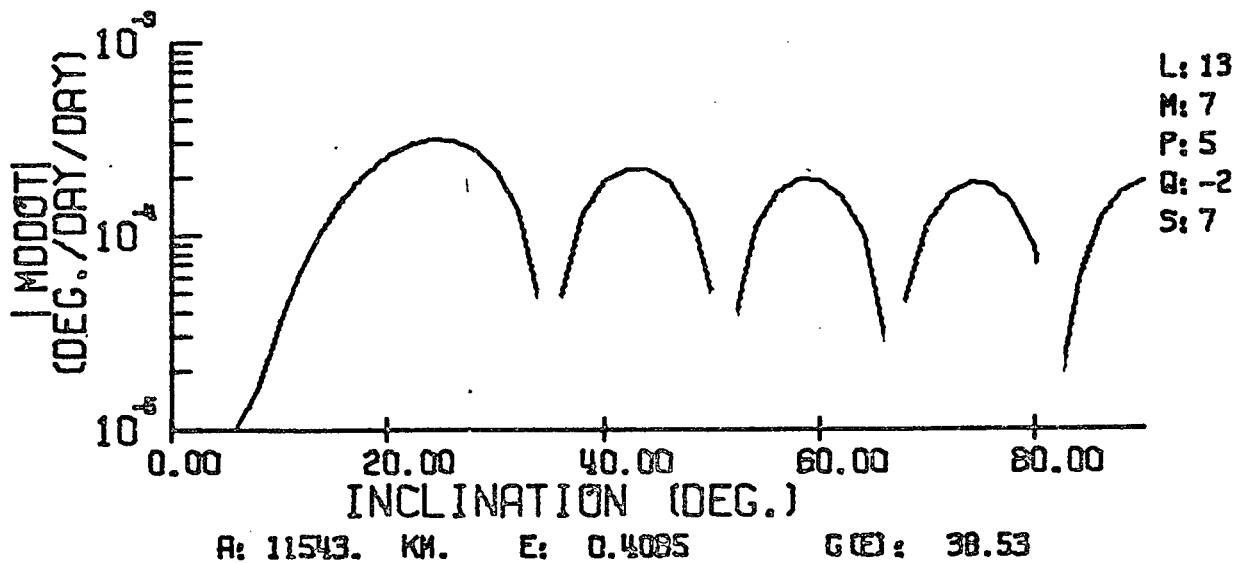
- 3-12. Chapman, S. and Bartels, J., Geomagnetism, vol. 2, Oxford University Press, London, 1940.
- 3-13. Hendricks, S.J., and Cain, J.C., "Magnetic Field Data for Trapped-Particle Evaluations," J. of Geophysical Res., vol. 71, no. 1, Jan. 1966.
- 3-14. Kalman, R.E., and Bucy, R.S., "New Results in Linear Filtering and Prediction Theory," J. of Basic Engineering, 83D, March 1961.
- 3-15. White, J.S., Shigemoto, F.H., and Bourquin, K., "Satellite Attitude Control Utilizing the Earth's Magnetic Field," NASA TN D-1068, Washington, D.C., Aug. 1961.
- 3-16. Marshall, S.V., "An Analytical Model for the Fluxgate Magnetometer," IEEE Transactions on Magnetics, vol. MAG-3, no. 3, Sept. 1967.
- 3-17. Bryson, A.E., Jr. and Ho, Y.C., Applied Optimal Control, Blaisdell Publishing Co., Waltham, Mass., 1968.
- 3-18. Sonnabend, D., "A Magnetic Control System for an Earth-Pointing Satellite," Proc. of the Symposium on Attitude Stabilization and Control of Dual-Spin Spacecraft, Aerospace Rept. No. TR-0158(3307-01)-16, Aerospace Corp., El Segundo, California, Nov. 1967.
- 3-19. Sorensen, J.A., "Precision Magnetic Attitude Control of Spinning Spacecraft," to be published as SUDAAR 380, Dept. of Aeronautics And Astronautics, Stanford University, Stanford, Calif., 1969.
- 3-20. Lange, B.O., "The Control and Use of Drag-Free Satellites," Ph.D. Dissertation, Dept. of Electrical Engineering, Stanford University, Stanford, Calif., June 1964, published also as SUDAER 194.
- 3-21. Gopinath, B. and B.O. Lange, "On the Identification and Control of Linear Systems," Ph.D Dissertation, Dept. of Aeronautics and Astronautics, Stanford University, Stanford, Calif., Jun 1968, SUDAAR No. 351.
- 3-22. Singer, R., "The Design & Synthesis of Linear Multivariable Systems With Application to State Estimation," Stanford Electronics Laboratory, Stanford University, Stanford, Calif., Jun 1968, SEL No. 68-030.
- 3-23. Scott, E.D., "Pseudo-Rate Sawtooth-Pulse Reset Control System Analysis and Design," 1966 AIAA Guidance and Control Conference, Seattle, Washington, Aug. 1966.

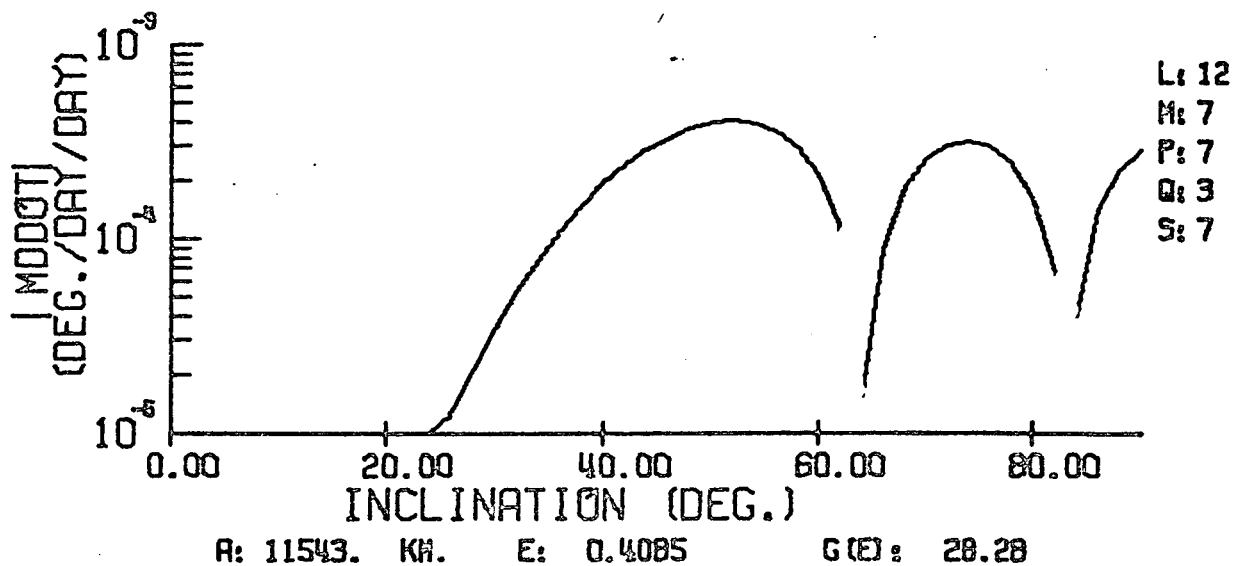
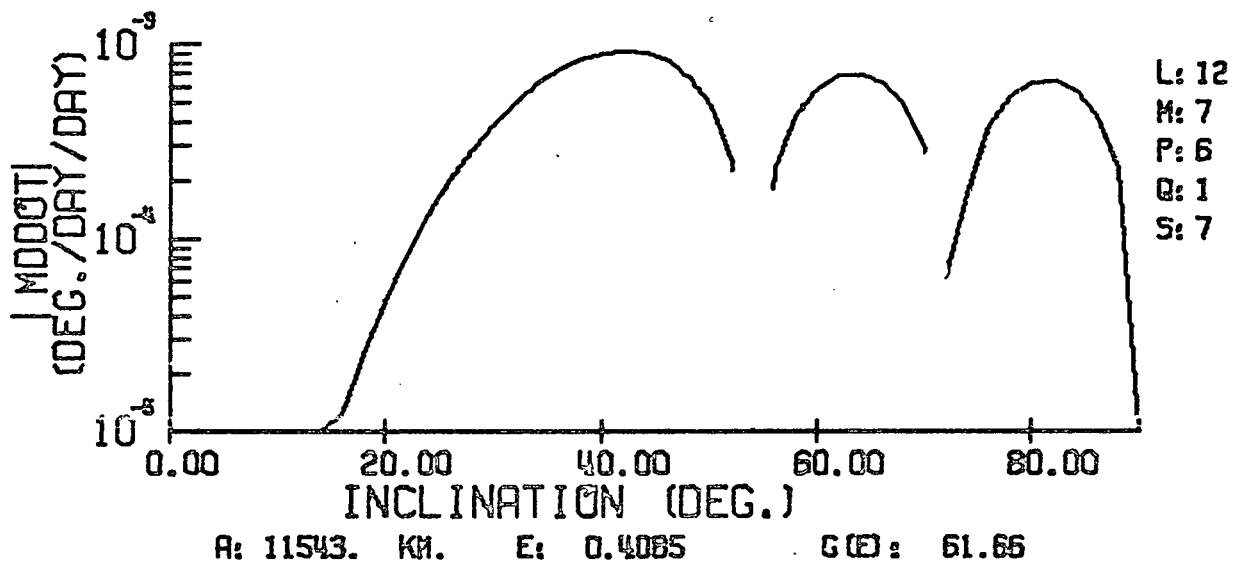
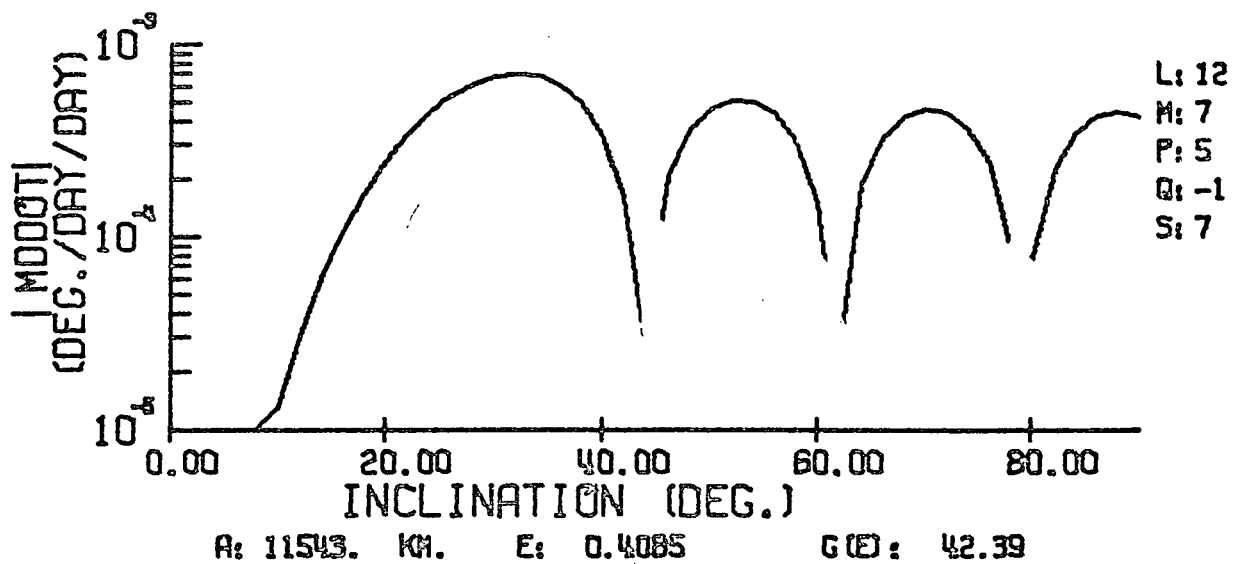
## APPENDIX A

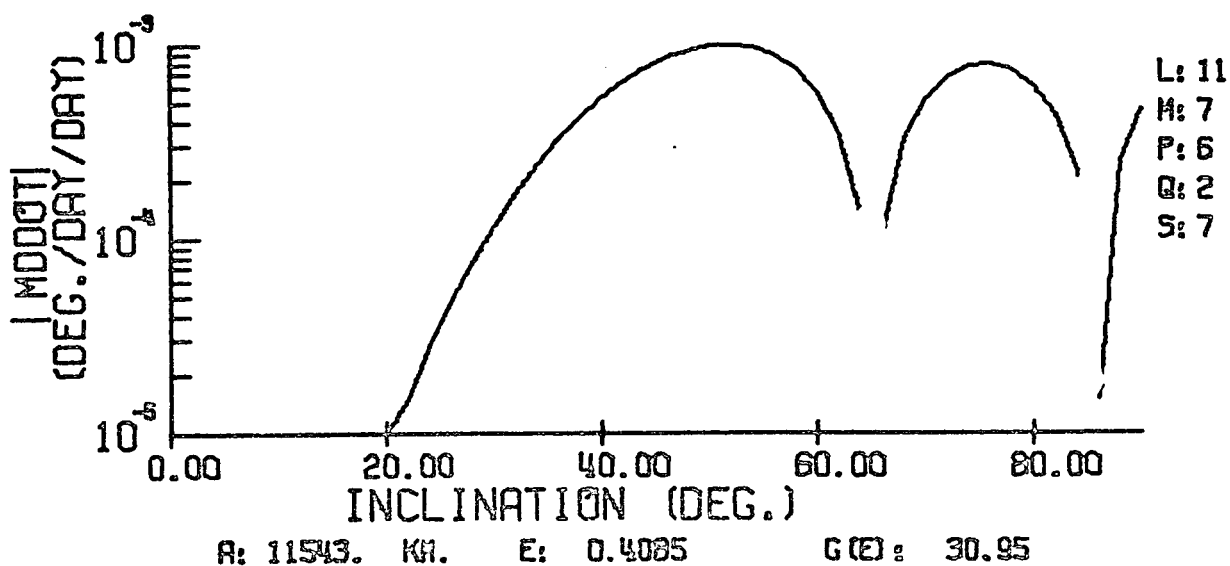
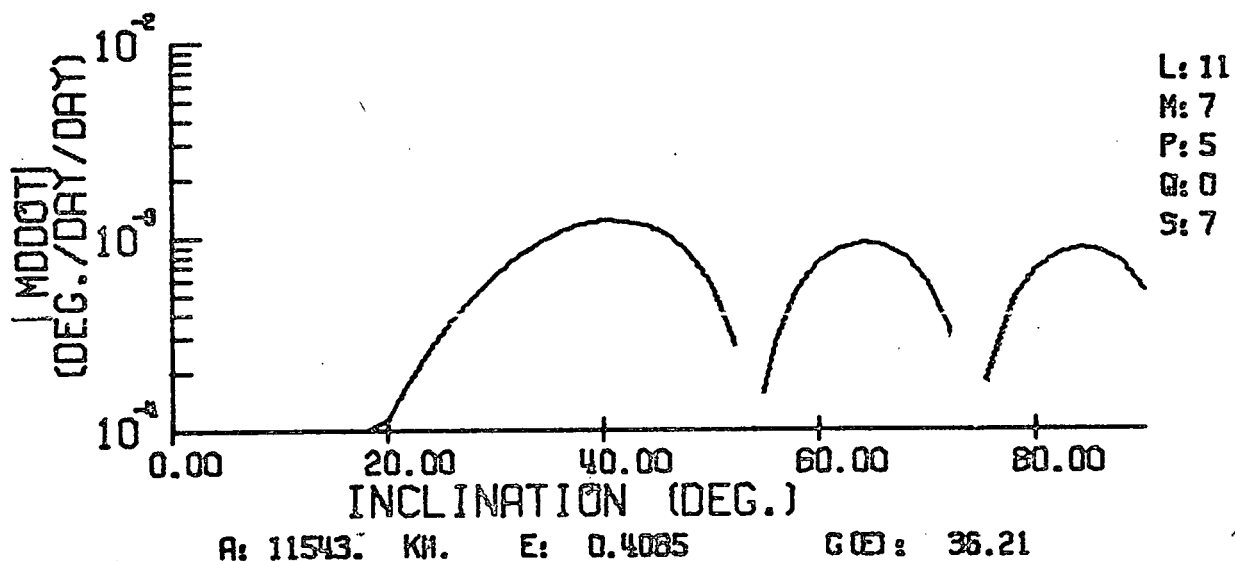
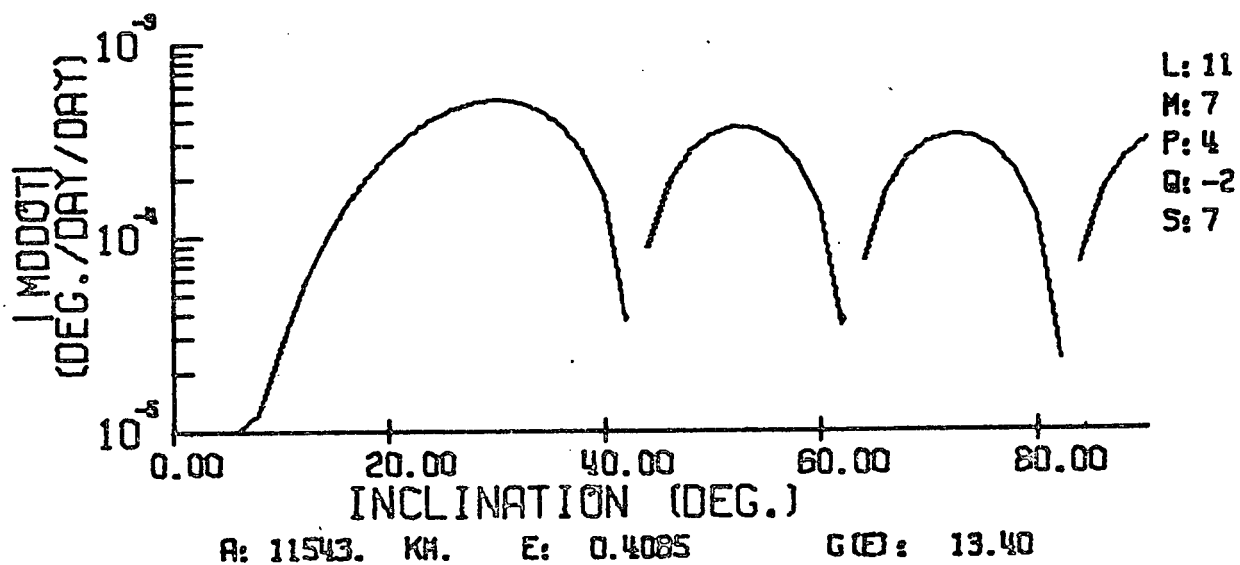
The plots of this Appendix show acceleration of mean anomaly as a function of inclination of 450 km and orbital frequency,  $s$ , of 7 rev/day. The degree,  $\ell$ , ranges from 7 through 15.

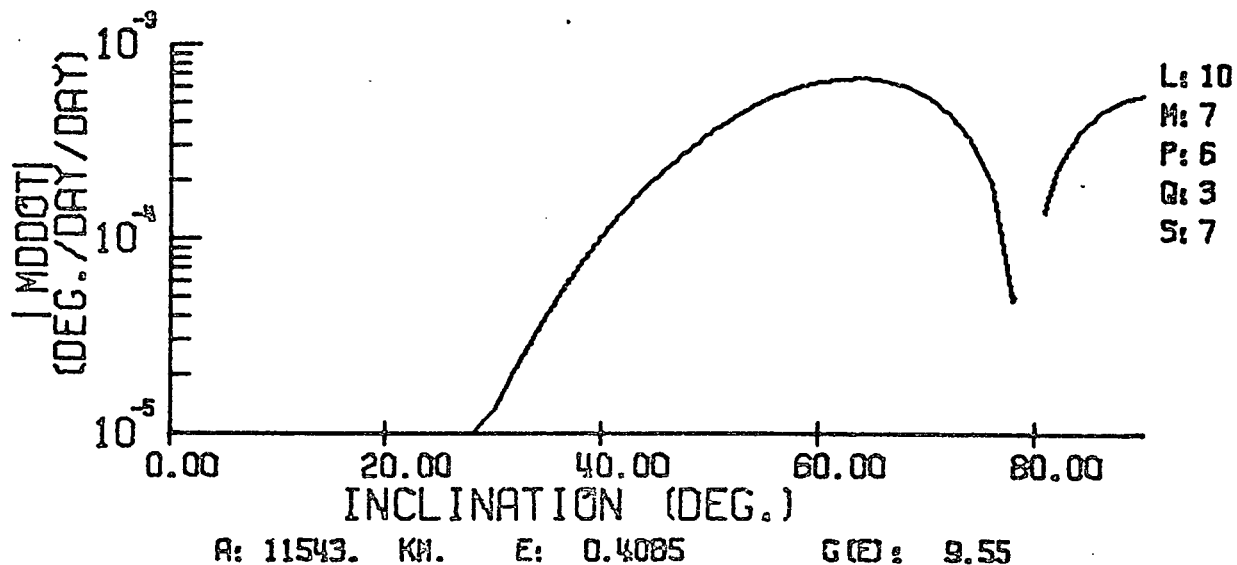
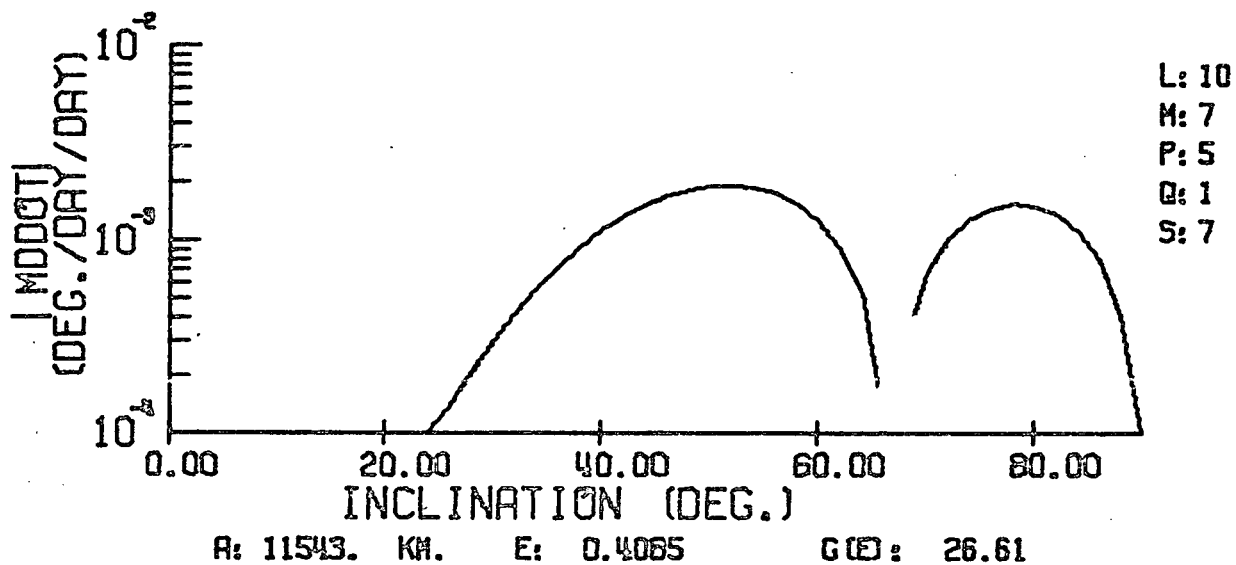
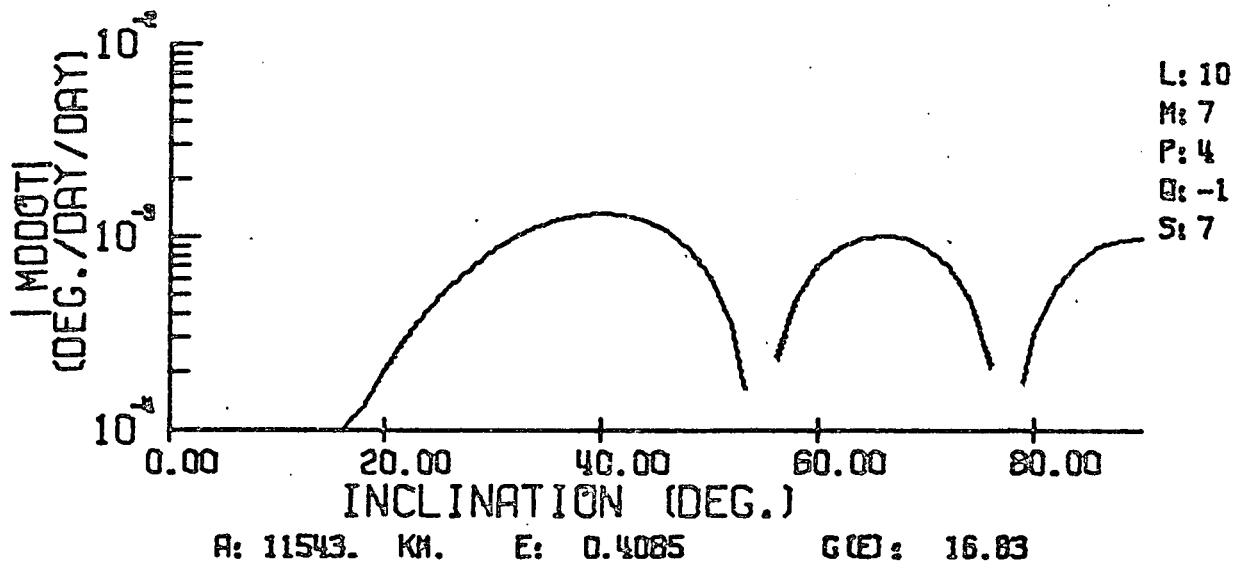


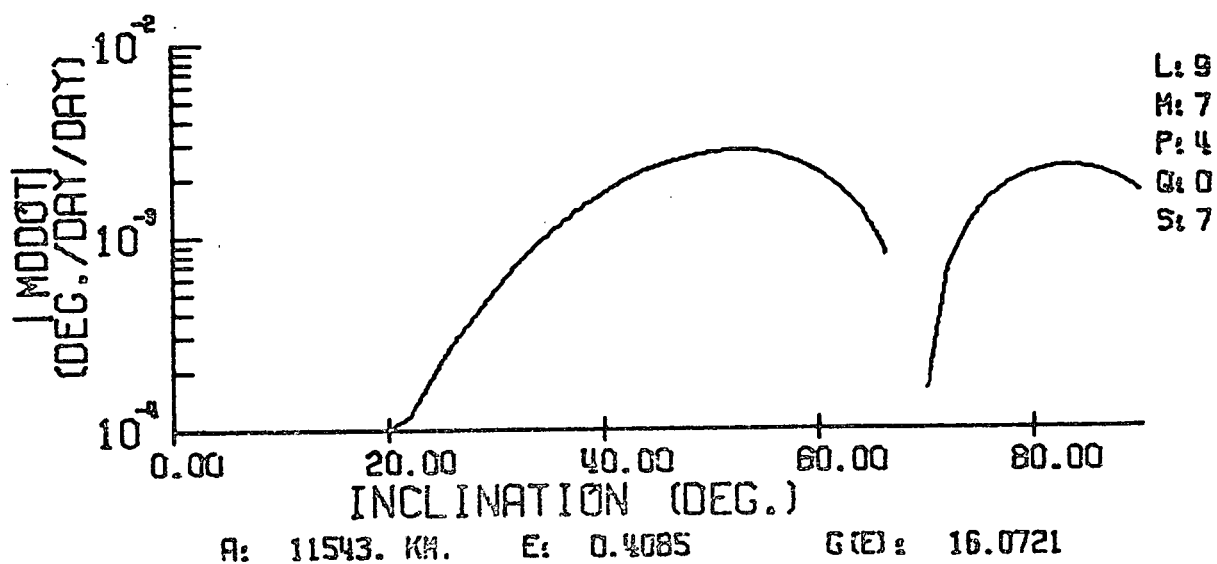
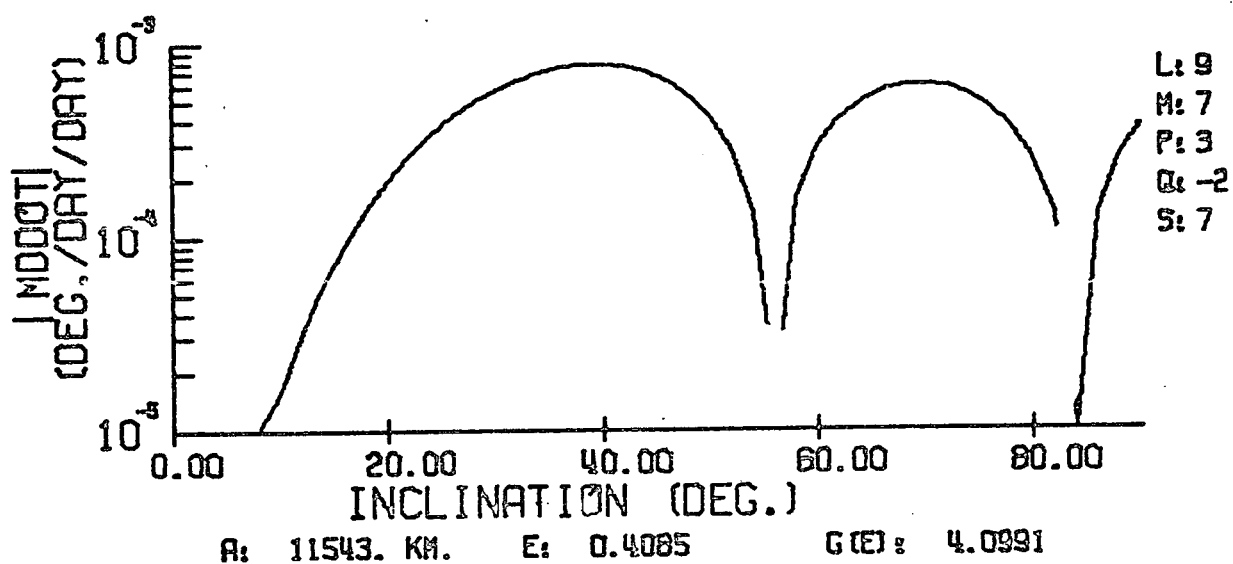
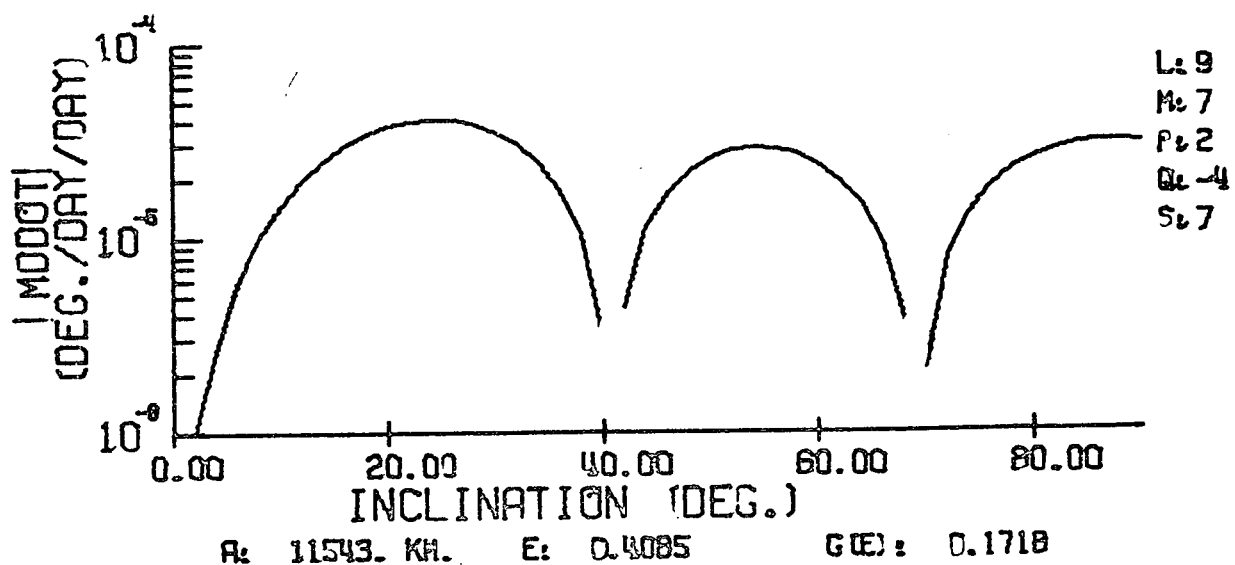


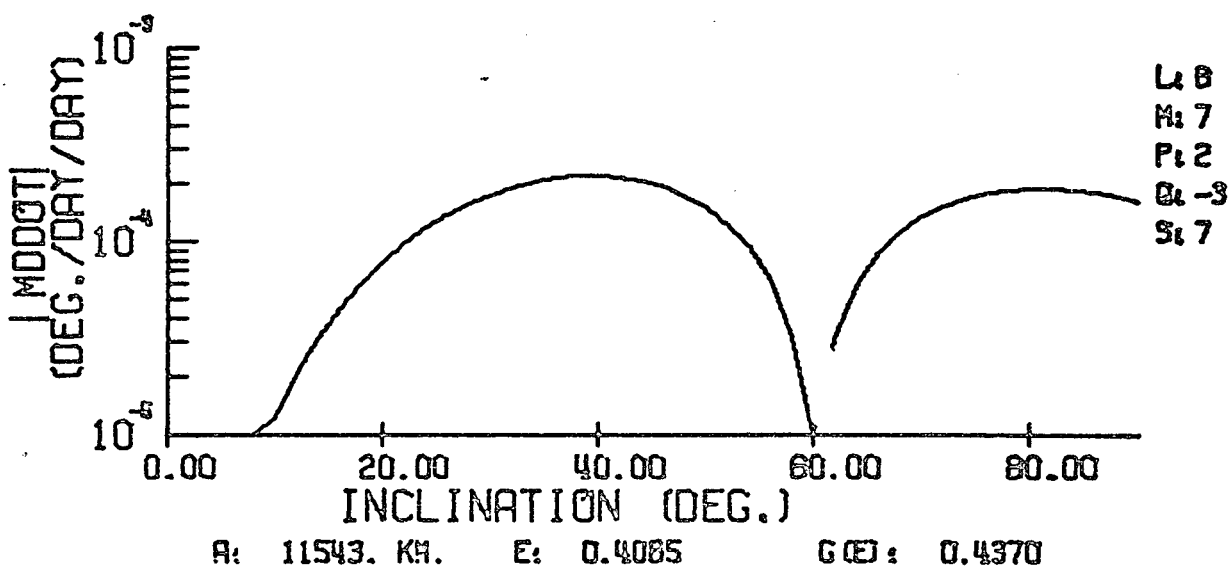
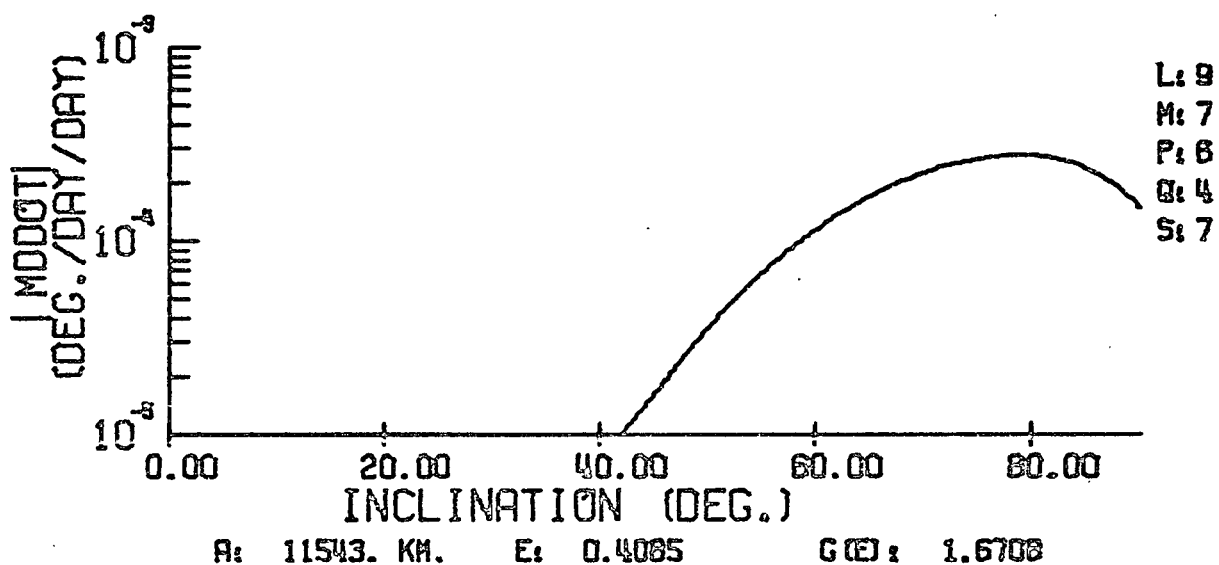
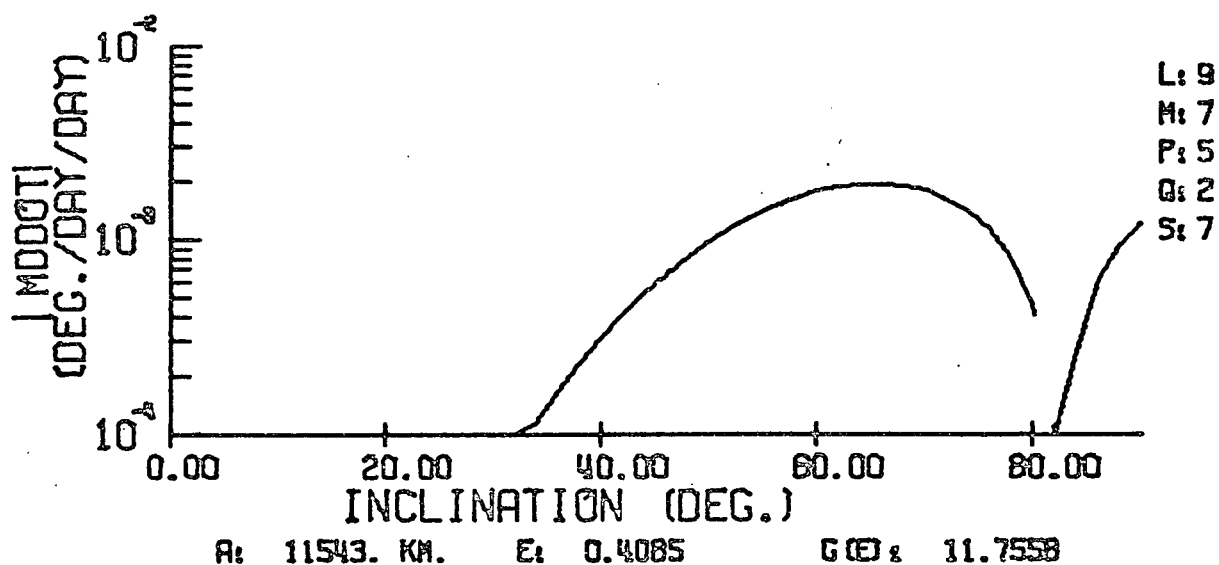


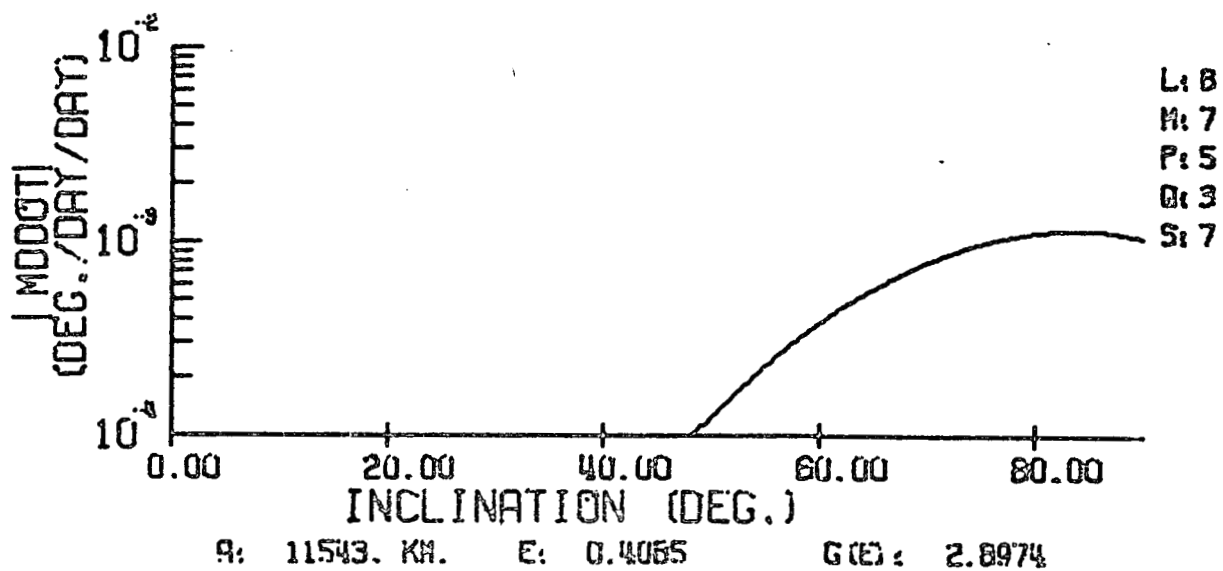
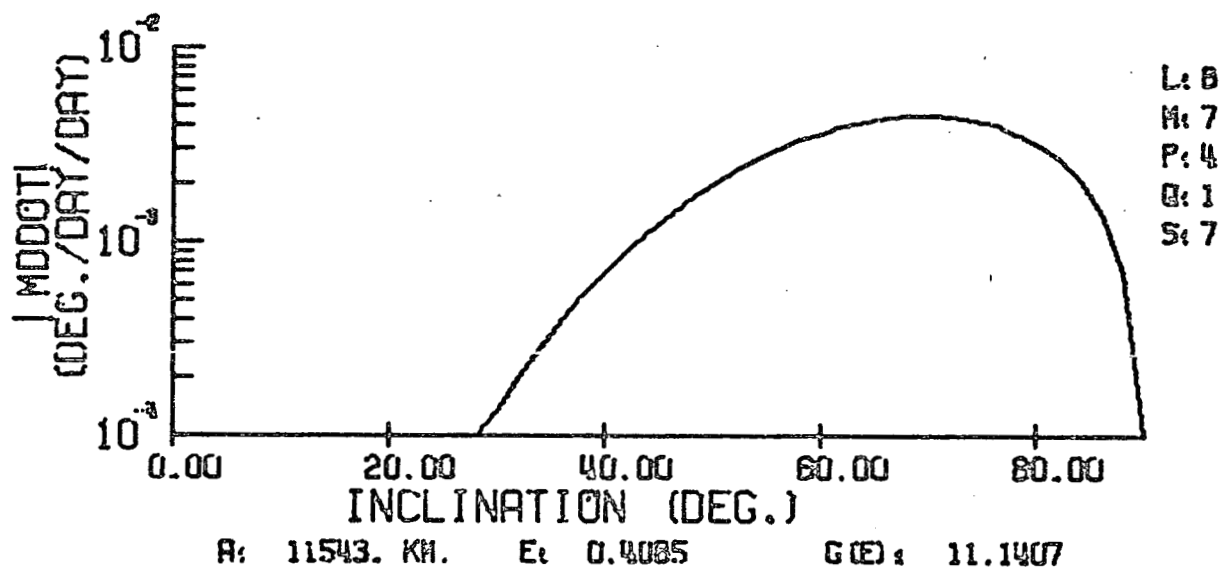
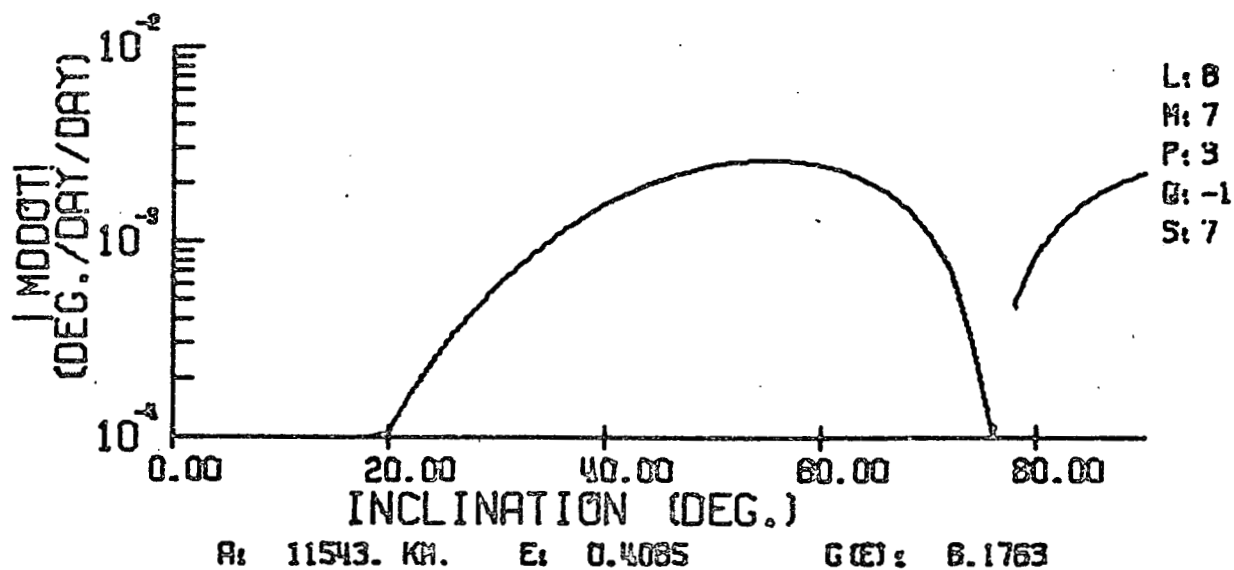


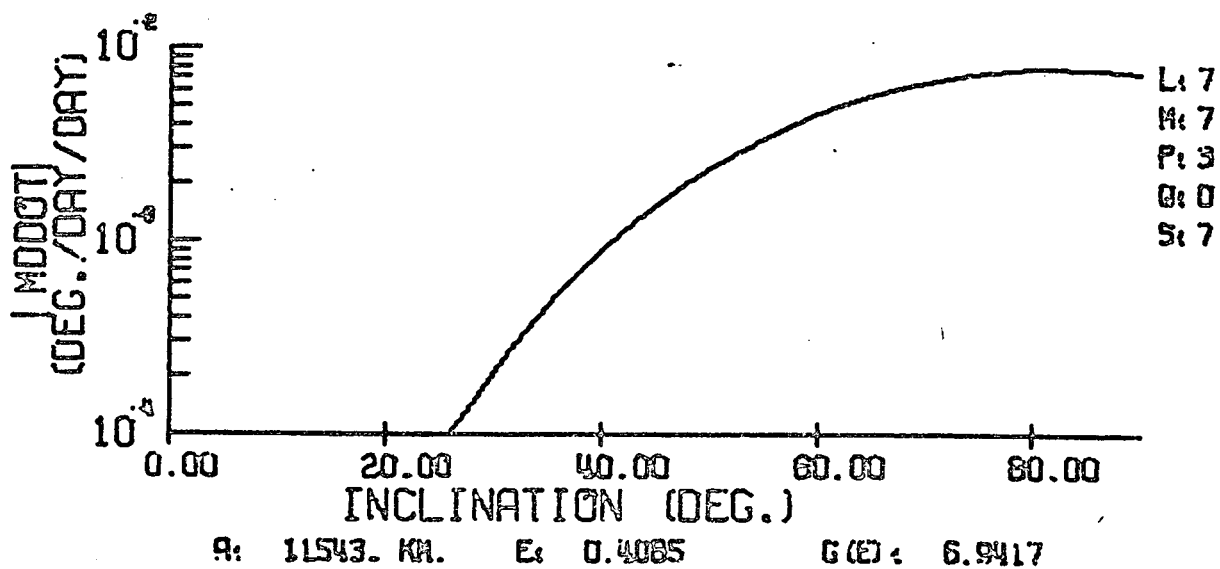
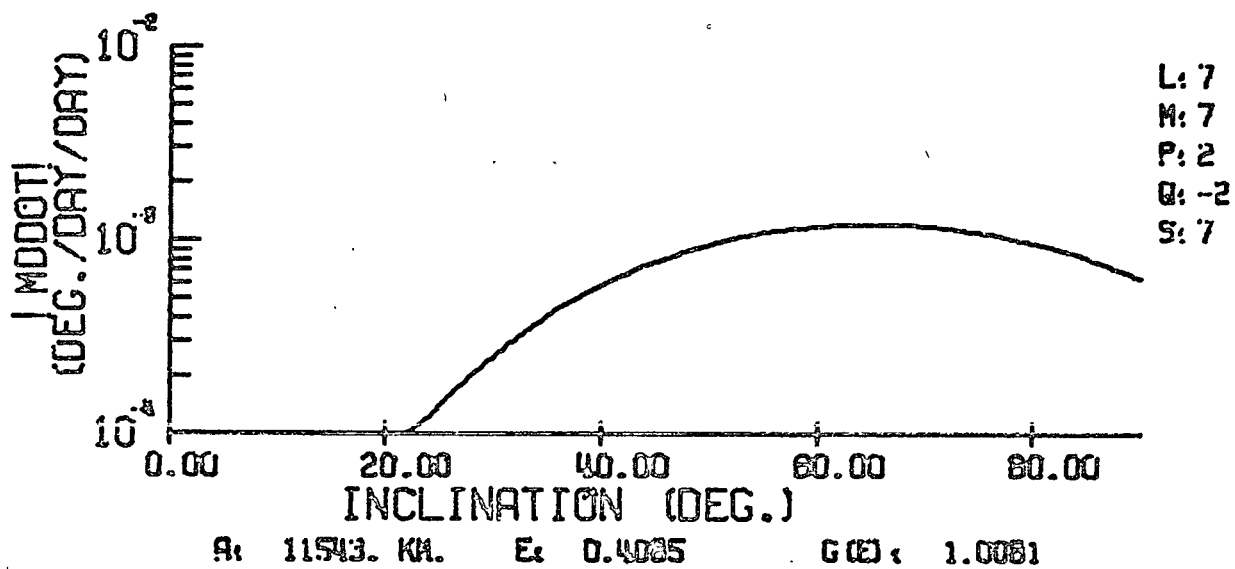
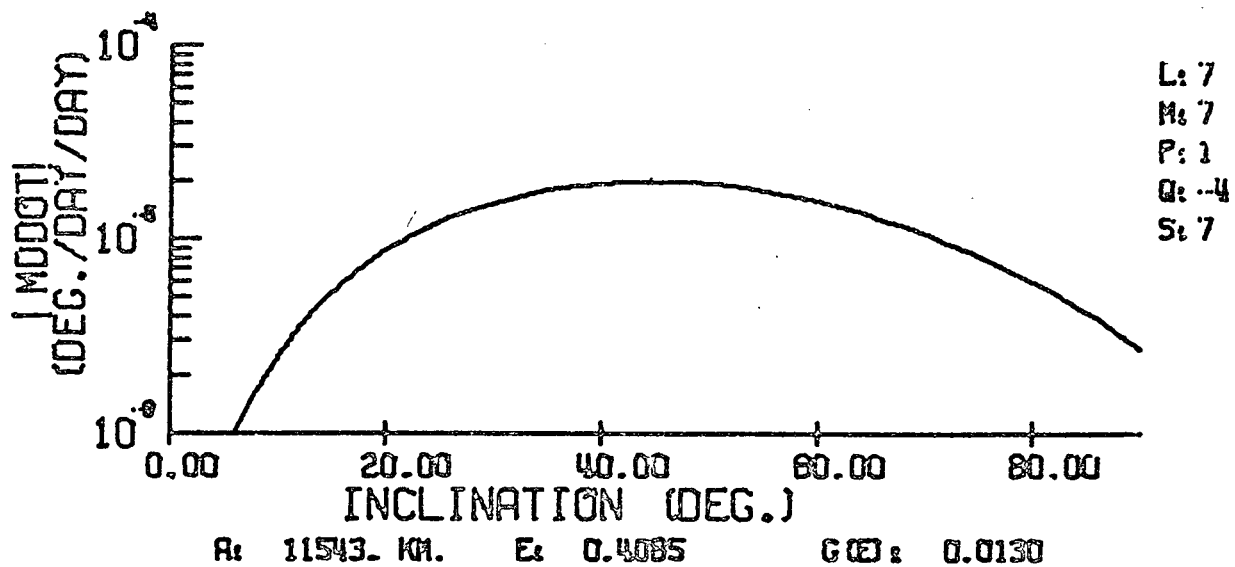




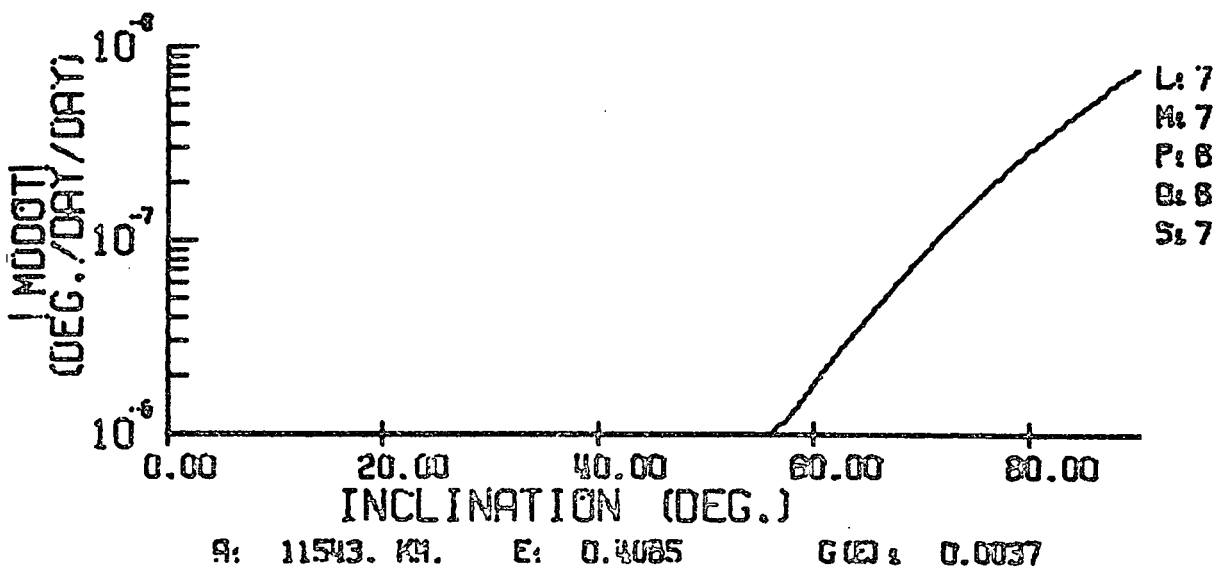
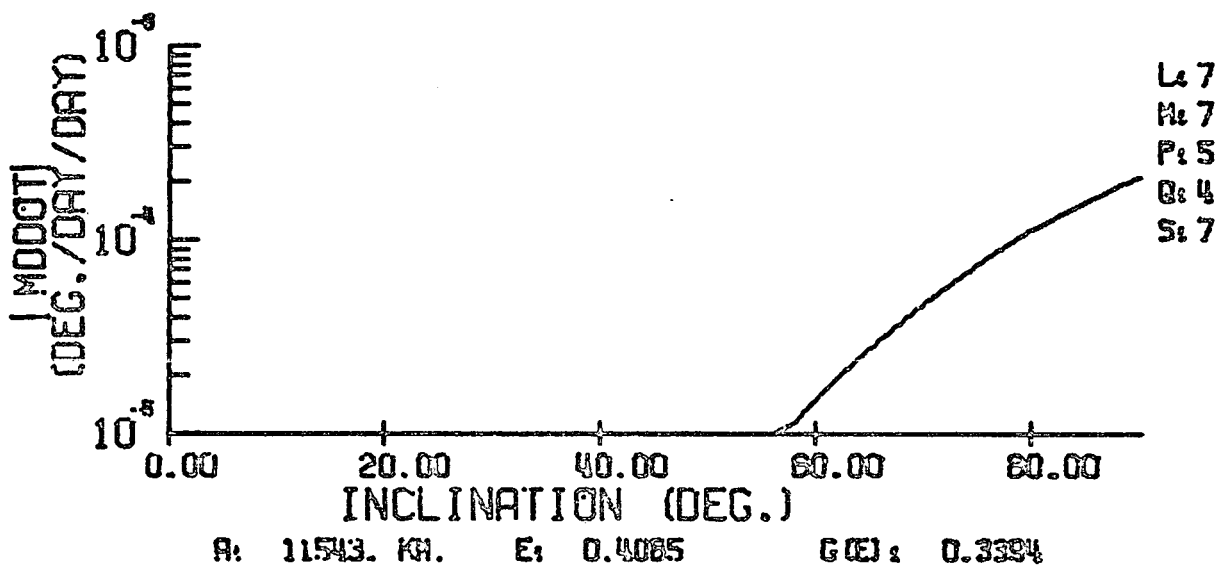
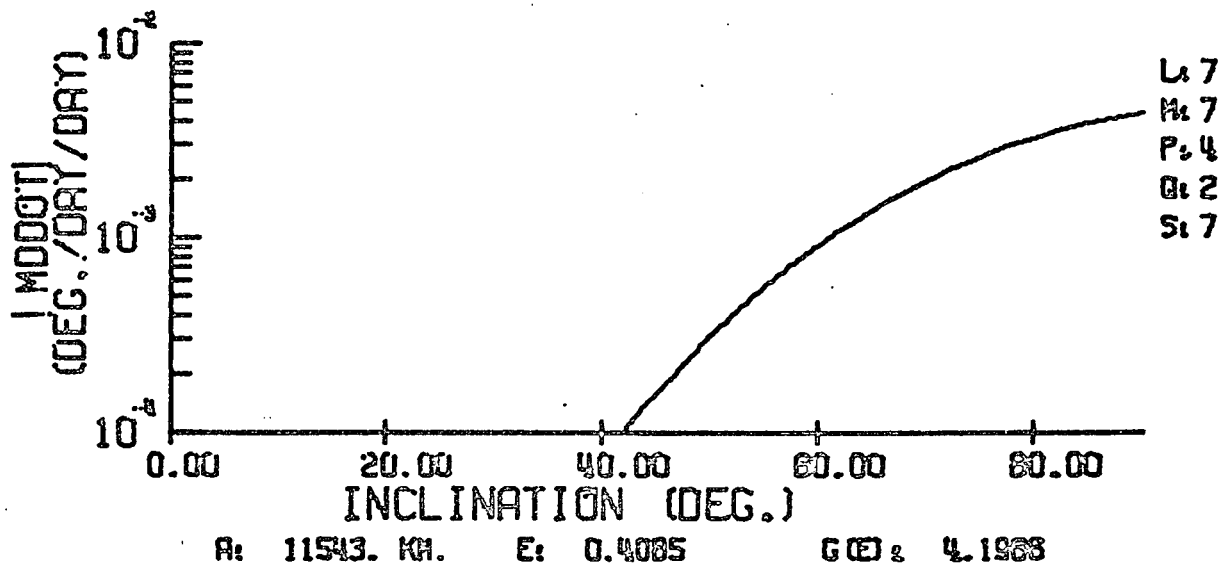






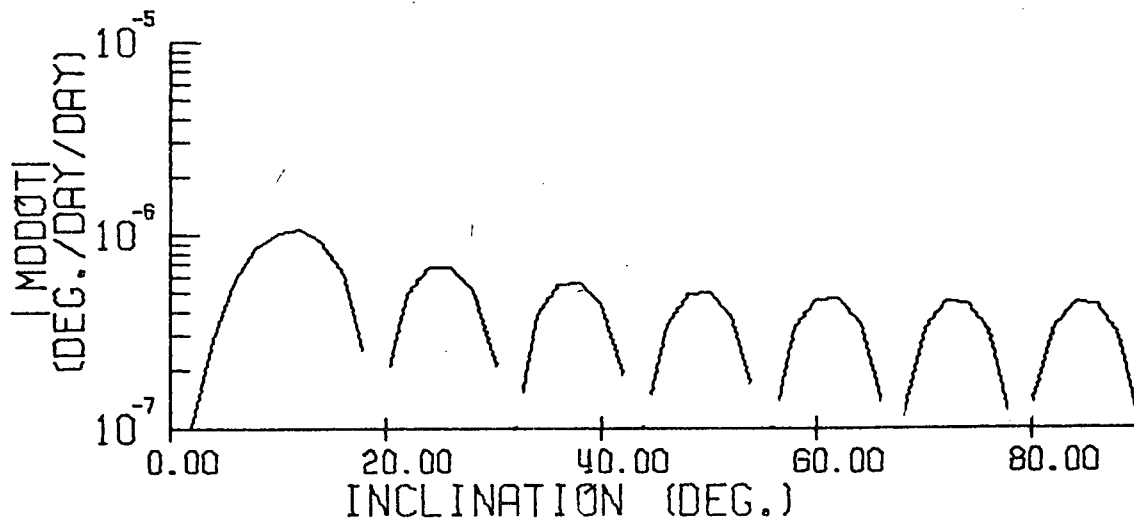






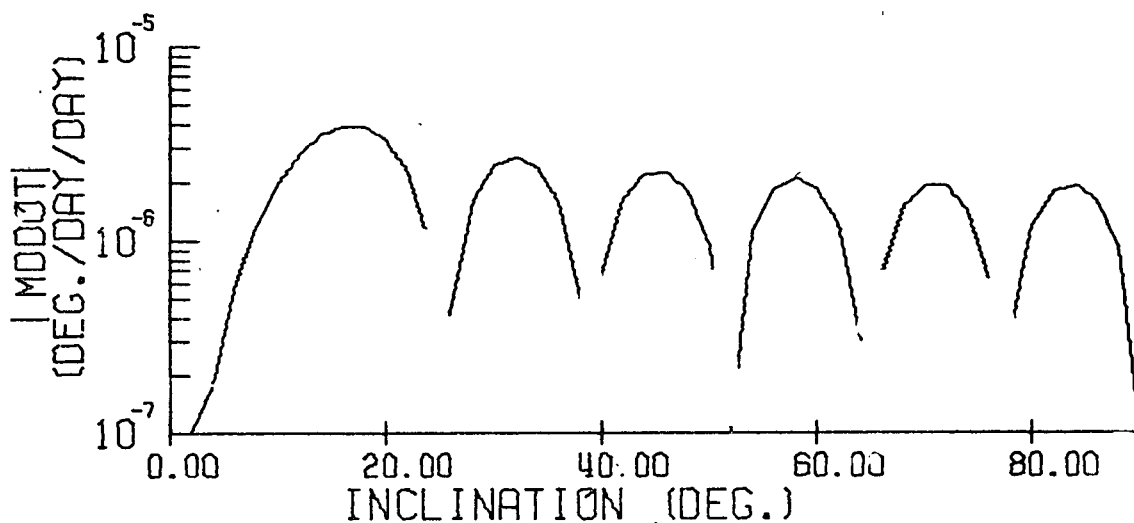
## APPENDIX B

The figures presented in this Appendix are of acceleration of mean anomaly as a function of inclination for perigee altitude of 450 km and  $s = m$  of 3 through 6 and 8 through 12. The degree,  $\ell$ , is varied from 7 through 15.



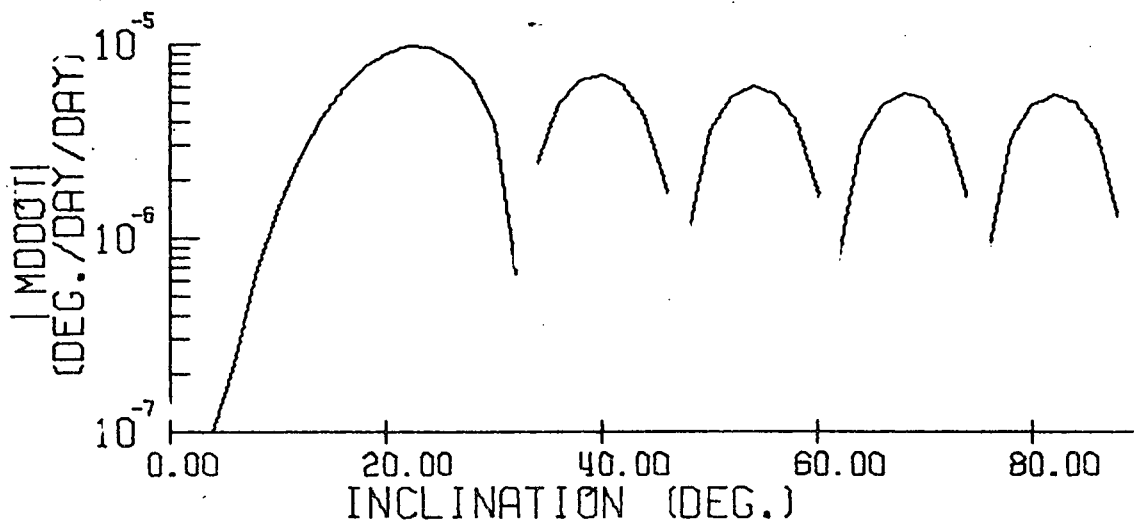
L: 15  
M: 3  
P: 7  
Q: 0  
S: 3

A: 20307. KM. E: 0.6638 G(E): 12522.55



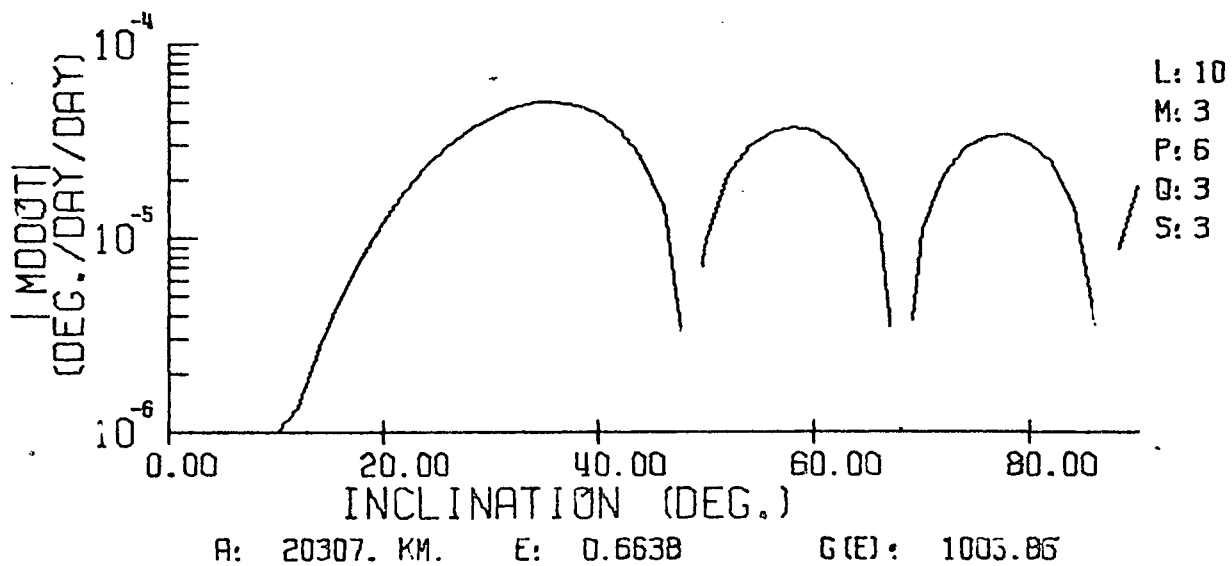
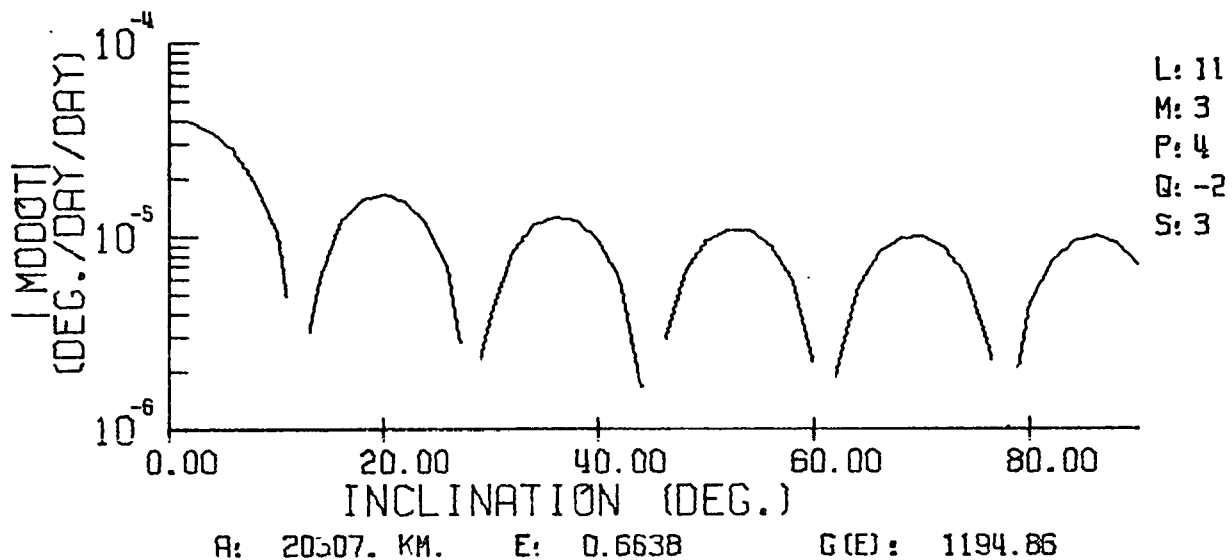
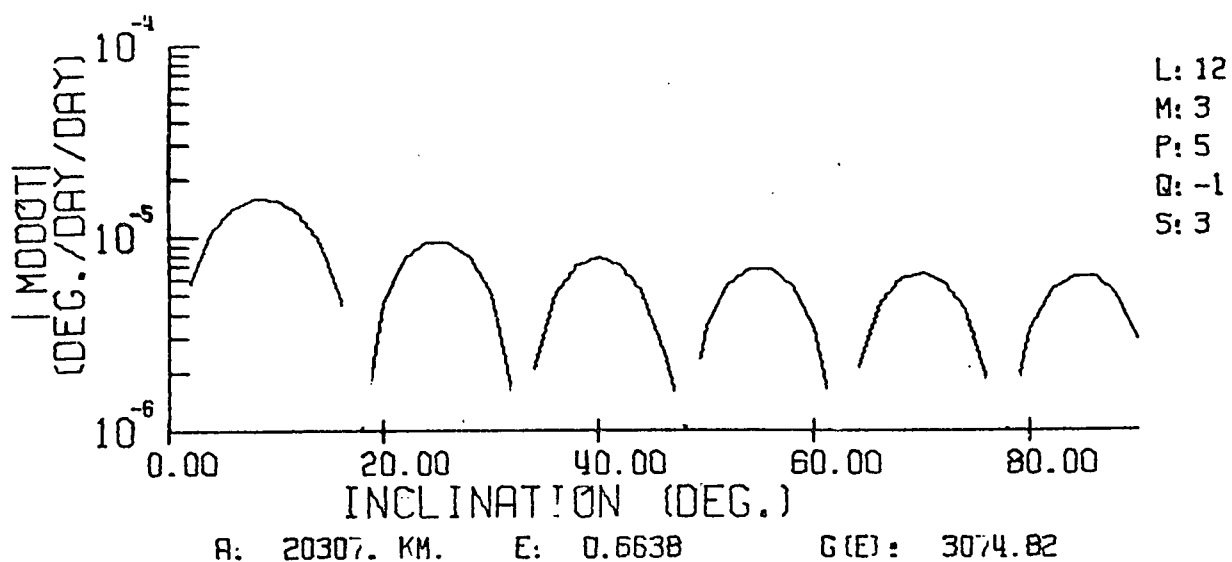
L: 14  
M: 3  
P: 7  
Q: 1  
S: 3

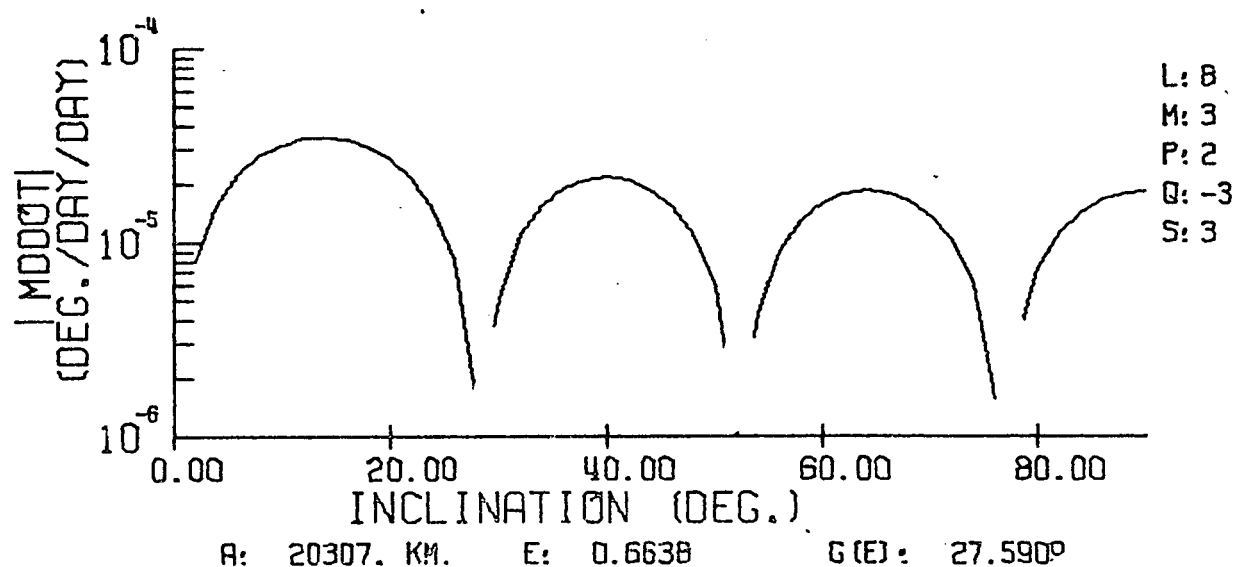
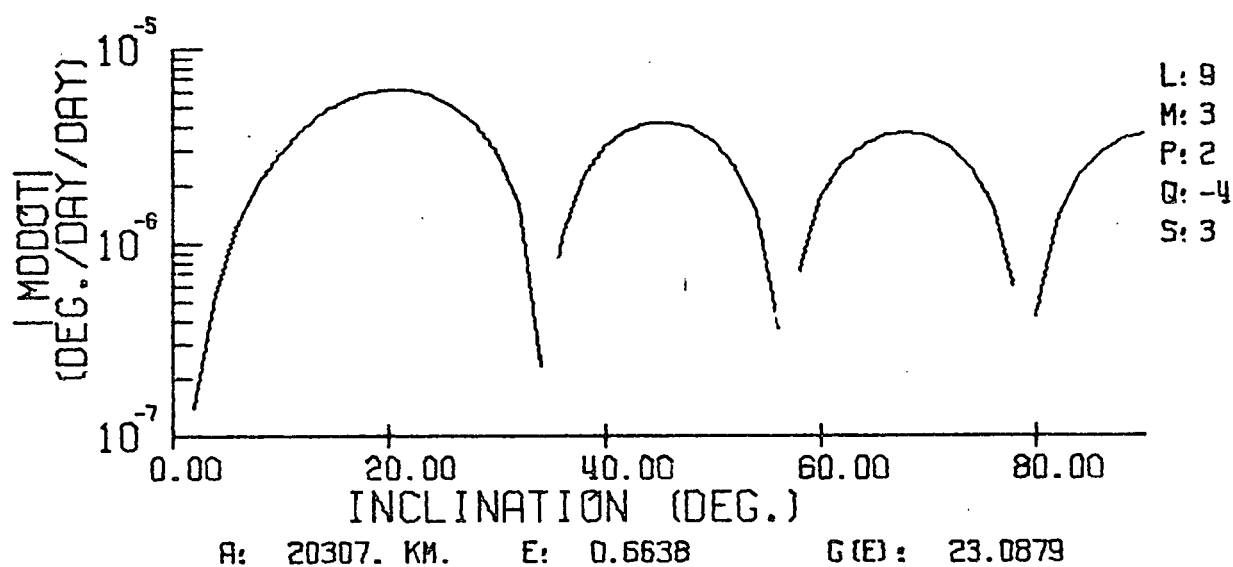
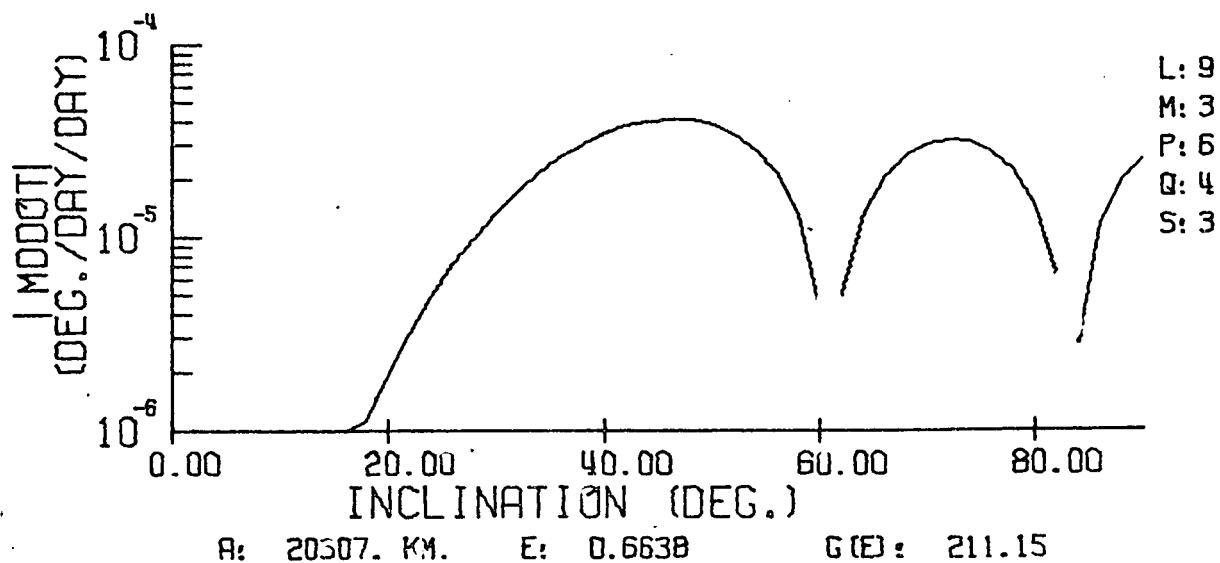
A: 20307. KM. E: 0.6638 G(E): 14126.78

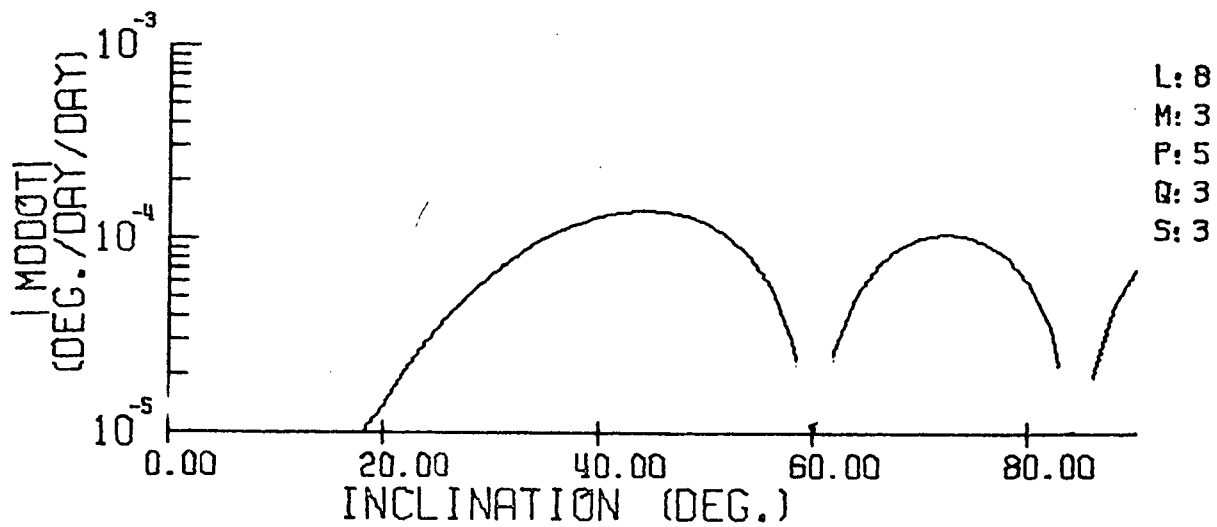


L: 13  
M: 3  
P: 7  
Q: 2  
S: 3

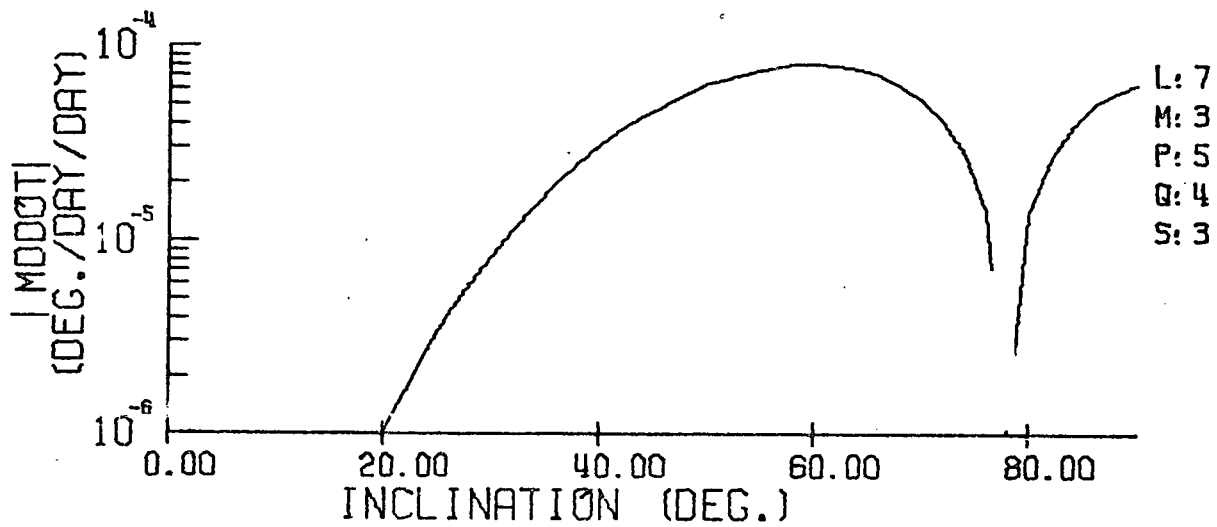
A: 20307. KM. E: 0.6638 G(E): 10252.76



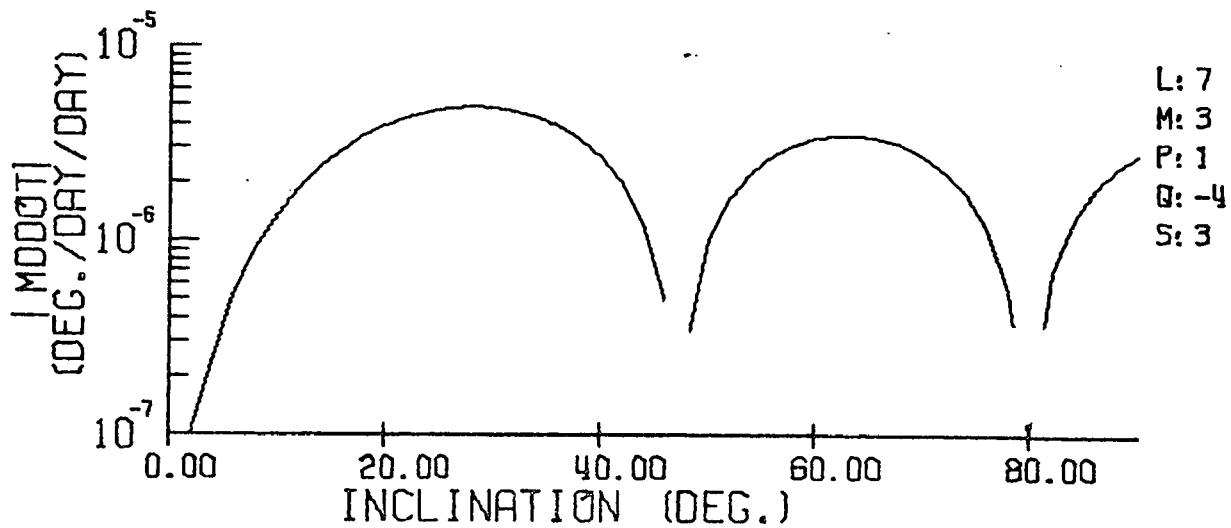




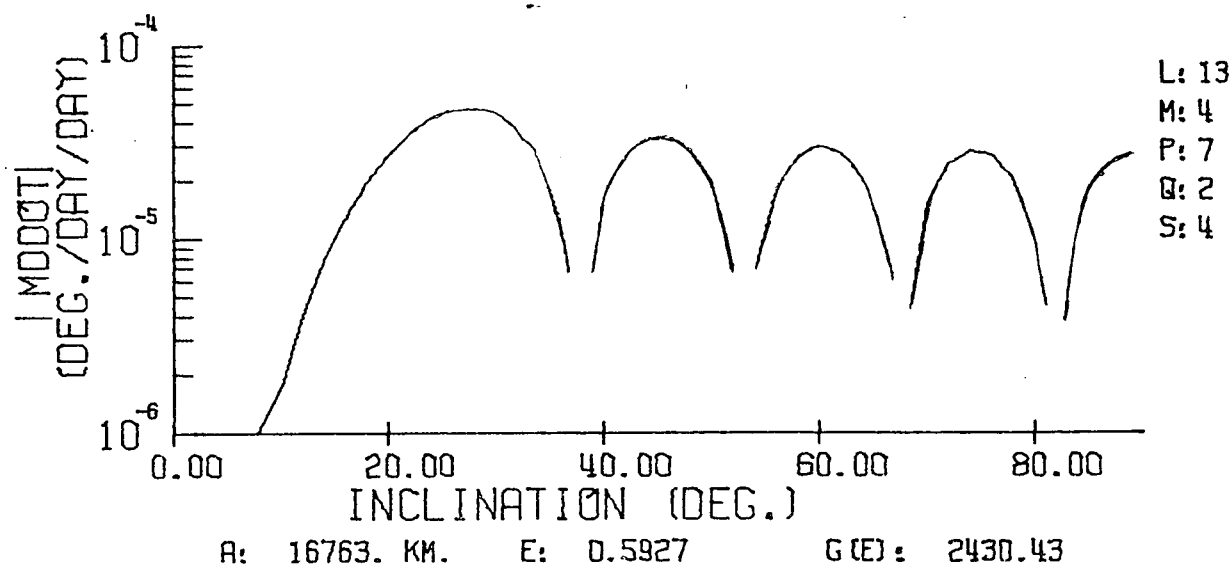
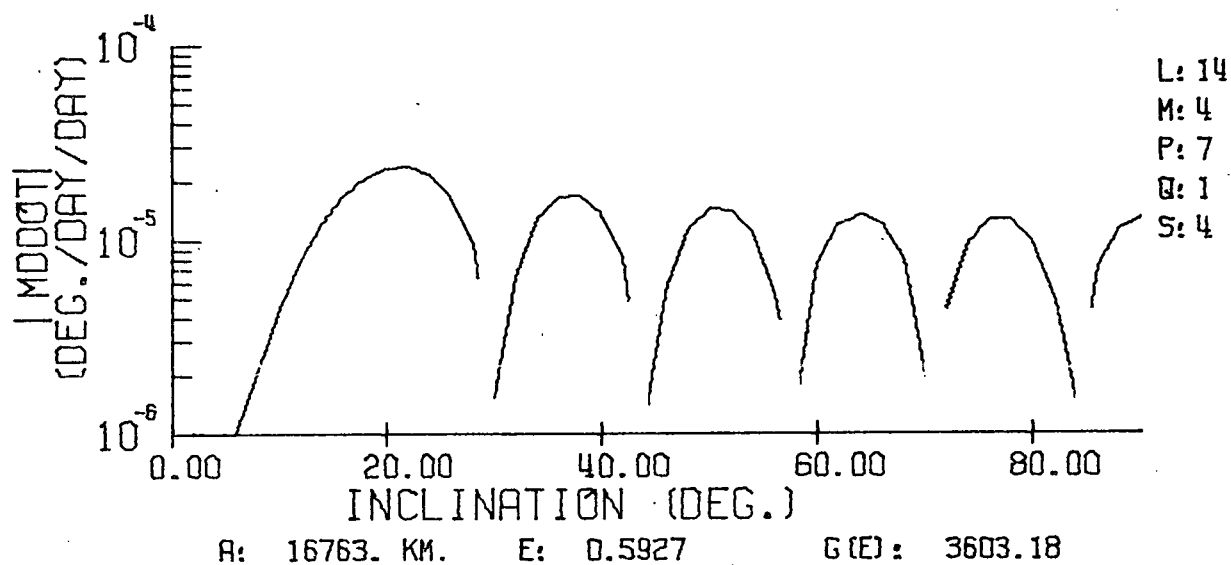
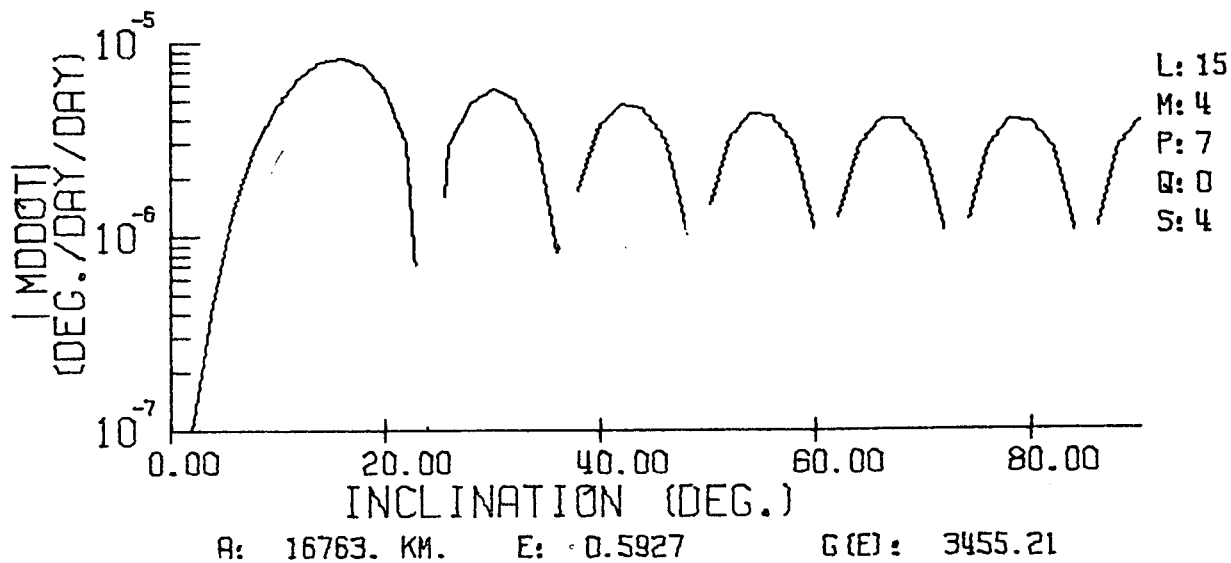
A: 20307. KM. E: 0.6638 G(E): 173.90

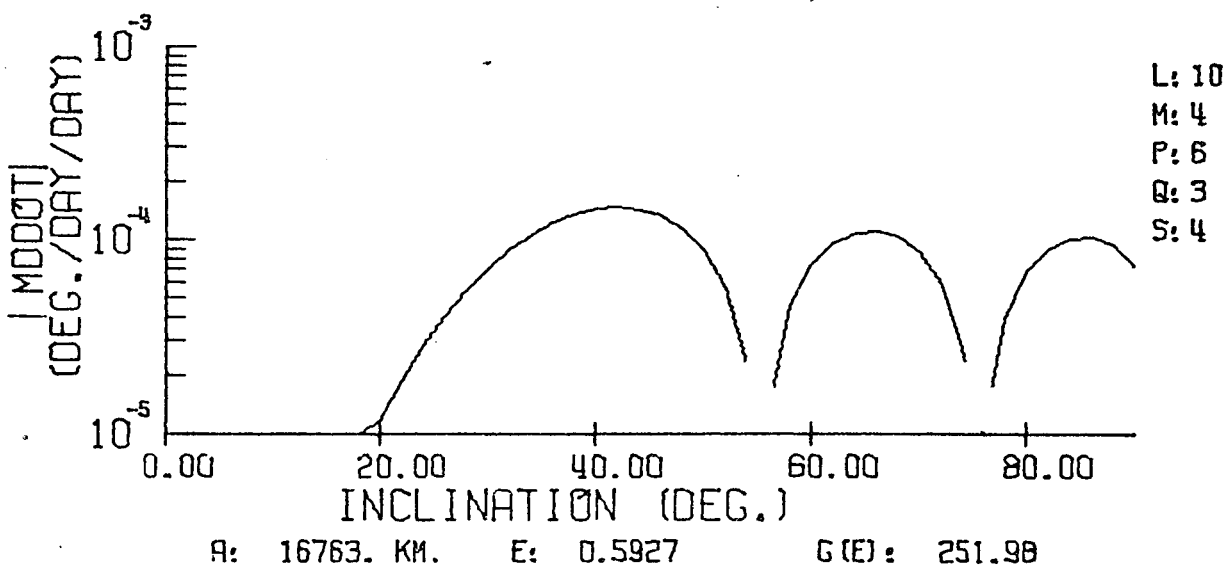
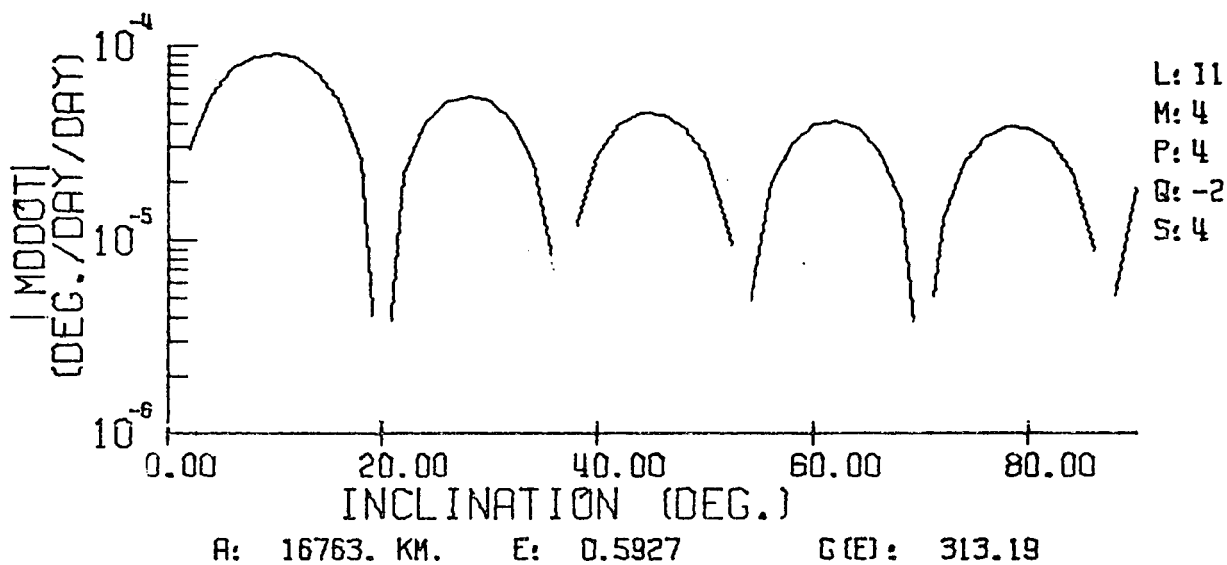
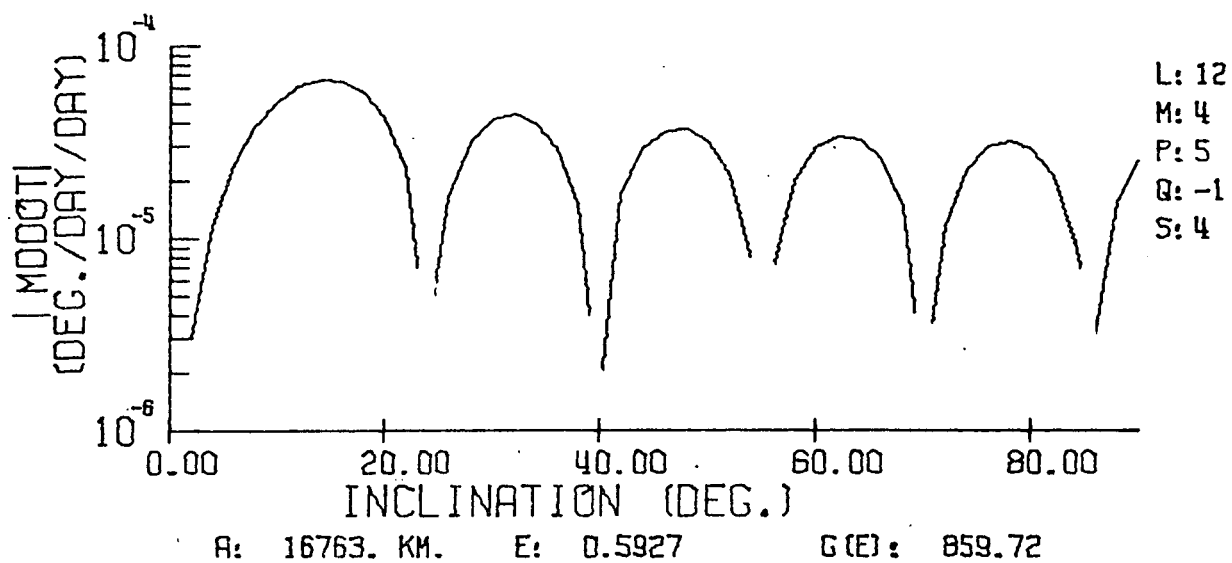


A: 20307. KM. E: 0.6638 G(E): 23.6048

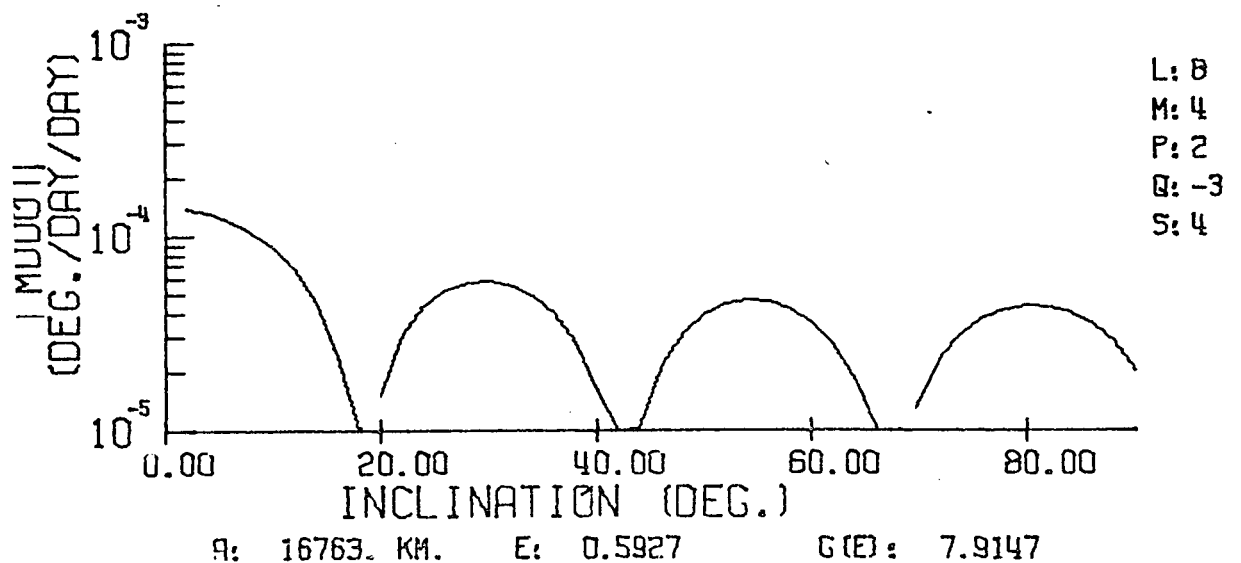
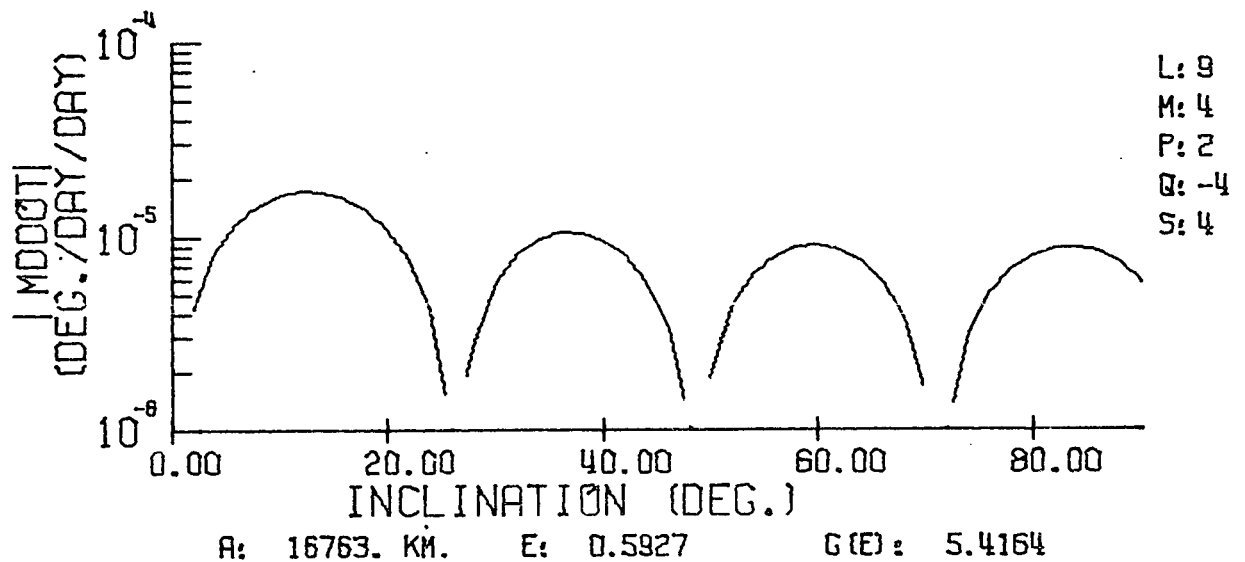
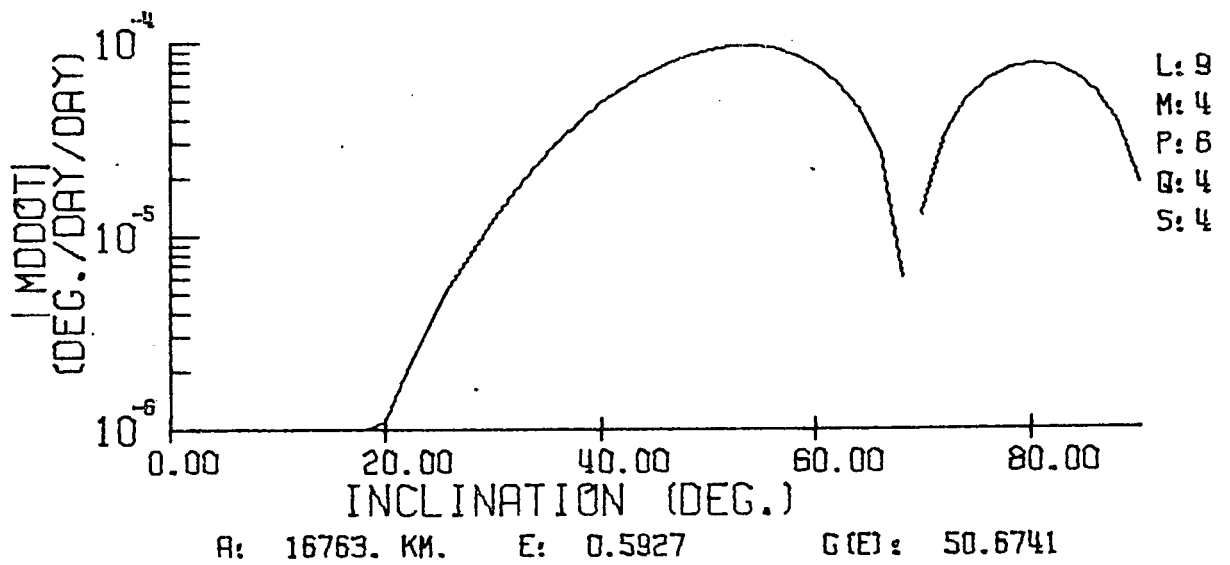


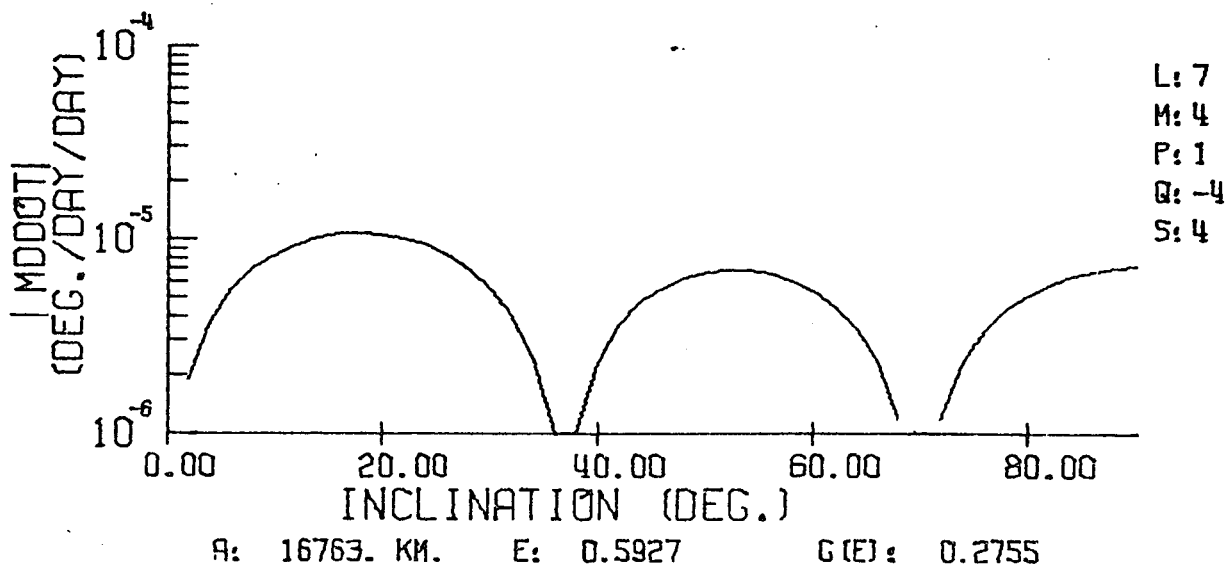
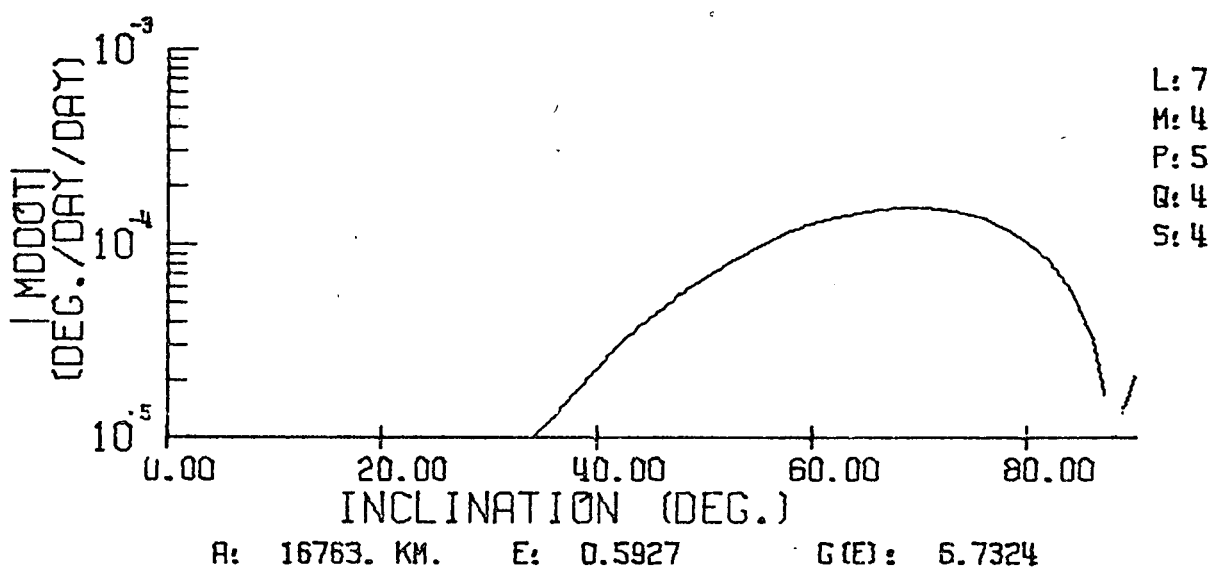
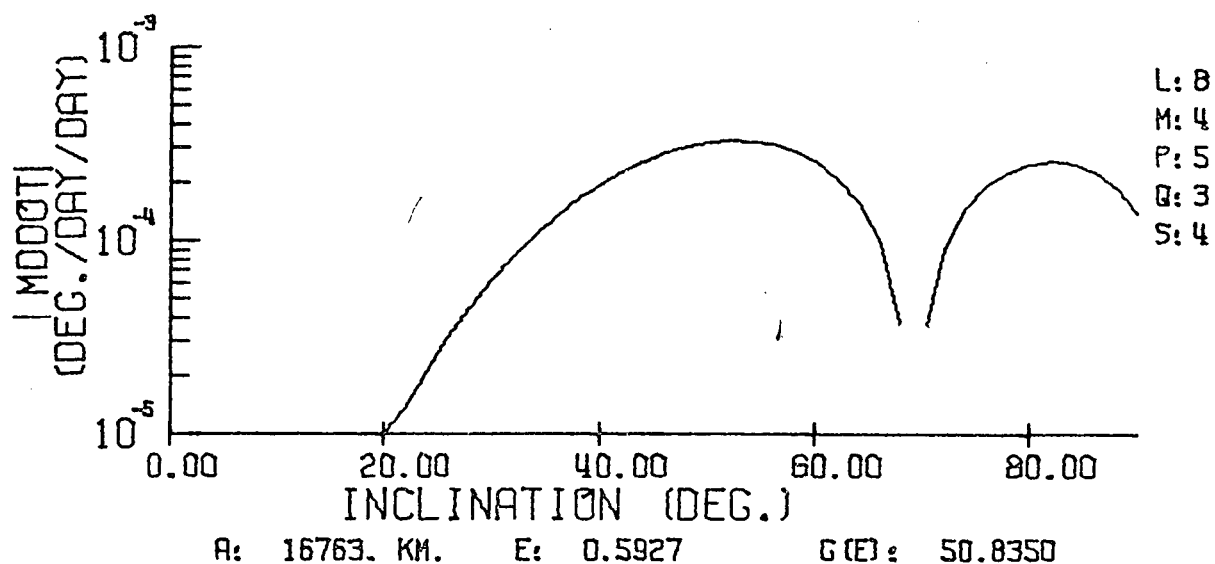
A: 20307. KM. E: 0.6638 G(E): 0.9983

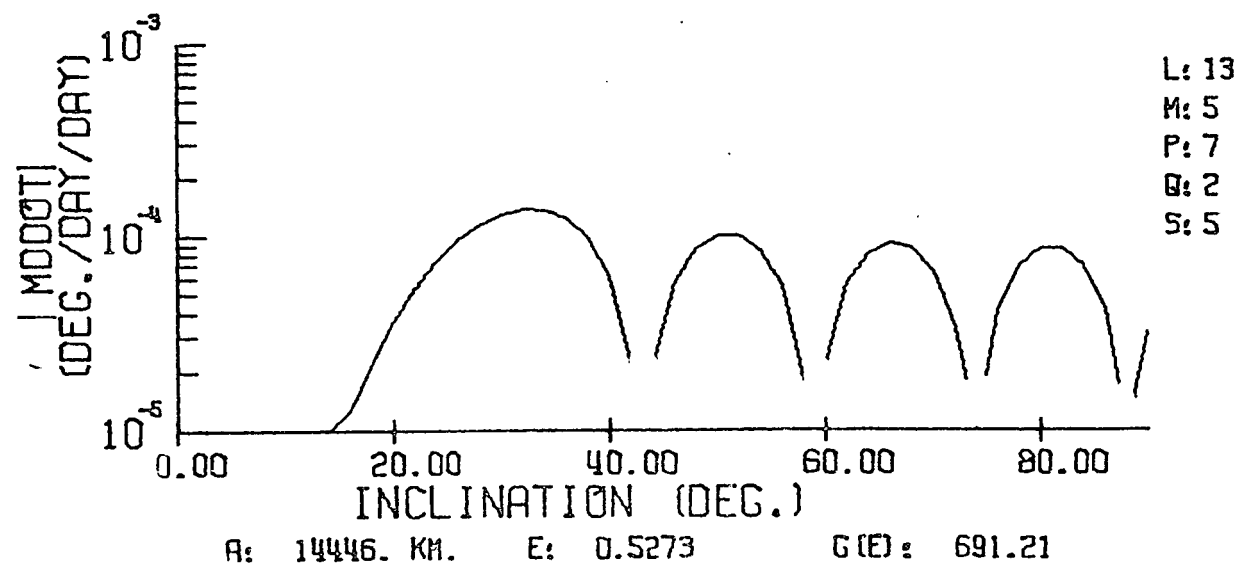
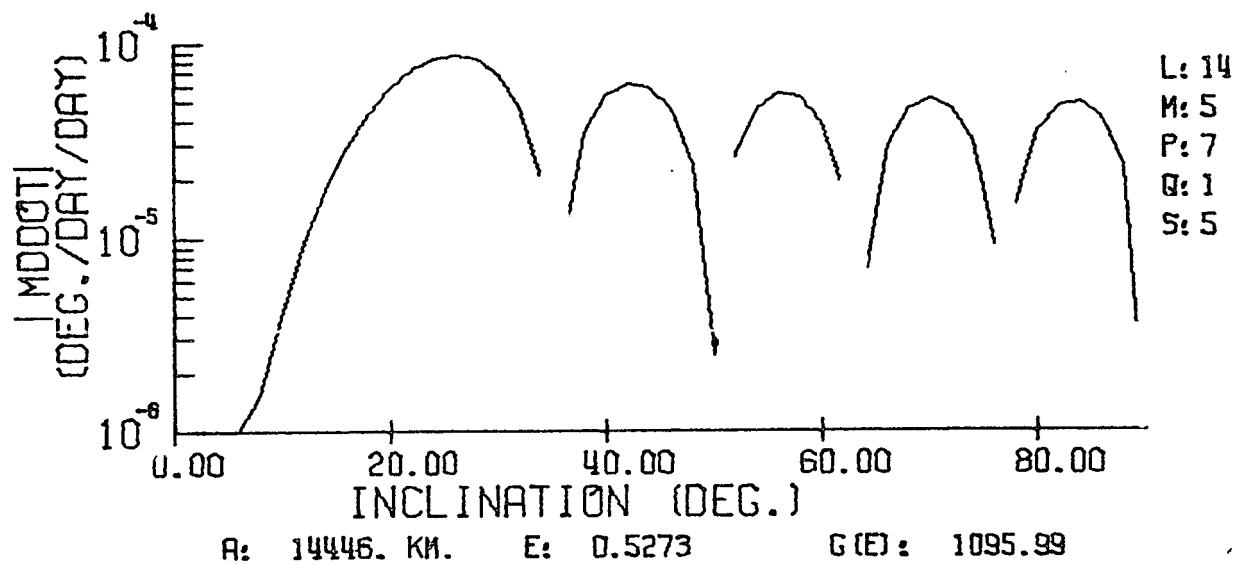
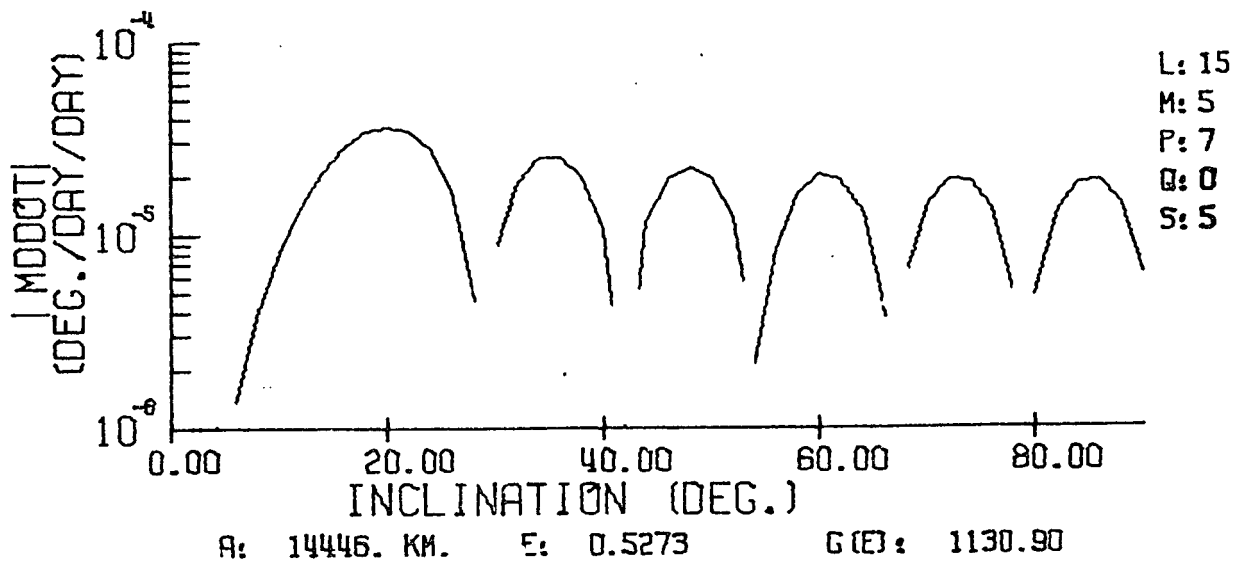


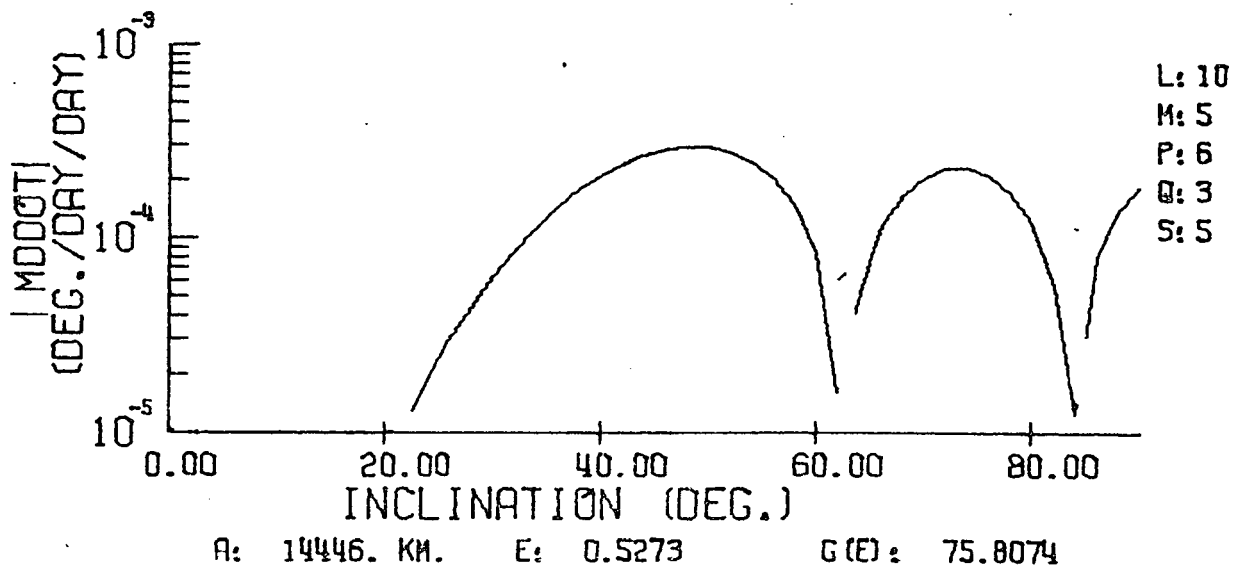
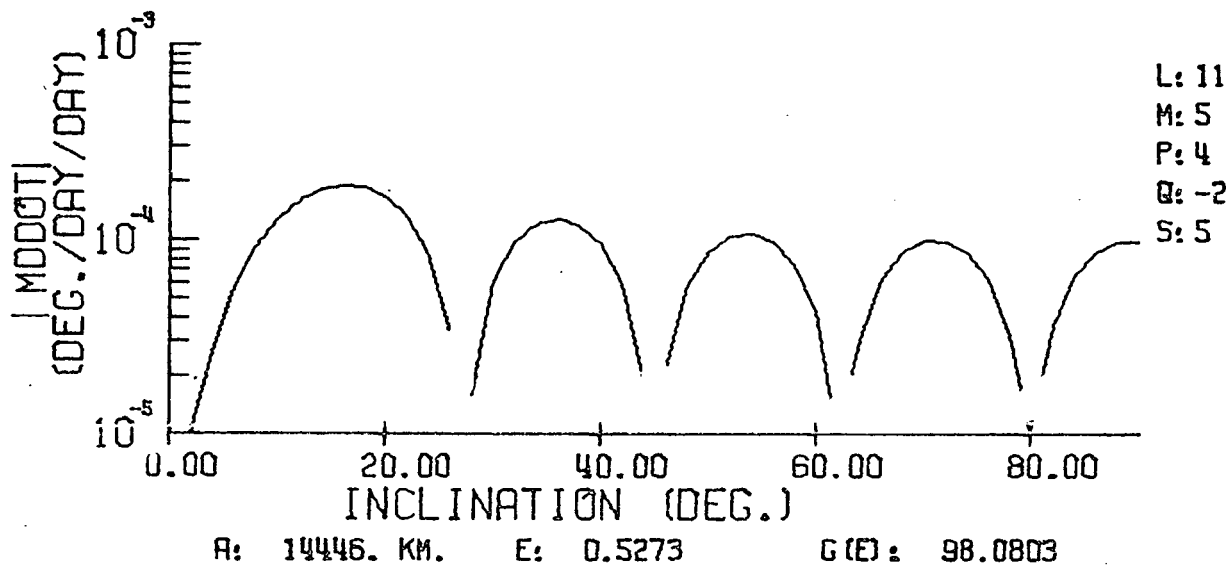
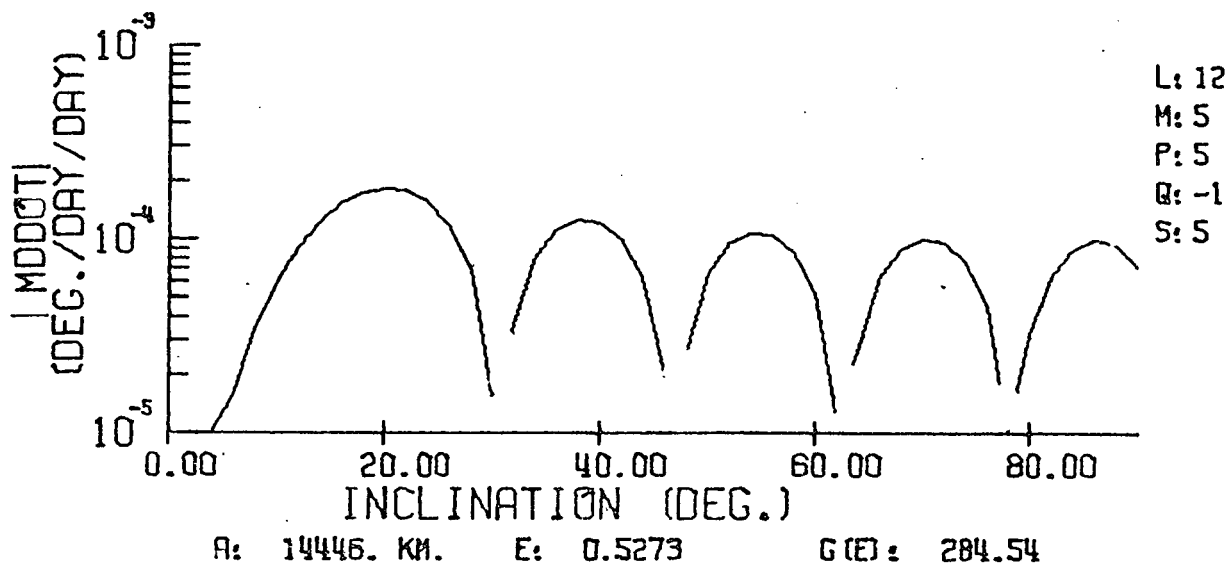


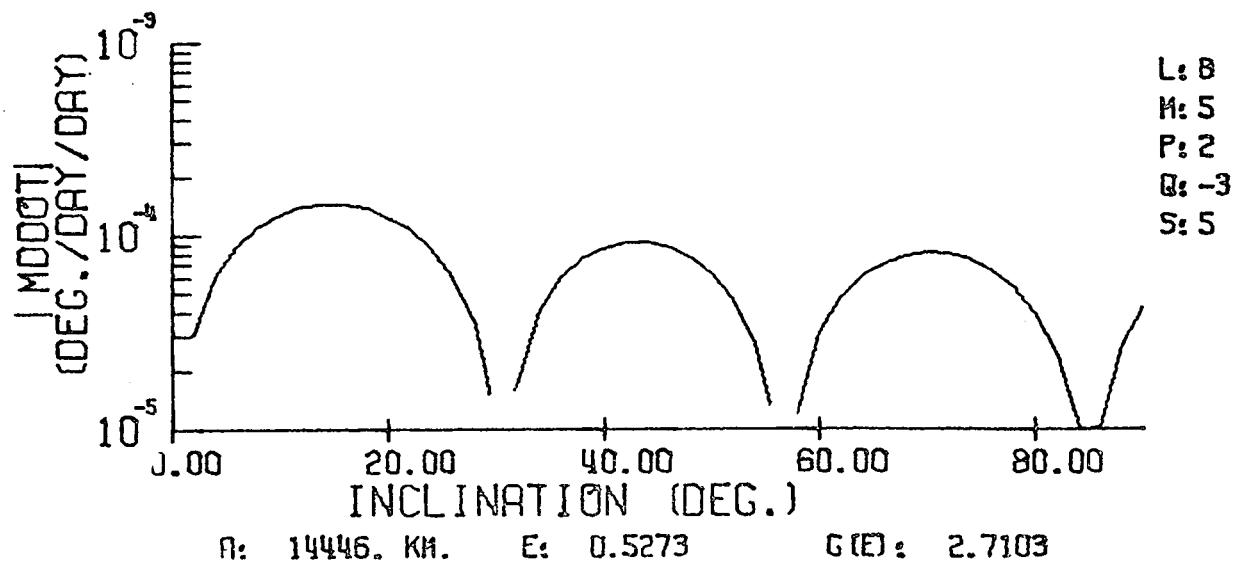
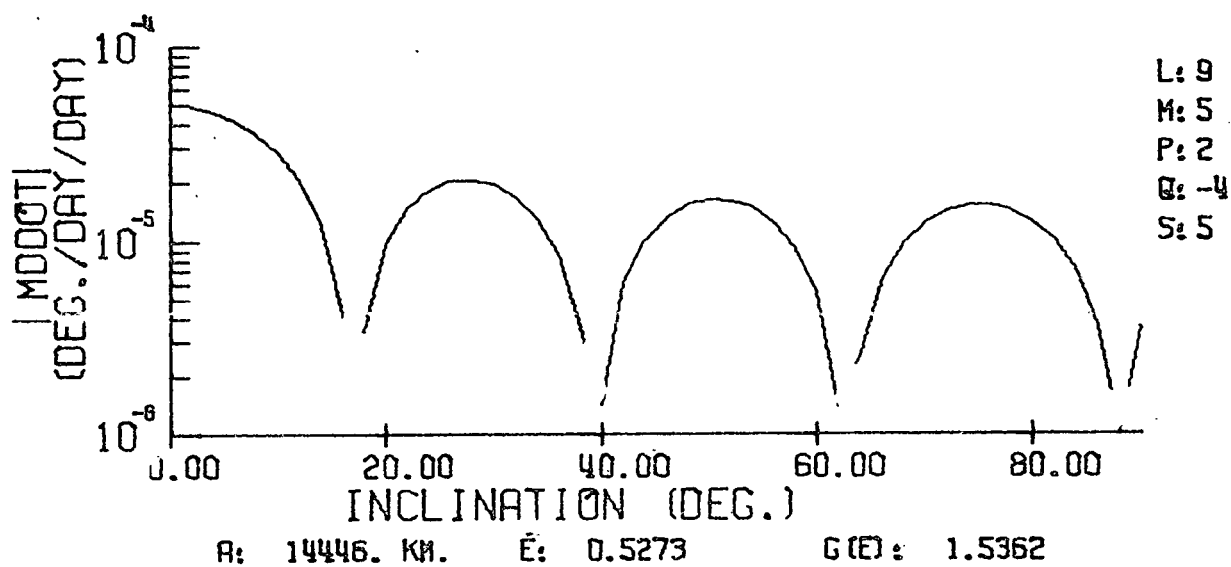
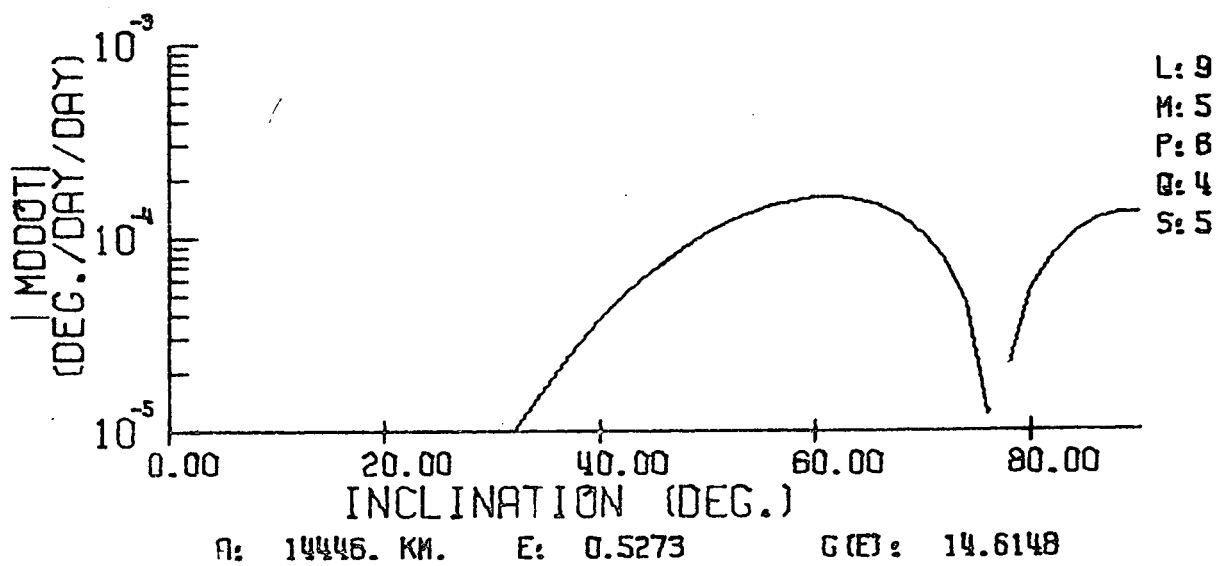


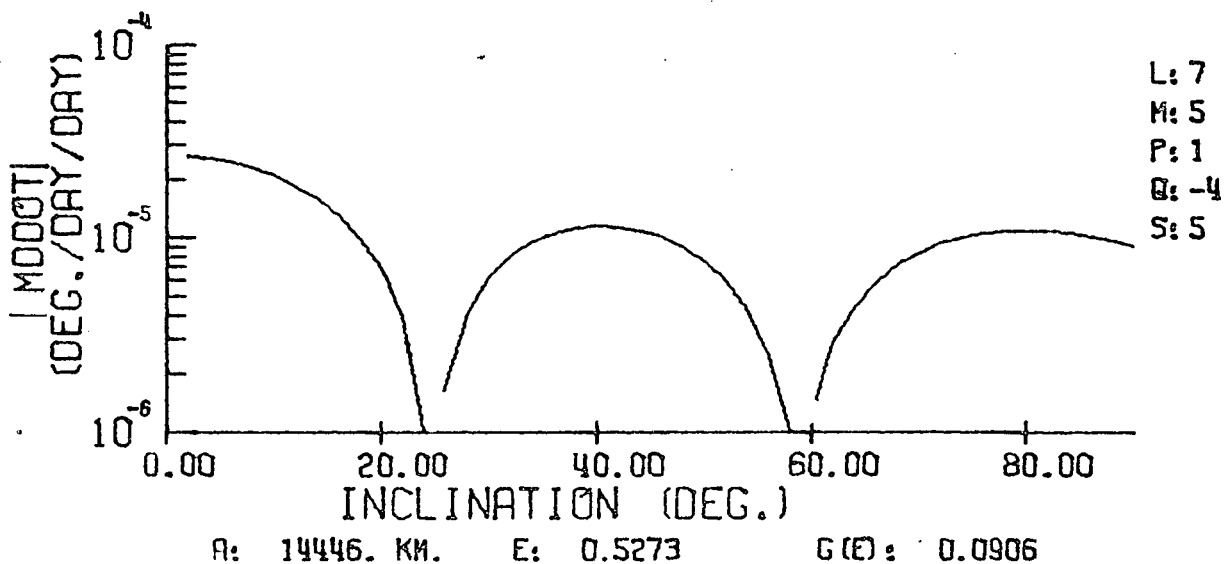
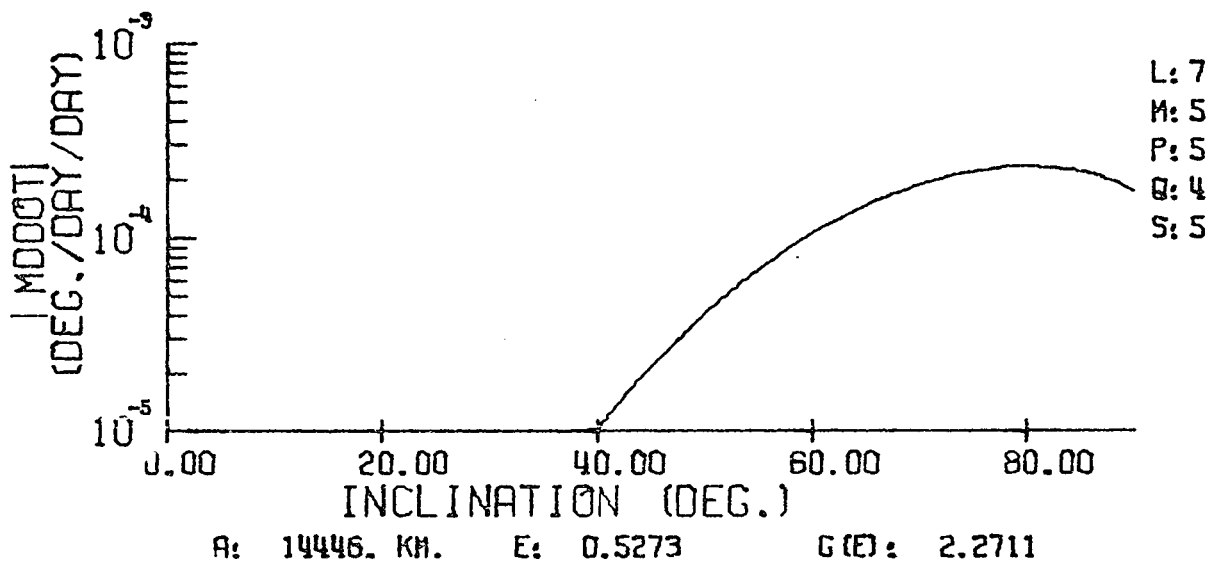
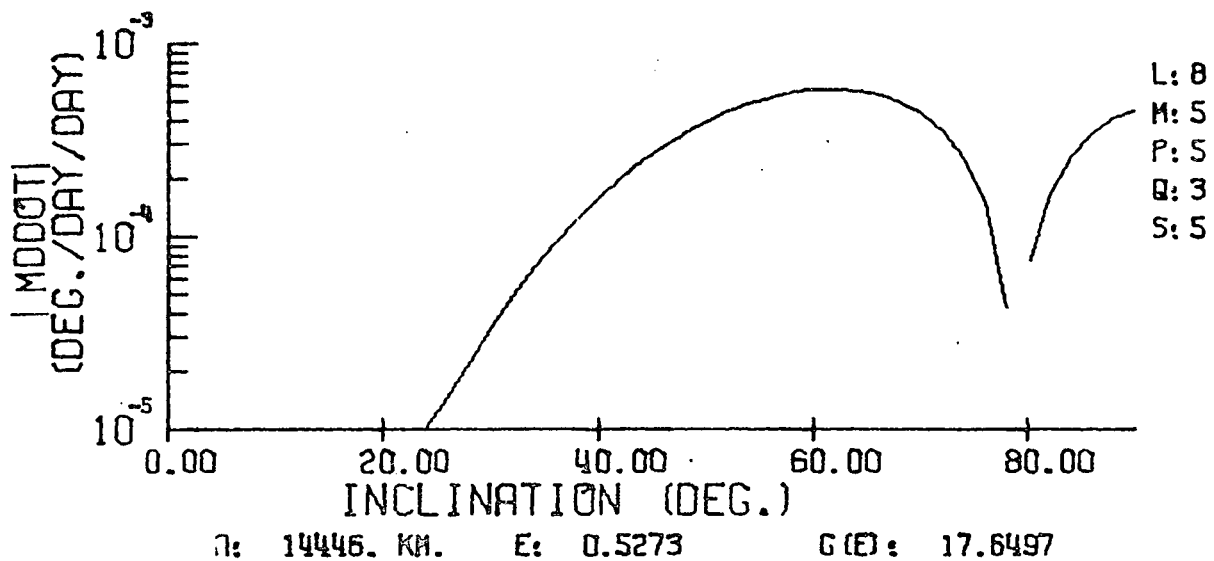


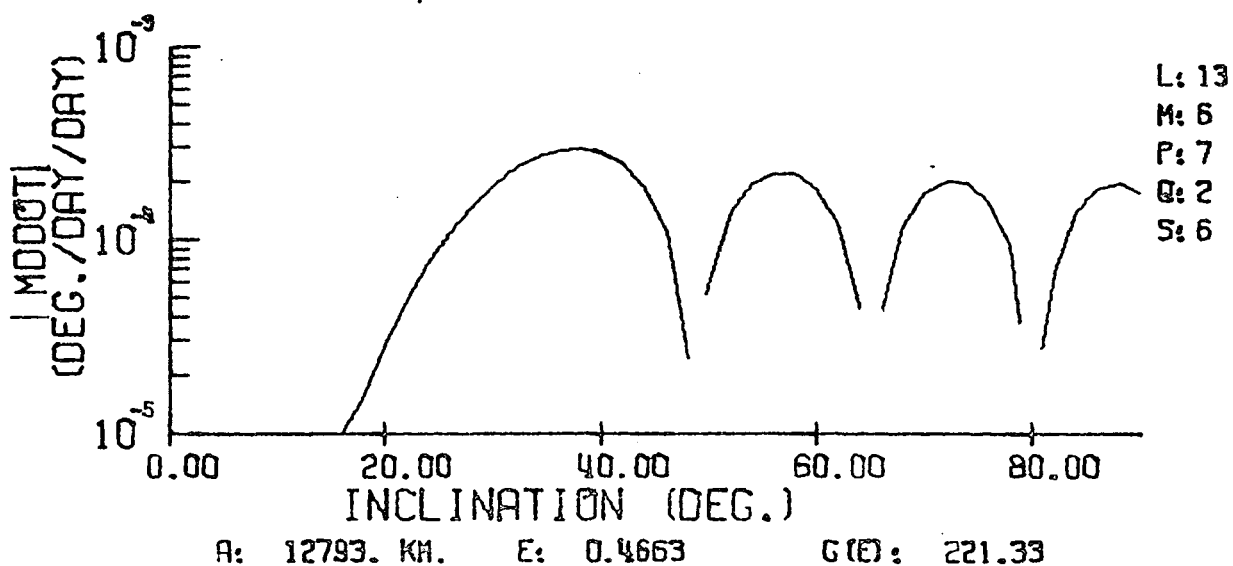
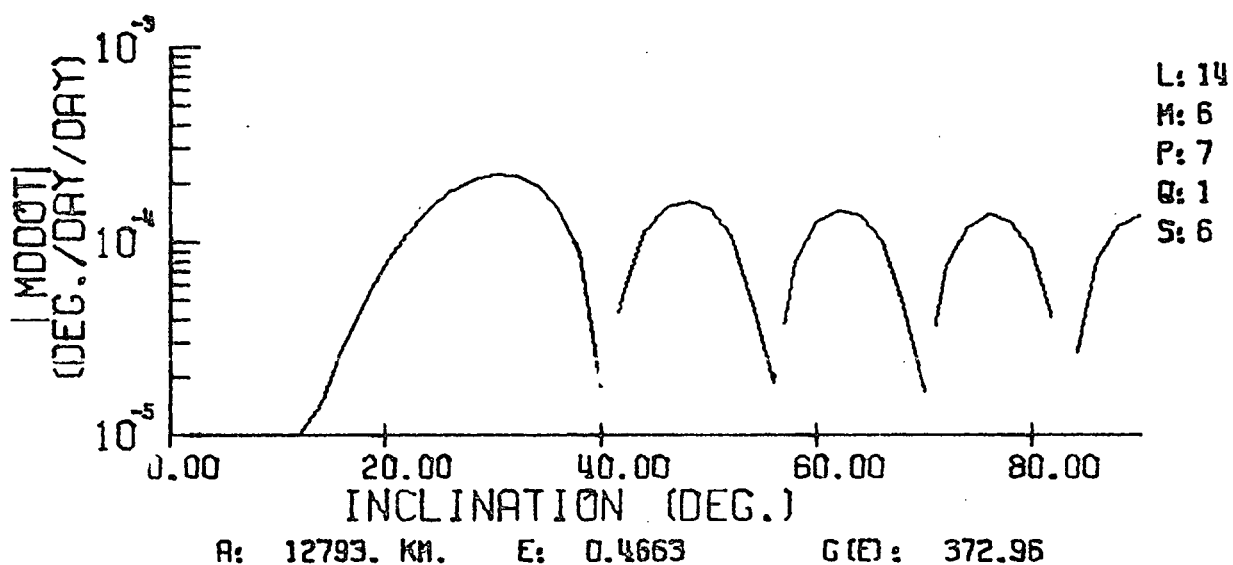
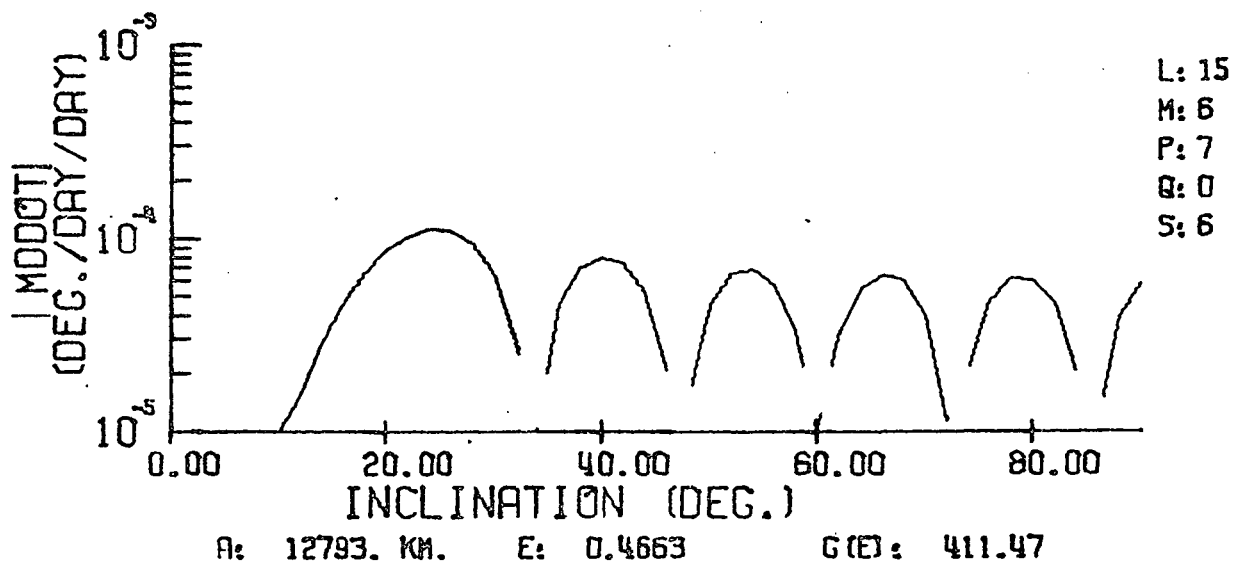


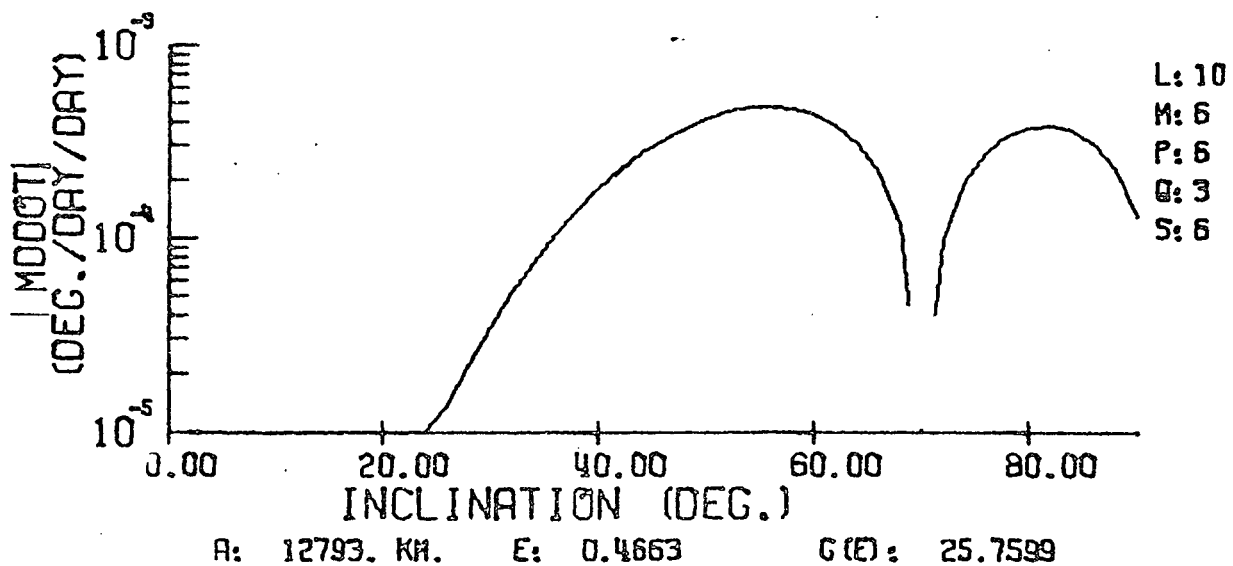
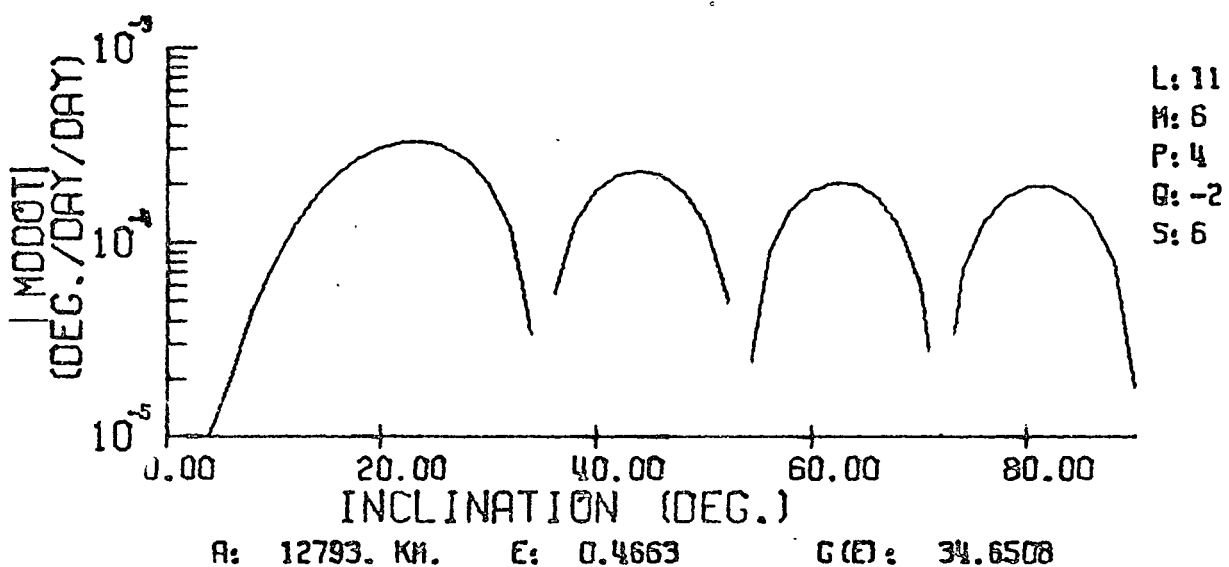
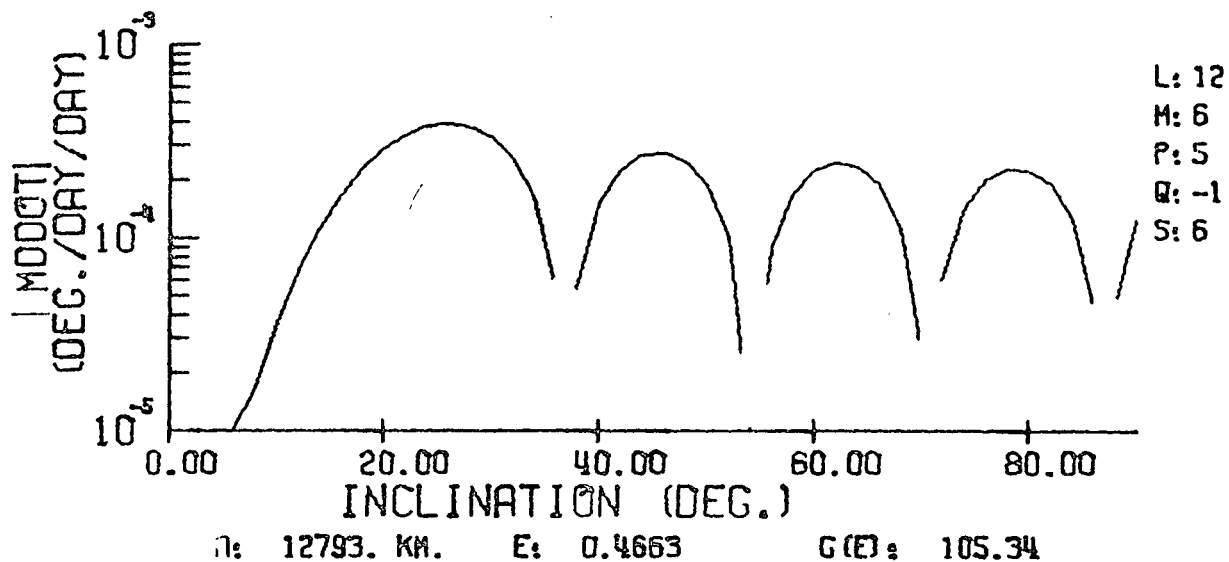




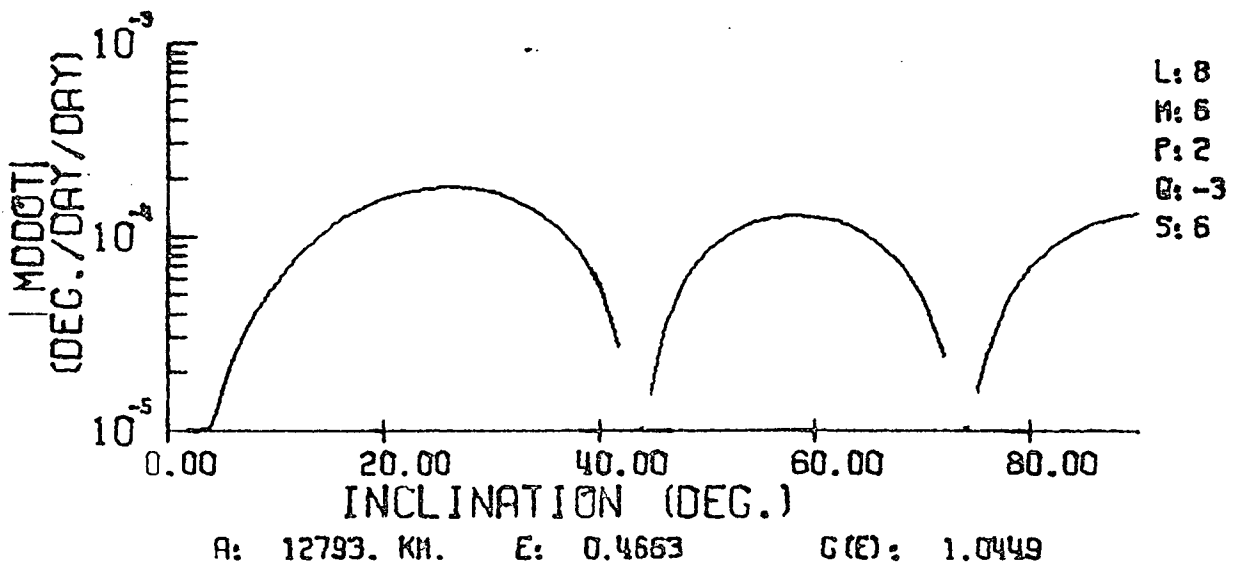
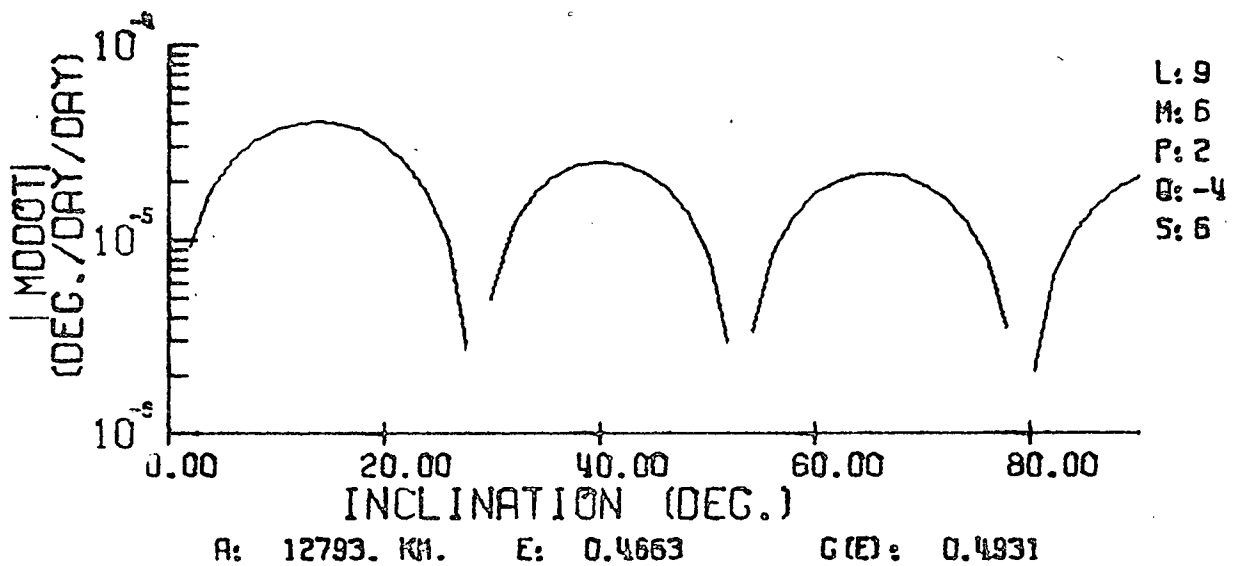
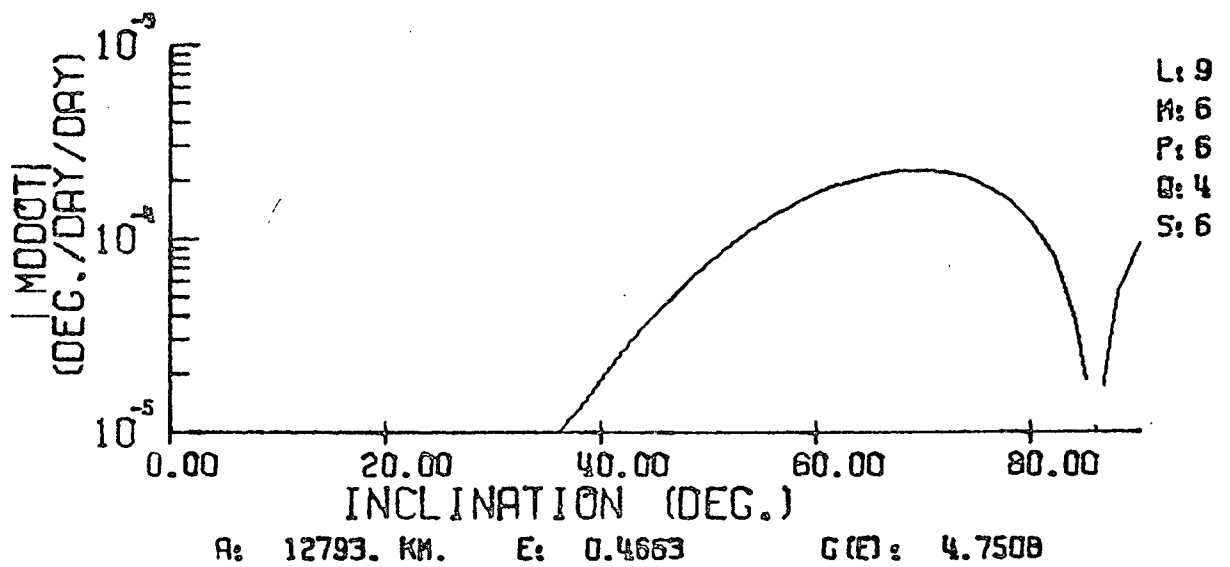


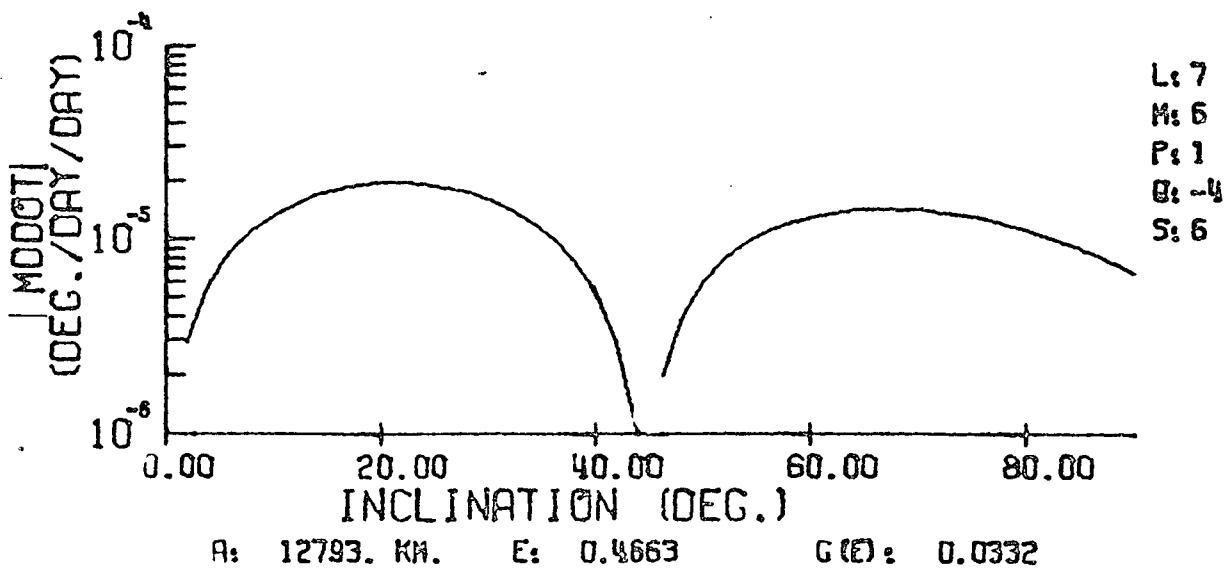
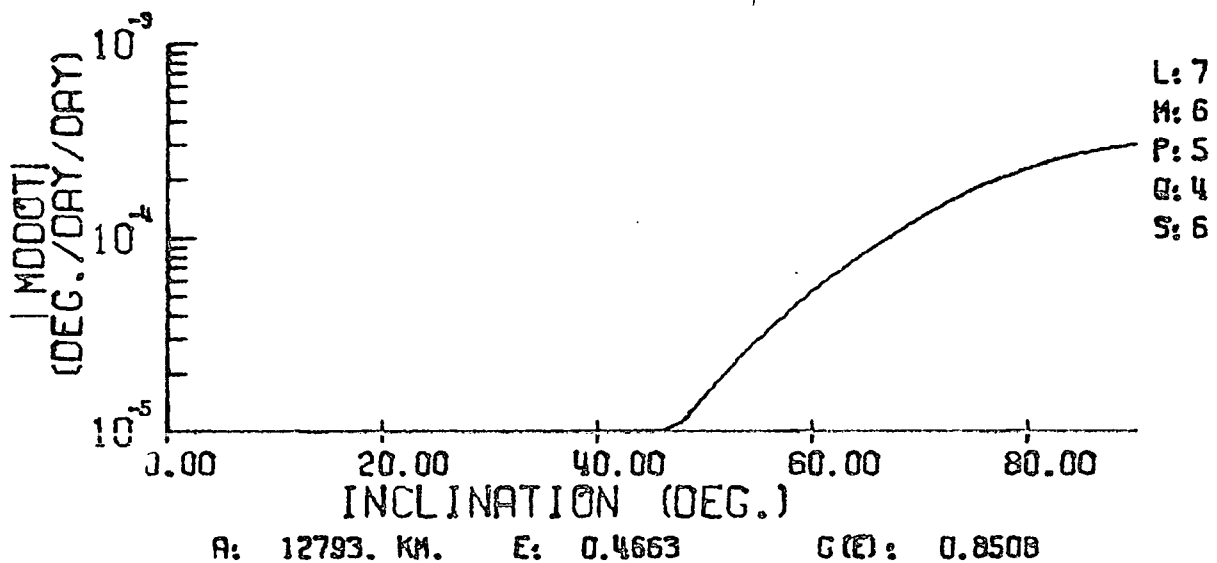
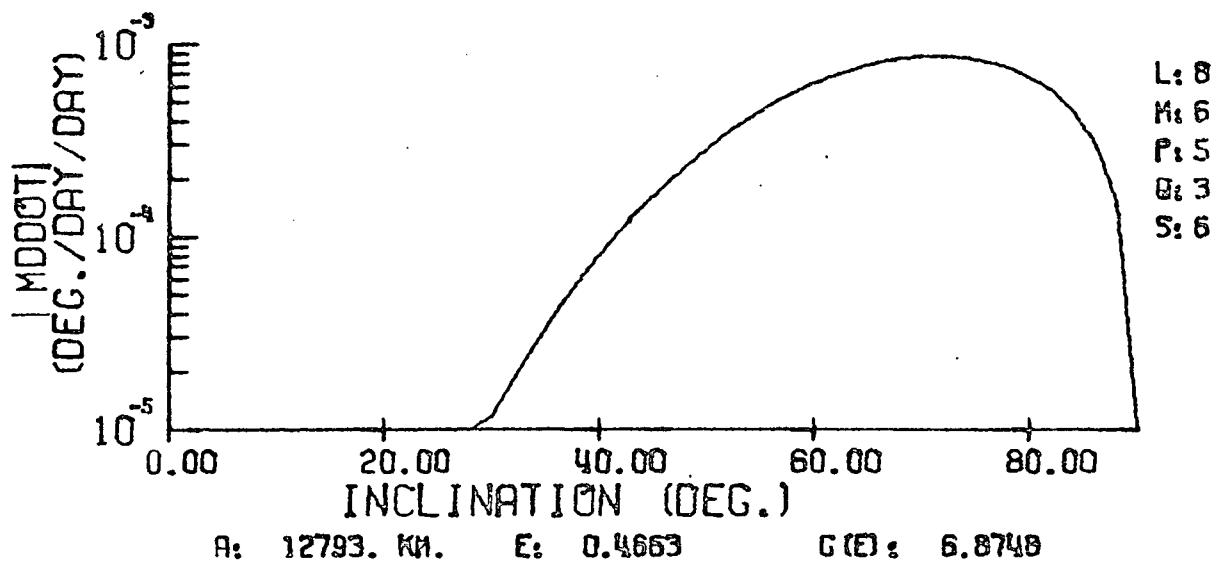


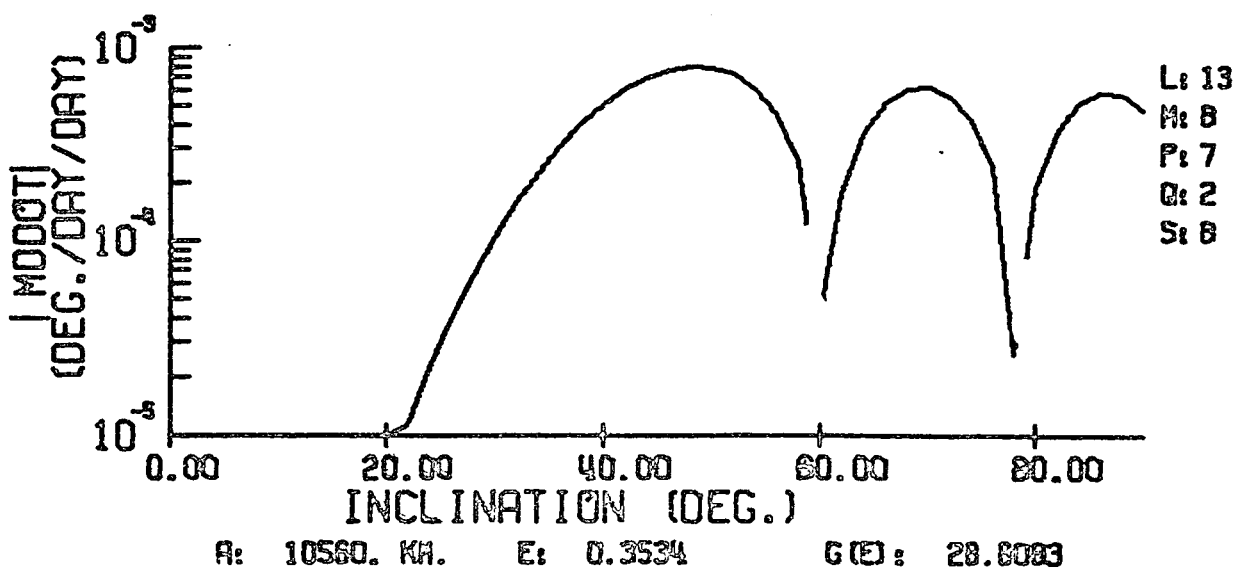
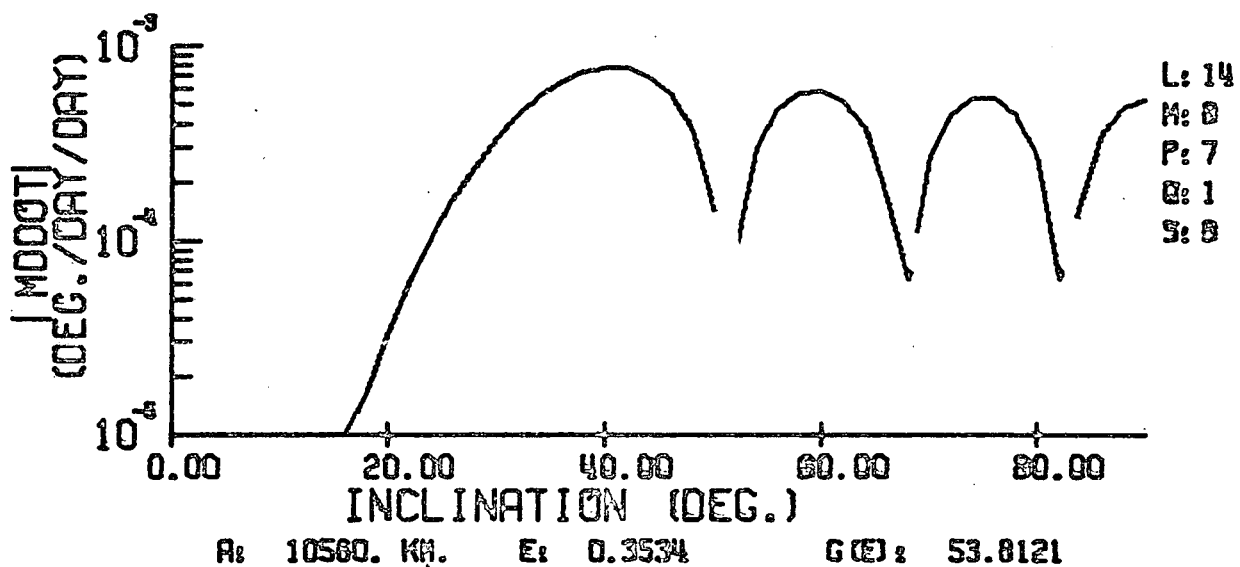
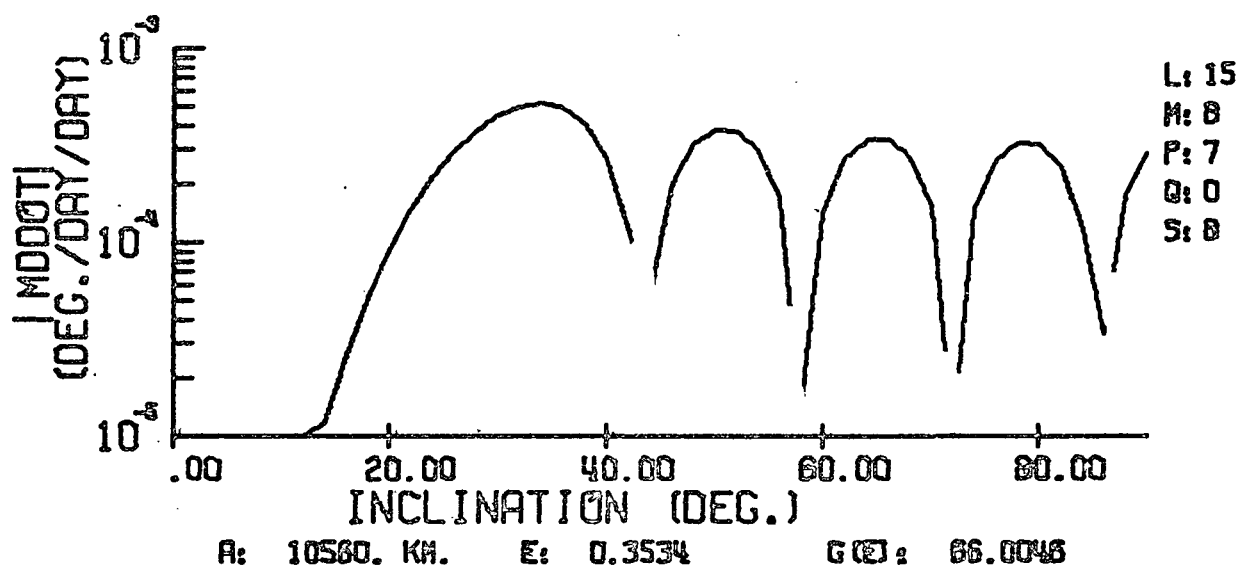


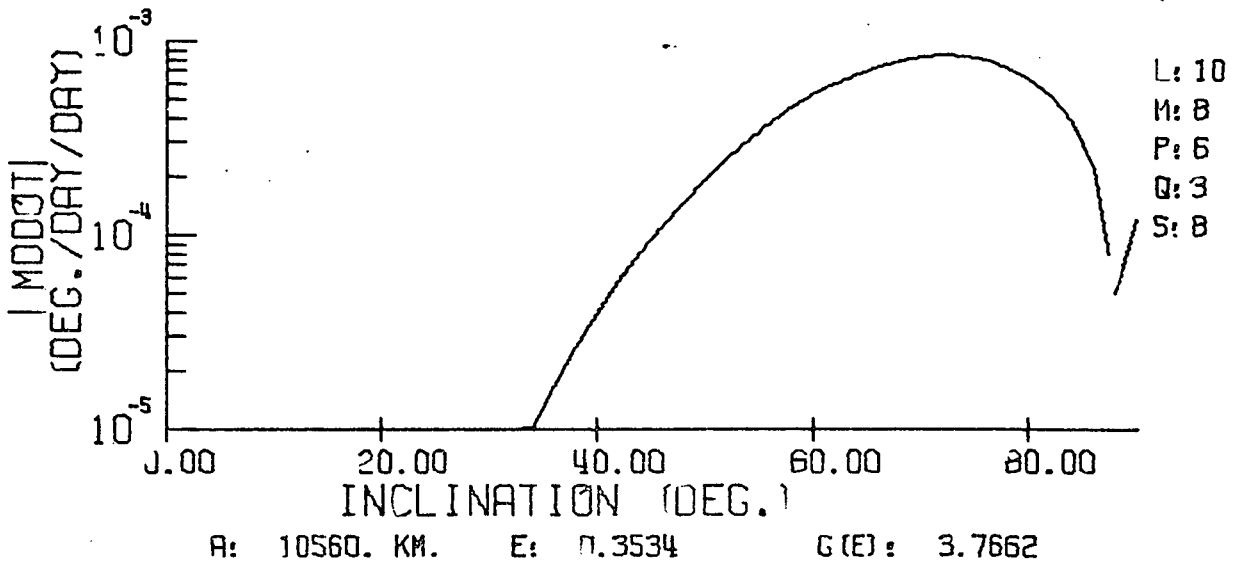
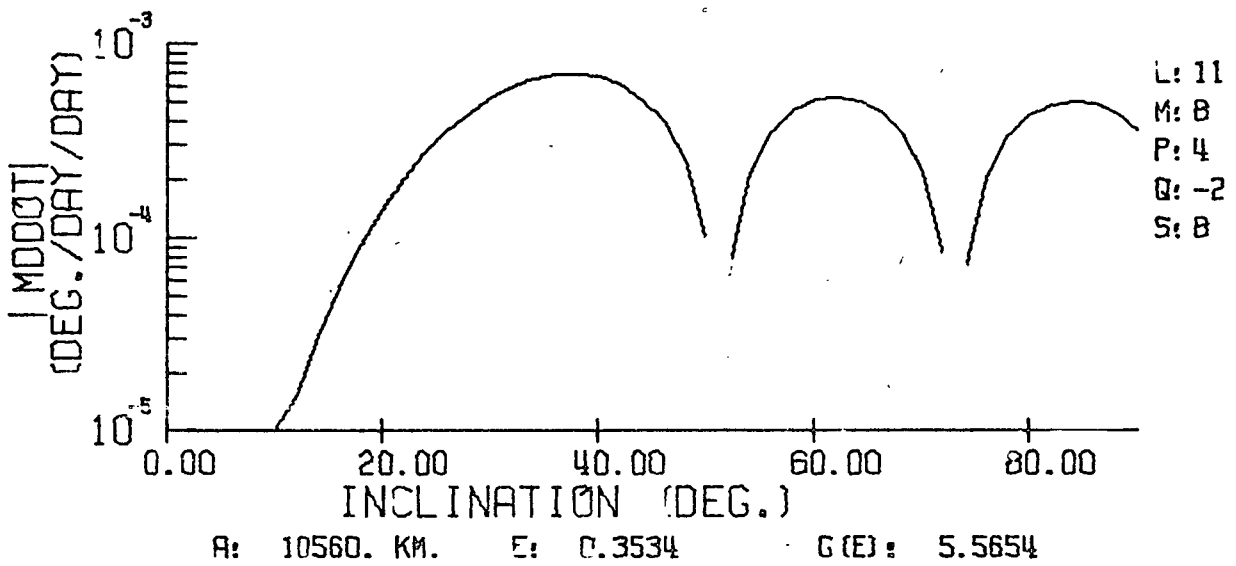
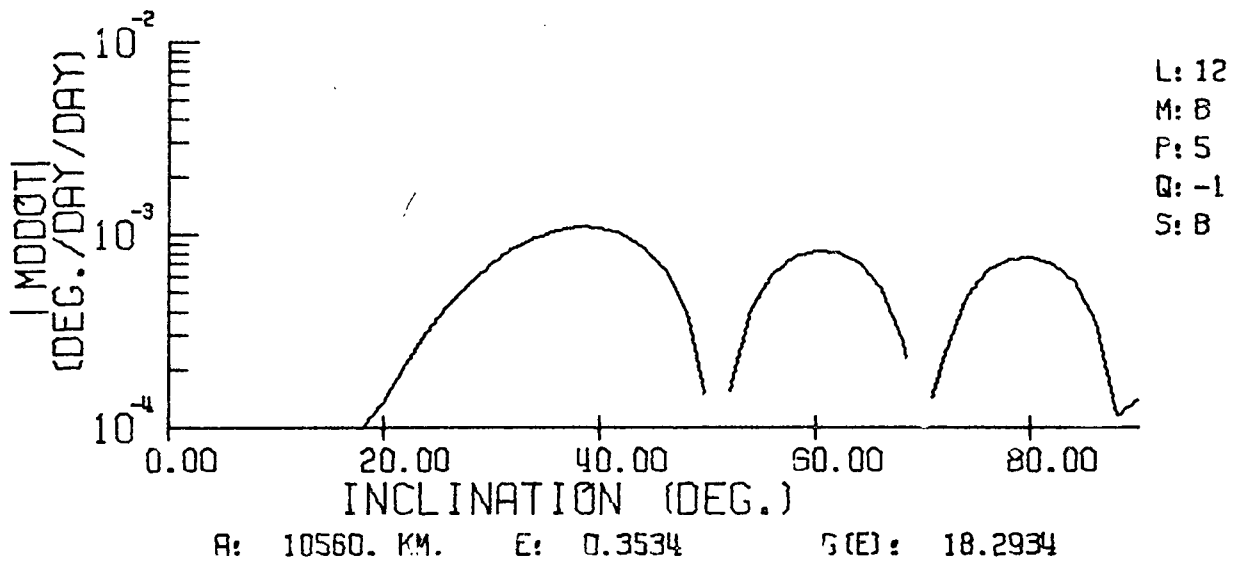


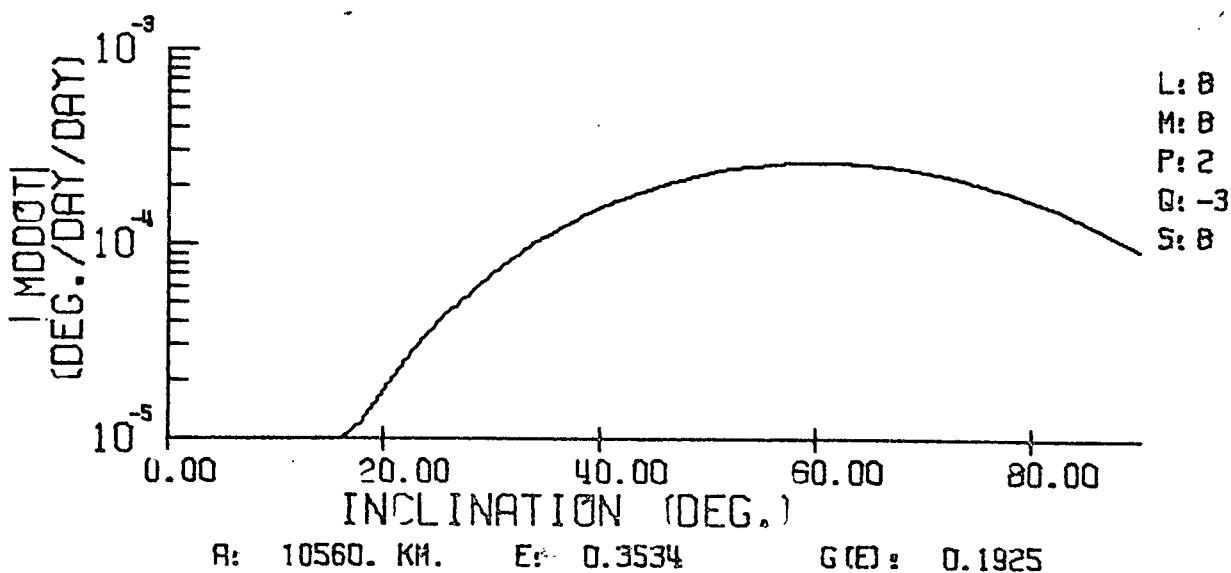
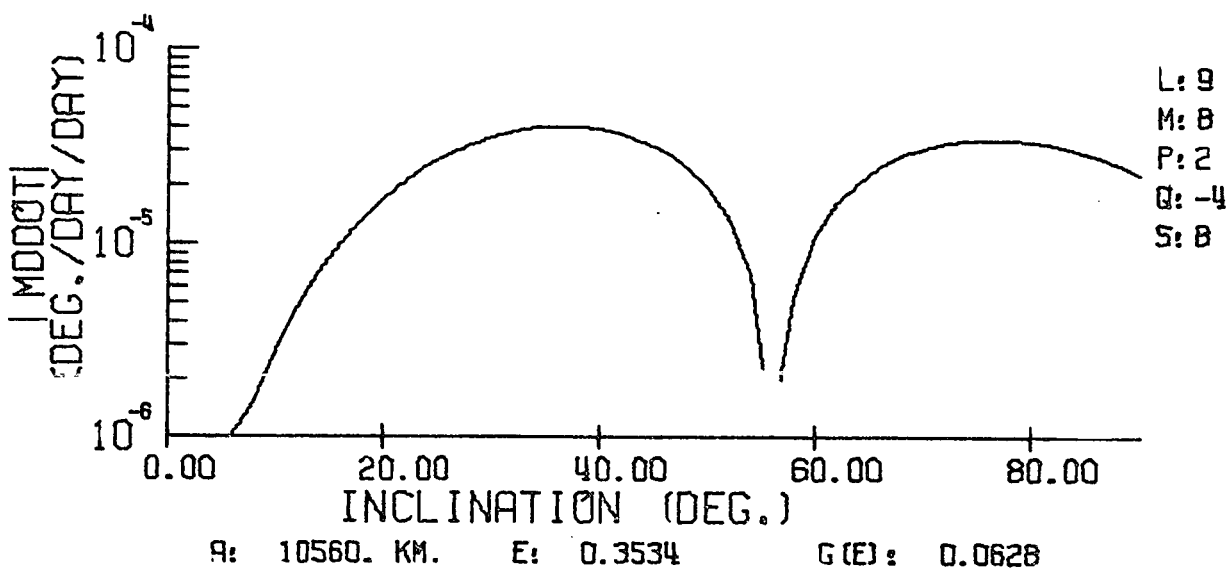
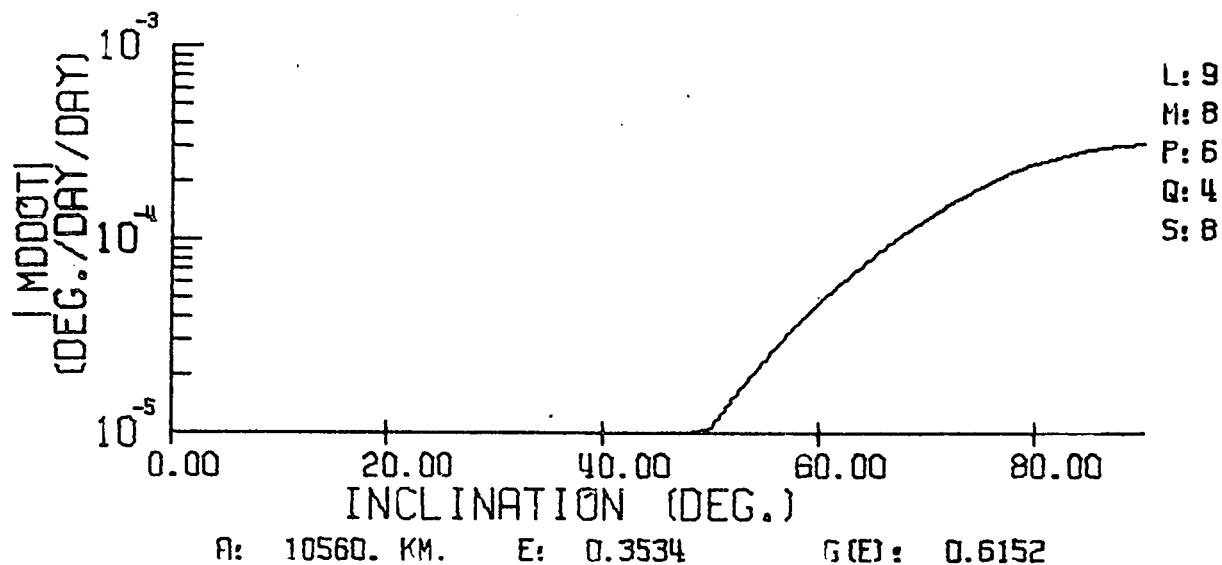


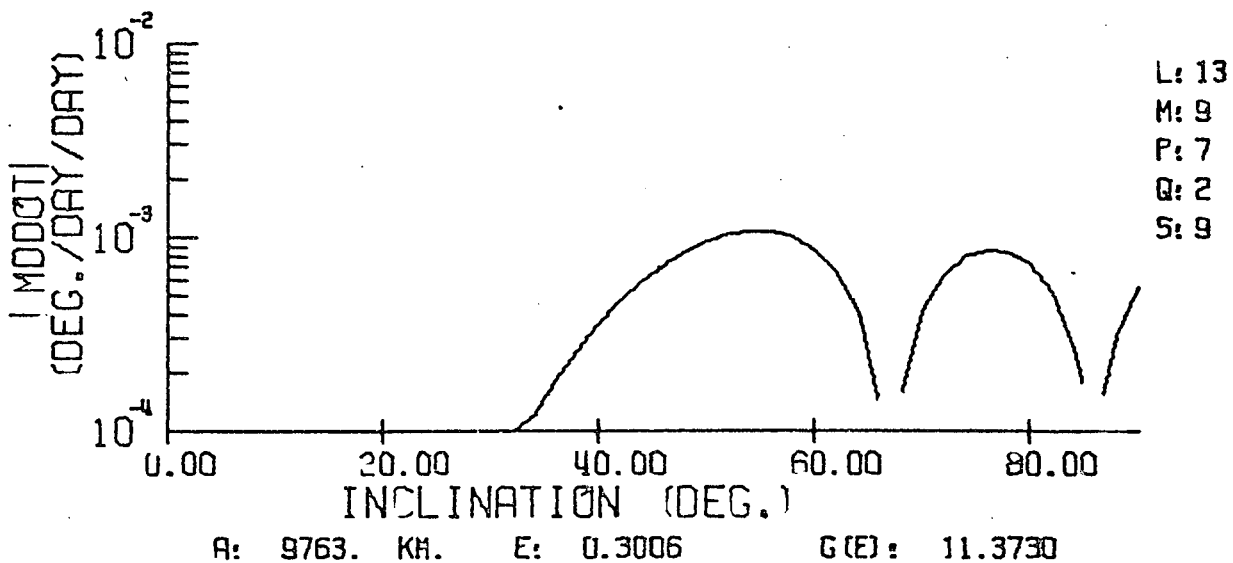
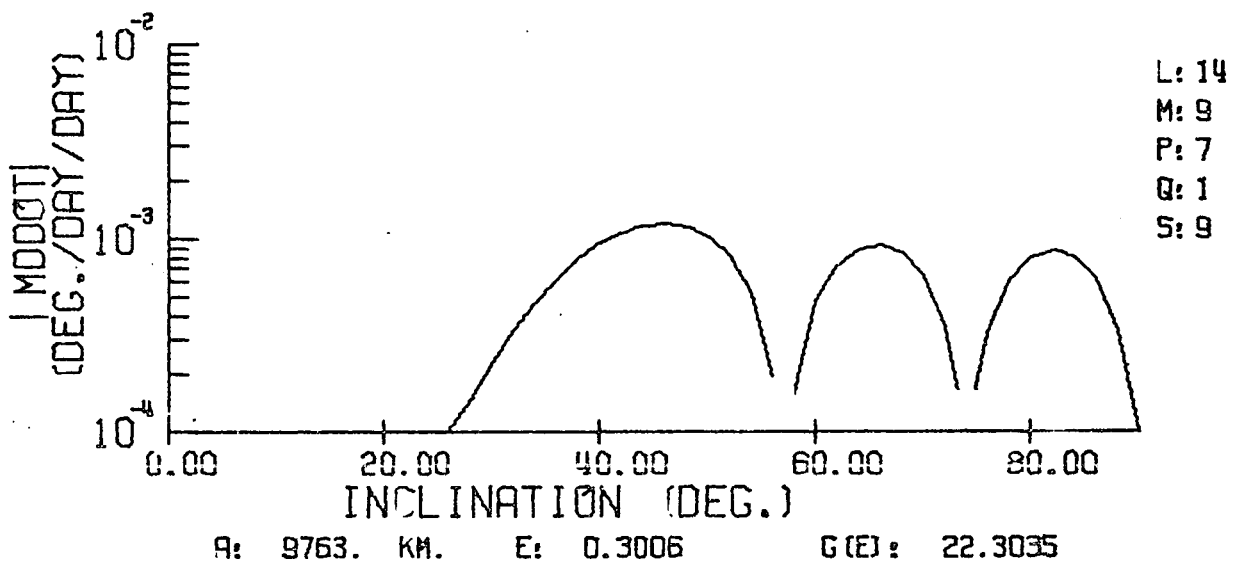
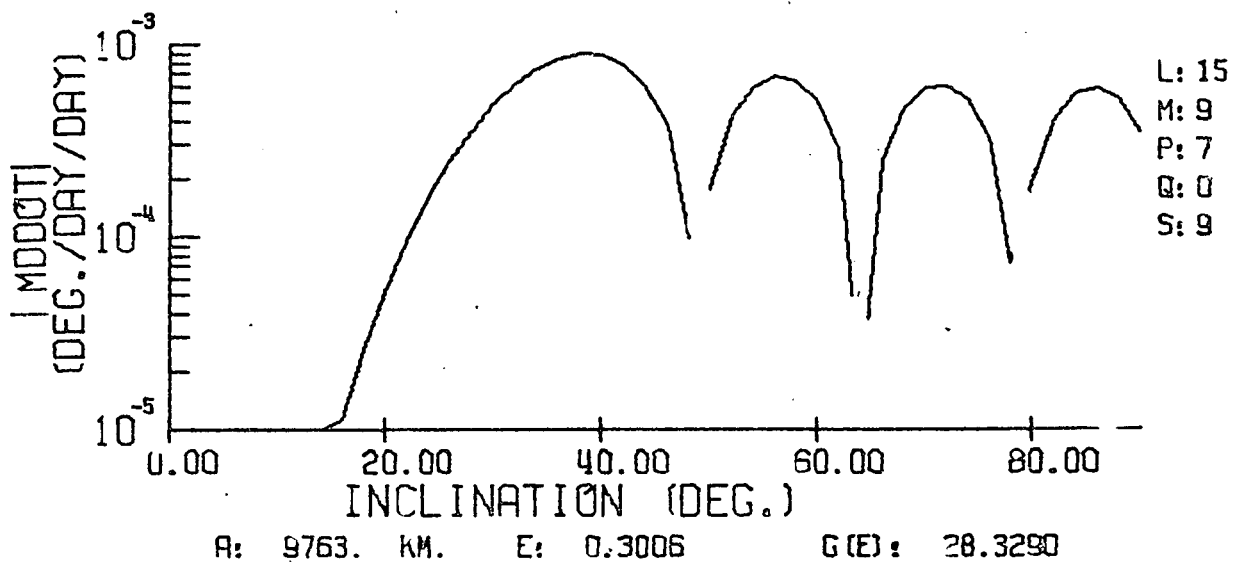


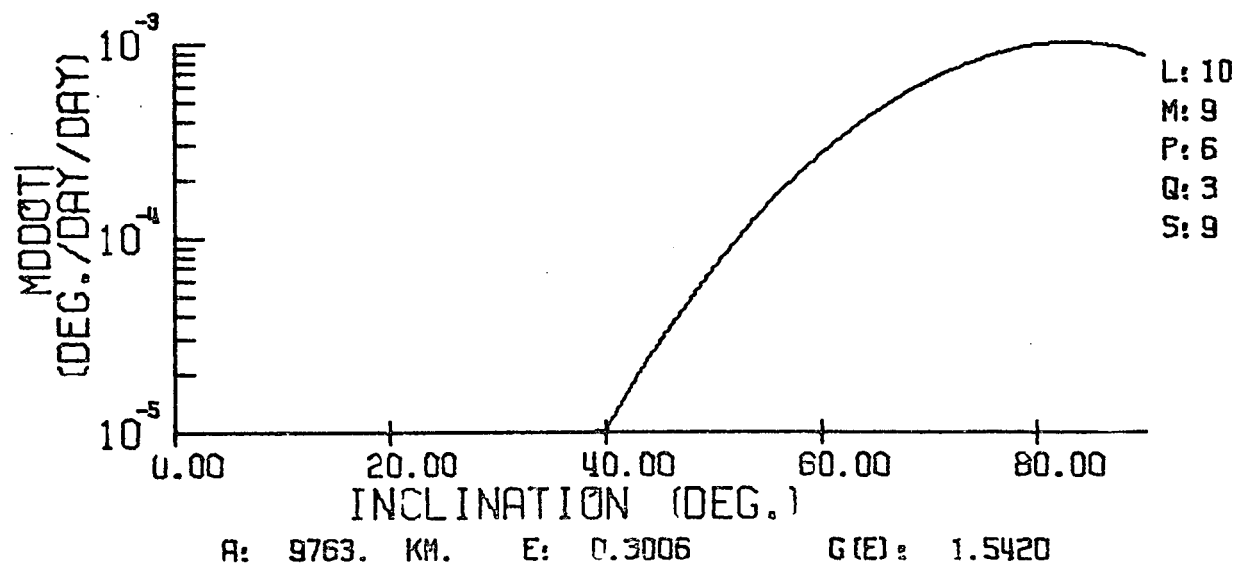
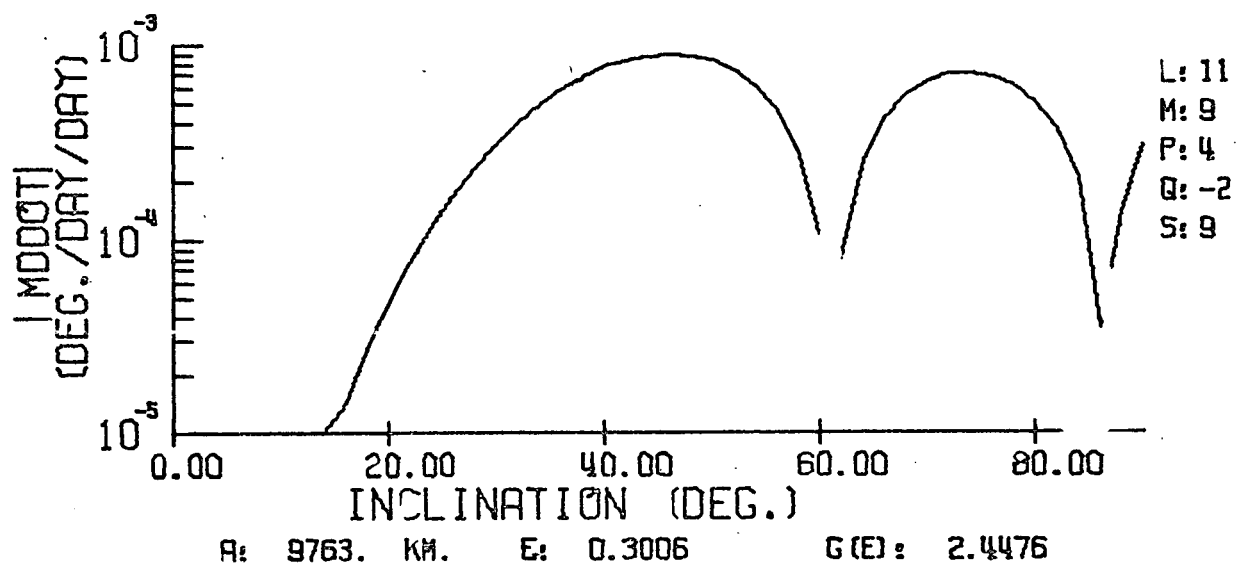
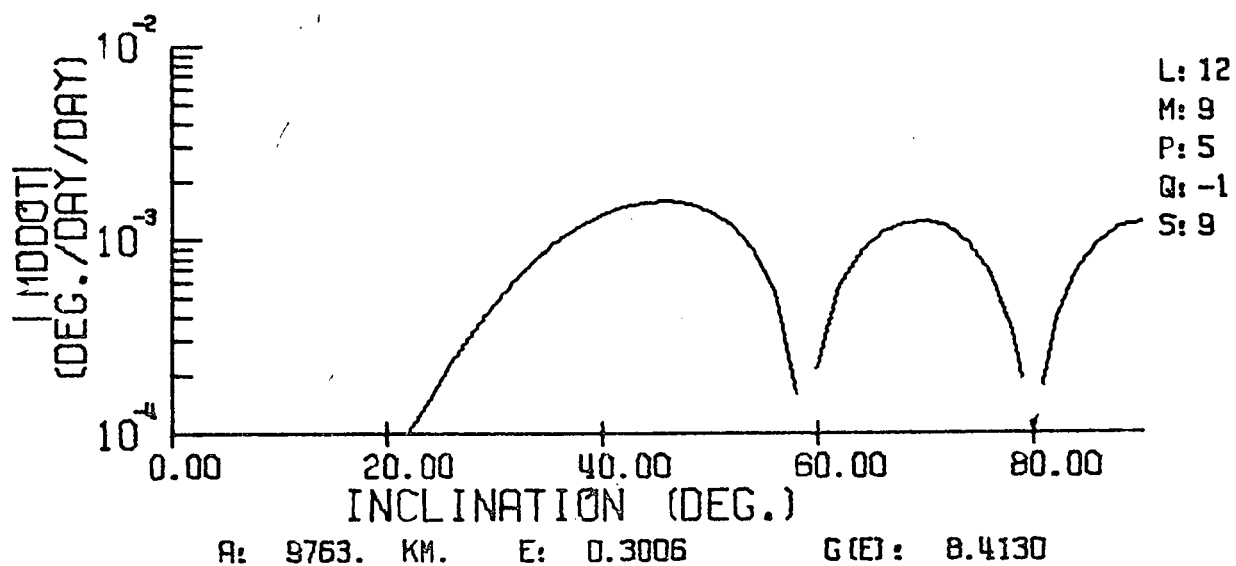


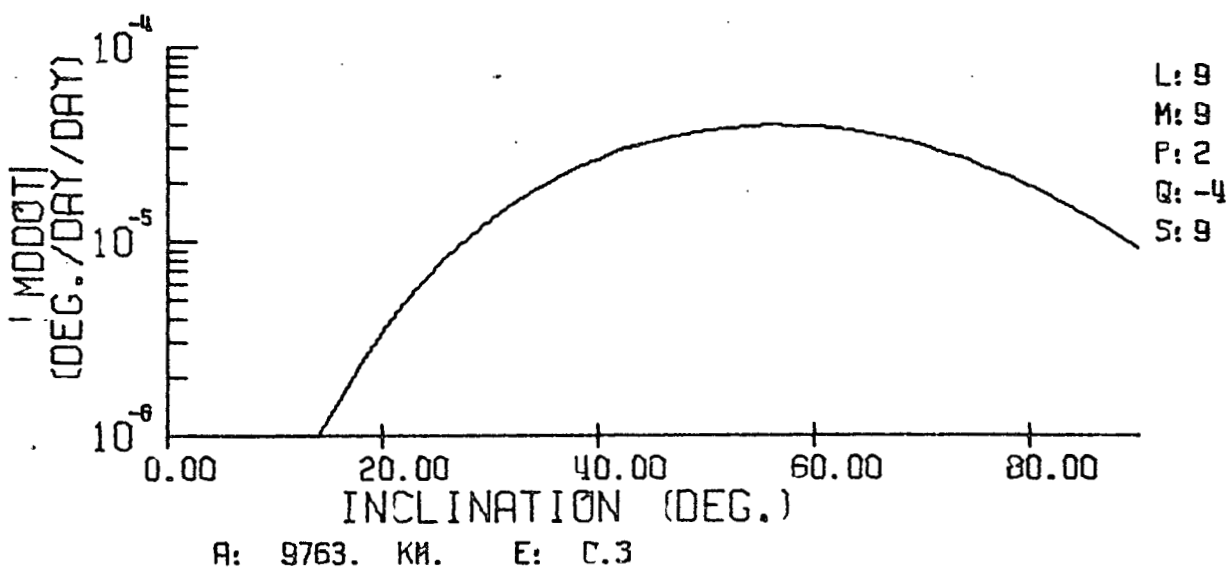
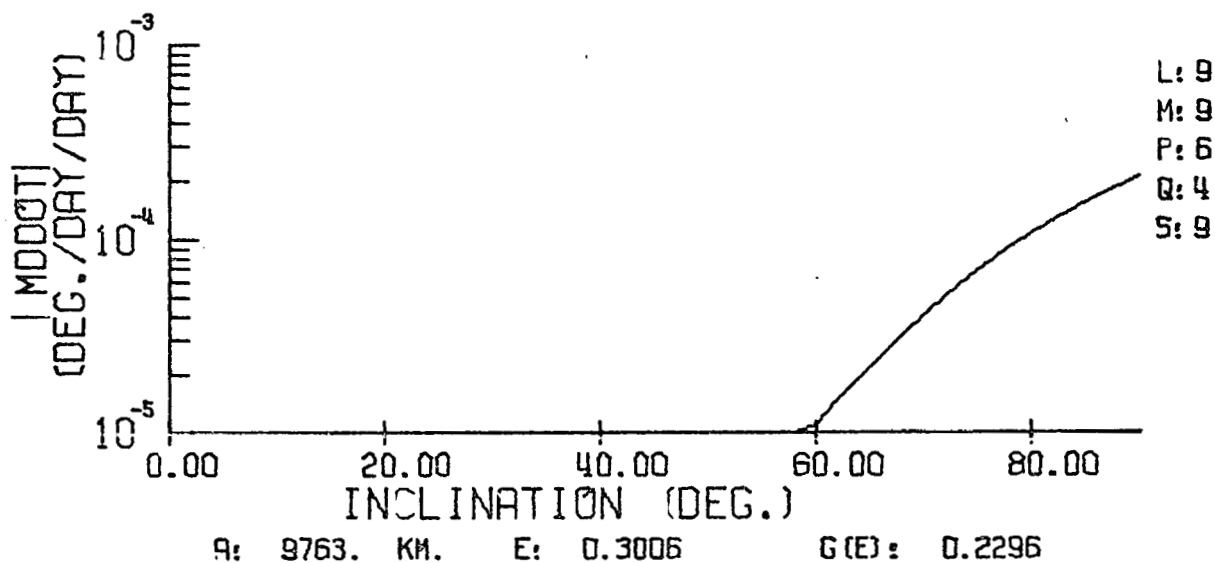
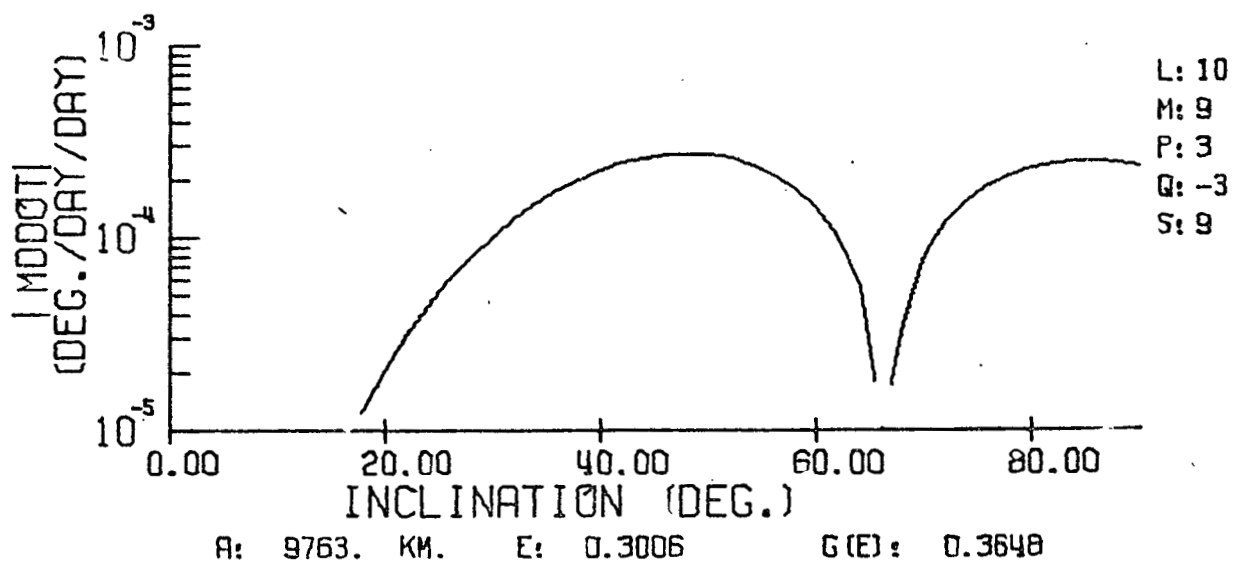




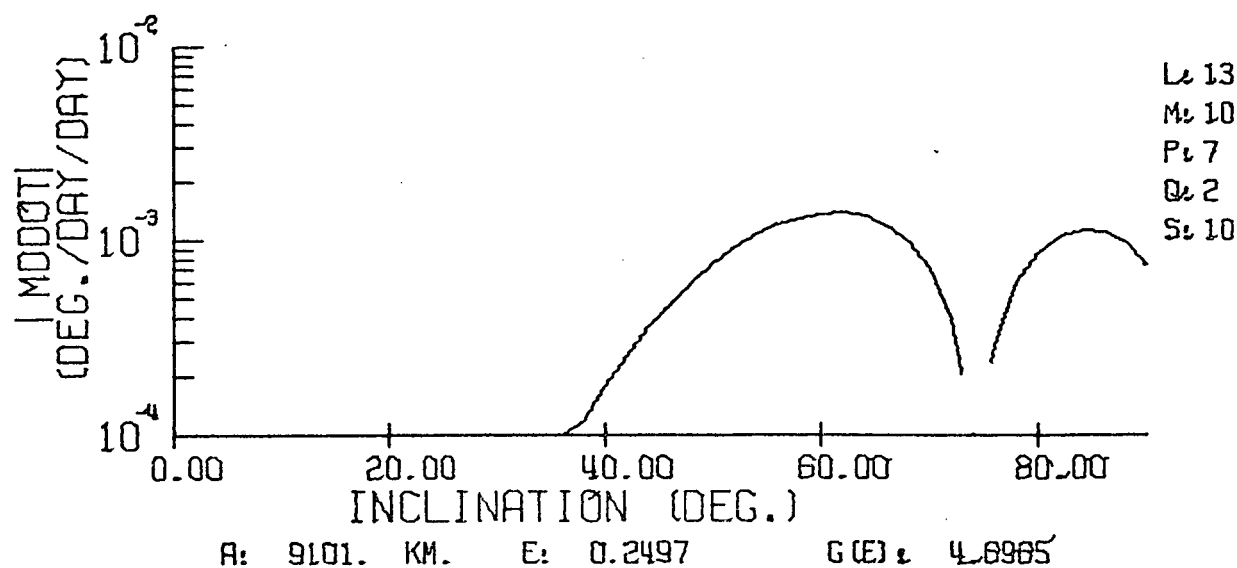
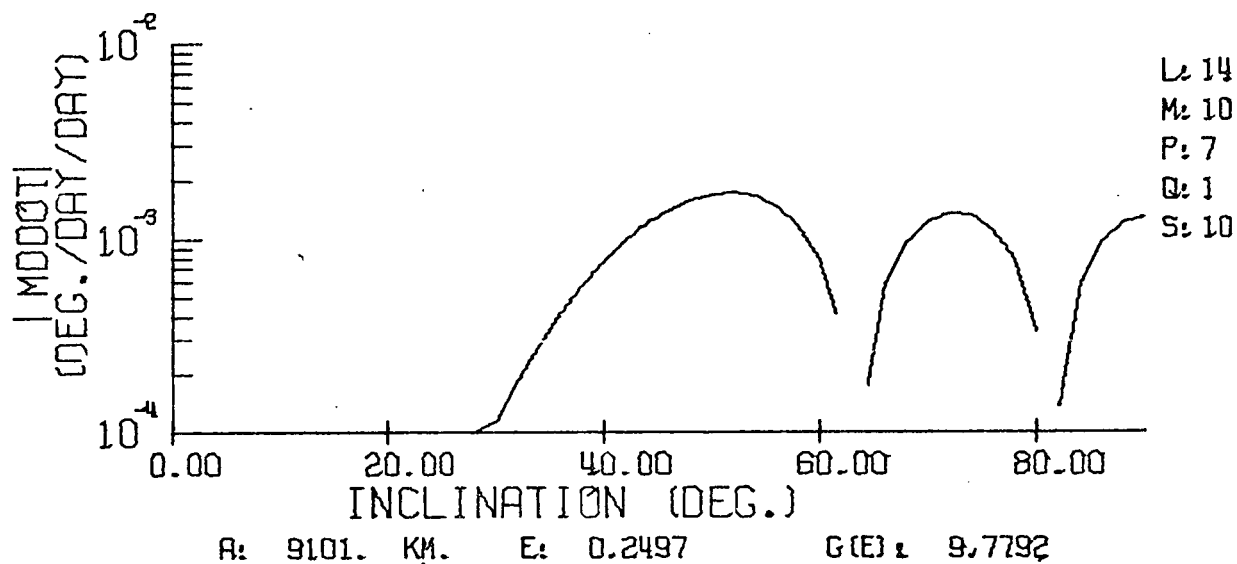
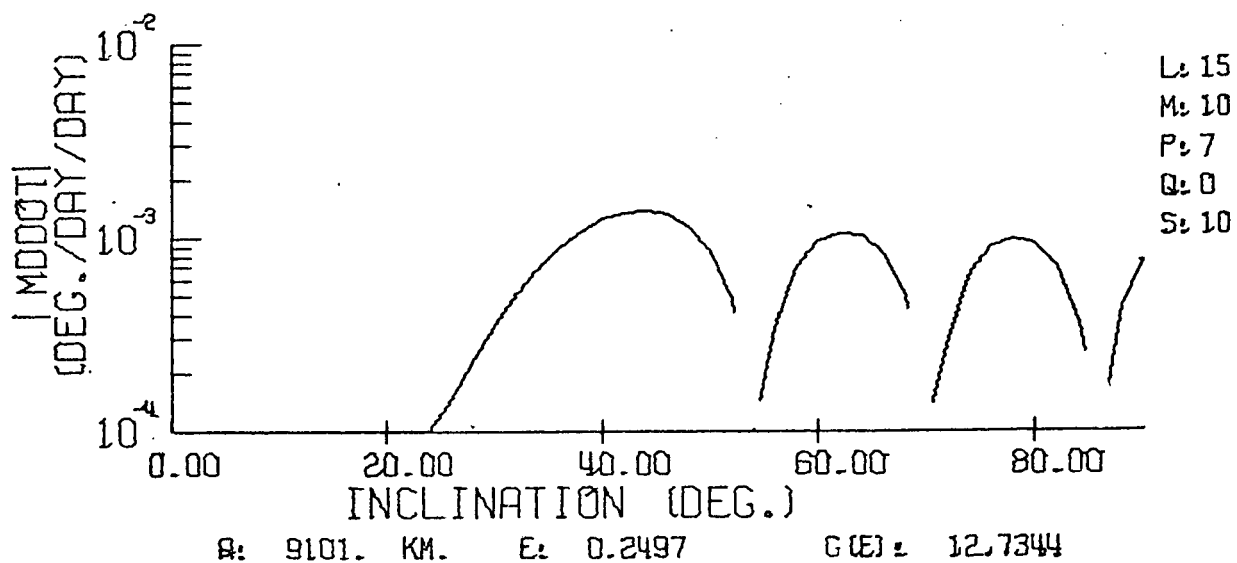


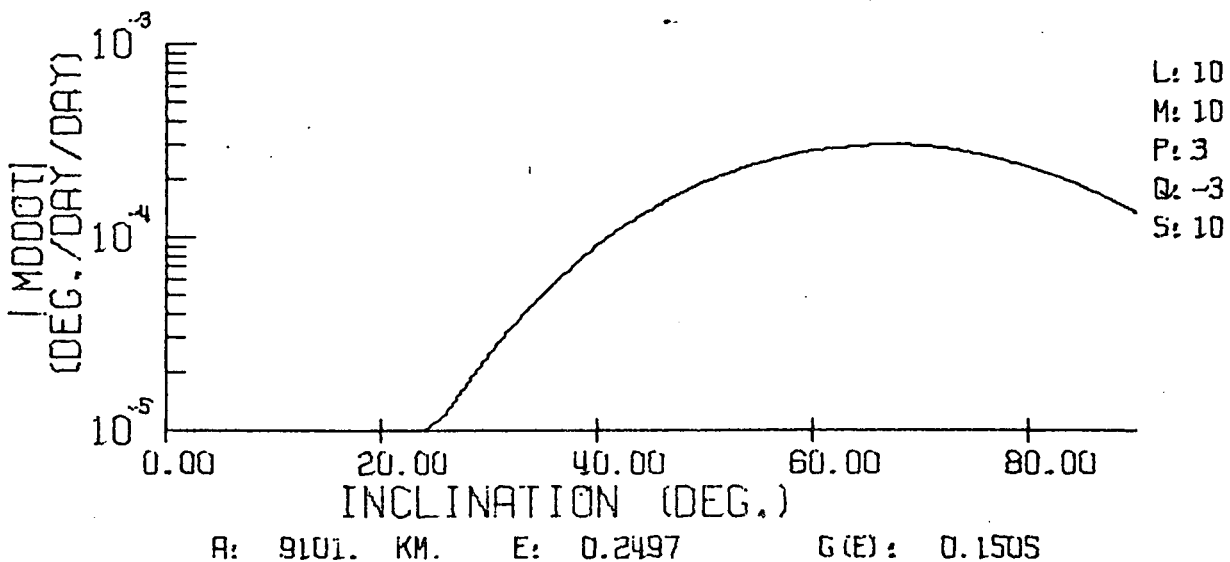
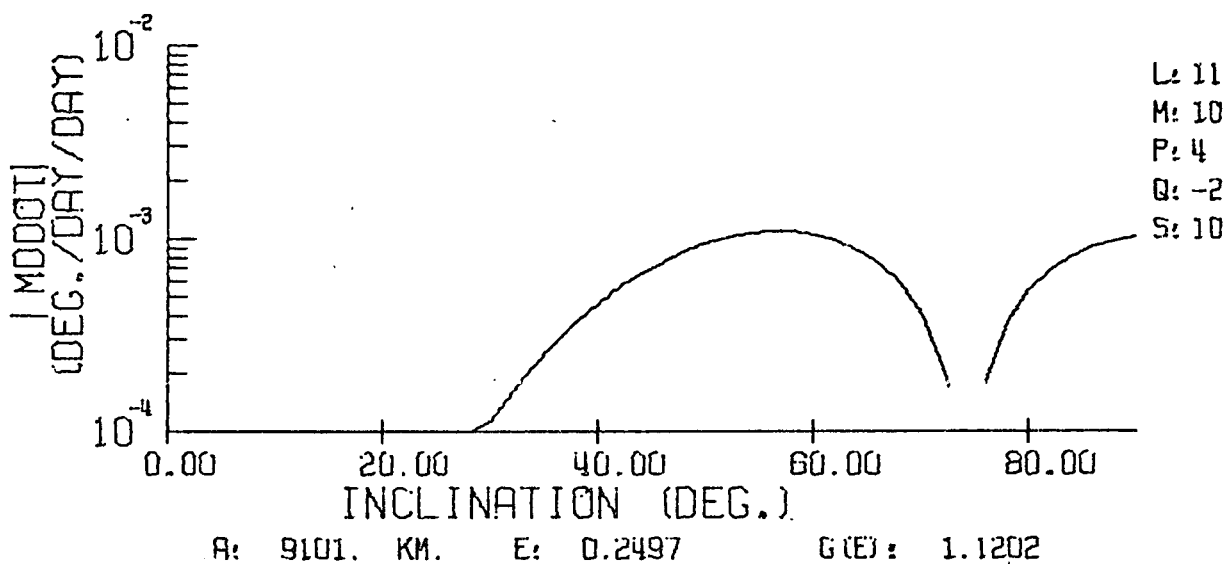
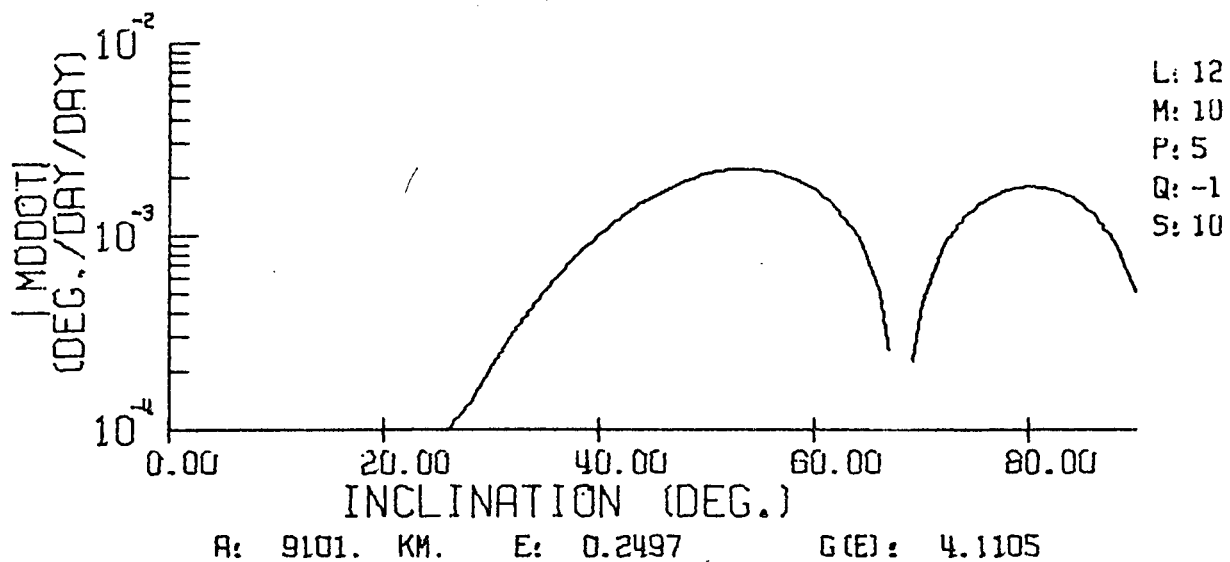


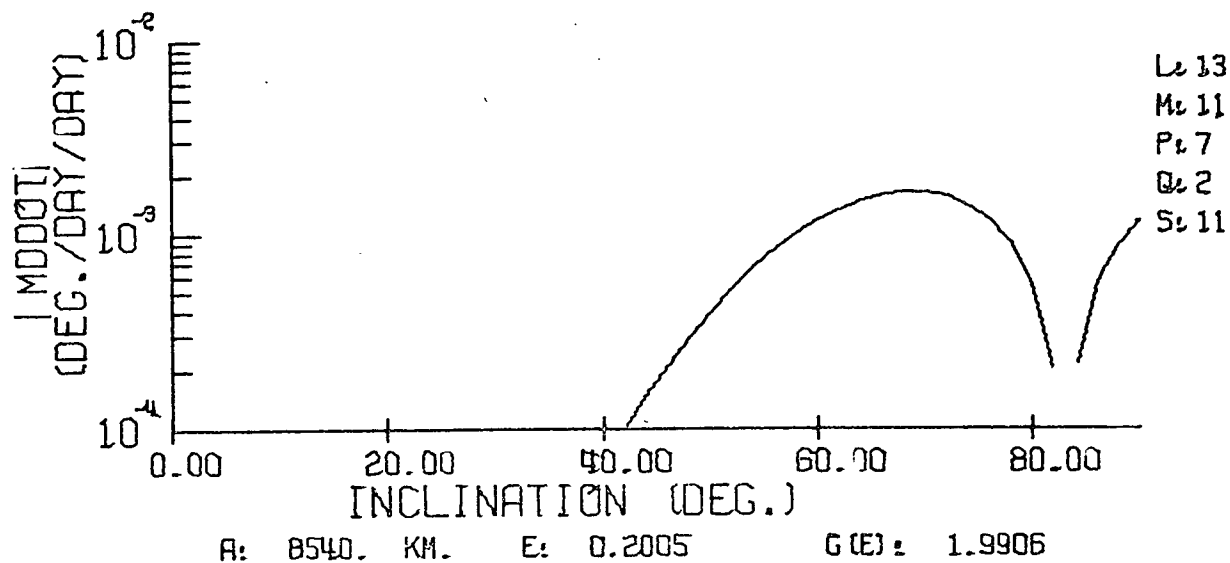
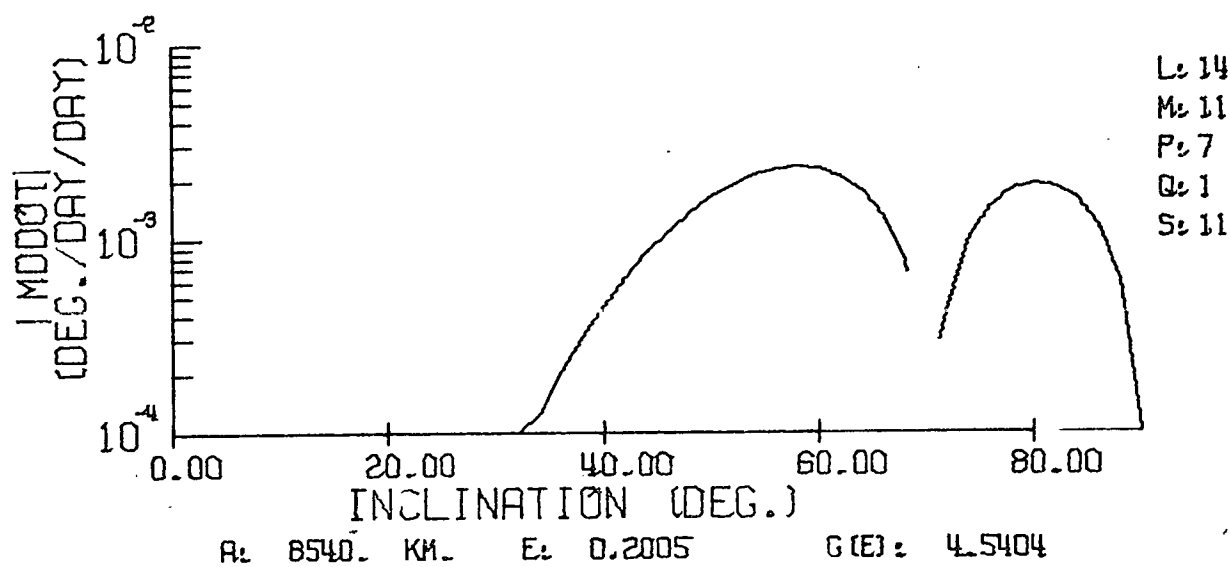
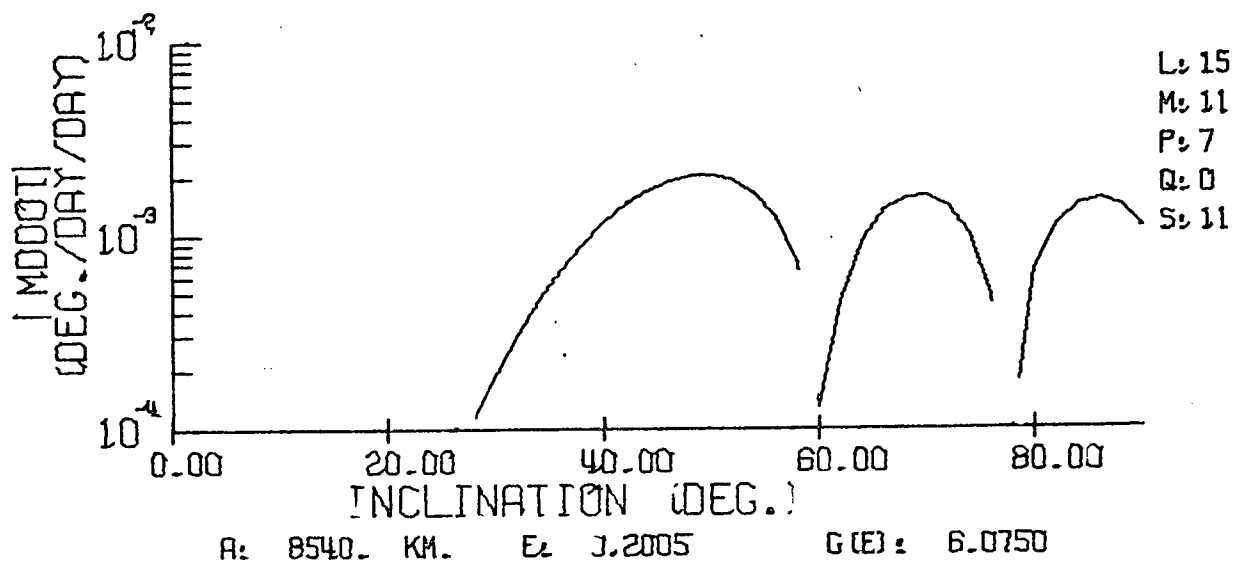


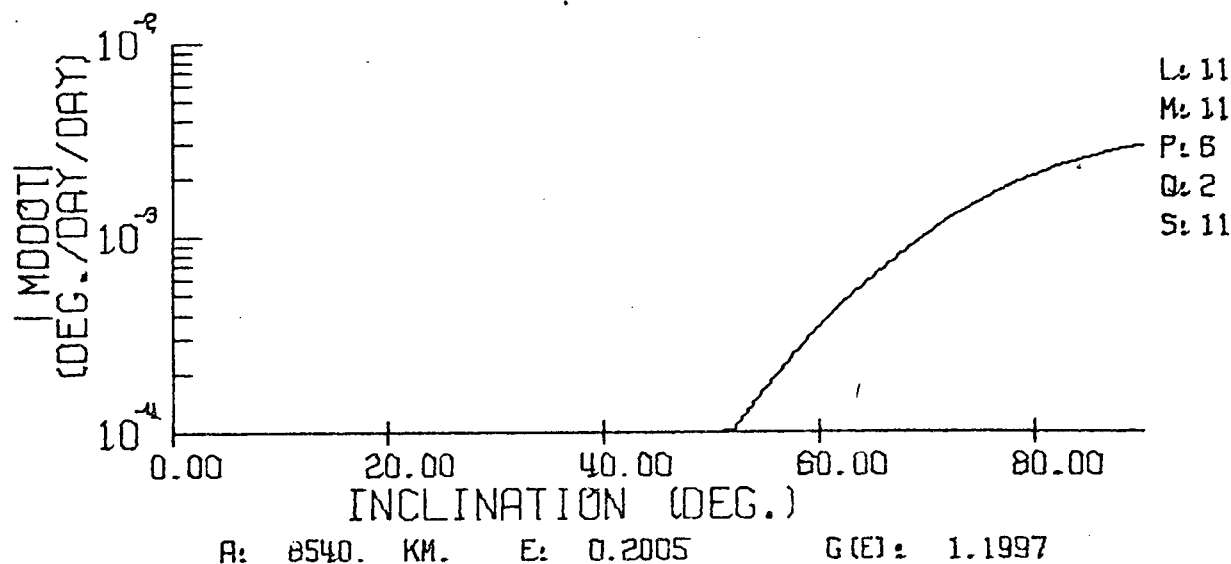
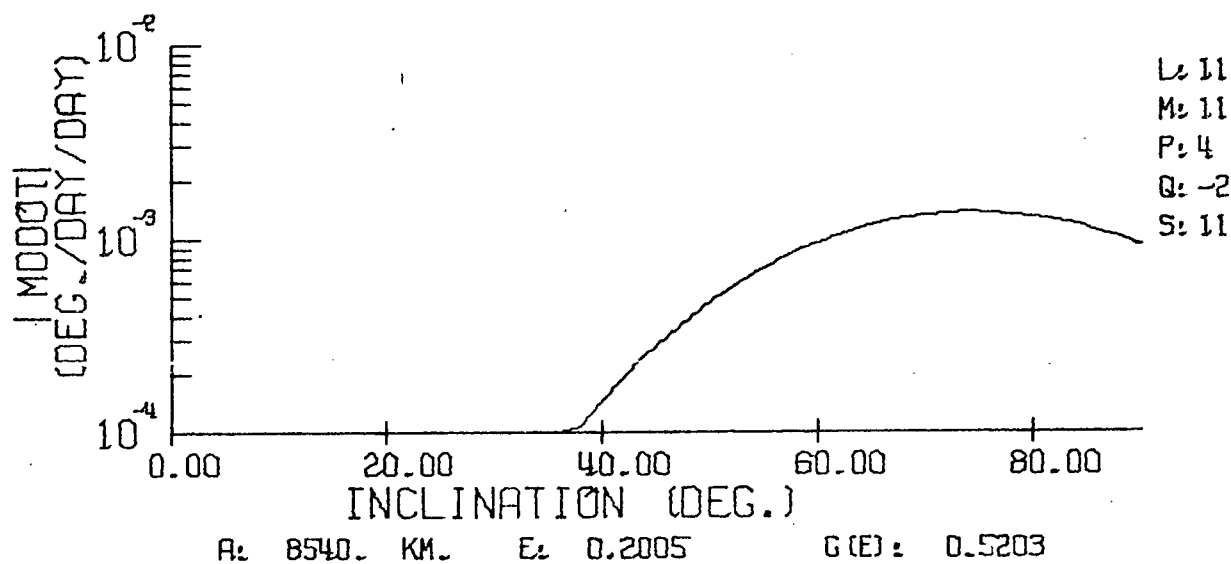
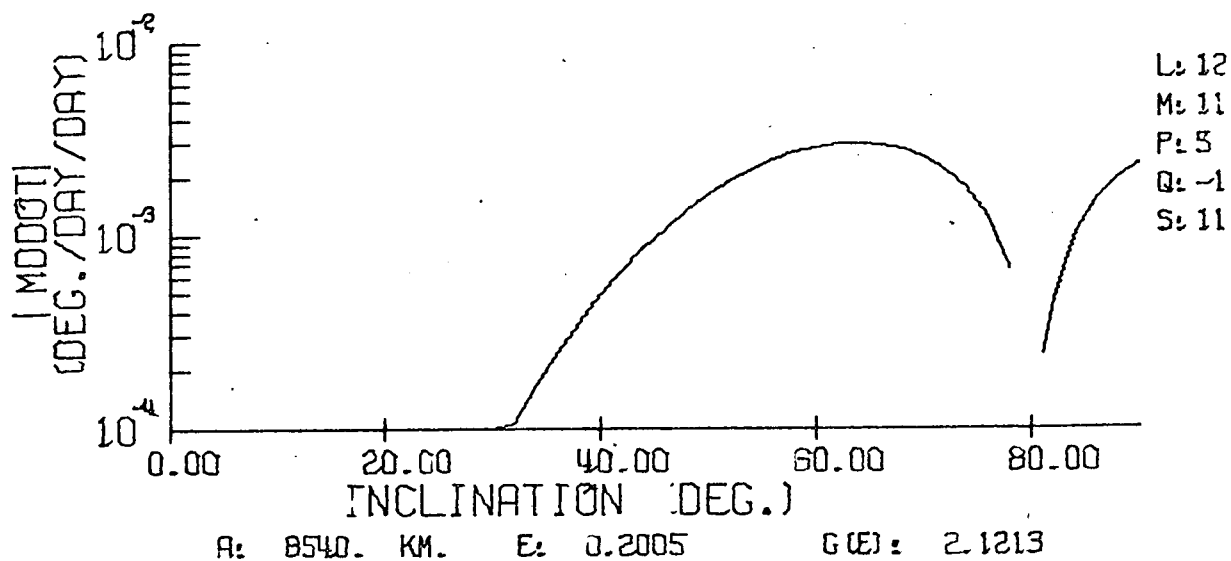


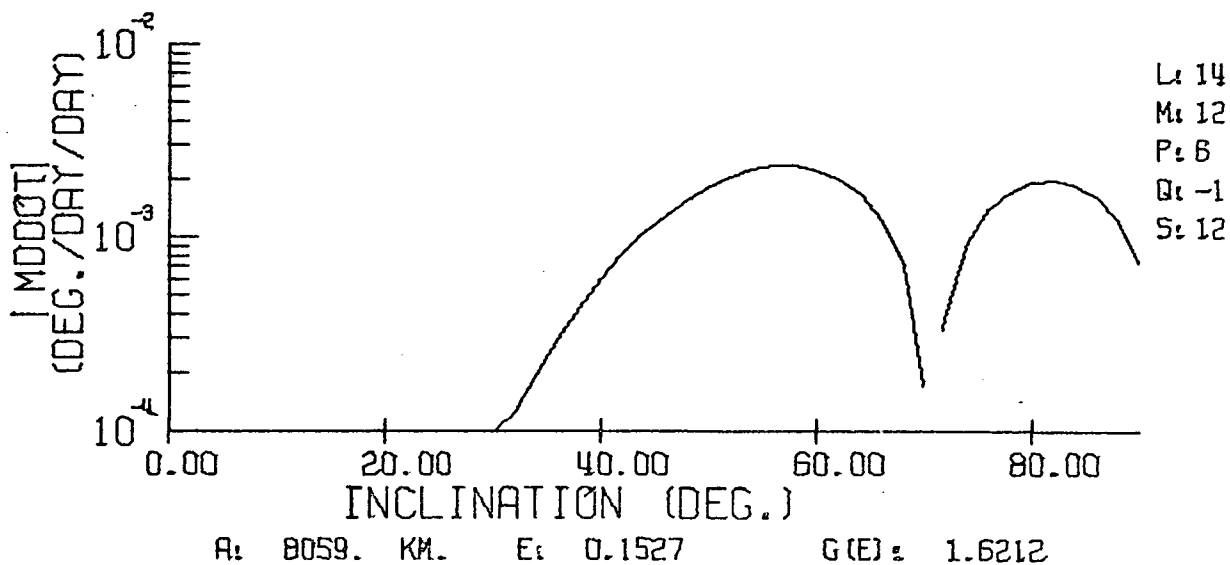
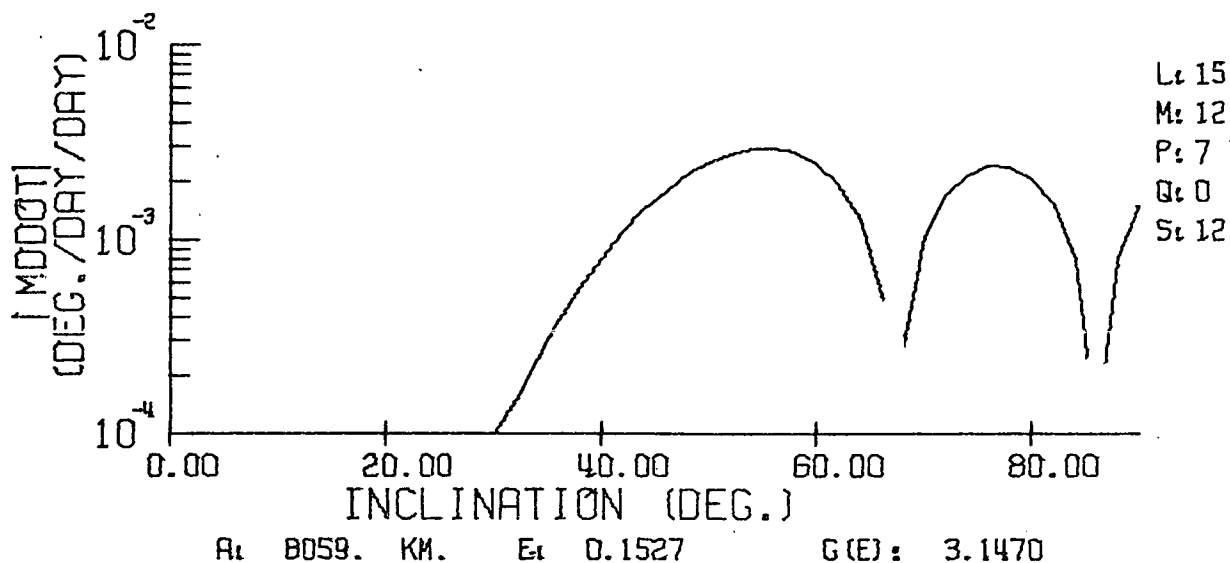
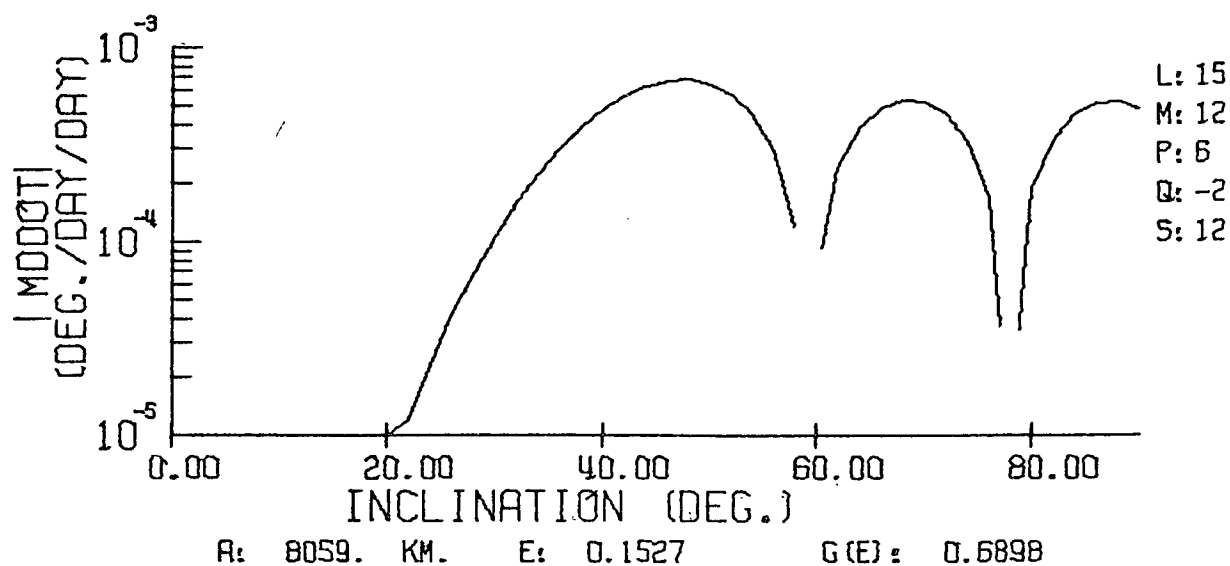


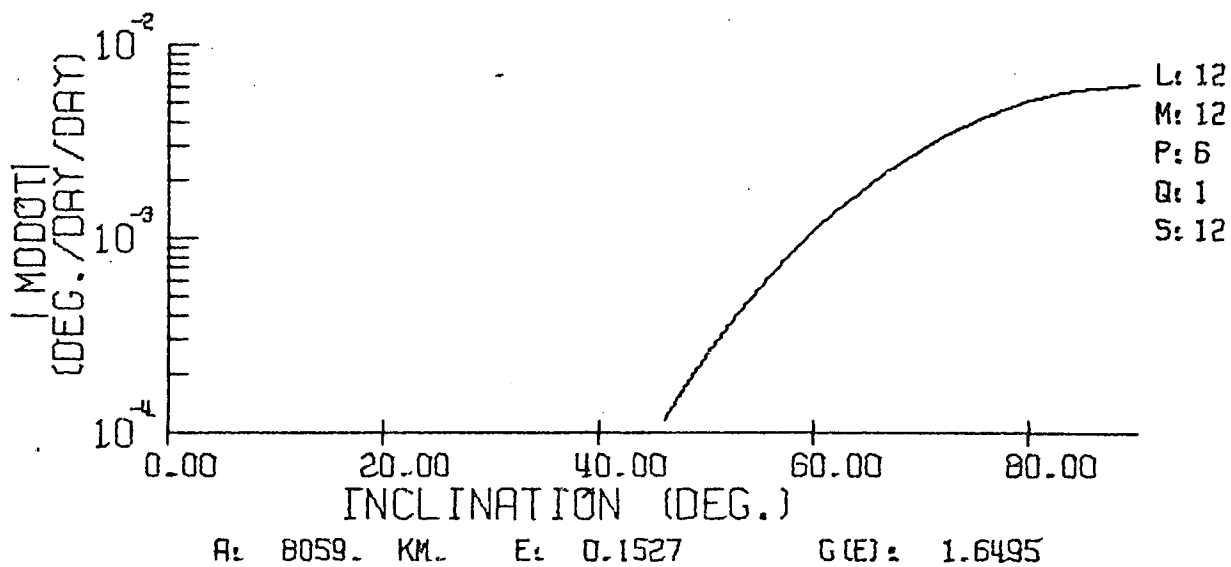
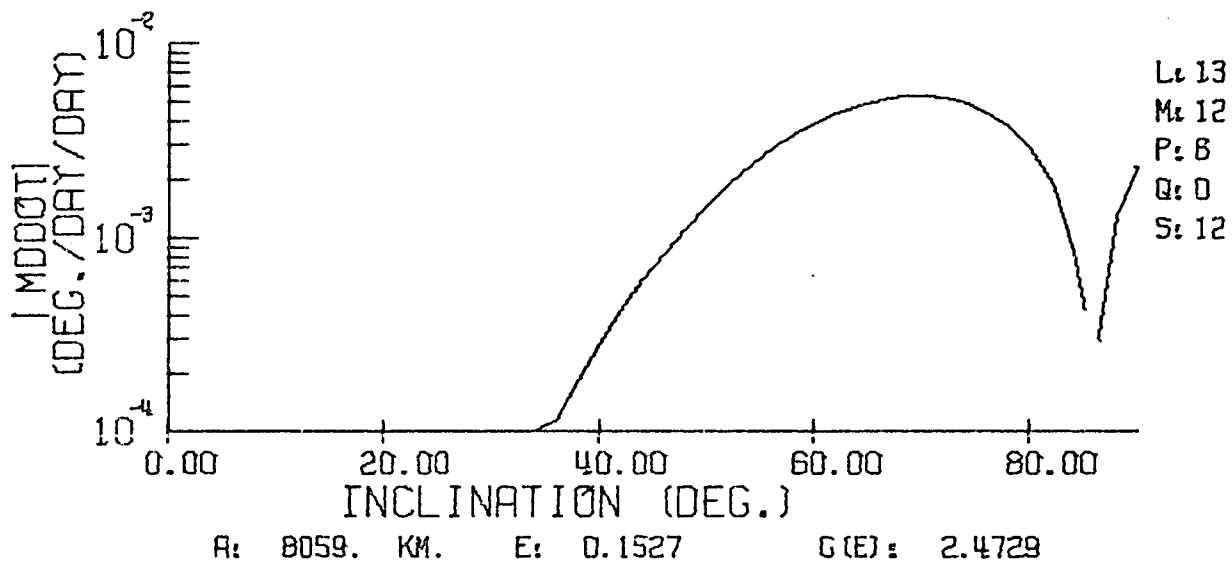
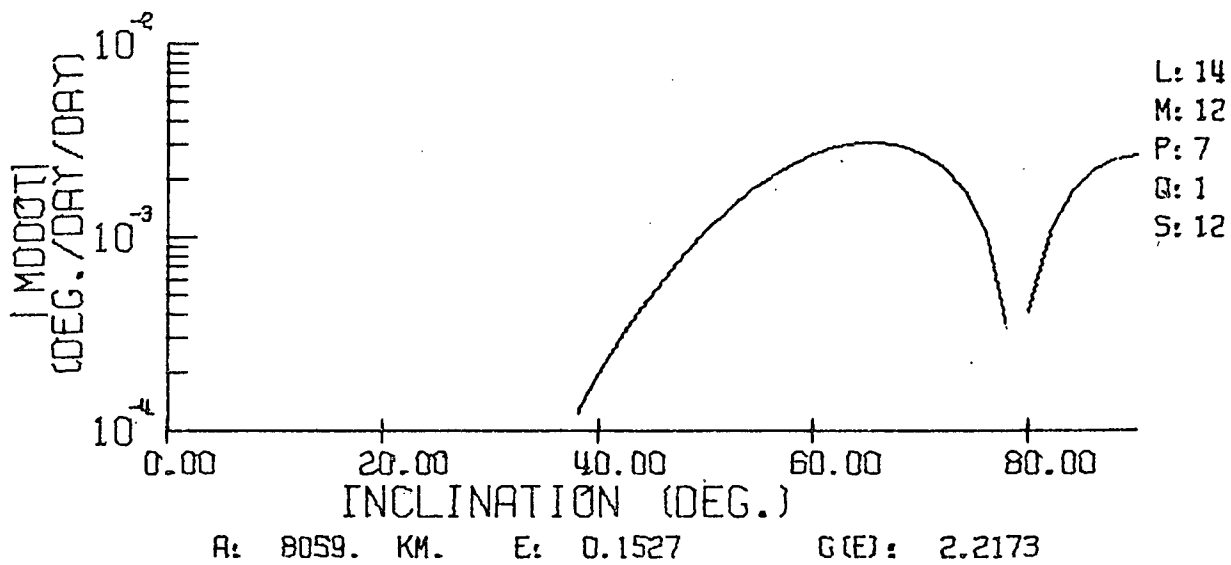






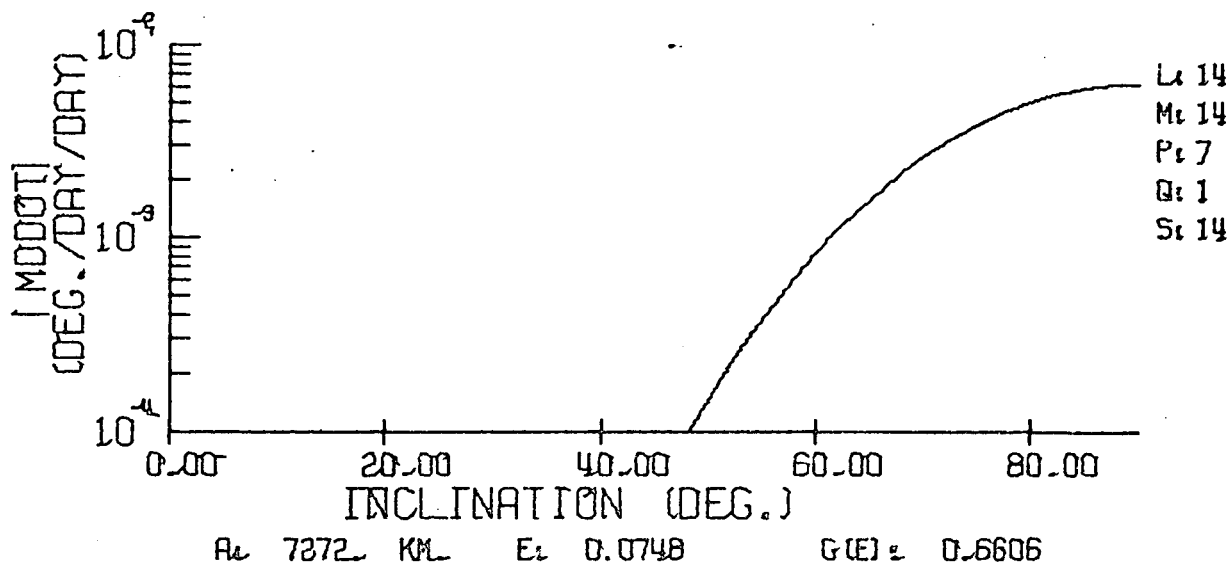
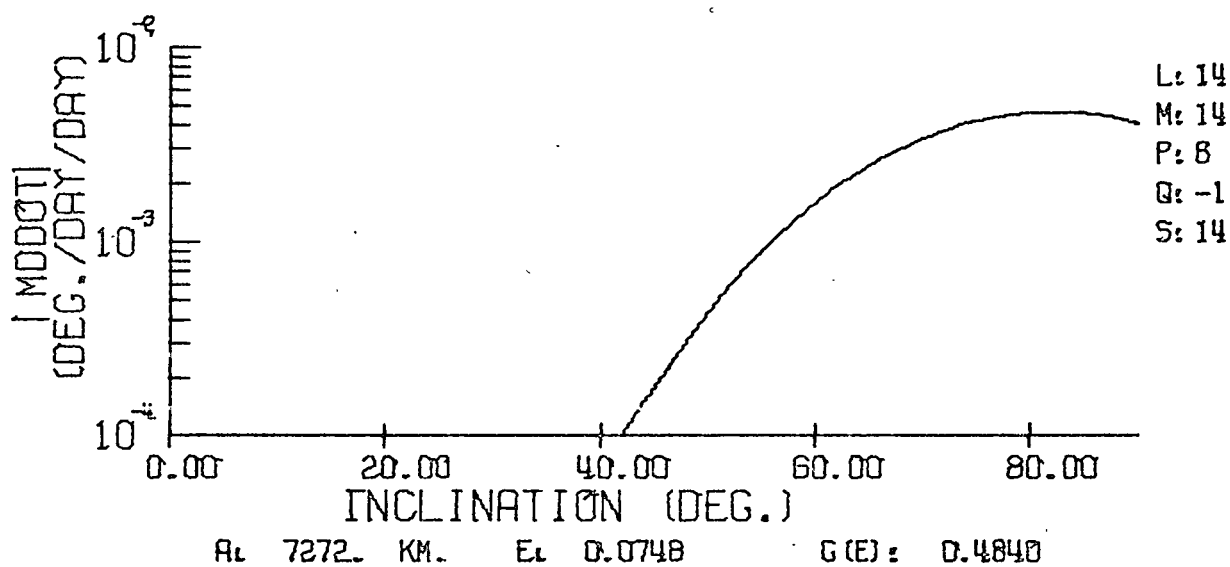
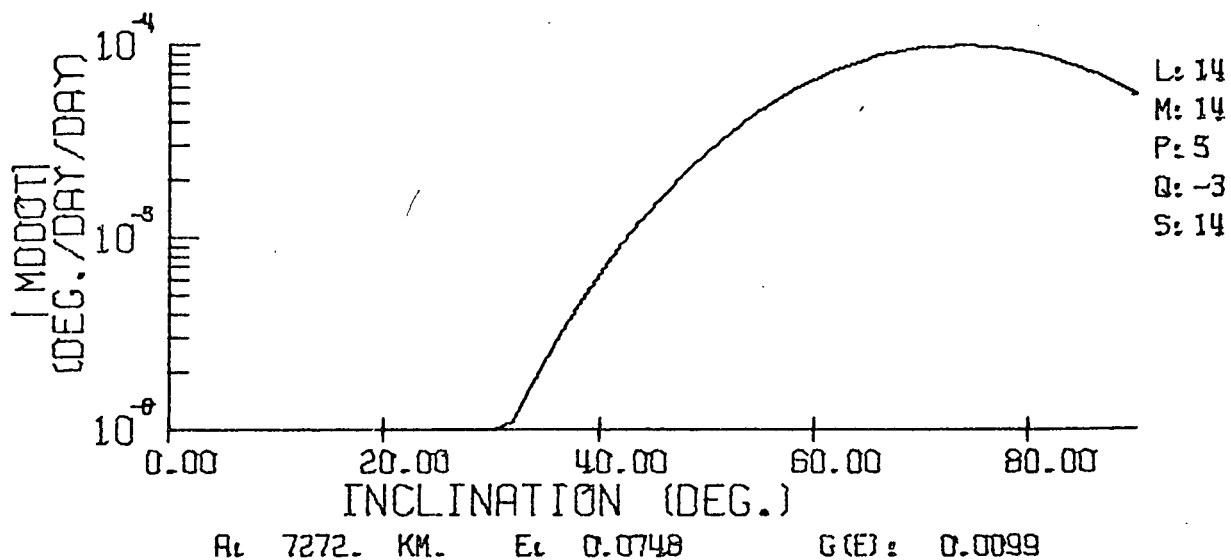




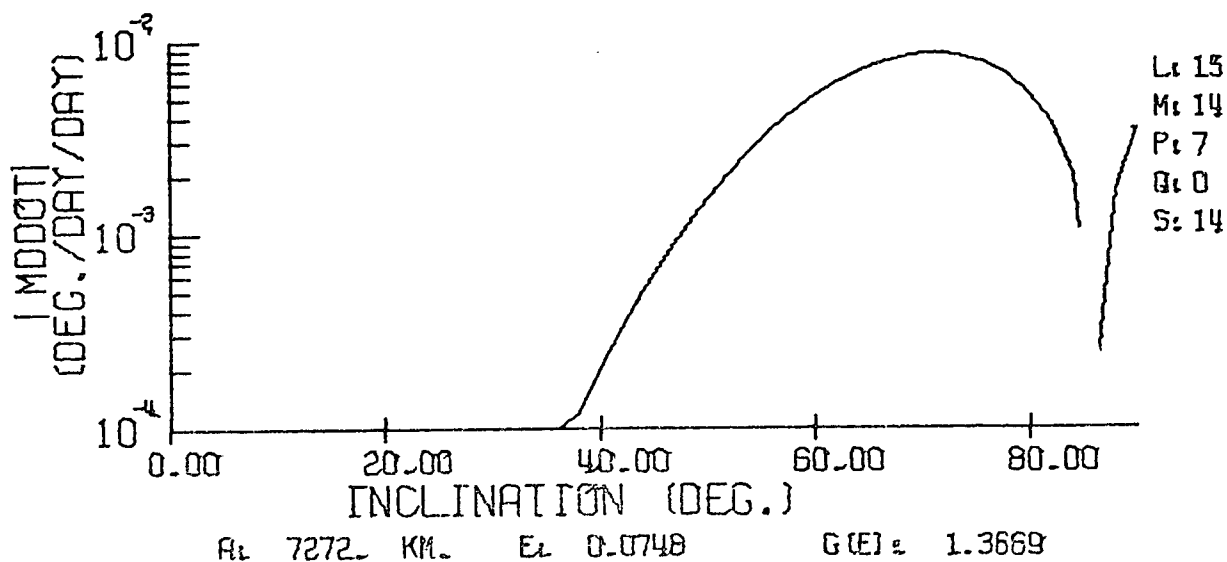
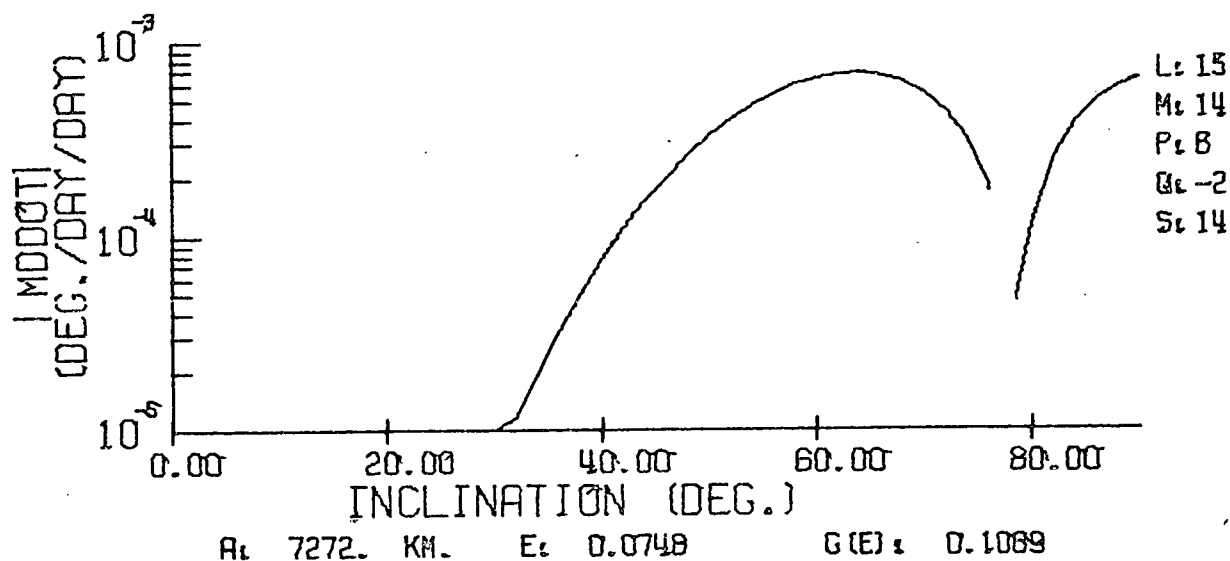
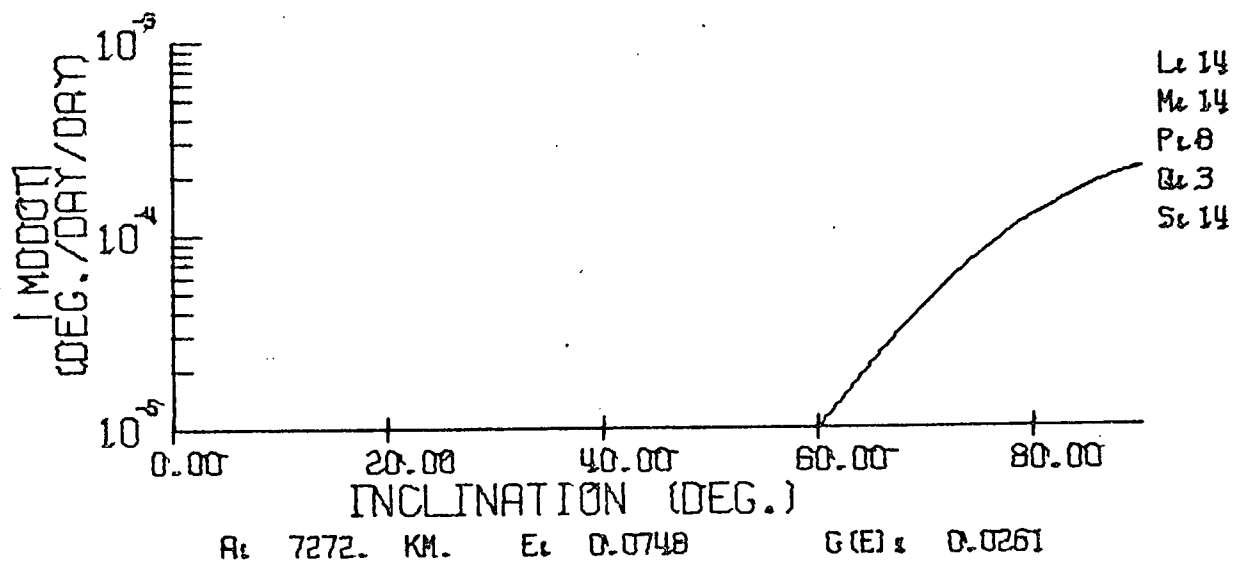


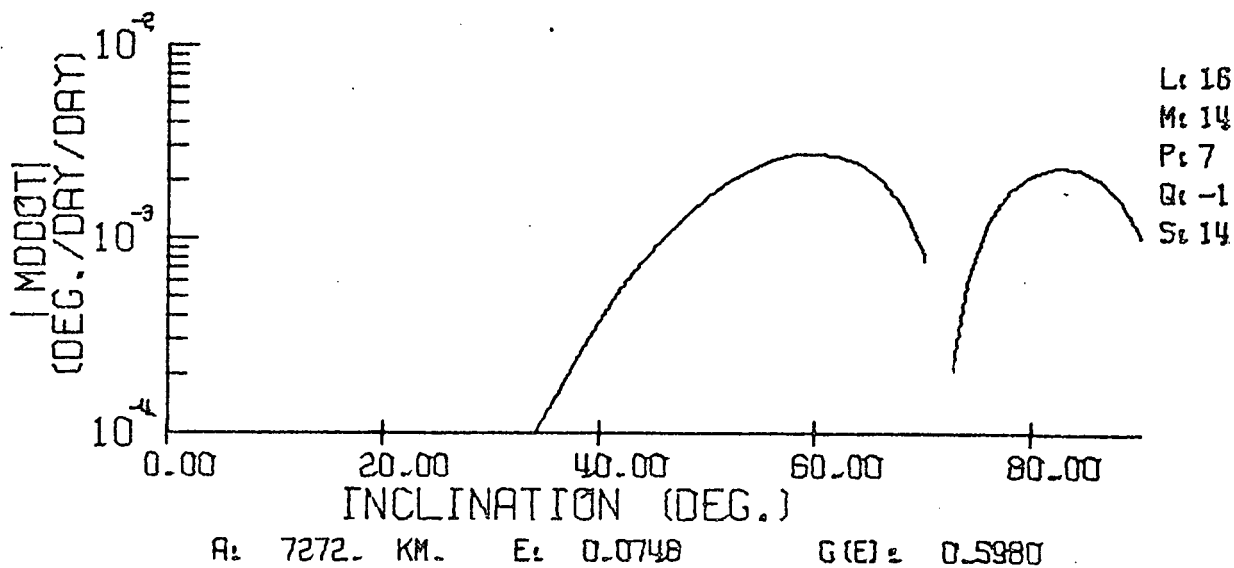
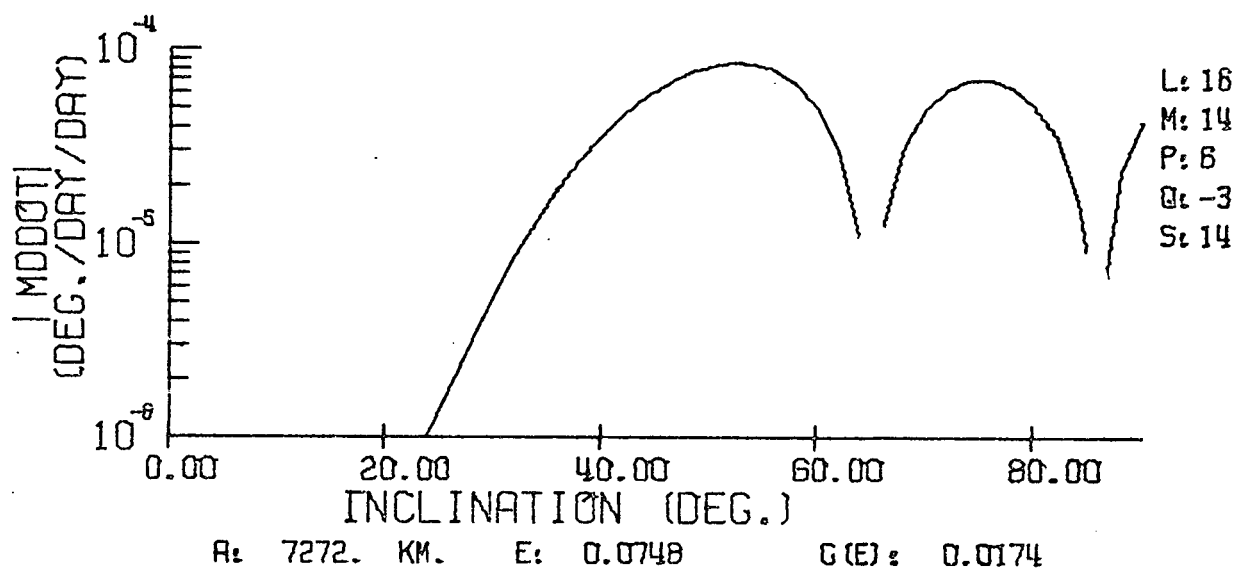
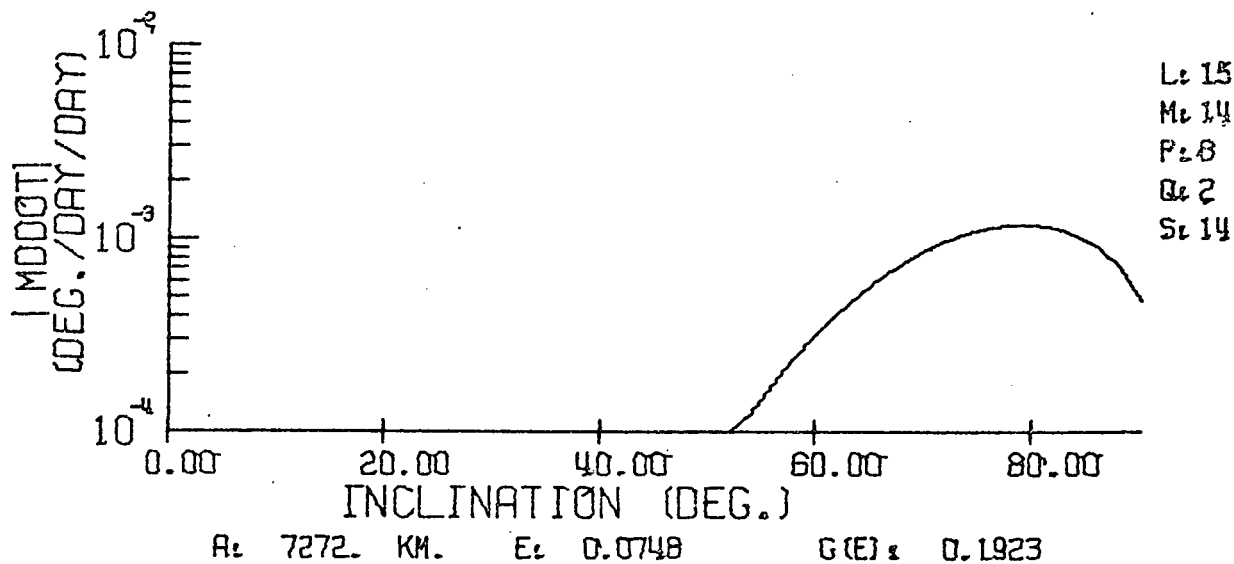
## APPENDIX C

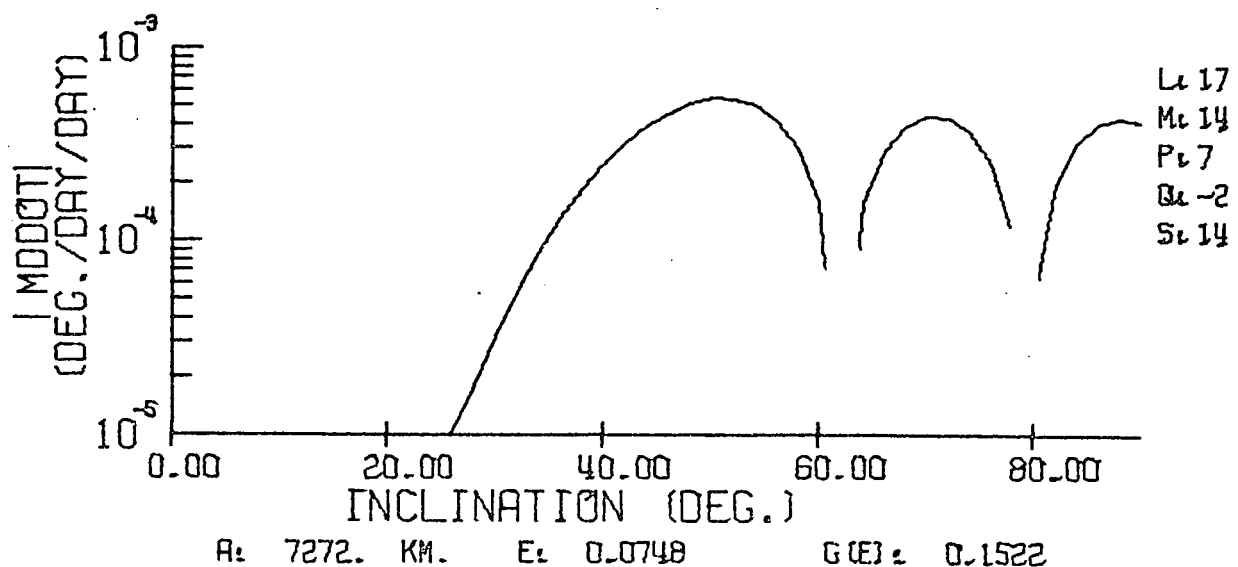
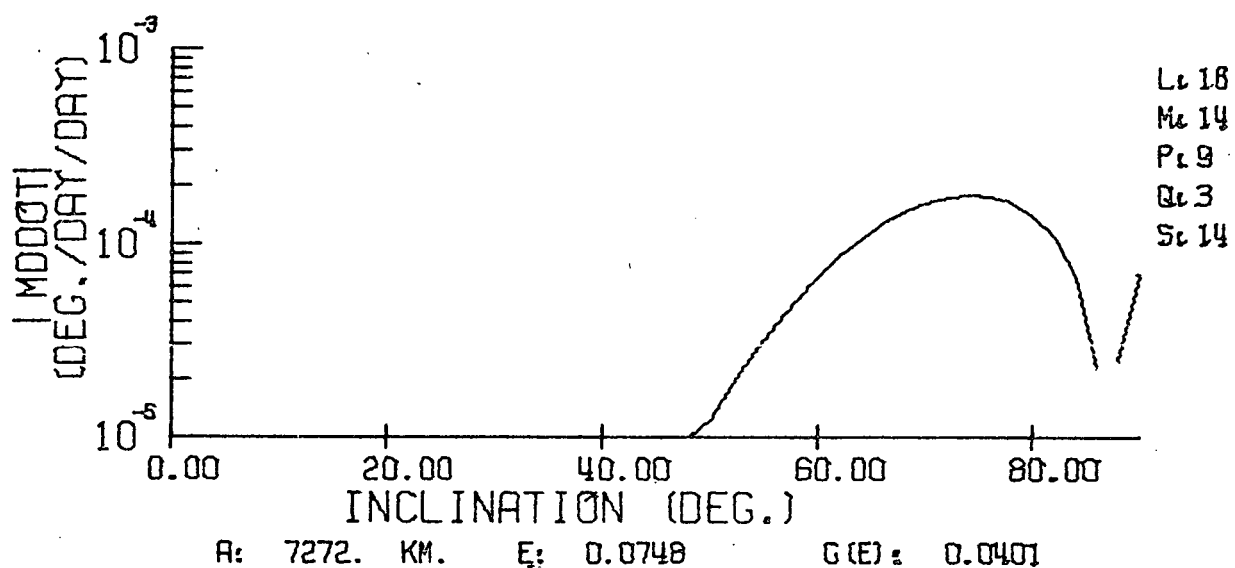
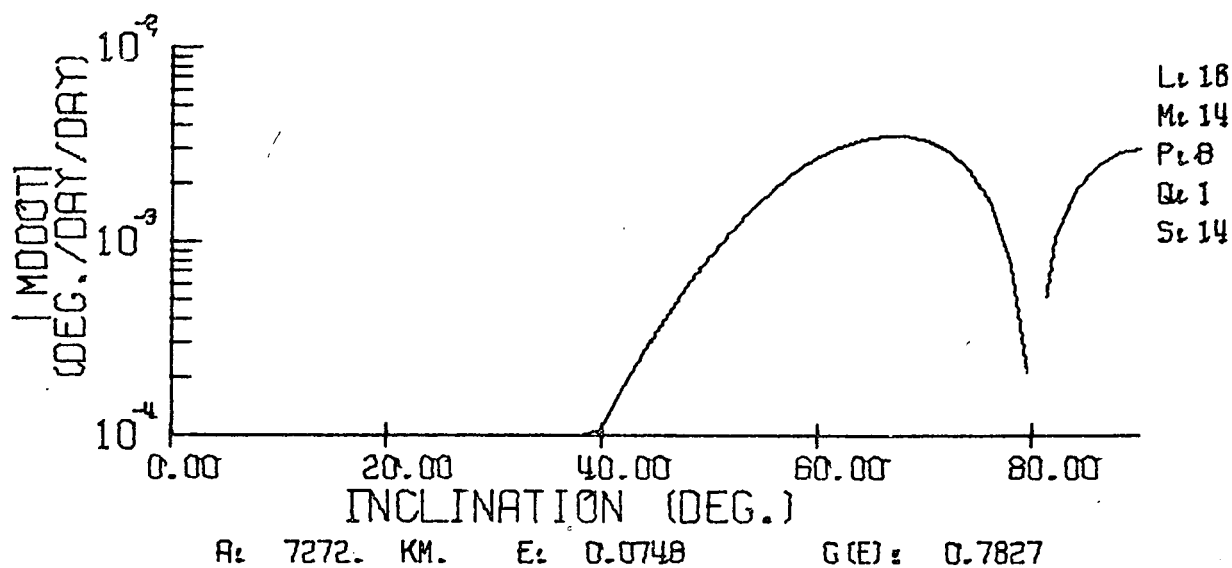
For this Appendix, acceleration of mean anomaly is shown for  
 $s = m = 14$ , perigee altitude of 350 km.

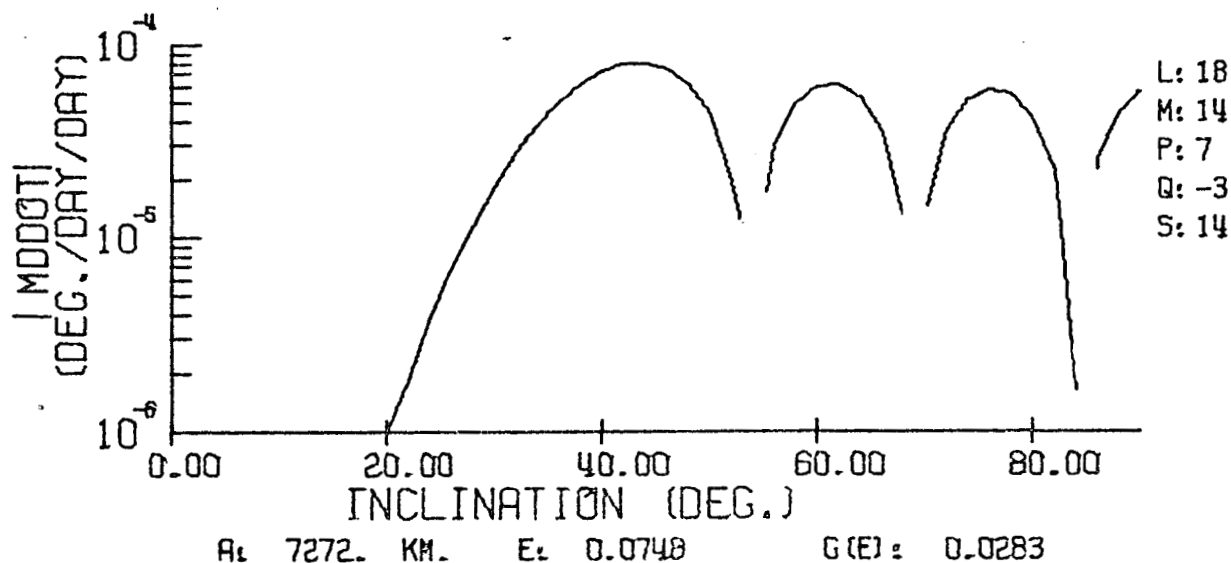
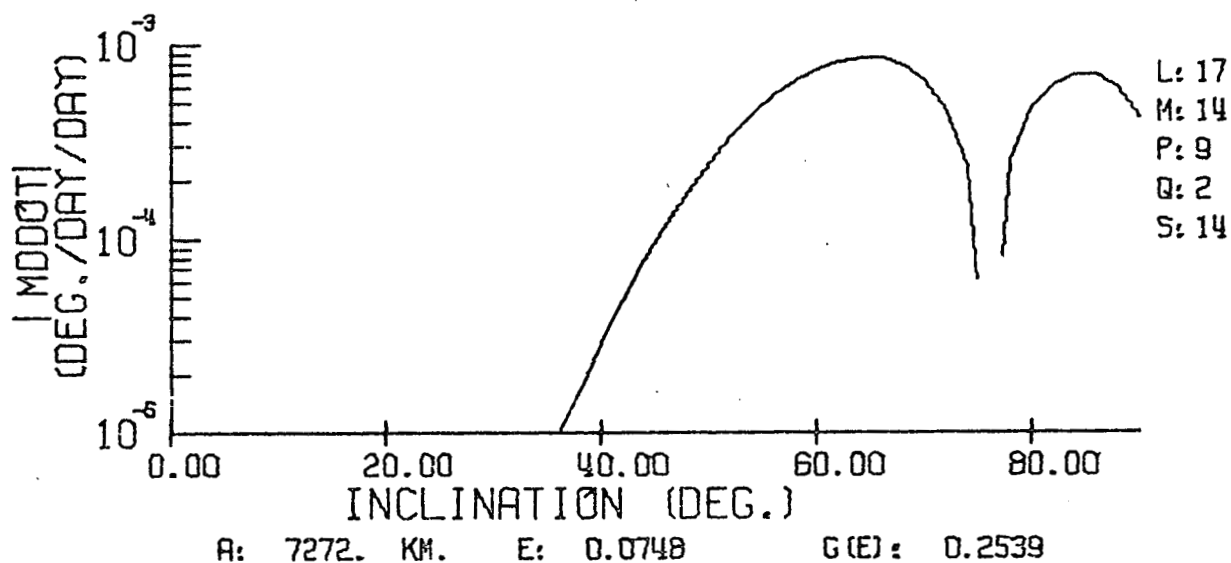
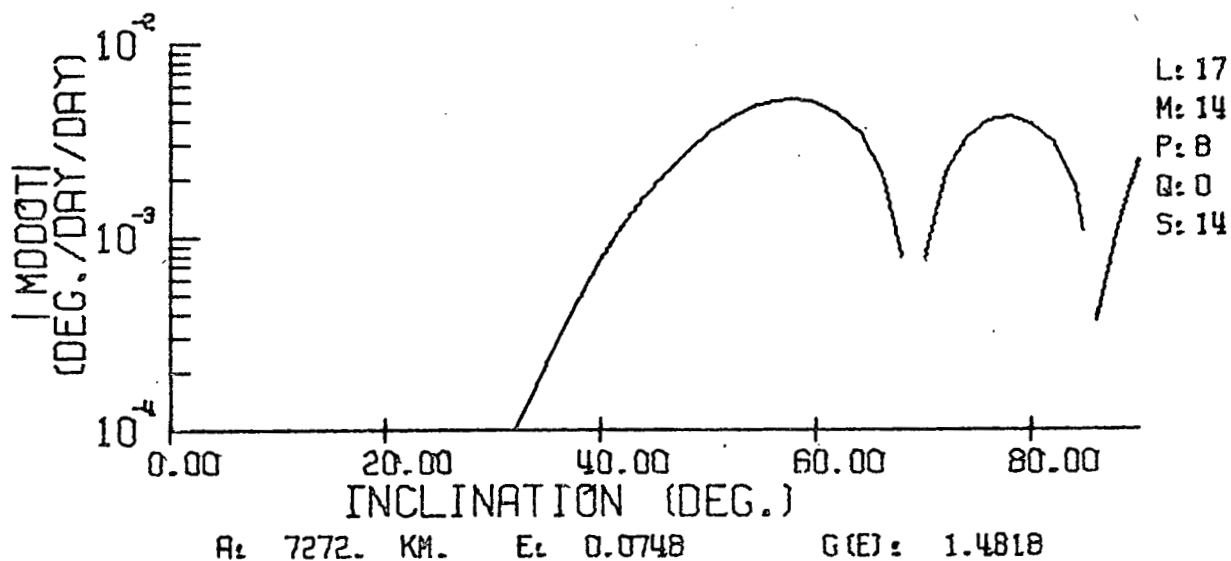


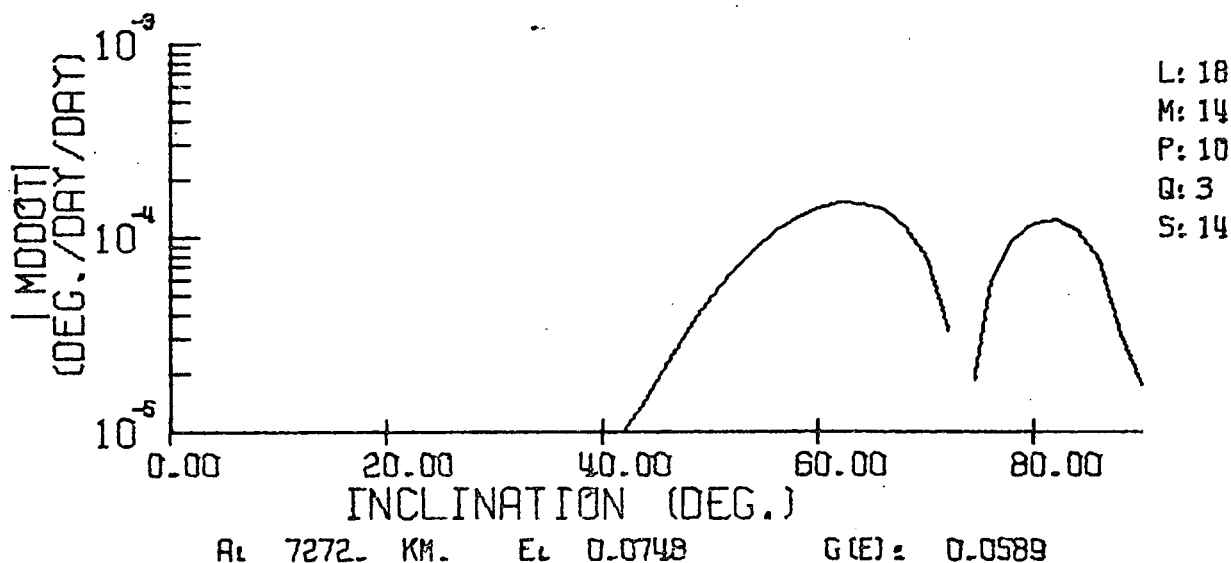
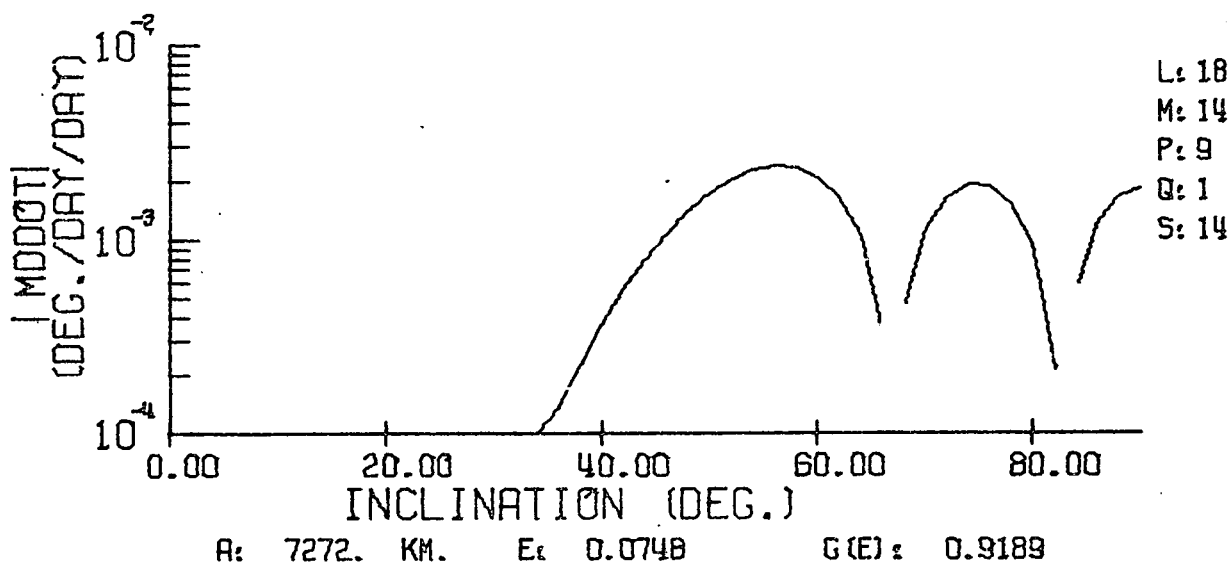
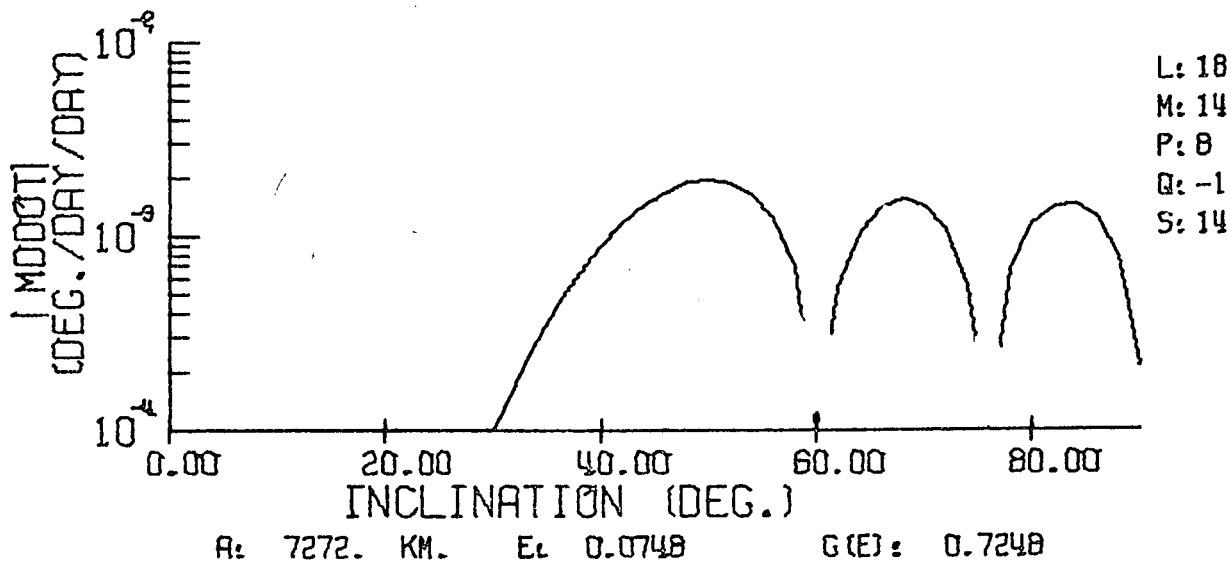


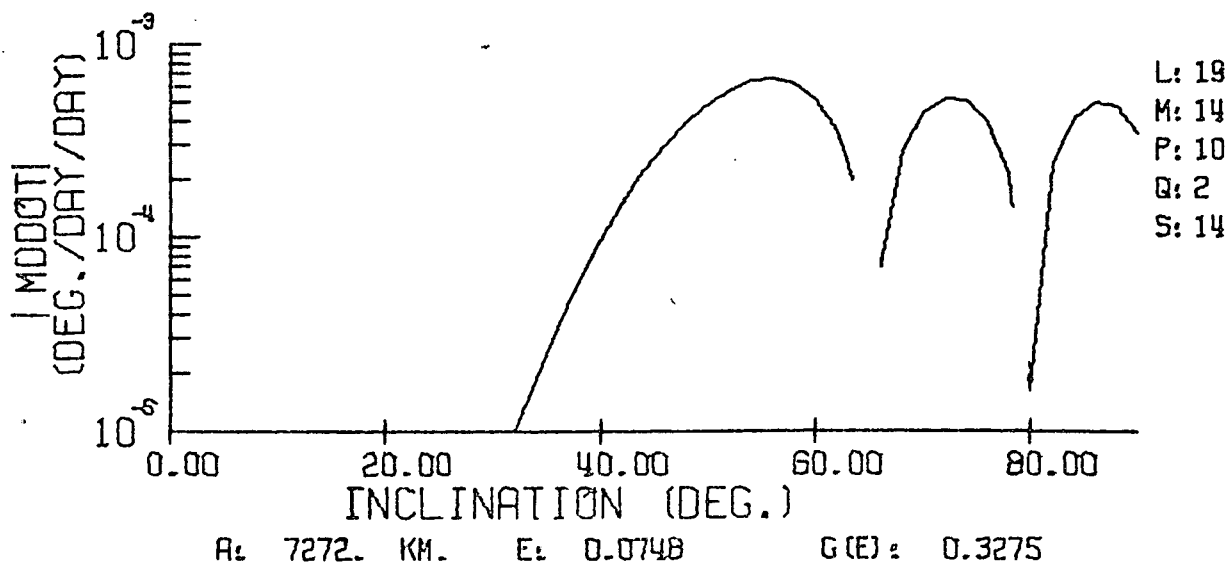
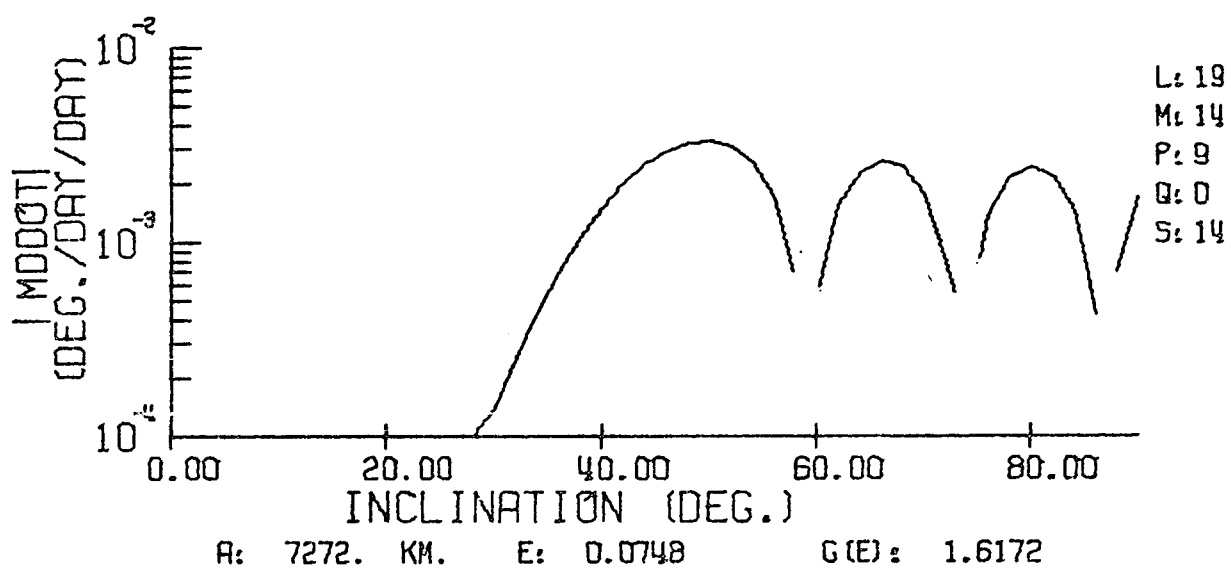
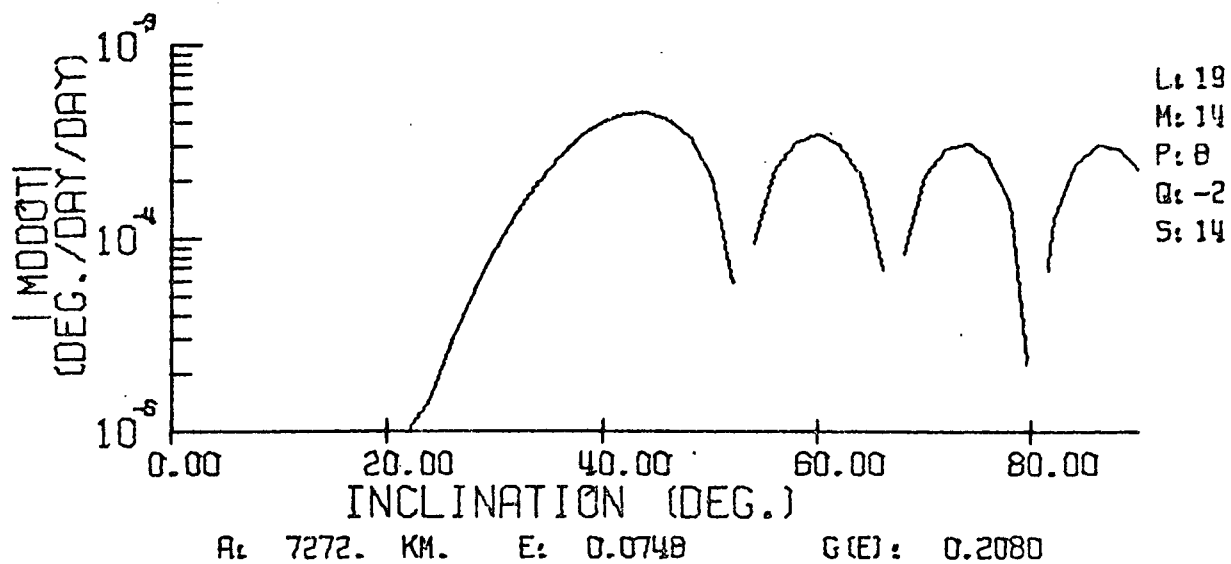


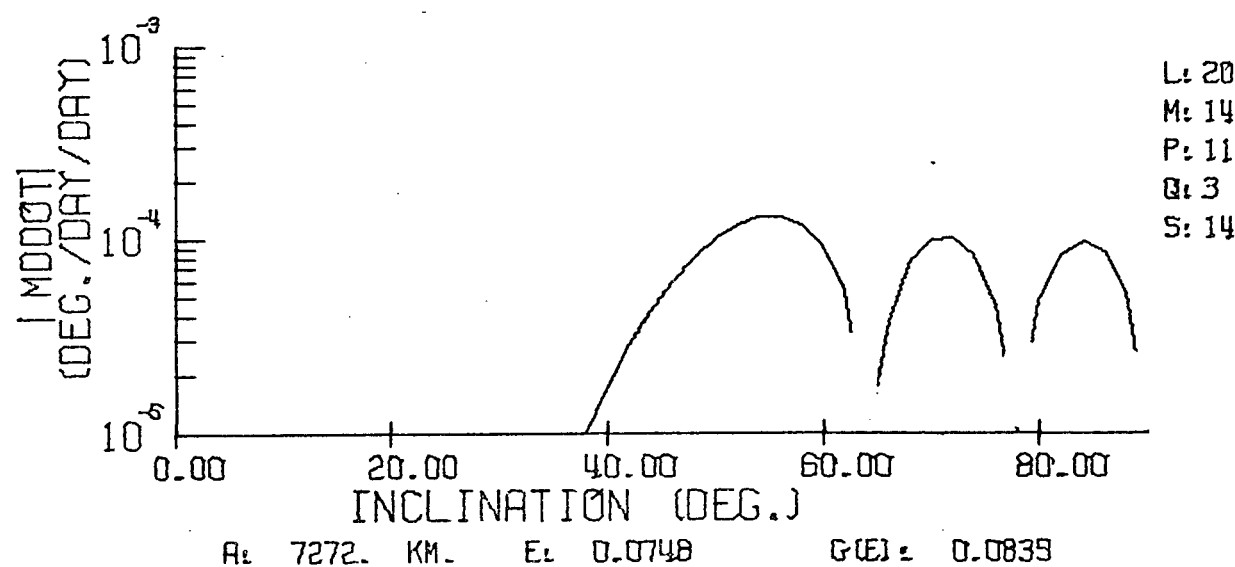
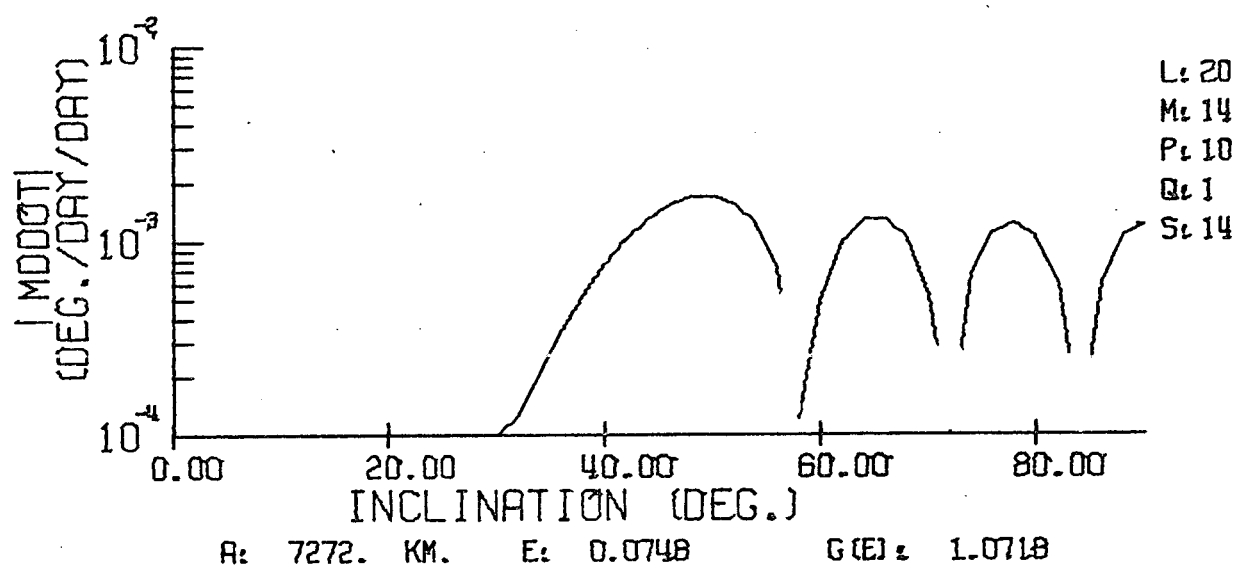
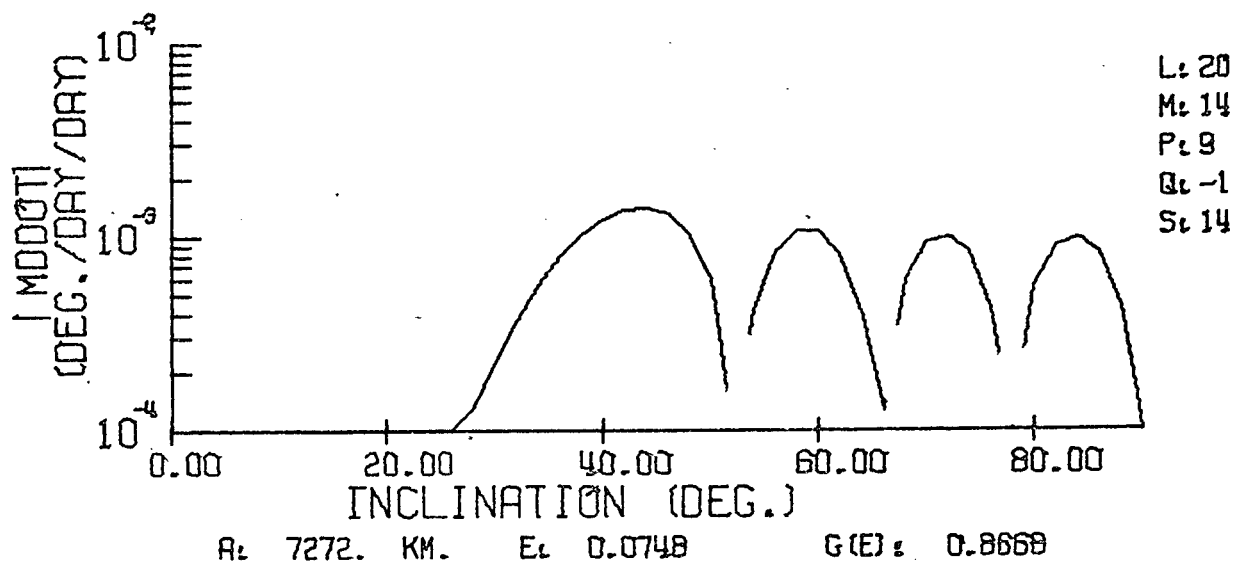












## APPENDIX D

### DOCUMENTATION OF DRAG-FREE SATELLITE FUEL COMPUTATION PROGRAM

#### PURPOSE

DFSFUEL is a digital program written in Fortran IV, level H, version II, which computes the translational control propellant required for sustaining a Drag-Free Satellite in a prescribed orbit for one year. Included in the computation are the effects of

- 1) atmospheric density
- 2) control system limit cycle
- 3) transient recovery from external perturbations
- 4) solar radiation pressure
- 5) vertical offset of mass center from position sensor null
- 6) effect of upper atmospheric winds.

#### PROCEDURE

The heart of the program is the dynamic, 2-degree-of-freedom atmospheric model of Jacchia [Ref. 1] as modified by Keating and Prior [Ref. 2] for asymmetry of the diurnal bulge. For computational reasons, it has been found convenient to use the 2-degree-of-freedom polynomial fit of this model given by Sorenson [Ref. 3] rather than use the original equations of Jacchia which require an integration. The polynomial agrees with the model to at least 3 places so it is adequate for present purposes. The program steps the satellite around in the given orbit calculating density at each step and numerically integrating the drag to get the total drag impulse for the orbit. To this is added "worst-case" impulses for limit cycle, solar radiation pressure, transient recovery, and vertical bias in pickoff null.

To account for the possibility that satellite surface forces need not be aligned with the control thrusters, a factor of  $\sqrt{3}$  is used in the impulse computation. A further factor of conservatism is provided for in a special factor called SAFTY by which the total impulse is multiplied, before computing the propellant mass.

#### VARIABLES

Listed only will be the variables which can be controlled by input. Most of them have default values assigned internally if they are not overridden by input specification.



INC	orbit inclination in degrees (no default)	
INCO	initial orbit inclination	} in cases where several different inclinations are to be examined.
INCI	orbit inclination increment	
INCF	final orbit inclination	
EP	orbit eccentricity (no default)	
EPO	initial eccentricity	} in cases where several different eccentricities are to be examined.
EPI	eccentricity increment	
EPF	final eccentricity	
HP	perigee altitude in km (no default)	
HPO	initial perigee altitude	} in cases where several different perigee altitudes are to be examined.
HPI	perigee increment	
HPF	final perigee altitude	
S	orbital frequency in revs/day (no default)	
SO	initial orbital frequency	} in cases where several orbital frequencies are to be examined.
SI	orbital frequency increment	
SF	final orbital frequency	
ISP	effective $I_{sp}$ of the propellant in sec (default value = 30 for nitrogen plus tanks).	
CD	satellite drag coefficient (default value = 2.2)	
MASS	satellite mass in kg (default value = 86.5)	
AOM	satellite area to mass ratio in $m^2/kg$ (default value = $1.2 \times 10^{-2}$ )	
DB	controller deadband in m (default value = $1.5 \times 10^{-3}$ )	
DVMIN	thruster minimum velocity change in m/sec (default = $4.4 \times 10^{-6}$ )	
VOFF	vertical offset from pickoff null to mass center in m (default value = $1. \times 10^{-2}$ )	
DIST	magnitude of impulsive transient disturbances in m (default = $2 \times 10^{-3}$ )	
NUMDIST	number of transient disturbances (default value = $1.0 \times 10^4$ )	
RSTIM	time to damp transient disturbance in sec (default value = 30.)	
OMG	satellite orbit right ascension in degrees (default value = -4.6)	
W	orbit argument of perigee in deg (default value = 270.)	
CWIND	ratio of rotational rate of upper atmosphere to earth's rotational rate (default value = 1.3)	
BLGO	angle between Greenwich and Equinox at time 0 in deg (default value = 0)	
FIO	index of solar decimetric flux in units of $10^{-22}$ watts/ $m^2$ /cps band- width (default value = 175)	
FIOB	monthly average of FIO (default value = 175)	
AP	index of magnetic activity in units of $2 \times 10^{-5}$ gauss (default value = 10.)	

DAY day of the year (default value = 170.)

DF increment in true anomaly to be used in impulse computation in deg  
(default = 5)

SAFTY factor of conservatism used in obtaining total impulse (default  
value = 1.2)

PRINT } These variables were included to give the option of plotting.  
PLOT } However, plot routines are not yet included so these variables  
should not be changed from their default values.

#### PROGRAM INPUT

In general, the order and quantity of input data is arbitrary for any combination of the variables listed above. Any variable which is not explicitly given a value by input will be assigned its default value. To input a value for a particular variable, the name of the variable is placed on the card (or card image) left justified to column 1 and the value is placed anywhere in columns 9 thru 20 as an E or F format number with explicit decimal point. Thus, there is always one variable name and value per card except when inputting a range of values for eccentricity, perigee altitude, orbital frequency, or inclination. In these cases, the name of the variable representing the initial value is placed on the card left justified to column 1, its corresponding value in E or F format in columns 9 thru 20, and the increment and final values in columns 29 thru 40, and 49 thru 60 respectively.

The set of variables (HP, EP, S) is redundant in that any one of them may be calculated from the other two, values must always be input for any two--and only two--of them. This gives some flexibility in specifying the orbital parameters. (See samples on page 185 and 186.)

#### OUTPUT

The output generated by DFSFUEL is generally self-explanatory. The only part which requires interpretation is the table labeled "default overrides." The order of the variables listed in this table is

INC	EP	HP	S	INCO	INCI	INCF	EPO
EPI	EPF	HPO	HPI	HPF	SO	SI	SF
ISP	CD	MASS	AOM	DB	DVMIN	VOFF	DIST
NUMDIST	RSTIM	OMG	W	BLGO	CWIND	DF	DAY
FIO	FIOB	AP	PRINT	PLOT	SAFTY		

Whenever one of these variables has been specified as input, the value will be shown explicitly in the table, otherwise the default value was used and the symbol \*\*\* ... will be shown in the table.

A sample output is included here to illustrate the result of running the sample input shown previously.

#### REFERENCES

- D-1. Jacchia, L.G., "Static Diffusion Models of the Upper Atmosphere With Empirical Temperature Profiles," Smithsonian Contributions to Astrophysics, vol. 8, no. 9, Smithsonian Institution Astrophysical Observatory, Washington, D.C., 1965.
- D-2. Keating, C.M., and Prior, E.J., "Latitude and Seasonal Variations in Atmospheric Densities Obtained During Low Solar Activity by Means of the Inflatable Air Density Satellite," Space Research VII, vol. 2, North Holland Publishing Co., Amsterdam, 1967.
- D-3. Sorensen, J.A., Ph.D Dissertation, Dept. of Aeronautics and Astronautics, SUDAAR 380, to be published.

# SAMPLE OUTPUT

PROPELLANT REQUIRED FOR DRAG FREE SATELLITE OPERATION FOR ONE YEAR

## DEFAULT VARIABLE OVERRIDES

45.000000	0.100000	*****	*****	*****	*****	*****	*****
*****	*****	300.000000	50.000000	800.000000	*****	*****	*****
*****	*****	100.000000	*****	*****	*****	*****	*****
*****	*****	10.000000	*****	*****	*****	*****	*****
200.000000	*****	*****	*****	*****	*****	*****	*****

## FIXED WORST CASE IMPULSES (N.SEC)

SOLAR RADIATION

235.966

LIMIT CYCLE

15.263

TRANSIENT RESPONSE

66.667

INCLINATION = 45.00 DEG

ECCENTRICITY = 0.10000

PERIGEE ALT (KM)	REVS/DAY	CM OFFSET IMP (N.SEC)	DRAG IMP (N.SEC)	TOTAL IMP (N.SEC)	MASS OF PROP + TANKS (KG)
300.000	13.604	61.732	19216.930	15596.550	63.659
350.000	13.453	60.364	6361.234	6739.488	27.508
400.000	13.304	59.037	2817.167	3194.099	13.037
450.000	13.158	57.748	1335.324	1710.968	6.984
500.000	13.014	56.496	656.115	1030.507	4.206
550.000	12.874	55.281	336.130	709.307	2.895
600.000	12.735	54.100	177.644	349.640	2.243

650.000	12.600	52.952	97.491	468.330	1.912
700.000	12.466	51.837	55.512	425.245	1.736
750.000	12.335	50.752	33.033	401.681	1.640
800.000	12.206	49.698	20.511	388.106	1.584

COMPILE TIME= 2.58 SEC, EXECUTION TIME= 6.97 SEC, OBJECT CODE= 18896 BYTES, ARRAY AREA= 546 BYTES, UNUSED= 230560 BYTES  
 \$STOP 521.  
 \$STOP 521.

APPENDIX D

(Cont)

PROGRAM LISTING

```

1. //DFSDRAG JOB (J363,414,1,2),*A FLEETING*,MSGLEVEL=1
2. //JOB LIB DD DSN=SYS2.PROGLIB,DISP=(OLD,PASS)
3. //KENT EXEC WATFOR
4. //GO.SYSIN DD *
5. SWATFOR
6. REAL*8 VAR(30),*INC *,'EP *,'HP *,'S *,'INCO
7. 1 *,'EPO *,'HPO *,'SO *,'ISP *,'CD *,'HASS
8. 2 *,'AOM *,'DB *,'DVNIN *,'VOFF *,'DIST *,'NUMDIS
9. 3 *,'ASTIR *,'DMG *,'U *,'BLGO *,'CWIND *,'DF
10. 4 *,'DAY *,'FIO *,'FIOB *,'AP *,'NO PRINT *,'PLOT
11. 5 *,'SAFTY
12. REAL*8 RLO2,RLO5,RLO9,DEFLT1,DEFLT2,DEFLT3
13. REAL*8 DEXP,DLOG,RLO12
14. REAL*8 RLO3,RLO4,RLO5,RLO7,RLO8,RLO10,TNP,RLO,LRO,RMI
15. REAL*8 OUTDUM(30)/30*1.010/
16. REAL ISP,HASS,NUMDIS,INCO,INCI,INCF,KOAB,IMPLC,IMPTN,
17. 1IMPSOL,INC,INCD,IMPDG,H,LONG,FASTOT,IMPTOT,IMPCNO
18. INTEGER PRINT,PLOT,UPDN
19. C
20. C INITIALIZE SATELLITE PARAMETERS TO DEFAULT VALUES
21. C
22. ISP = 30.0
23. CD = 2.2
24. HASS = 86.5
25. AOM = 1.2E-2
26. DB = 0.0015
27. DVNIN = 4.4E-6
28. VOFF = 0.01
29. DIST = 2.0E-3
30. NUMDIS = 1.0E4
31. RESTIR = 30.0
32. C
33. C INITIALIZE SATELLITE ORBIT AND SOLAR PARAMETERS TO DEFAULT VALUES
34. C
35. DMG = -4.6
36. W = 270.
37. CWIND = 1.3
38. BLGO = 0.0
39. FIO = 175.
40. DF = 5.0
41. FIOB = 175.
42. DAY = 170.
43. AP = 10.
44. PRINT = 2
45. PLOT = 1
46. SAFTY = 1.2
47. KOPT = 0
48. C
49. C START MAIN PROGRAM BY READING IN ANY DEFAULT OVERRIDES
50. C
51. 1 READ (5,100,END=2) DEFLT1,DUM1,DEFLT2,DUM2,DEFLT3,DUM3
52. 100 FORMAT (3(A8,G12))
53. DO 3 J=1,30
54. IF (DEFLT1 .EQ. VAR(J)) GO TO (4,5,6,7,8,9,10,11,12,13,14,15
55. ,16,17,18,19,20,21,22,23,24,25,26,27,28,29,30,31,32,33),J
56. 3 CONTINUE
57. GO TO 1
58. 4 INCO = DUM1
59. INCF = DUM1 +0.01
60. INCI = 1.

```

```

61.      OUTDUM(1) = INCO
62.      GO TO 1
63.      5  EPO = DUM1
64.      EPF = DUM1 + 0.01
65.      EPI = .1
66.      KOPT = KOPT + 1
67.      OUTDUM(2) = EPO
68.      GO TO 1
69.      6  HPO = DUM1
70.      HPF = DUM1 + 1.
71.      HPI = 100.
72.      KOPT = KOPT + 2
73.      OUTDUM(3) = HPO
74.      GO TO 1
75.      7  SO = DUM1
76.      SF = DUM1 + 0.1
77.      SI = 1.0
78.      KOPT = KOPT + 3
79.      OUTDUM(4) = SO
80.      GO TO 1
81.      8  INCO = DUM1
82.      INCI = DUM2
83.      INCF = DUM3
84.      OUTDUM(5) = INCO
85.      OUTDUM(6) = INCI
86.      OUTDUM(7) = INCF
87.      GO TO 1
88.      9  EPO = DUM1
89.      EPI = DUM2
90.      EPF = DUM3
91.      KOPT = KOPT + 1
92.      OUTDUM(8) = EPO
93.      OUTDUM(9) = EPI
94.      OUTDUM(10) = EPF
95.      GO TO 1
96.      10 HPO = DUM1
97.      HPI = DUM2
98.      HPF = DUM3
99.      KOPT = KOPT + 2
100.     OUTDUM(11) = HPO
101.     OUTDUM(12) = HPI
102.     OUTDUM(13) = HPF
103.     GO TO 1
104.     11 SO = DUM1
105.     SI = DUM2
106.     SF = DUM3
107.     KOPT = KOPT + 3
108.     OUTDUM(14) = SO
109.     OUTDUM(15) = SI
110.     OUTDUM(16) = SF
111.     GO TO 1
112.     12 ISP = DUM1
113.     OUTDUM(17) = ISP
114.     GO TO 1
115.     13 CO = DUM1
116.     OUTDUM(18) = CO
117.     GO TO 1
118.     14 MASS = DUM1
119.     OUTDUM(19) = MASS
120.     GO TO 1
121.     15 AUM = DUM1

```



```

122.      OUTDUM(20) = AOM
123.      GO TO 1
124. 10  UB = DUM1
125.      OUTDUM(21) = UB
126.      GO TO 1
127. 17  DVMIN = DUM1
128.      OUTDUM(22) = DVMIN
129.      GO TO 1
130. 18  VOFF = DUM1
131.      OUTDUM(23) = VOFF
132.      GO TO 1
133. 19  DIST = DUM1
134.      OUTDUM(24) = DIST
135.      GO TO 1
136. 20  NUMDIS = DUM1
137.      OUTDUM(25) = NUMDIS
138.      GO TO 1
139. 21  RSTIM = DUM1
140.      OUTDUM(26) = RSTIM
141.      GO TO 1
142. 22  CMG = DUM1
143.      OUTDUM(27) = CMG
144.      GO TO 1
145. 23  W = DUM1
146.      OUTDUM(28) = W
147.      GO TO 1
148. 24  HLG0 = DUM1
149.      OUTDUM(29) = HLG0
150.      GO TO 1
151. 25  CWIND = DUM1
152.      OUTDUM(30) = CWIND
153.      GO TO 1
154. 26  DF = DUM1
155.      OUTDUM(31) = DF
156.      GO TO 1
157. 27  DAY = DUM1
158.      OUTDUM(32) = DAY
159.      GO TO 1
160. 28  F10 = DUM1
161.      OUTDUM(33) = F10
162.      GO TO 1
163. 29  F10B = DUM1
164.      OUTDUM(34) = F10B
165.      GO TO 1
166. 30  AP = DUM1
167.      OUTDUM(35) = AP
168.      GO TO 1
169. 31  PRINT = 1
170.      OUTDUM(36) = PRINT
171.      GO TO 1
172. 32  PLOT = 2
173.      OUTDUM(37) = PLOT
174.      GO TO 1
175. 33  SAFETY = DUM1
176.      OUTDUM(38) = SAFETY
177.      GO TO 1
178. 2  CONTINUE
179.      IF (PRINT.EQ.1) GO TO 27
180.      WRITE (6,101)
181. 101 FORMAT ('1774, *ACCELERANT REQUIRED FOR DRAG FREE SATELLITE OPER',
182.          '1, *ATION F - ONE YES */////////8X, *DEFAULT VARIABLE OVERRIDES')

```

```

183.      WRITE (6,102) (OUTDUM(I),I=1,36)
184. 102 FORMAT (///(' ',B(2X,F13.6)/))
185. 47 CONTINUE
186. C
187. C ASSIGN FIXED CONSTANTS AND PERFORM DEGREES TO RADIANS CONVERSION
188. C
189.      WE = 0.7292E-4
190.      TP = 0.0
191.      FO = 0.0
192.      GME = 3.9858E5
193.      RE = 6371.
194.      FSTOP = 360.0
195.      TO = 0.0
196.      DAYP = 4.
197.      ASU = 1.496E8
198.      SUTNC = 23.45
199.      MSU = -77.59749
200.      KOPT = KOPT - 2
201.      IF (KOPT.EQ. 2) GO TO 80
202.      RPF = HPF + RE
203.      RPO = HPD + RE
204.      RPI = MPI
205. 80 CONTINUE
206.      SECPY = 365.*24.*60.*60.
207.      KRAD = .8
208.      SQRT3 = SQRT(3.0)
209.      DTR = 1./57.29578
210.      RTD = 57.29578
211.      INCO = DTR*INCO
212.      INCI = DTR*INCI
213.      INCF = DTR*INCF
214.      OMC = DTR*OMC
215.      W = DTR*W
216.      BLGO = DTR*BLGO
217.      FO = DTR*FO
218.      FSTOP = DTR*FSTOP
219.      PI = 3.1415927
220.      TPI = 2.*PI
221.      KEVCCN = 60.*60.*24./TPI
222.      CO = COS(OMC)
223.      SO = SIN(OMC)
224.      PUT = PI/2.
225.      TPUT = 3.*PUT
226.      DF = DTR*DF
227. C
228. C DETERMINE SOME TEMPERATURE PARAMETERS
229. C
230.      TFO = 414. +3.6*FIOB +1.8*(FIO-FIOB)*(0.37+0.14*SIN(TPI*(DAY-151.
231.      I 1/365.)))*FIOB*SIN(2.*TPI*(DAY-59.)/365.)
232.      KK45 = 45.*DTK
233.      KK12 = 12.*DTK
234.      APM = AP +125.*41. -EXP(-0.085*AP)
235. C
236. C COMPUTE FULL IMPULSE FOR LIMIT CYCLE, TRANSIENT RECOVERY, AND
237. C SLEW DATA, ASSUMING WORST CASE CONDITIONS)
238. C
239.      TAUIC = 4.*M/DVXIN
240.      TAUIC = 3.*MASS*VME*SECPY/TAUIC
241.      IMPTR = DIST*MMDIS*MASS/KESTIN
242.      IMPSL = 30.*MASS*AD*4.5E-6*SECPY*KRAD
243.      IF (KOPT.EQ. 1) GO TO 42

```

```

244. WRITE (6,103) INPSOL,IMPLC,IMPTR
245. 103 FORMAT (////44X,'FIXED WORST CASE IMPULSES (N,SEC)'/13X,'SOLAR RA
246. IRIATION',27X,'LIMIT CYCLE',25X,'TRANSIENT RESPONSE'//3(15X,F10.3,
247. 215X))
248. 64 CONTINUE
249. C
250. C DETERMINATION OF SUN POSITION
251. C
252. EPSU = 1.672592E-02
253. WSU = DTR*WSU
254. SUINC = DTR*SUINC
255. DFSU = 0.9856091*DTR
256. SUM = DFSU*(DAY-DAYP)
257. ESU = SUM
258. DO 41 I=1,5
259. 41 ESU = SUM + EPSU*SIN(ESU)
260. CES = COS(ESU)
261. CFS = (CES - EPSU)/(1. - EPSU*CES)
262. SFS = (SIN(ESU)*SQRT(1.-EPSU*EPSU))/(1.-EPSU*CES)
263. SMS = SIN(WSU)
264. CWS = COS(WSU)
265. SUS = SMS*CFS + CWS*SFS
266. CUS = CWS*CFS - SMS*SFS
267. SULM = ARSIN(SUS*SIN(SUINC))
268. SUOL = ARCUS(CUS/COS(SULM))
269. IF (SUS.LT.0.0) SUHL = TPI - SUOL
270. C
271. C INITIALIZE THE FAMILY OF ORBITS TO BE INVESTIGATED, COMPUTE ORBITAL
272. C PARAMETERS, AND THEN INCREMENT THROUGH THE FAMILY
273. C
274. 64 INC = INCO - INCI
275. 52 INC = INC + INCI
276. IF (INC.GT.INCF) GO TO 1000
277. 65 IF (PRINT.EQ. 1) GO TO 69
278. INCD = RTD*INC
279. WRITE (6,104) INCD
280. 104 FORMAT (////7X,'INCLINATION = ',F7.2,' DEG')
281. 49 CONTINUE
282. GO TO (53,56,54), K*PT
283. 53 EP = EPJ - EPI
284. 54 EP = EP + EPI
285. IF (EP.GT.EPF) GO TO 52
286. IF (PRINT.EQ. 1) GO TO 70
287. WRITE (6,105) EP
288. 105 FORMAT (////7X,'ECCENTRICITY = ',F7.5)
289. WRITE (6,107)
290. 107 FORMAT (/// 2X,'PERIGEE ALT (KM)', 8X,'REVS/DAY', 5X,'CM OFFSET IN
291. IP (N,SEC)', 1X,'OPAG IMP (N,SEC)', 1X,'TOTAL IMP (N,SEC)', 1X,'MAS
292. 25 OF PROP + TANKS (KG)')
293. 70 CONTINUE
294. RP = RPO - RPI
295. 55 RP = RP + RPI
296. IF (RP.GT.RPF) GO TO 54
297. S = REVCUN*SQRT(GME/(RP*(1. - EP)))**3)
298. GO TO 62
299. 56 S = SO - SI
300. 57 S = S + SI
301. IF (S.GT.SFI) GO TO 52
302. IF (PRINT.EQ. 1) GO TO 71
303. WRITE (6,106) S
304. 106 FORMAT (////7X,'REVOLUTIONS PER DAY = ',F7.3)

```

```

305.      WRITE (6,108)
306. 108  FORMAT (/// 2X,'ECCENTRICITY', 8X,' PER ALT (KM)', 5X,'CM OFFSE',
307. 107. 1X,'IMP IN (N.SEC)', 1X,'DRAG IMP (N.SEC)', 1X,'TOTAL IMP (N.SEC)', 1X,
308. 2X,'MASS OF PROP + TANKS (KG)')
309. 71  CONTINUE
310.      EP = EPO - EPI
311. 58  EP = EP + EPI
312.      IF (EP.GT.EPFF) GO TO 57
313.      RP = (1.-EP)*(GME*REVCON**2/S**2)**(1./3.)
314.      GO TO 62
315. 59  S = SO - S1
316. 60  S = S + S1
317.      IF (S.GT.SF) GO TO 52
318.      IF (PRINT.EQ. 1) GO TO 72
319.      WRITE (6,106) S
320.      WRITE (6,109)
321. 109  FORMAT (/// 2X,'PER ALT (KM)', 8X,'ECCENTRICITY', 5X,'CM OFFSET IN
322. 1P (N.SEC)', 1X,'DRAG IMP (N.SEC)', 1X,'TOTAL IMP (N.SEC)', 1X,'MASS
323. 2 OF PROP + TANKS (KG)')
324. 72  CONTINUE
325.      RP = RPO - RPI
326. 61  RP = RP + RPI
327.      IF (RP.GT.RPFF) GO TO 60
328.      EP = 1. - RP*(S**2/(GME*REVCON**2))**(.1/3.)
329. 62  CONTINUE
330.      A = RP/(1. - EP)
331.      HP = RP - RE
332.      ORF = SQRT(GME/A**3)
333.      OOA = 1./A
334.      PER = TPI/ORF
335. 63  CONTINUE
336.      SINC = SIN(INC)
337.      CINC = COS(INC)
338.      SOCINC = SO*CINC
339.      COCINC = CO*CINC
340. C
341. C  THIS SECTION UPDATES THE ORBITAL POSITION OF THE SATELLITE
342. C  USING A CENTRAL FORCE FIELD MODEL.
343. C
344. 40  F2 = FO - DF
345.      T1 = TO
346.      IMPDG = 0.
347. 38  F2 = F2 + DF
348.      F = F2
349.      IF (F.GT.TPI) F = F - TPI
350.      COSF = COS(F)
351.      CE = (EP + COSF)/(1. + EP*COSF)
352.      E = ARCOS(CE)
353.      IF (F.GT.PI) E = TPI - E
354.      M = F - EP*SIN(F)
355.      T = TP + M/ORF
356.      IF (F2.GT.TPI) T = T + PER
357.      SINFI = SIN(F)
358.      R = A*(1. - EP*CE)
359.      V = SQRT(GME*(2./R - OOA))
360.      DUM = 1./SQRT(1. + 2.*EP*COSF + EP*EP)
361.      SG = EP*SINFI*DUM
362.      CG = (1. + EP*COSFI)*DUM
363.      U = M + F
364.      IF (U.GT.TPI) U = U - TPI
365.      SU = SIN(U)

```

```

366.      CU = COS(U)
367.      CL = SQRT(1. - (SU*SINC)**2)
368.      IF(ABS(SINC - POT).LT.0.0001) GO TO 77
369.      IF(U.LE.PI) GO TO 78
370.      BLAM = OMC * TPI - APCOS(CU/CL)
371.      GO TO 79
372. 78 BLAM = OMC + APCOS(CU/CL)
373.      GO TO 79
374. 77 IF(U.LE.POT) GO TO 34
375.      IF(U.GT.POT) GO TO 34
376.      BLAM = OMC + PI
377.      GO TO 79
378. 34 BLAM = OMC
379. 79 IF(BLAM.GT.TPI) BLAM = BLAM - TPI
380.      VSG = V*SG
381.      VCG = V*CG
382.      XID = (CO*CU - SOCINC*SU)*VSG -(CO*SU + SOCINC*CU)*VCG
383.      YID = (SO*CU + COCINC*SU)*VSG -(SO*SU - COCINC*CU)*VCG
384.      ZID = SINC*SU*VSG + SINC*CU*VCG
385.      VM = C*WIND*WE*RC*CL
386.      SBL = SIN(BLAM)
387.      CBL = COS(BLAM)
388.      XRD = XID + VM*SBL
389.      YRD = YID - VM*CBL
390.      ZRD = ZID
391.      SL = SU*SINC
392.      LAM = ARSIN(SL)
393.
394. C      DETERMINE ATMOSPHERIC DENSITY VIA SORENSEN POLYNOMIAL
395. C      FIT TO JACCHIA TWO PARAMETER MODEL
396. C
397.      ETT = 0.5*ABS(LAM-SULM)
398.      THT = 0.5*ABS(LAM+SULM)
399.      HA = BLAM - SUBL
400.      TASU = HA - RK45 + RK12*SIN(HA+RK45)
401.      IF (TASU.LT.-PI) TASU = TASU+TPI
402.      IF (TASU.GT.PI) TASU = TASU-TPI
403.      TIEP = TEN*(1. + 0.28*SIN(ETT) + 0.28*(COS(THT)-SIN(ETT))*(COS(0.5*
404. 1 TASU))**2.5)
405.      TIF = TIEP + APK
406.      FX = (TIF-900.)/1750. + 11.722E-04*(TIF-800.)*2)
407.      FS = 0.0291*EXP(-FX*FX/2.)
408.      HE = R - RF/SQRT(1. + (6.7385E-03)*SL*SL)
409.      TMP = TIF - (TIF-355.)*EXP(-FS*(HE-120.))
410.      KRN = 1
411.      IF (HE.LT.120.) GO TO 81
412.      IF (HE.LT.200.) GO TO 42
413.      IF (HE.LT.300.) GO TO 43
414.      IF (HE.LT.400.) GO TO 44
415.      IF (HE.LT.500.) GO TO 45
416.      IF (HE.LT.600.) GO TO 46
417.      IF (HE.LT.700.) GO TO 47
418.      IF (HE.LT.800.) GO TO 48
419.      IF (HE.LT.900.) GO TO 49
420.      GO TO 50
421. 81 WRITE (6,110) HE
422. 110 FORMAT ('X,HEIGHT =',F7.1,'IS OUT OF RANGE')
423.      GO TO 73
424. 42 RL012 = -11.*ALOG(2.461)
425.      HLO = 120.
426.      KRN = 2

```

```

427.      RLO = RLO12*1.25
428. 43 RLO2 = -0.30543570+02 +TMP*(0.29147450-02+TMP*(-0.10723230-05
429.      1 +0.39342890-11*TMP))
430.      IF (KRO.EQ.2) RHI = RLO2*1.25
431.      IF (KRO.EQ.2) GO TO 51
432.      HLO = 200.
433.      KRO = 2
434.      RLO = RLO2
435. 44 RLO3 = -0.38173060+02 +TMP*(0.12018970-01+TMP*(-0.63458190-05
436.      1 +0.11506960-08*TMP))
437.      IF (KRO.EQ.2) RHI = RLO3
438.      IF (KRO.EQ.2) GO TO 51
439.      HLO = 300.
440.      KRO = 2
441.      RLO = RLO3
442. 45 RLO4 = -0.41947990+02+TMP*(0.14433360-01+TMP*(-0.70408650-05
443.      1 +0.12043880-08*TMP))
444.      IF (KRO.EQ.2) RHI = RLO4
445.      IF (KRO.EQ.2) GO TO 51
446.      HLO = 400.
447.      KRO = 2
448.      RLO = RLO4
449. 46 RLO5 = -0.45682130+02 +TMP*(0.17523010-01+TMP*(-0.83043900-05
450.      1 +0.13963050-08*TMP))
451.      IF (KRO.EQ.2) RHI = RLO5
452.      IF (KRO.EQ.2) GO TO 51
453.      HLO = 500.
454.      KRO = 2
455.      RLO = RLO5
456. 47 RLO6 = -0.49373530+02+TMP*(0.20306900-01+TMP*(-0.94092410-05
457.      1 +0.15592820-08*TMP))
458.      IF (KRO.EQ.2) RHI = RLO6
459.      IF (KRO.EQ.2) GO TO 51
460.      HLO = 600.
461.      KRO = 2
462.      RLO = RLO6
463. 48 RLO7 = -0.50692830+02 +TMP*(0.20471030-01 +TMP*(-0.89800820-05
464.      1 +0.14249710-08*TMP))
465.      IF (KRO.EQ.2) RHI = RLO7
466.      IF (KRO.EQ.2) GO TO 51
467.      HLO = 700.
468.      KRO = 2
469.      RLO = RLO7
470. 49 RLO8 = -0.49687380+02 +TMP*(0.15525720-01 +TMP*(-0.56217010-05
471.      1 +0.73357390-09*TMP))
472.      IF (KRO.EQ.2) RHI = RLO8
473.      IF (KRO.EQ.2) GO TO 51
474.      HLO = 800.
475.      KRO = 2
476.      RLO = RLO8
477. 50 RLO9 = -0.45953530+02 +TMP*(0.67329910-02+TMP*(-0.26290550-06
478.      1 -0.30583030-09*TMP))
479.      IF (KRO.EQ.2) RHI = RLO9
480.      IF (KRO.EQ.2) GO TO 51
481.      HLO = 900.
482.      RLO = RLO9
483.      RLO10 = -0.42505970+02 +TMP*(-0.50244030-03+TMP*(0.37461300-05
484.      1 -0.10186550-08*TMP))
485.      RHI = RLO10
486. 51 LRO = RLO + (HLO-HLO)*(RHI-RLO)*0.01
487.      RMD = DEXP(LRO)*1.0E1

```

```

484.      C
485.      C COMPUTE ATMOSPHERIC DRAG IMPULSE
486.      C
487.      DELT = T - T1
488.      VMAGS = (XPD**2 + YRD**2 + ZRD**2)**.5
489.      IMPDG = 0.5*RHQ*ACM*MASS*VMAGS*CD*DELT*SQR3 + IMPDG
490.      T1 = T
491.      39 IF (F2.LT.FSTOP) GO TO 38
492.      IMPDG = IMPDG*.965
493.      VACC = 2.*(GME/(A**3))*VOFF
494.      IMPCMO = MASS*SECPY*VACC
495.      IMPTOT = IMPDG + IMPLC + IMPTR + IMPSOL + IMPCMO
496.      MASTOT = IMPTOT*SAFTY/(9.8*ISP)
497.      IF (PRINT .EQ. 1) GO TO 73
498.      GO TO (74,75,76),KOPT
499.      74 WRITE (6,111) HP,S,IMPCMO,IMPDG,IMPTOT,MASTOT
500.      111 FORMAT (' ',6(5X,F9.3,4X)/)
501.      GO TO 73
502.      75 WRITE (6,111) EP,HP,IMPCMO,IMPDG,IMPTOT,MASTOT
503.      GO TO 73
504.      76 WRITE (6,111) HP,EP,IMPCMO,IMPDG,IMPTOT,MASTOT
505.      73 CONTINUE
506.      GO TO (55,58,61),KOPT
507.      1000 CONTINUE
508.      RETURN
509.      END
510.
511.      $DATA
512.      INC          45.
513.      EP           0.1
514.      HPO          300.      50.      800.
515.      MASS         100.
516.      OXC          10.
517.      F10          200.
518.      $STOP
519.      /*

```